Masters Theses   Graduate School

5-1994

Structure, Stratigraphy, and Metamorphism of a Part of the Columbus Promontory, Western Inner Piedmont, North Carolina

Gregory M. Yanagihara
University of Tennessee - Knoxville

Follow this and additional works at: https://trace.tennessee.edu/utk_gradthes

Part of the Geology Commons

To the Graduate Council:

I am submitting herewith a thesis written by Gregory M. Yanagihara entitled "Structure, Stratigraphy, and Metamorphism of a Part of the Columbus Promontory, Western Inner Piedmont, North Carolina." I have examined the final electronic copy of this thesis for form and content and recommend that it be accepted in partial fulfillment of the requirements for the degree of Master of Science, with a major in Geology.

Robert D. Hatcher, Major Professor

We have read this thesis and recommend its acceptance:

Bill Dunne, Hap McSween
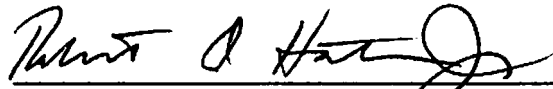
Accepted for the Council:
Carolyn R. Hodges

Vice Provost and Dean of the Graduate School

(Original signatures are on file with official student records.)

To the Graduate Council:
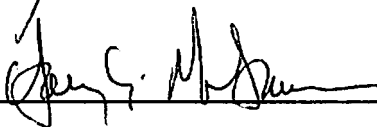
I am submitting herewith a thesis written by Gregory Masakatsu Yanagihara entitled"Structure, Stratigraphy, and Metamorphism of a Part of the Columbus Promontory, Western Inner Piedmont, North Carolina." I have examined the final copy of this thesis for form and content and recommend that it be accepted in partial fulfillment of the requirements for the degree of Master of Science, with a major in Geology.
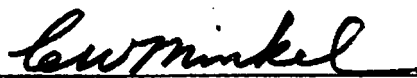
Robert D. Hatcher, Jr., Major Professor

We have read this thesis
and recommend its acceptance:

Accepted for the Council:
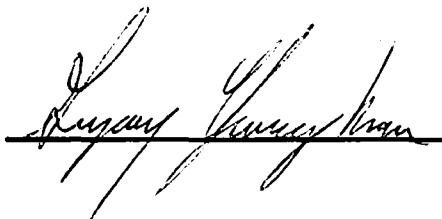
Associate Vice Chancellor
and Dean of The Graduate School

STATEMENT OF PERMISSION TO USE

In presenting this thesis in partial fulfillment of the requirements for a Master's degree at the University of Tennessee, Knoxville, I agree that the Library shall make it available to borrowers under rules of the Library. Brief quotations from this thesis are allowable without special permission, provided that accurate acknowledgement of the source is made.

Permission for extensive quotation from or reproduction of this thesis may be granted by my major professor, or in his absence, by the Head of Interlibrary Services when, in the opinion of either, the proposed use of the material is for scholarly purposes. Any copying or use of the material in this thesis for financial gain shall not be allowable without my written permission.

Signature _____

Date _12-21-93_____

STRUCTURE, STRATIGRAPHY, AND METAMORPHISM OF A PART OF THE COLUMBUS PROMONTORY, WESTERN INNER PIEDMONT, NORTH CAROLINA

A Thesis
Presented for the
Master of Science
Degree
The University of Tennessee, Knoxville

Gregory M. Yanagihara
May, 1994

ACKNOWLEDGEMENTS

So many people have had a positive impact on my thesis that a complete list of them would be too long. My greatest thanks goes to my advisor, Dr. Robert D. Hatcher, Jr., whose patience with a dyslexic Californian for three and a half years is unparalleled. His moral and financial support has made my experience as a graduate student a truly positive one. I also want to thank the other two members of my committee, Drs. Bill Dunne and Hap McSween, for their insight and help during the course of this study. Special thanks goes to Bill Dunne whose advice and friendship helped me to make the right decisions early in graduate school. Funding for this thesis was provided, in part by National Science Foundation grant EAR-90046004 awarded to Drs. R. D. Hatcher, Jr., and J. R. Tabor.

I am grateful to the "Hatchery" staff— Gina, Don, Mary, and Nancy for their moral support and assistance. Two graduate students have contributed directly to the content of my thesis: Tim Davis who got me started on my thesis project and with whom I later had lengthy discussions with, and Chris Jayne who showed a clueless southern Californian the difference between a poison ivy rash and a swarm of chigger bites. Marvin Bennett, Tony Caldanaro, Tim Davis, Mike Green, Beth McClellan, Qu Qi, and Ian Richards, were also helpful by editing parts of my thesis or helping me operate equipment that I was otherwise ignorant in using.

I would like to thank the many friends I have made at UT to whom I am known as Gonogorhea, Dr. Clue, and Goobenhaufer. After going to football games, drinking, rock climbing, skiing, field trips, and GSA meetings with these folks, I feel that graduate school has been one of the greatest experiences in my life, and will be a memory that I will cherish forever. If there is anybody I could "unthank", it would be Ralph Harvey, who provided us with a number of video games that, among other things, prolonged completion of my thesis.

Finally, I would like to thank my family, especially my parents, Daniel and Amy Yanagihara. It is to their credit that they raised a sick child who was so severely dyslexic

that he was initially thought to be retarded (many still think I am) to eventually receive a

Masters degree. I am also appreciative of my grandmother, Haruko Arakaki, who taught me

why I should be proud to be a Japanese American and that being myself isn't so bad after all.

ABSTRACT

The geology of the Inner Piedmont in a part of southwestern North Carolina, called the Columbus Promontory, is characterized by a complex history involving high grade metamorphism and penetrative ductile deformation. This study involved detailed (1:24,000) geologic mapping, petrography, whole rock geochemical analysis, and structural analysis to study the stratigraphy, structural geology, and metamorphism of a part of the Columbus Promontory.

Rocks in the study area can be divided into three major lithotectonic units, each separated by a ductile thrust fault, and strike NE and dip gently to the SE. Unit 1, the structurally lowermost and northwesternmost unit in the study area is composed entirely of Henderson Gneiss, a 509 Ma granitic augen gneiss. It also contains a 438 Ma intrusion of granitic gneiss. Unit 2 contains rocks of the upper Mill Spring complex with biotite gneiss and pelitic schist and the Poor Mountain Formation, dominated by amphibolite and quartzite. Unit 3, the structurally highest and southeasternmost unit, contains a lower unit of biotite gneiss associated with the upper Mill Spring complex and an upper unit of undifferentiated biotite gneiss, amphibolite, granitic gneiss, and pelitic schist. Based on the ordering of lithologies, the Poor Mountain Formation and Mill Spring complex are interpreted to be correlative with rocks in other parts of the Inner Piedmont and eastern Blue Ridge of Virginia, North Carolina, South Carolina, Georgia, and Alabama.

The structure of the Columbus Promontory is dominated by a series of SE-dipping, penetratively deformed, ductile, thrust sheets. Five episodes of deformation (D_1 to D_5) have been recognized but the two most significant were D_2 and D_3. Of these two episodes, D_2 accounts for virtually all the shear strain observed in the Inner Piedmont and is synchronous with peak M_2 metamorphism. D_2 deformation is associated with a regionally penetrative mylonitic C-fabric (S_2), mineral lineation, folds, and S-C fabrics. The penetrative nature of

these structures, the parallel orientations of the foliation, thrust faults, fold girdles, and great circle defined by mineral lineations, the parallel orientation of fold axes and mineral lineations, and the presence of sheath folds indicate that D_2 involved very high shear strains ($\gamma >> 10$) and that the Inner Piedmont represented a crustal-scale ductile shear zone. D_3 occurred during the cooling stages of M_2 metamorphism and forms a continuum with D_2 deformation. Shear sense during D_2, as indicated by mineral lineations, winged porphyroclasts, S-C fabrics, and snowball garnets, varied gradually from W-directed in areas to the SE to SW-directed in areas to the NW. Hansen analysis of F_2 and F_3 folds suggest that shear sense did not change significantly between D_2 and D_3 deformation. This change in the orientation of shearing from W to SW-directed transport is probably related to a dextral component of shearing along the primordial Brevard fault zone.

M_2 metamorphism reached the lower sillimanite zone in pelitic schist and upper amphibolite facies in amphibolite. Textural relationships and optical zoning in garnet indicate that sillimanite grew by a series of continuous reactions involving garnet growth and garnet consumption. These observations are consistent with relationships observed in other parts of the Columbus Promontory suggesting that sillimanite growth occurred along the retrograde portion of the P-T path.

Whole rock geochemical analysis was conducted on Poor Mountain Amphibolite using X-ray fluorescence. Covariation diagrams and Niggli trends indicate that the amphibolite was metamorphosed from a tholeiitic basalt. Tectonic discrimination diagrams and spider diagrams suggest they evolved from a mid-ocean ridge basalt.

TABLE OF CONTENTS

LIST OF FIGURES

LIST OF TABLES

LIST OF PLATES

I. INTRODUCTION

The southern Appalachian Piedmont is characterized, in general, by low topography and poor exposure relative to the Blue Ridge. Consequently, little detailed geologic mapping has been completed in the Piedmont, leaving it one of the most poorly understood geologic provinces in the southern Appalachians. Parts of the western Inner Piedmont of North and South Carolina, however, locally contain Blue Ridge topography. Here, a number of authors (Griffin, 1967, 1969, 1971a, 1974; Hatcher, 1969, 1970, 1971a; Lemmon, 1973; Hatcher and Acker, 1984; Hopson and Hatcher, 1988; Yanagihara and others, 1992; Davis, 1993a) have conducted detailed geologic mapping of most of the Inner Piedmont from northeastern Georgia to southwestern North Carolina. This thesis involved detailed geologic mapping of a 200 km^2 area in the southern Appalachian Inner Piedmont in North Carolina (Fig. 1.1) with supporting petrographic, structural, and geochemical analysis. The goal of this study was to provide data and interpretations that would lead to a better understanding of the Inner Piedmont and the southern Appalachian orogen as a whole.

REGIONAL GEOLOGY

The southern Appalachian Piedmont is bounded to the west by the Blue Ridge geologic province (Fig. 1.1). The boundary between the two provinces is the Brevard fault zone, a multiply deformed fault zone whose last movement was dextral strike-slip (Reed and Bryant, 1964; Bobyarchick, 1984; Edelman and others, 1987; Vauchez, 1987; Vauchez and Brunel, 1988; Bobyarchick and others, 1988). The Piedmont can be further subdivided into several terranes and lithotectonic units (Fig. 1.1). To the east of the central Piedmont suture is the Carolina (Avalon) exotic terrane that are believed to have been emplaced before the Alleghanian orogeny (Williams and Hatcher, 1983; Hatcher, 1987).

Figure 1.1. Tectonic map showing major tectonostratigraphic units in the southern

Appalachians. The study area is located in the shaded rectangle southeast of

Asheville. Modified from Hatcher (1987).
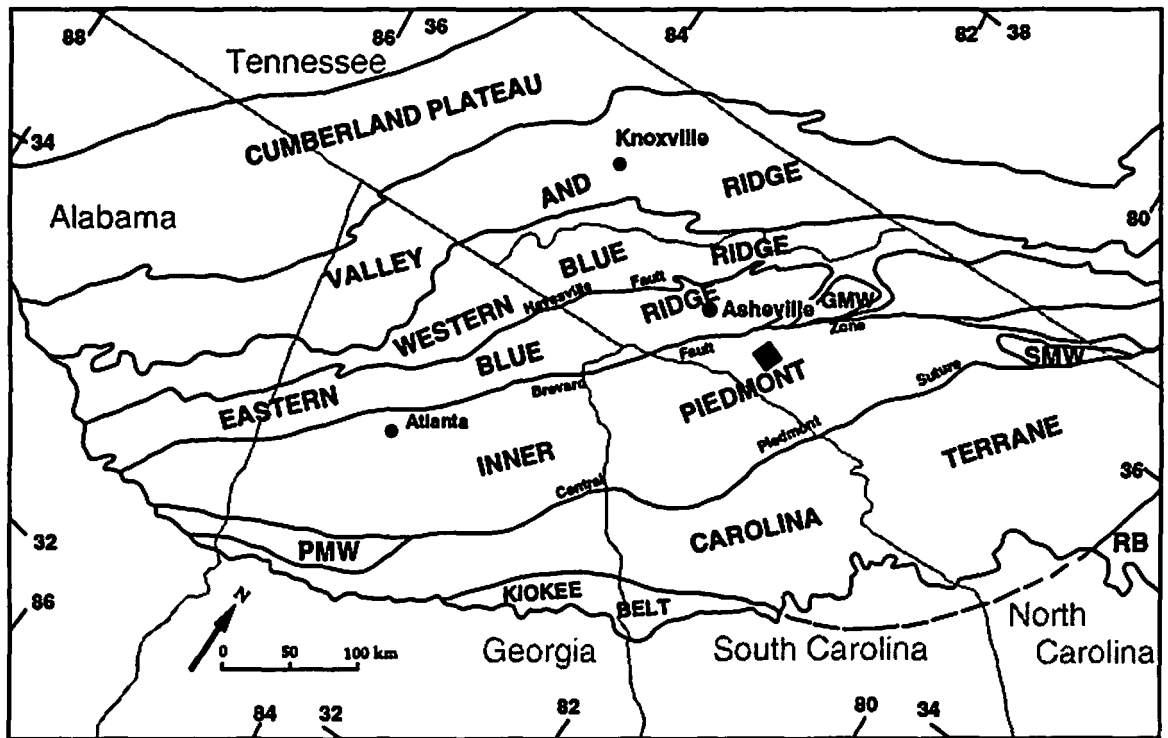
West of the central Piedmont suture is the Inner Piedmont, which includes areas covered by this study. In South Carolina, it has been subdivided into three lithotectonic units and includes from NW to SE in ascending structural order: (1) the Chauga belt (Hatcher, 1972, 1978), (2) the Walhalla nappe, and (3) the Six Mile nappe (Griffin, 1969, 1971a, 1974). Rocks of the Chauga belt include (1) the Chauga River Formation, (2) the Poor Mountain Formation and (3) the Henderson Gneiss (Hatcher, 1969). The Chauga River Formation is mainly confined to areas along the Brevard fault zone and is believed to be a facies equivalent of the Poor Mountain Formation (Hatcher, 1969, 1970). Hatcher (1972) originally defined the Chauga belt as the area of low-grade metamorphism (upper greenschist to lower amphibolite facies) which contrasted with middle to upper amphibolite facies conditions in the Walhalla and Six Mile nappes. In North Carolina, however, metamorphic conditions in the Chauga belt are upper amphibolite facies, identical to those of the Walhalla nappe (Davis and others, 1990a). Because part of the region between the areas mapped by Hatcher, Griffin, and Liu, and the Inner Piedmont in southwestern North Carolina, has not been mapped in detail, it is not clear how or where this change in metamorphic grade occurs.

The Walhalla nappe consists of migmatitic biotite gneiss, granitic gneiss, and amphibolite, while the Six Mile nappe contains migmatitic biotite gneiss, mica schist, granitic gneiss, and amphibolite (Griffin, 1967, 1969, 1971a, 1971b, 1974). The metamorphic grade of these two units remains middle to upper amphibolite facies throughout the Piedmont of northeastern Georgia, South Carolina, and southwestern North Carolina (Griffin, 1974; Hopson and Hatcher, 1988; Davis and Tabor, 1988; Davis and others, 1990a). Based on lithologic similarities, Hatcher (1972, 1978), Hopson and Hatcher (1988) and Davis (1993a) concluded that rocks of the Inner Piedmont are correlative with rocks of the Tallulah Falls Formation in the eastern Blue Ridge.

While it is clear that the western Inner Piedmont underwent one episode of upper greenschist to upper amphibolite facies metamorphism, possibly erasing any trace of previous metamorphism, there is also evidence for multiple episodes of deformation. The Brevard fault

zone records at least three episodes of movement, one associated with Taconic or Acadian nappe emplacement, the other two associated with early and late Alleghanian movement (Reed and Bryant, 1964; Hatcher, 1969, 1970, 1972, 1978, 1987; Edelman and others, 1987). Multiple episodes of deformation have also been documented in the Inner Piedmont by Griffin (1974), Hopson and Hatcher (1988), Davis and Tabor (1988), and Liu and others (1991).

The goals of this thesis include comparison of the stratigraphy and metamorphism of the area for comparison with areas already studied. In addition, the problems associated with the deformational history will be addressed and should lead to a better understanding of the tectonic history of the western Inner Piedmont.

PREVIOUS WORK

The earliest studies conducted in the Inner Piedmont included reconnaissance mapping and other studies focusing on resource potential by Keith (1905, 1907), Sloan (1908), and Conley and Drummond (1963, 1965, 1981). The earliest work focusing on deformation and metamorphism is Conley and Drummond (1965). In South Carolina, Griffin and Hatcher conducted extensive field studies in the Inner Piedmont that documented the stratigraphy, metamorphic history, and structure of the Chauga belt, Walhalla nappe, and Six Mile nappe (Griffin, 1967, 1969, 1974; Hatcher, 1969, 1970, 1971a, 1971b). The two differed on the tectonic development of the Inner Piedmont— Griffin (1971b) supported a regional "stockwork" model for the development of the entire Piedmont geologic province based on Wegman's (1935) models, and did not recognize any stratigraphic order, whereas Hatcher (1972, 1978, 1989) and Hopson and Hatcher (1988) recognized a stratigraphic order and favored a more complex deformational history arguing that a stockwork model assumed a single episode of deformation. With more mapping completed by the early 1970's, a clearer tectonic picture of the Inner Piedmont and the Appalachian orogen emerged favoring a more complex, polydeformational history (Hatcher,

1970, 1978). Regional compilations based, in part, on studies conducted in the Inner Piedmont include Hatcher (1972, 1978, 1987) and Hatcher and others (1987). Hatcher (1987) proposed that rocks of the Piedmont formed on the late Precambrian continental slope, rise, and ocean floor immediately adjacent to the North American craton. They were later obducted onto the craton during the Taconic orogeny and metamorphosed during both the Taconic and Acadian orogeny.

A fundamental question facing those studying southern Appalachian tectonics concerns the Brevard fault zone. It has been interpreted as a continent-continent suture (Dewey and Kidd, 1974; Rankin, 1975), an arc-continent suture (Odom and Fullagar, 1973), a dextral strike-slip fault (Reed and Bryant, 1964; Bobyarchick, 1984; Bobyarchick and others, 1988), a sinistral strike-slip fault with a thrust component (Reed and others, 1970), and a multiply reactivated fault that includes dextral as well as thrust movement (Edelman and others, 1987). The Appalachian Ultradeep Core Hole (ADCOH) Project sought to resolve part of the Brevard question targeting it as an intermediate-depth drilling objective (Liu, 1991). In association with ADCOH, a Bouguer anomaly map, a compiled aeromagnetic anomaly map, and a high- resolution seismic-reflection profile were produced that gave a clearer picture of Blue Ridge and Piedmont structure at depth (Fabbri, 1986; Coruh and others, 1987; Hatcher and others, 1987; Favret and Williams, 1988). Davis (1993a), using some of the results from ADCOH and geochemical studies and field work, proposed that the Brevard fault zone sutured a back-arc basin and an ancient arc-system to the North American craton. The basin was probably in its intitial stages of development before spreading stopped and accretion began.

Other works that specifically dealt with the western Inner Piedmont include Roper and Dunn (1973), Hopson and Hatcher (1988) in northeast Georgia and South Carolina, Liu (1991), and Hatcher and Acker (1984) in South Carolina. In North Carolina, Lemmon (1973) and Lemmon and Dunn (1973a, 1973b) completed geologic mapping of two quadrangles a few miles west of the present study area and documented a WNW-directed thrust sheet. Based on radiometric-age dating of plutons, Lemmon (1973) concluded the timing of thrusting was

Acadian. Lemmon's work provided some of the basic framework from which this project was begun. Studies associated with the present study began in 1987 and have continued to the present with theses by Davis (1993a) and the present work.

Extensive radiometric-age dating has been conducted throughout the Chauga belt and Inner Piedmont. In general, age dating focused on crystallization ages of granitoids and granitic gneisses as well as timing of peak metamorphism. Age dates of granitic gneisses show progressively younger crystallization ages eastward (Harper and Fullagar, 1981; Sinha and others, 1989). Dallmeyer (1988) used $^{40}Ar/^{39}Ar$ data to suggest a Late Devonian (Acadian) age for metamorphism.

STUDY AREA

The study area is located in Rutherford, McDowell, and Buncombe counties about 25 mi (40 km) ESE of Asheville and 150 mi (250 km) ESE of Knoxville. It covers an area of roughly 70 mi^2 (180 km^2; Fig. 1.2). Detailed geologic mapping was conducted at a scale of 1:24,000 in the Lake Lure, Shingle Hollow, Sugar Hill, and Moffitt Hill 7.5 minute quadrangles ENE of areas mapped by Davis, Tabor, and Lemmon. Chris Jayne (unpublished) also began mapping approximately 3 mi^2 (8 km^2) in an area located south of the study area.

Geologic mapping was conducted over a period of 7 months in summer, 1991, and winter-spring, 1992. The study area is located mostly in a sparsely populated agricultural and resort area with relief that ranges from 800 (245 m) to 3500 ft (1065m) above sea level. The western half of the field area is characterized by moderate relief dominated by Hickorynut Mountain and Young's Mountain exposing cliffs of Henderson Gneiss. These cliffs are especially spectacular in Hickorynut Gorge (Plate III), just west of the study area, and this area was the filming site for the movies *Last of the Mohicans* and *Dirty Dancing*. Farther east are isolated clusters of mountains and hills that also yield excellent exposures and unlimited control. Between these mountains, the

Figure 1.2. Map showing the location of the study area (shaded rectangle) and areas mapped

by T. L. Davis, J. R. Tabor, and R. E. Lemmon in North Carolina, and by V. S. Griffin,

R. D. Hatcher, Jr., and J. L. Hopson in South Carolina and Georgia.

TENNESSEE

Buncombe
County

McDowell
County

Asheville

NORTH CAROLINA

Rutherford
County

Brevard fault zone

Lemmon (unpublished); Davis and
Tabor (1987-1991)

GEORGIA

Hatcher and Griffin
(1969);
Liu (1991)

SOUTH CAROLINA

Hopson and Hatcher (1988)
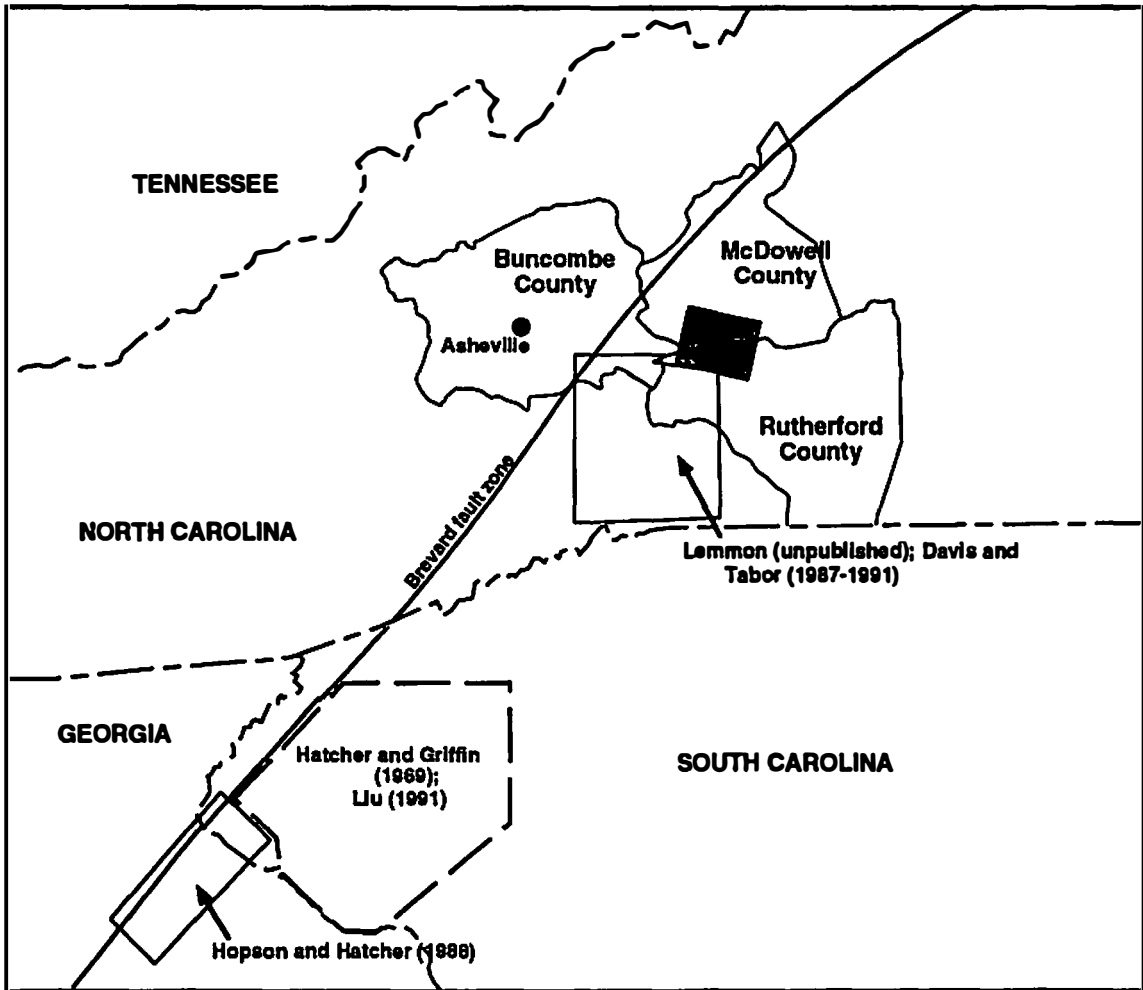
relief is low providing more limited exposure, particularly within the areas of active or recent farming. The geology controls the landforms in a number of ways. Within 10 miles (16 km) of the Brevard fault zone, the ridgecrests parallel the fault zone itself and the regional strike of the foliation (Plate III). The rock unit in which the parallelism occurs is mostly Henderson Gneiss and it appears that the foliation, which dips gently to the southeast, controls ridge erosion. The northwestern slopes of the ridges are steep and are nearly perpendicular to the foliation whereas the southeast slopes are gently dipping and are roughly parallel to the foliation so that they consist of hogbacks (Plate I). Exfoliation, most prominent in the Henderson Gneiss, is controlled by the foliation on the southeast slopes while it appears to be influenced little by foliation on the northwest slopes. Many of the stream paths, particularly in the granitic gneisses, are controlled by fracture orientations. This geometry is best observed in Hickorynut Gorge and Chimney Rock Park, west of the study area (Plate III). The trend of the canyon and the orientation of the canyon walls and cliffs parallel a system of WNW-stiking subvertical fractures (Clark, 1993).

OBJECTIVES OF THIS STUDY

The primary objectives of this study are as follows:

(1) To produce a detailed geologic map of the study area and to construct high quality cross sections.

(2) To describe the stratigraphic relationships in the study area including detailed descriptions of the lithology and internal stratigraphy in each of the lithotectonic unit recognized.

(3) To provide detailed descriptions of the structure at the regional, mesoscopic, and microscopic scales. In addition, variations in direction of transport, deformation mechanisms, and postmetamorphic deformation through the use of structural analysis will be described.

(4) To describe the metamorphic assemblages as well as P-T relations during peak thermal metamorphism. The relative timing between metamorphism and deformation will also be addressed.

(5) To present a few of the possible protolith assemblages and the nature of metamorphism for various amphibolites collected in the study area.

(6) To compare stratigraphic, structural, and metamorphic relationships observed within the study area with such relationships in the Inner Piedmont of South Carolina and northeastern Georgia.

METHODS USED IN THIS STUDY

Detailed geologic mapping was conducted at the 1:24,000 level in 1991-92 using USGS base maps. The objectives of the field work included locating all mappable lithologic contacts, measurement of orientation of foliations, lineations, fold axial planes, and fold axes, as well as observation of shear-sense indicators, fold vergence, and any other relevant features. Measurements made at about 1700 stations were made using a Brunton compass over a period of 6 months. Final map compilation and cross-section construction were completed in fall, 1992.

Some 50 oriented and nonoriented rock samples were collected, cut to make thin sections, and detailed petrographic descriptions were compiled with special attention given to mineral

assemblages, microtextural relationships, and shear-sense indicators. 20 representative thin sections were point counted (at least 1,000 points were counted on each) and assessed for error to give a more accurate account of the modal compositions of all major lithologic units. Structural analysis included observation of shear-sense indicators in the field and in thin section, stereonet analysis of the foliations and lineations, and Hansen analysis of fold axes (Hansen, 1971).

The bulk-rock chemistry of 23 amphibolite samples from the Poor Mountain Formation and Mill Spring formation, 4 granitic gneiss samples from the Poor Mountain Formation, and 1 granitic gneiss sample from the Henderson Gneiss were obtained using X-ray flourescence techniques. The data were collected using an energy dispersive EG&G ORTEC X-ray flourescence spectrometer. The volcanic protoliths for the amphibolites were obtained by compiling trace element chemistry data and plotting them on tectonic discrimination diagrams (Pearce and Cann, 1973).

II. STRATIGRAPHY AND LITHOLOGY

Because rocks in the study area experienced high grade metamorphism (upper-amphibolite facies) and intense deformation, textures from the original protolith have been completely erased in most areas. Although many of the rocks are layered, most textures observed in the Inner Piedmont are interpreted to result from metamorphic differentiation, partial melting, and ductile deformation. Therefore, most inferences about the protolith must be made on the basis of mineral and chemical composition alone. The stratigraphy of the Inner Piedmont is characterized by a wide variety of lithologies revealing a complex tectonic history that may never be fully resolved. Modal compositions of these lithologies were obtained using point counting and plagioclase compositions were determined using the Michel-Levy method.

STRATIGRAPHIC FRAMEWORK

The earliest workers in the Columbus Promontory focused most of their studies on the Henderson Gneiss (Keith, 1905, 1907; Sloan, 1908; Stuckey and Conrad, 1958; Reed and Bryant, 1964; Conley and Drummond, 1965; Bryant and Reed, 1970; Hadley and Nelson, 1971). Subsequent studies on the adjacent stratigraphy include Lemmon (1973, 1982) and Lemmon and Dunn (1975). More recent works include those of Davis and Tabor (1988), Davis and others (1989, 1990a, 1990b, 1991a, 1991b, 1992), Tabor and others (1990), Yanagihara and others (1992), Yanagihara and Davis (1992), and Davis (1993a).

Odom and Fullagar (1973) determined the age of the Henderson Gneiss to be 535 Ma using Rb-Sr. This was later revised to 509 Ma by Sinha and others (1989). Lemmon (1973) recognized a younger intrusion of granitoid gneiss within the Henderson Gneiss. Odom and Russell (1975) dated this intrusion within the Henderson Gneiss at 438±22 Ma using Rb-Sr. Lemmon (1973) also subdivided adjacent Inner Piedmont rocks into three units collectively called the Sugarloaf

Mountain group. He recognized a similarity between rocks of the Sugarloaf Mountain group with the Poor Mountain Formation in South Carolina but failed to correlate the two. Davis (1993a) and Yanagihara and others (1992) have subsequently referred to these rocks as correlatives of the Poor Mountain Formation.

Farther east, a sequence of biotite gneiss, granitoid gneiss, amphibolite, and amphibolite gneiss was named the Mill Spring group by Conley and Drummond (unpublished, 1975). Davis (1993a) subdivided the Mill Spring complex into amphibole-rich and amphibolite-poor units, termed the lower and upper Mill Spring complexes, respectively. Davis (1993a) also speculated that the Mill Spring group is correlative with the Tallulah Falls Formation in the eastern Blue Ridge. These lithologies are also similar to those observed in the Inner Piedmont of northwestern South Carolina (Griffin, 1969, 1971a, 1971b, 1974; Hatcher and Acker, 1984; Liu, 1991) and northeastern Georgia (Hopson, 1984; Hopson and Hatcher, 1988). Griffin (1967, 1969) recognized a series of southeast-dipping ductile thrust sheets southeast of the Chauga belt and named them, from NW to SE, the Walhalla nappe and the Six Mile nappe. The rocks in these two nappes are similar to those of the Mill Spring complex (Davis, 1993a).

LITHOLOGIES IN THE STUDY AREA

The study area is composed of three major tectonic units and lithologies will be discussed by tectonic unit (Fig. 2.1 and 2.2). These thrust sheets are stacked in ascending structural order from NW to SE. While the structural thicknesses of the stratigraphic units can be easily calculated, true stratigraphic thickness is impossible to determine due to extensive recumbent folding and internal deformation. Unit 1, the northwesternmost, structurally lowest lithotectonic unit, is composed almost entirely of Henderson Gneiss within the study area. The lower contact lies outside the field area and its thickness is unknown (the structural thickness within the study area is 3000 m). Unit 2, lying above unit 1, is composed of a basal unit of biotite-granitoid gneiss

Figure 2.1. Generalized tectonostratigraphic column showing relationships between various lithologic units in the study area. Dashed lines represent lithologic contacts and solid lines represent thrust faults.

Biotite gneiss, granitoid gneiss,
amphibolite, and pelitic schist

— — — — — — — — — — — — — —

Upper Mill Spring complex
(biotite gneiss and biotite-
muscovite schist)

THRUST FAULT ——————▶

Unit 3

Poor Mountain
Quartzite (Poor Mountain
Formation)

— — — — — — — — — — — — — —

Poor Mountain
Amphibolite (Poor Mountain
Formation)

— — — — — — — — — — — — — —

Biotite gneiss (upper Mill Spring complex)
and granitoid gneiss

THRUST FAULT ——————▶

Unit 2

Biotite-rich Henderson Gneiss

Henderson
Gneiss

— — — — — — — — — — — — — —

Fine-grained
Henderson Gneiss

HRUST FAULT ——————▶

Poor Mountain
Formation (not exposed)

Unit 1

17

Figure 2.2. Simplified geologic map of the study area showing spatial relationships of the major lithologic units. In general, these units strike NE and dip gently to the SE.

ROCK UNITS

N

KILOMETERS

0   1   2   3
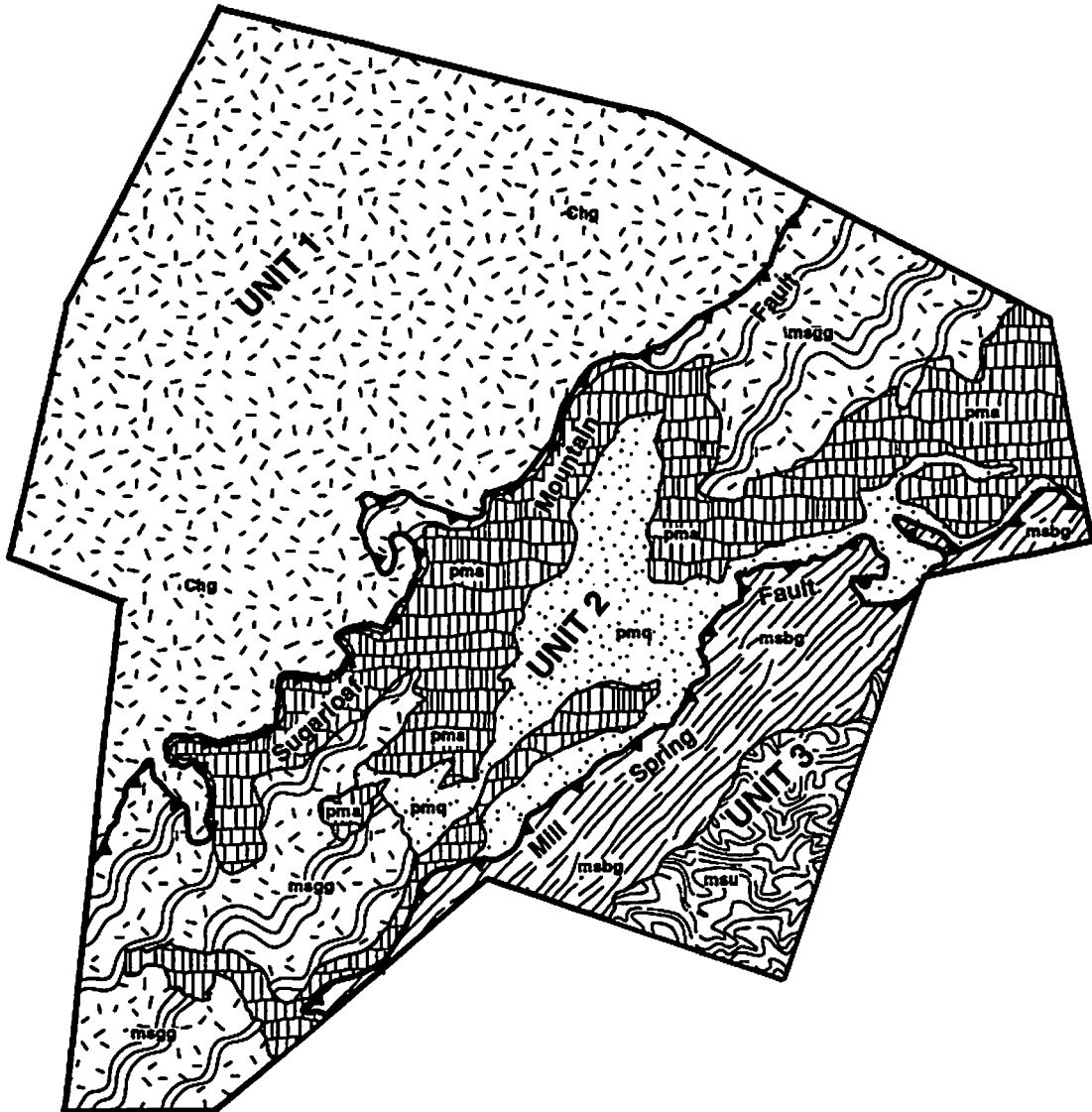
Unit 3, upper unit	
Unit 3, lower unit	
Unit 2, Poor Mtn. quartzite	
Unit 2, Poor Mtn. amphibolite	
Unit 2, granitic gneiss	
Unit 1, Henderson gneiss	

and quartz-rich schist, correlative with the upper Mill Spring complex of Davis (1993a). Above this unit, in stratigraphic contact with the upper Mill Spring complex, are rocks of the Poor Mountain Formation. The structural thickness of unit 2 varies from 1000 m in the south to 1800 m in the north. Unit 3, the structurally highest unit in the study area, contains a basal unit of migmatitic biotite gneiss (upper Mill Spring complex) and an upper undifferentiated unit of biotite gneiss, biotite-muscovite schist, amphibolite, and granitoid gneiss with minor pelitic schist and quartzite. Because the upper contact of unit 3 lies outside of the study area, the true thickness is unknown (structural thickness within the study area is 1200 m).

Overall, the stratigraphic units were very distinct, making delineation of contacts easy. A few exceptions do occur, such as the contact between Henderson Gneiss in unit 1 and granitoid gneiss in unit 2. Both have similar compositions and textures in hand sample. Beyond that, the accuracy of the placement of contacts in the field was limited only by the amount of exposure.

UNIT 1

Unit 1 is composed almost entirely of Henderson Gneiss, a granitic orthogneiss. The Henderson Gneiss was first described by Keith (1905, 1907) as the Henderson Granite. Reed and Bryant (1964) redefined it as the Henderson Gneiss whose protolith is interpreted to be granite or rhyolite that was subsequently metamorphosed. Its contact with the structurally lower Poor Mountain and Chauga River Formations was originally thought to be stratigraphic (Cazeau, 1967; Hatcher, 1969), but is now believed to be a fault (Hatcher and Acker, 1984; Edelman and others, 1987; Liu, 1991; Davis, 1993a). Regionally, the Henderson Gneiss extends from the Georgia-South Carolina border through northwestern South Carolina to central-western North Carolina, immeidately southeast of the Grandfather Mountain window (Bryant and Reed, 1970).

Most gneiss in unit 1 is characterized by a coarse-grained mylonitic augen texture with porphyroblasts of K-feldspar and plagioclase and bands of schist composed mostly of biotite and

muscovite (Fig. 2.3). There are also isolated, widely scattered pods of Poor Mountain amphibolite. It is not clear if the contact between the Henderson Gneiss and the Poor Mountain Amphibolite in these pods is a fault, as observed by Davis (1993a) or a lithologic contact, as observed by Hatcher and Acker (1984). Based on the absence of truncated layering observed in the Tumblebug Creek fault (Davis, 1993a), and Stumphouse Mountain thrust (Liu, 1991), I believe the contact is lithologic. A single sample of ultramafic rock that was retrograded to chlorite and clinozoisite was also found within the Henderson Gneiss. The sample was found as float and thus its relationship with the Henderson Gneiss is unknown.

In the NW, at the lowest known part of the unit, the rocks are fine-grained, with well developed foliation but poorly developed gneissic banding and an absence of feldspar augen that are distinctive of the Henderson Gneiss (Fig. 2.4). This texture is similar to the fine-grained quartzofeldspathic gneiss near the base of the Henderson Gneiss in South Carolina (Hatcher, 1970). In unit 1, however, the compositions of these gneisses, determined by point counting, are roughly the same as the coarse-grained rocks. It is not clear why rocks towards the NW are relatively fine-grained. It may be due to increased shearing in the vicinity of the Brevard fault zone that has led to grain-size reduction.

Fine-grained textures dominate the lower 500 m of unit 1, but higher up they quickly give way to the coarse-grained textures that dominate most of the upper part of the unit. The transition between the two textures is characterized by alternating bands of coarse-grained gneiss and fine-grained gneiss, similar to that in South Carolina (Hatcher, 1970). The coarse-grained augen texture is dominant for the rest of the unit. In the top 50 m of the unit, however, grain size decreases and while the augen remain large, they are very flattened. The composition remains fundamentally the same and both factors are probably related to increased shearing in the proximity of the Sugarloaf Mountain fault that separates unit 1 from unit 2.

About 100 to 200 m below the top of unit 1 are thin, discontinuous lenses of gneiss that are texturally and compositionally different from "regular", coarse-grained Henderson Gneiss. These

Figure 2.3. Two common forms of Henderson Gneiss. (A) Augen textures that dominate most of

unit 1. The length of the photograph is approximately 25 cm and was taken on

Hickorynut Mountain, Moffitt Hill quadrangle. (B) Feldspar-rich layers alternating

with mica-rich layers at Chimney Rock Park, Bat Cave quadrangle. Many of these

layers are granitic dikes that intruded the Henderson Gneiss during M_2

metamorphism. Note the man's head for scale at the bottom-left corner of the

photograph. Length of field is approximately $2^1/2$ m.

Figure 2.4. Photomicrographs of Henderson Gneiss taken in cross-polarized light. (A) Coarse-

grained lithology typical of most of the Henderson Gneiss. Photograph includes

biotite, quartz, plagioclase, and sphene (upper left corner). Sample was collected at

Buffalo Creek, Lake Lure quadrangle. (B) Fine-grained lithology typical of the lower

parts of the Henderson Gneiss. Sample was collected at Sally Gap, south of

Davistown, Moffitt Hill quadrangle. Width of both photographs is approximately 2

mm.
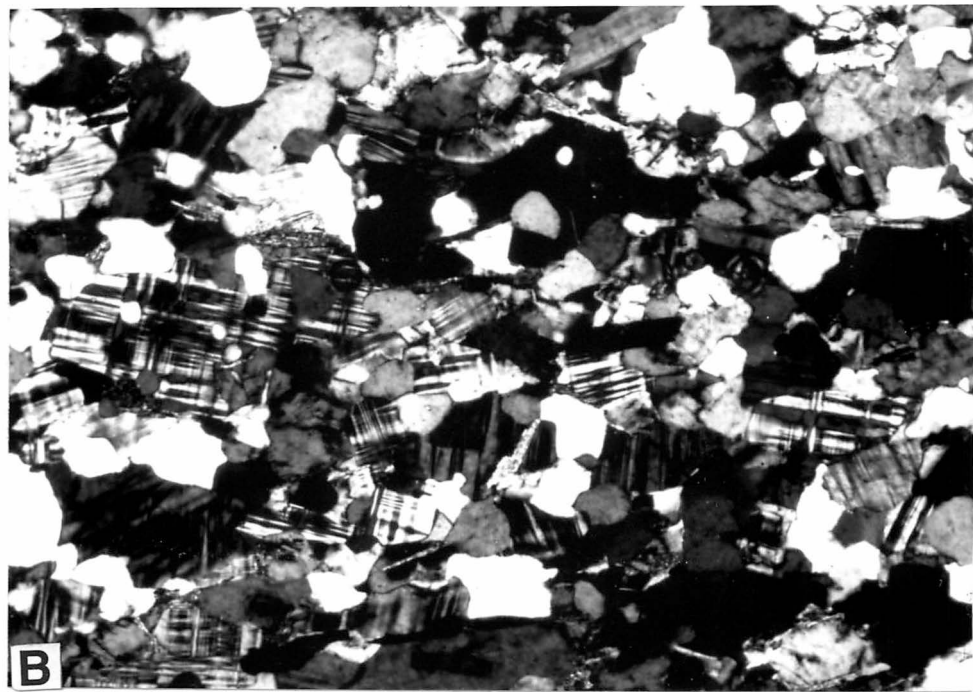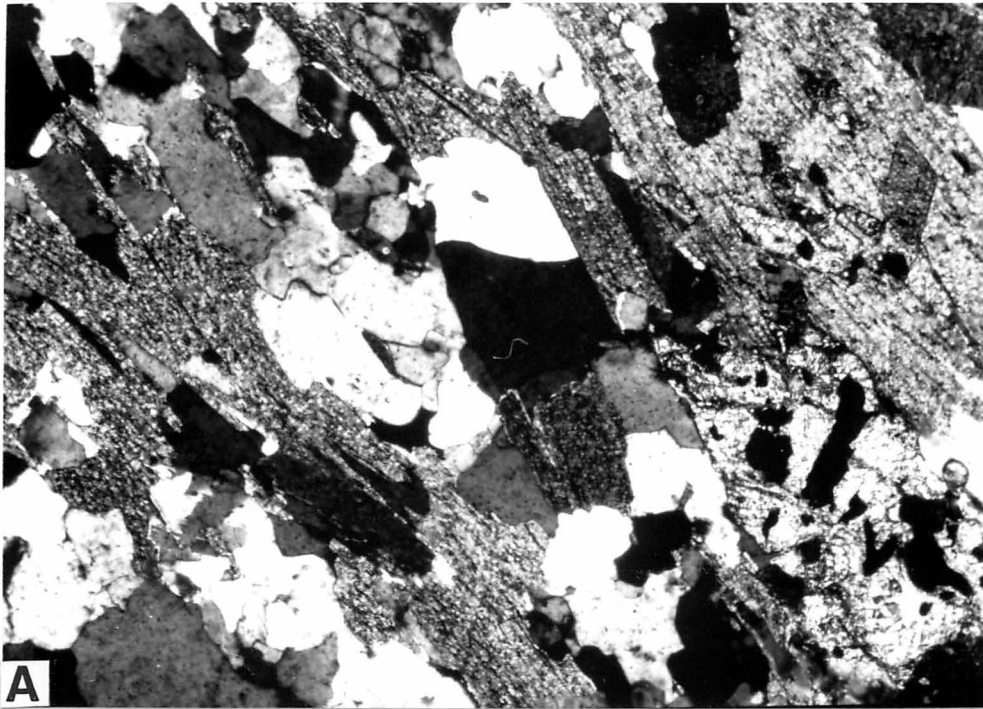
lenses contain larger amounts of biotite and smaller amounts of feldspar and quartz. The felsic parts of the lenses also contain increased amounts of plagioclase and decreased amounts of microcline (Table 2.1, sample LL 359). The augen in the bodies are considerably larger (up to 5 cm long) and, have a well-defined sigma shape yielding good shear-sense. In addition, the gneisses are very coarse-grained and tend to have a migmatitic texture. The bodies measure about 50 to 100 m thick, up to 3000 m long and are widely scattered (3 were mapped in the study area— Plate I). Associated with these rocks is fine-grained biotite schist, and fine-grained quartzofeldspathic gneiss similar to those seen in areas to the northwest.

The Henderson Gneiss is distinctive petrographically in that the biotite has a dark greenish-brown color, it has large (up to 2 mm) crystals of sphene and epidote, and the plagioclase is myrmekitic. No other granitoid gneiss in the study area has this combination of features. Individual porphyroblasts are composed exclusively of either plagioclase or microcline, are optically continuous, and measure up to 2 cm long. Quartz is rare within the porphyroblasts but tends to form pressure shadows on the ends. Schist layers between the porphyroblasts are composed mostly of biotite and muscovite grains up to 8 mm long along with significant amounts of relatively fine-grained quartz, plagioclase (An_{15-20}), and microcline that rarely exceed 3 mm in length. Sphene, although rare, forms large, embayed crystals up to 5 mm long. In addition, there are trace amounts of epidote, chlorite, and opaque minerals (Table 2.1).

UNIT 2

Unit 2 in the study area is composed of rocks of the Poor Mountain Formation and the upper Mill Spring complex and is correlative with the Sugarloaf Mountain thrust sheet of Lemmon (1973) and Davis (1993a). Yanagihara and others (1992) speculated that the contact between the Poor Mountain Formation and the upper Mill Spring complex is an early, premetamorphic fault, but the absence of fault-related textures, such as truncation of

Table 2.1: Mineral compositions determined by point counting in the study area. Errors are shown below each mineral were calculated using the graph of Van der Plas and Tobi (1965). Those phases that don't have errors indicated have errors that are substantially less than 1%.

Sample	Qtz (1-2.5%)	Plag (2-3%)	Kspar (2-3%)	Biot (1-3%)	Musc (1-3%)	Chl	Epl (1-2.5%)	Clz (2%)	Hbl (2.5-3%)	Gar	Sph	Zir	Opq	Points counted
Unit 1														
Mo 158 (hg)	25.0	36.8	24.4	7.6	5.2	0.4	—	—		—	0.6	—	—	1004
LL 2 (hg)	27.4	35.2	22.8	13.8	0.2	—	—	—	—	—	0.2	—	0.4	1573
LL 359 (hg)	22.6	57.1	2.1	14.6	2.2	1.3	—	—	—	—	0.1	—	—	1064
LL 227 (hg)	24.0	44.1	22.7	7.4	1.2	—	0.4	—	—	—	0.1	—	0.1	1074
Unit 2									—					
LL 271 (sch)	24.9	38.3	1.4	29.3	5.6	0.2	—	—	—	—	0.1	—	0.2	1078
LL 591 (gr)	37.5	33.2	21.5	1.9	5.9	—	—	—	—	—	—	—	—	1959
LL 563a (gr)	27.8	32.2	37.8	1.2	0.5	1.1	0.1	—	—	0.3	—	—	0.1	1304
LL 563b (gr)	33.5	31.8	27.6	6.5	0.6	—	—	—	—	—	—	—	—	1434
Su 54 (bg)	37.3	28.9	0.1	17.9	15.8	—	—	—	—	—	—	—	—	1073
Su 148 (amp)	3.2	15.0	—	31.8	—	—	—	2.1	46.0	—	1.6	0.3	—	1083
Su 112 (amp)	—	—	—	—	—	—	—	—	98.5	—	—	—	1.5	1024
LL 526 (amp)	1.0	11.2	—	—	—	0.1	22.4	13.0	47.0	—	2.9	0.9	1.5	1344
ShH 20 (amp)	4.2	40.2	—	0.2	tr	—	6.0	8.2	37.6	tr	1.3	—	2.3	1043
Su 410 (qzt)	48.8	18.6	3.6	1.5	25.0	—	—	—	—	1.9	—	—	0.1	2484
ShH 40 (qzt)	46.6	22.8	—	10.9	6.0	—	—	—	—	—	—	—	10.1	1044
ShH 1 (qzt)	38.2	18.5	—	15.3	27.6	0.4	—	—	—	—	—	—	—	1038
LL 448 (qzt)	57.3	29.0	—	3.6	6.9	—	0.9	—	—	—	—	—	1.6	1042
Unit 3														
LL 587 (sch)	46.2	0.7	—	5.6±1	42.4	0.2	—	—	—	—	—	—	5.0	1220
Su 100 (bg)	47.5	23.5	—	10.1	20.9	—	—	—	—	tr	—	—	—	1044
Sh 207 (bg)	39.8	16.0	—	30.5	12.3	—	—	—	—	1.2	—	—	0.2	1549
Su 150 (amp)	—	0.5	—	—	0.1	0.3	14.0	12.0	73.0	—	—	—	0.1	1018
Sh 272 (amp)	17.7	39.0	—	—	—	—	0.2	—	43.1	—	—	—	—	1250

ABBREVIATIONS: Hg = Henderson Gneiss, sch = schist, gr = granitic gneiss, bg = biotite gneiss, amp = amphibolite, qzt = quartzite, Qtz = quartz, Plag = plagioclase, Kspar = alkali feldspar, Biot = biotite, Musc = muscovite, Chl = chlorite, Epl = epidote, Clz = clinozoisite, Hbl = hornblende, Gar = garnet, Sph = sphene, Zlr =zircon, Opq = opaque minerals.

compositional layering and reduced grain size in the vicinity of the contact observed by Davis (1993a) in early faults to the SW, and the observation that Mill Spring gneisses interfinger with the amphibolites above make such an interpretation less likely. Unlike areas mapped by Davis and Tabor (Davis, 1993a), the upper Mill Spring complex in the study area also contains considerable amounts of granitoid gneiss.

Upper Mill Spring Complex. The structurally lowest lithology in unit 2 is composed mostly of complexly interlayered granitoid gneiss and biotite gneiss with widely distributed interlayers of Poor Mountain Amphibolite, metagraywacke, and metasiltstone. The relationship between biotite gneiss and granitoid gneiss is complex and the contact between the two units is typically gradational (Fig. 2.5). Some granitoid gneiss in the study area is similar in mineralogy and texture to the Sugarloaf gneiss in the Bat Cave quadrangle, but it lies below the Poor Mountain Formation, whereas the Sugarloaf gneiss overlies the Poor Mountain Formation to the south (Lemmon, 1973; Davis, 1993a).

The upper Mill Spring complex in unit 2 varies in structural thickness from at least 150 m in the southern part of the study area to less than 10 m farther north to 1100 m in the far north. Thickening and thinning may be attributed not only to changes in original stratigraphic thicknesses but also to map-scale recumbent isoclinal folding. Biotite gneiss and granitoid gneiss are distinguished in the field on basis of mica content— biotite gneiss typically contains more than 30% mica, whereas granitoid gneiss contains less than 10% mica but transitional lithologies are common. When the mica content is somewhere between 10% and 30%, the gneiss is sometimes difficult to distinguish from Henderson Gneiss because they may have similar mineral assemblages and textures. Because they are nearly identical mineralogically, they must be distinguished on the basis of texture and structural (stratigraphic?) relationships. The Henderson Gneiss commonly has numerous, large augen (up to 2 cm long) that give good sense of shear whereas granitoid gneiss is usually banded and is sometimes migmatitic. It is when the granitoid

Figure 2.5. Lithologies in the upper Mill Spring complex. (A) Interlayered coarse-grained granitoid gneiss (light-colored rock) and fine-grained biotite gneiss (metagraywacke) on the south slope of Youngs Mountain, Lake Lure quadrangle. Such relationships are common in the upper Mill Spring complex in the study area making delineation of the two lithologies at the map-scale difficult. Width of the photograph is approximately 75 cm. (B) Photomicrograph of granitoid gneiss taken in cross-polarized light showing microcline, plagioclase, quartz, and garnet (extinct mineral in the upper-left center). The sample was collected in the Bills Creek Community near Bills Creek, Lake Lure quadrangle. Width of the photograph is approximately 2 mm.

gneiss contains augen textures that it becomes difficult to distinguish from the Henderson Gneiss. While augen are pervasive throughout much of the upper Henderson Gneiss, their extent in upper Mill Spring gneiss is more limited. In the upper Mill Spring complex, augen-rich bands are usually less than 10 m thick and are typically interlayered with migmatitic gneiss. Furthermore, granitoid gneiss is sometimes interlayered with Poor Mountain Amphibolite. If the granitoid gneiss was interpreted to be Henderson Gneiss, this would imply the Sugarloaf Mountain fault, separating the Poor Mountain Amphibolite and upper Mill Spring complex from the Henderson Gneiss, was isoclinally folded during D_2 deformation. Because the Sugarloaf Mountain fault is a D_2 fault, it has never been observed to be folded except by gentle to open F_4 folding in the study area or in areas mapped by Lemmon (1973) and Davis (1993a), this interpretation is highly unlikely. Poor Mountain Amphibolite has been mapped in fault contact with Henderson Gneiss by Davis (1993a) in the Columbus Promontory. This fault, however, is premetamorphic and juxtaposes Henderson Gneiss onto Poor Mountain Amphibolite.

Granitoid gneiss is characterized by the mineral assemblage plagioclase (An_{12-20}), quartz, microcline, biotite, muscovite, and minor amounts of garnet, epidote, sphene, opaque phases, and allanite (Fig. 2.5b and Table 2.1). In many areas, particularly west of Youngs Mountain (Plate I), biotite and muscovite are present only in trace amounts leaving only plagioclase, microcline, and quartz as the most common minerals. The biotite gneiss is identical in major mineral assemblage to granitoid gneiss but contains larger amounts of biotite and muscovite and less feldspar. It also contains opaque minerals and rare garnet. The granitoid gneiss is generally coarse-grained and its relationship to the biotite gneiss is gradational. As biotite content increases, the gneiss is sometimes interlayered with fine-grained gneiss that is identical in composition to the coarse-grained gneiss. Allanite, a common accessory mineral in igneous rocks but not in metamorphic rocks, is present in the granitoid gneiss. Allanite is compositionally zoned and has an incomplete rim of epidote, possibly a product of retrograde metamorphism. Schist in the Mill Spring complex contains a high quartz and feldspar content with biotite and muscovite forming mica

fish and is interpreted to be equivalent to Hatcher's (1970) Brevard-Poor Mountain transitional unit (Table 2.1— LL 271). XRF analysis was conducted on granitoid gneiss and the results indicate they have a granitic composition.

Based on modal compositions, biotite gneiss is interpreted to have originated as a graywacke or an arkose (Fig. 2.6). The protolith for granitoid gneiss is not clear but its composition, determined by point counting, is similar to the Sugarloaf gneiss in areas mapped by Lemmon (1973) and Davis (1993a). Lemmon (1973), based on Rb-Sr isotopic data and zircon shapes, speculated that the Sugarloaf gneiss represents a recycled sedimentary rock but could not definitively rule out an igneous protolith. Davis (1993a) noted that a group of granitoid gneiss bodies in the Chauga belt of South Carolina has a Rb-Sr age of 423 Ma and maintains a similar structural (stratigraphic?) position as the Sugarloaf Gneiss above the Poor Mountain Formation. Granitoid gneiss in the study area, however, lies below the Poor Mountain Formation, but the presence of allanite, interpreted to be a relict mineral, suggests that the gneiss is derived from a granite or a sediment shed from a granite.

Poor Mountain Formation. The Poor Mountain Formation was first described by Sloan (1908) and later by Shufflebarger (1961) as the Poor Mountain sequence in South Carolina. It was subsequently redesignated as a formation by Hatcher (1969, 1970). In South Carolina, it consists of fine-grained amphibolite, fine-grained feldspathic quartzite, metasiltstone, phyllite, marble, pelitic schist, and metagraywacke (Sloan, 1908; Shufflebarger, 1961; Hatcher, 1969, 1970). Shufflebarger (1961) and Hatcher (1970, 1972) speculated that the Poor Mountain Formation is correlative with the Chauga River Formation farther to the northwest (Fig. 2.7), and that these rocks are preserved in a map-scale synform cored by Henderson Gneiss. In the Columbus Promontory, the Poor Mountain Formation is dominated by fine-grained amphibolite and fine-grained feldspathic quartzite with minor amounts of metagraywacke, metasiltstone, and pelitic schist (Yanagihara and Davis, 1992; Davis, 1993a). Davis (1993a) also described a basal unit of

Figure 2.6. Ternary QFM diagram plotted with rocks interpreted to be metasediments. In the diagram, Q=quartz, F=feldspar, M=mica. Subdivision of the diagram is from Pettijohn (1954).

EXPLANATION

○ Unit 2: Mill Spring gneiss

● Unit 2: Poor Mountain quartzite

■ Unit 3: biotite gneiss and
    pelitic schist
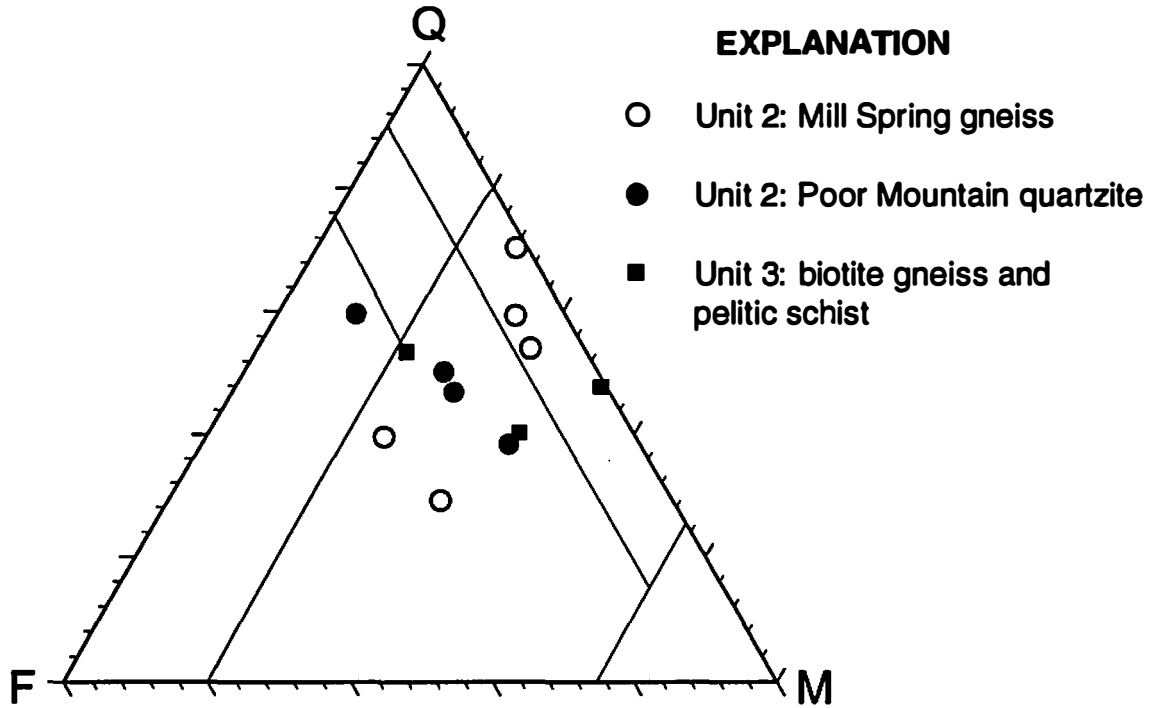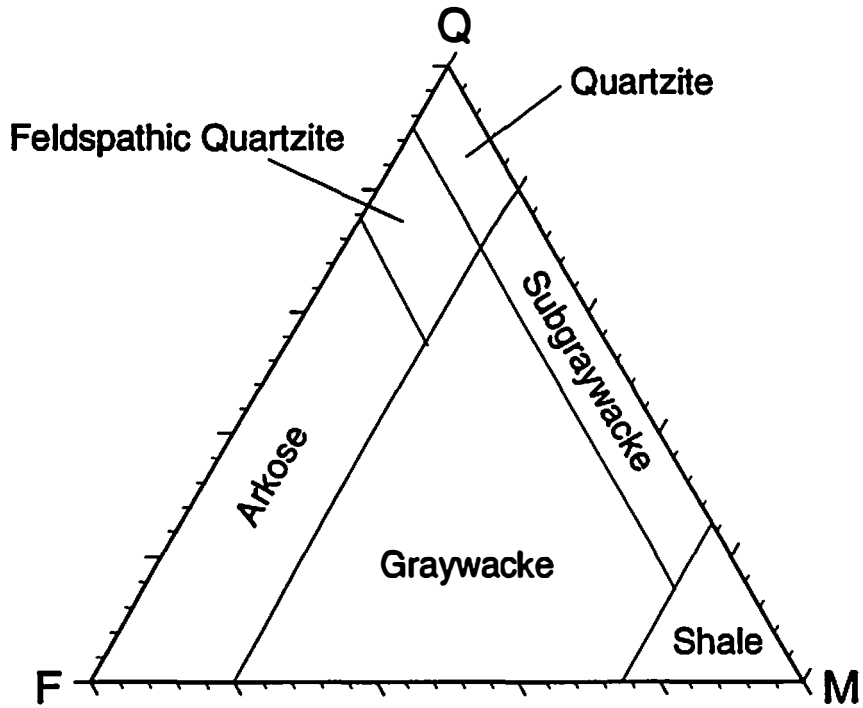
Figure 2.7. Possible facies relationships between the Chauga River and the Poor Mountain

Formations in South Carolina. From Hatcher (1970).

Chauga River
Area

Poor Mountain
Area

Henderson Gneiss

NW   Chauga River Sequence   Poor Mountain Sequence   SE

Brevard-Poor Mtn.
transitional

marble-calcareous
quartzite

graphitic phyllite

Brevard carbonate

feldspathic
quartzite

amphibolite

transitional
amphibolite

Brevard phyllite

graphitic phyllite

Brevard-Poor Mountain transitional

feldspathic biotite
quartzite

Brevard phyllite

——?——?——?——?——?——?——?——?——

——?

garnet mica schist, which he called Poor Mountain schist and speculated that it may be equivalent to the Brevard-Poor Mountain transitional unit. This schist can have similar textures and mineralogy to upper Mill Spring complex schist but the two are distinguished on the basis of their association with Poor Mountain amphibolite: Poor Mountain schist commonly contains interlayers of Poor Mountain Amphibolite or is found as interlayers in amphibolite whereas upper Mill Spring schist has no such association with the Poor Mountain amphibolite (Davis, 1993a). In the study area, Poor Mountain schist occurs as thin (usually a few meters or less) layers within the amphibolite and quartzite but does not occur as a mappable unit at the base of the Poor Mountain Formation. Lemmon (1973) also found marble lenses up to 6 feet thick near the Brevard fault zone but no marble was found by Davis (1993a) or by myself.

The Poor Mountain Formation in the study area is divided into two units— an amphibolite-rich/quartzite-poor unit and a quartzite-rich/amphibolite-poor unit. Minor amounts of pelitic schist, metagraywacke, and metasiltstone are present in both units. In general, amphibolite lies structurally below the quartzite and above the granitoid gneiss but recumbent isoclinal folding has reversed the order in several areas. Quartzite is located in thrust contact below rocks of unit 3 and in stratigraphic contact above the Poor Mountain Amphibolite. This unit pinches out in the southern part of the study area along the Mill Spring fault leaving Poor Mountain Amphibolite in contact with unit 3 rocks (Plate I; Plate II). The contact between the amphibolite and upper Mill Spring gneiss in most of the study area is sharp with rare interlayering of the amphibolite and gneiss. Farther south, however, in the vicinity of the Bills Creek Community, amphibolite often interfingers with granitoid gneiss (Plate I) and is probably the result of isoclinal folding.

The Poor Mountain Amphibolite is fine-grained, unlike the gneiss that underlies it. Interlayered with the amphibolite is laminated feldspathic quartzite that is commonly a few millimeters to a few centimeters thick, although it may reach several meters thick (Fig. 2.8). The layers are usually continuous over long distances (at least tens of meters) and are commonly folded. They are considered here to be primary layers of quartzite and not produced by

Figure 2.8. Photographs of the Poor Mountain Amphibolite. (A) Amphibolite with a single felsic folded felsic layer on the southeast ridge of Youngs Mountain, Lake Lure quadrangle. Density of the felsic layers can vary considerably from dozens to less than one per meter of section. Diameter of the lens cap is 5 cm. (B) Photomicrograph of Poor Mountain Amphibolite (right) next to a felsic layer (left) taken in cross-polarized light. Note the foliated texture of the amphibolite, composed mostly of hornblende along with tiny inclusions of sphene and zircon. The felsic layer has a more granoblastic appearence and is composed mostly of plagioclase, epidote, and clinozoisite. The latter two minerals are probably the product of retrograde metamorphism. Width of the photograph is approximately 2 mm.
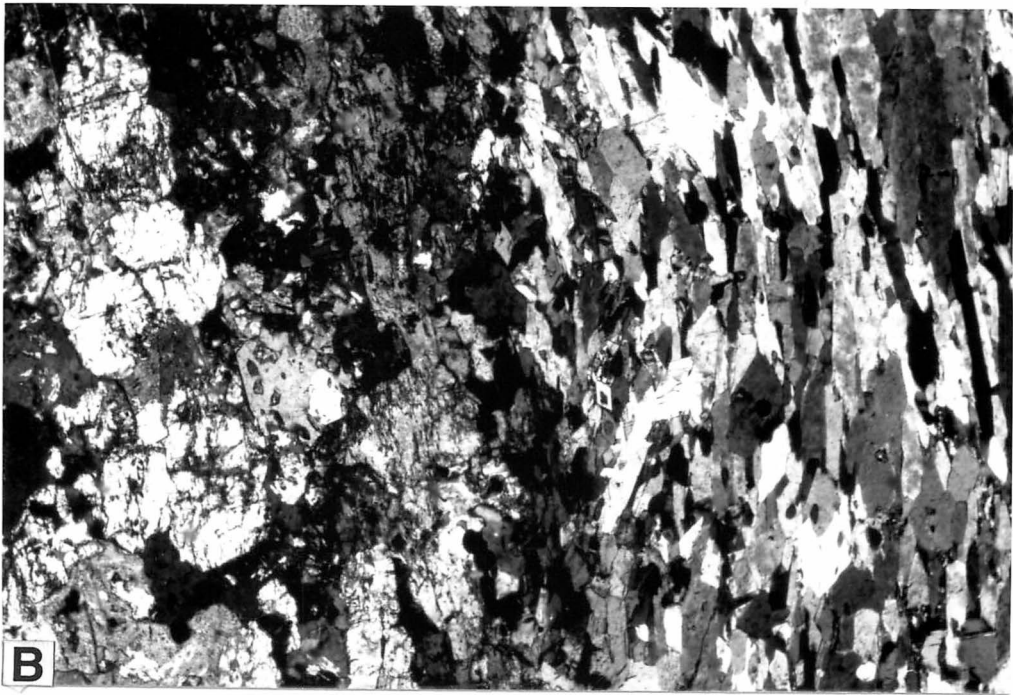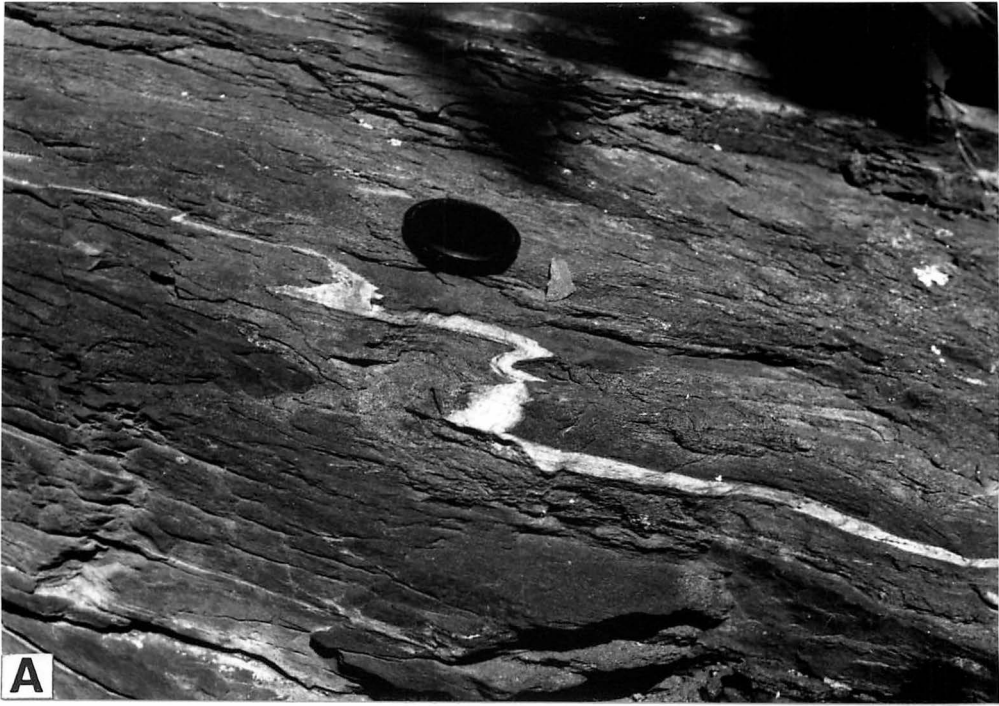
metamorphic differentiation. Also within the amphibolite are thin, discontinuous layers or boudins of granitoid gneiss, metagraywacke, biotite-muscovite schist, and sillimanite-bearing pelitic schist. The contact between amphibolite and overlying quartzite is gradational with increasing amounts of quartzite layers occurring within amphibolite towards the east. This transition occurs over tens of meters in areas to the south, whereas it is more sharp to the north, occurring over a few meters.

In general, brownish-green to yellowish-green hornblende and plagioclase (An$_{30-35}$) are the two consistently dominant minerals, but biotite, quartz, epidote, and clinozoisite can also occur in large amounts (Fig. 2.8b and Table 2.1). Amphibolite in the northeastern part of the study area can contain large amounts of biotite, constituting up to 32 percent of the rock. In addition, trace amounts of sphene, zircon, chlorite, rutile, garnet, muscovite, colorless amphibole, and opaque phases occur. The opaque phases, determined by reflection petrography, include pyrite, ilmenite, magnetite, and chalcopyrite. Grains in both the amphibolites and the felsic laminations rarely exceed 1 mm long although in rare cases, they may be up to 10 mm long. Not all samples contain all the minerals mentioned above. Some samples are composed almost entirely of hornblende (Table 2.1- Su 112), while other samples contain all of the minerals mentioned above with relatively little hornblende. The thin, felsic laminations within the amphibolite are composed mostly of plagioclase and quartz but may also contain significant amounts of clinozoisite and epidote (Fig. 2.8b). Less commonly, the laminations may be composed of pure quartz. The thicker laminations that are up to several meters thick are more similar to Poor Mountain Quartzite containing quartz, plagioclase, microcline, and muscovite (Table 2.1- Su 410). XRF analysis was conducted on the amphibolites and the results are discussed in Chapter V.

The Poor Mountain Quartzite lies immediately above the Poor Mountain Amphibolite. This rock unit is structurally the highest lithology in unit 2, lying in fault contact with rocks of unit 3 (Fig. 2.1 and Plate II). In the southwest, however, it pinches out, sliced off by the Mill Spring

fault that separates unit 2 from unit 3 leaving amphibolite in contact with the gneiss of unit 3 (Plate I). Like the Poor Mountain Amphibolite, the quartzite is fine-grained and has widely scattered layers of amphibolite, metagraywacke, pelitic schist, and biotite-muscovite schist. Foliation is defined by the parallel orientation of muscovite and biotite and less so by slightly elongated crystals of quartz and feldspar (Fig. 2.9).

The composition of the Poor Mountain Quartzite can be as variable as the Amphibolite. In general, it is composed primarily of quartz and plagioclase plus variable amounts muscovite. Minor amounts of microcline, garnet, epidote, opaque phases (mostly pyrite and magnetite), biotite, and chlorite are also present (Table 2.1). Most of the thin, dark laminations are composed of biotite, but in rare cases, garnet and opaque minerals compose the laminations. Occasionally, muscovite is the secondmost common mineral, comprising up to 30 percent and making the rock appear as a muscovite schist (Fig. 2.9b). It is also present in two generations: an earlier, synmetamorphic phase that parallels the foliation (individual crystals measure up to 4 mm long) and a later, retrograde phase that is randomly oriented, coarse grained (up to several mm long), and grows around preexisting phases. This retrograde phase probably formed during postmetamorphic hydrothermal alteration of the quartzite. The micas define the foliation and tend to be segregated into thin (<1 mm thick) layers, while quartz and feldspar are granoblastic. The overall effect in the field is a thinly laminated rock that tends to break along the mica layers.

When plotted on the ternary diagram of Pettijohn (1954), the protolith for the quartzite is probably either a graywacke or an arkose (Fig. 2.6). This contrasts with quartzite in South Carolina which is often a true quartzite or contains calcite and other calcareous minerals (Shufflebarger, 1961; Hatcher, 1970). Also included in the plots in Figure 2.6 is the basal gneiss of unit 2 and the biotite gneiss of unit 3, both of which plot in the graywacke field. The complete absence of any protolithic textures in the Poor Mountain Quartzite as well as other Inner Piedmont metasediments, however, makes determination of the origin of the Poor Mountain Quartzite impossible.

Figure 2.9. Photomicrographs of Poor Mountain Quartzite. (A) Prograde muscovite layer

(middle of photograph) that typically defines layering in the Poor Mountain Quartzite.

Biotite and garnet may also define layering. Note that quartz and feldspar,

constituting the rest of the rock are slightly elongated so that the foliation can be

recognized even if the mica layers are absent. Sample was collected at Oak Mountain,

Sugar Hill quadrangle. (B) Muscovite-rich quartzite with pyrite (opaque minerals)

taken near Cove Creek, Shingle Hollow quadrangle. In hand sample, these rocks look

like a schist. Width of both photographs is 2 mm.
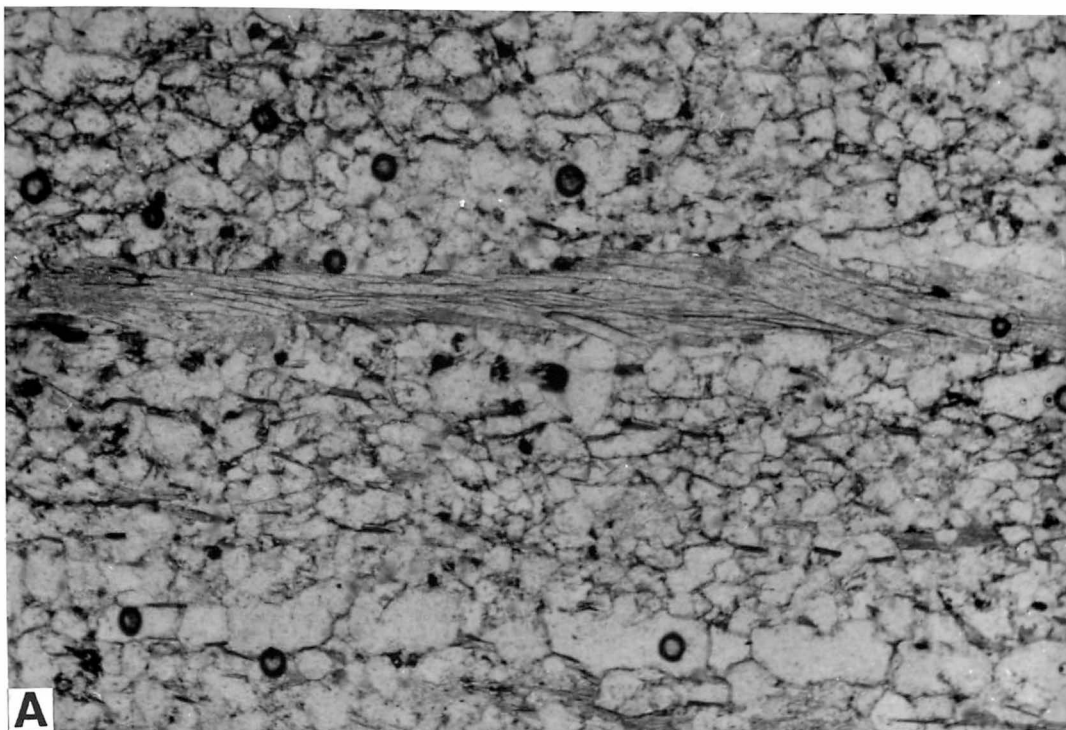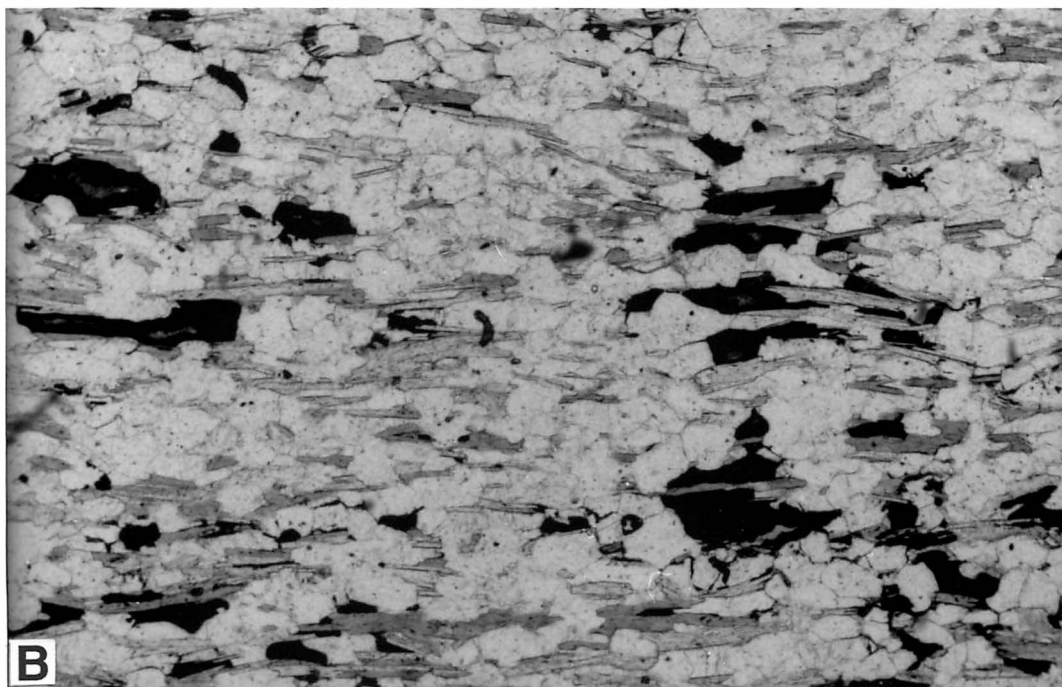
UNIT 3

The structurally highest unit contains rocks similar to those of Griffin's (1969) Walhalla and Six Mile nappes and is interpreted to be correlative with the Mill Spring thrust sheet of Davis (1993a). The tectonic stratigraphy in unit 3, however, differs from the stratigraphy in the Mill Spring thrust sheet. The Mill Spring thrust sheet contains mostly amphibole gneiss with lesser amounts of biotite gneiss and granitoid gneiss, whereas unit 3 contains mostly biotite gneiss with lesser amounts of amphibolite and granitoid gneiss but no amphibole gneiss. Because areas between the study area and areas studied by Davis (1993a) remained unmapped, the change in tectonic stratigraphy changes between the two areas is not clear.

In the study area, unit 3 has been divided into two units— a lower unit of biotite gneiss plus minor amounts of garnet-bearing biotite-muscovite schist and an upper unit of complexly interlayered biotite gneiss, granitoid gneiss, amphibolite, and minor amounts of pelitic schist and quartzite. The lower unit is similar in lithology to the upper Mill Spring complex but contains considerably less granitoid gneiss than upper Mill Spring rocks in unit 2. The lithologies and complex interlayering in the upper unit is similar to the lower Mill Spring complex as described by Davis (1993a) but contains relatively little amphibolite. This change may represent a transitional unit to more amphibolite-rich rocks in unmapped areas to the southeast.

Lower Unit. In the lower unit, coarse to very coarse-grained biotite gneiss and biotite-muscovite schist are interlayered but gneiss predominates. A few exceptions occur to the southwest and northeast where schist tends to be more common and even dominant. These relationships, however, may be more reflective of the greater susceptibility of biotite gneiss to chemical weathering than schist. South of the study area, biotite gneiss and schist are present as a mappable unit at the top of the Sugarloaf Mountain thrust sheet but not in the Mill Spring thrust sheet (Davis, 1993a). Isolated layers and boudins of Inner Piedmont amphibolite and granitoid

gneiss also occur in the lower unit. Overall, the thickness of the unit, about 300 m, remains constant throughout the study area. Modal percentages suggest that biotite gneiss and schist were metamorphosed from a graywacke (Fig. 2.6).

Both the schist and biotite gneiss contain the same mineral assemblages with dominant amounts of untwinned plagioclase, biotite, muscovite, and quartz (Table 2.1). There are also smaller amounts of garnet, which becomes more common as quartz and feldspar content decrease, and microcline and opaque minerals. In hand sample, both lithologies, but more commonly the schists, contain sillimanite. Petrographic analysis reveals, however, that some of the sillimanite has been retrograded to bands of very fine-grained muscovite and biotite containing only relict sillimanite. Sillimanite also occurs as tiny needle-like inclusions (less than 0.2 mm long) within quartz and muscovite. Unit 3 biotite gneiss differs from unit 2 gneiss in that quartz, sillimanite, garnet, biotite, and muscovite are much more common, and has less microcline. Unlike unit 2 gneiss, unit 3 gneiss seldom contains lenses or layers of fine-grained gneiss, and it is commonly migmatitic (Fig. 2.10a). The presence of migmatitic textures in unit 2 gneiss appears to be dependent on mica content because the higher the mica content, the more migmatitic it is. Such relationships are not well defined in unit 3, where fine-grained textures do exist but do not appear to be related to mica content.

Upper Unit. Above the gneiss and schist of the lower unit is an undifferentiated unit of biotite gneiss, amphibolite, granitoid gneiss, and minor pelitic schist and quartzite. The unit remains undifferentiated largely because of the complex interlayering of these rocks, the low relief, and the poor exposure that characterize the southeastern part of the study area. Most rocks in the upper unit have sustained considerable weathering and therefore, petrographic analysis could not be done on many of them. In hand sample, the granitoid gneiss can be distinguished from Unit 2 gneiss because they are coarse to very coarse-grained and have a higher content of biotite and muscovite. Biotite gneiss in the upper unit is identical in texture and mineralogy to those in

Figure 2.10. Lithologies in unit 3. (A) Biotite gneiss in the lower unit (upper Mill Spring

complex) near the Green River on I-26, Cliffield Mountain quadrangle (Plate III).

Note the migmatitic textures and the large porphyroblasts indicating sense of

shear (top to the left or west). Diameter of the lens cap is 5 cm. (B)

Photomicrograph of amphibolite in the upper unit at Piney Knob, Shingle

Hollow quadrangle (plane polarized light). The large, dark crystals are

hornblende and the light minerals include plagioclase and quartz. Amphibolites

in the upper unit are typically coarser-grained than Poor Mountain Amphibolite

(compare with Figure 2.8b). Width of the photograph is 2 mm.
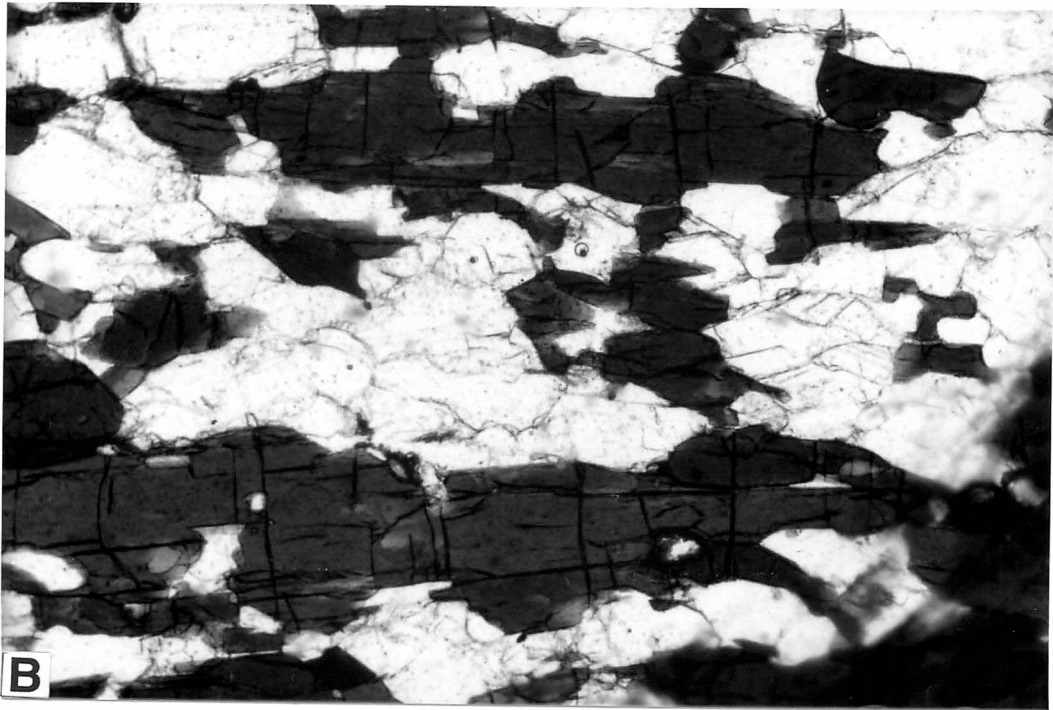
the lower unit. The quartzite, like the Poor Mountain Quartzite, appears to have a high feldspar and mica content, but is much coarser-grained.

The only lithology in which fresh samples could be obtained for petrographic analysis was amphibolite. They occur throughout the upper unit as thin layers and boudins less than a meter thick, but occasionally reach several tens of meters in thickness. In hand sample, the amphibolite is coarser-grained than Poor Mountain Amphibolite with individual hornblende crystals commonly measuring 5 to 10 mm in length but often reaching up to 2 to 3 cm in length (as opposed to hornblende in Poor Mountain Amphibolite which rarely exceed 5 mm in length, Fig. 2.10b). In addition, unit 3 amphibolite lacks the quartzofeldspathic laminations that are characteristic of Poor Mountain Amphibolite.

In thin section, unit 3 amphibolite contains blue-green amphibole, plagioclase, and quartz plus minor amounts of epidote, clinozoisite, tourmaline, and opaque minerals (ilmenite, chalcopyrite and pyrite; Table 2.1). Unlike the Poor Mountain Amphibolite, clinozoisite, sphene, zircon, garnet, biotite, muscovite, and chlorite are rare or nonexistent in Inner Piedmont amphibolite. Furthermore, quartz is more common in unit 3 amphibolite than it is in the Poor Mountain Formation.

MISCELLANEOUS ROCK UNITS

Granite and Pegmatite. Numerous, small intrusive bodies occur throughout the study area. Earlier dikes and sills have a variety of orientations with respect to the foliation, have undergone varying degrees of transposition, and appears to have served as ideal sites for ductile shearing (Fig. 2.11). These relationships suggest that intrusion probably occurred continuously during peak M_2 metamorphism and shortly afterwards. While no thin sections were prepared from the dikes and sills, inspection of hand samples indicates the presence of feldspar and quartz with

Figure 2.11. Granitic dikes in the Henderson Gneiss at Chimney Rock Park. The dikes exhibit varying degrees of cross-cutting relationships and transposition. Note that some of the dikes in the photograph behaved as ductile shear zones during deformation. Width of the photograph is approximately 5 m.

minor amounts of biotite, muscovite, and possibly sphene. Davis (1993a) also found mafic dikes in the lower Mill Spring complex.

The youngest dikes and sills are typically very coarse-grained, contain mostly white K-feldspar, plagioclase, quartz, muscovite, and biotite, and are variably oriented. In pegmatite, muscovite, K-feldspar, and quartz are the three most common minerals. Individual muscovite crystals can measure up to 10 cm long. None of the rocks that surround the granite and pegmatite bodies show any evidence of contact metamorphism which suggests that intrusion occurred when the rocks were still very hot. They do not appear to be related to metamorphic differentiation or partial melting because their mineralogy is different from the surrounding rock, including leucosome in the migmatite. Therefore, I believe they are related to an intrusive event occurring during the waning stages of metamorphism.

Vein Quartz. Most of the veins that occur in the study area are dominated by quartz. While many veins contain pure quartz, others also contain minor muscovite. A few veins, filling east-trending fractures, contain quartz, epidote, and chlorite. In the Henderson Gneiss and granitoid gneiss in unit 2, veins composed entirely of quartz occur parallel to the foliation and have been subsequently deformed, indicating that they formed before or during peak metamorphism. In other parts of the study area, however, the veins were emplaced after metamorphism. In these veins, very large crystals of milky quartz up to 60 cm across can be found.

CORRELATION OF UNITS AND REGIONAL RELATIONSHIPS

Multiple transposition, intrusion of granitic plutons, map-scale isoclinal recumbent folding, and thrusting have made establishment of the stratigraphy in the eastern Blue Ridge and Inner Piedmont exceedingly difficult. These processes have eliminated all premetamorphic textures and structures. Thus, all inferences about the nature of protoliths and correlations with units in

other thrust sheets must be made on the basis of composition, relationships with adjacent lithologies, and position in sequences of lithologies. Numerous studies employing such methods in the high grade parts of the eastern Blue Ridge and Inner Piedmont include Rankin (1970, 1975); Rankin and others (1973), Hatcher (1969, 1970, 1972, 1978, 1987), Wehr and Glover (1985), Hopson and Hatcher (1988), and Hatcher and Goldberg (1990).

Davis (1993a) subdivided rocks of the Columbus Promontory area into the Henderson Gneiss, upper (amphibolite-poor) and lower (amphibolite-rich) Mill Spring complex, and the Poor Mountain Formation. The upper Mill Spring complex is present in the study are at the bottom of unit 2 conformably underlying the Poor Mountain Formation and at the bottom of unit 3 (Fig. 2.12). The undifferentiated unit in unit 3 is interpreted to be part of the lower Mill Spring complex but this correlation is ambiguous. The amphibolites constitute a relatively small volume of the unit although they still are significant, amphibole gneiss is absent here but is dominant to the south, and granitoid gneiss constitutes the majority of the rocks in the unit. Furthermore, unit 3 rocks are interpreted to correlate with rocks of the Mill Spring thrust sheet of Davis (1993a) which is composed almost entirely of lower Mill Spring rocks. These rocks are dominated by amphibolite and amphibole gneiss although significant amounts of granitoid gneiss are also present. This implies that relationships within the Mill Spring thrust sheet must change considerably between the study area and those areas mapped by Davis and Tabor (Davis, 1993a).

Davis' (1993) division of the Mill Spring group into amphibolite-poor and amphibolite-rich units correlates well with other parts of the Inner Piedmont including northeast Georgia and South Carolina (Hopson and Hatcher, 1988), South Carolina (Griffin, 1969, 1971a, 1971b, 1974; Liu, 1991), and northwestern North Carolina in the Smith River allochthon (Conley and Henika, 1973). Such relationships have also been noted in the Tallulah Falls Formation of the eastern Blue Ridge in which amphibole-poor rocks lie on top of amphibole-rich rocks (Hatcher, 1971b, 1978). These relationships are also present in other parts of the eastern Blue Ridge including the Ashe,

Figure 2.12. Simplified geologic map showing lithologic relationships in the study area

(northeast corner) as well as adjacent areas to the southwest. Map is modified from

Davis (1993) and includes data by Jayne (unpublished), Davis (1993), Tabor

(unpublished), Lemmon (1973), and Conley and Drummond (1965).
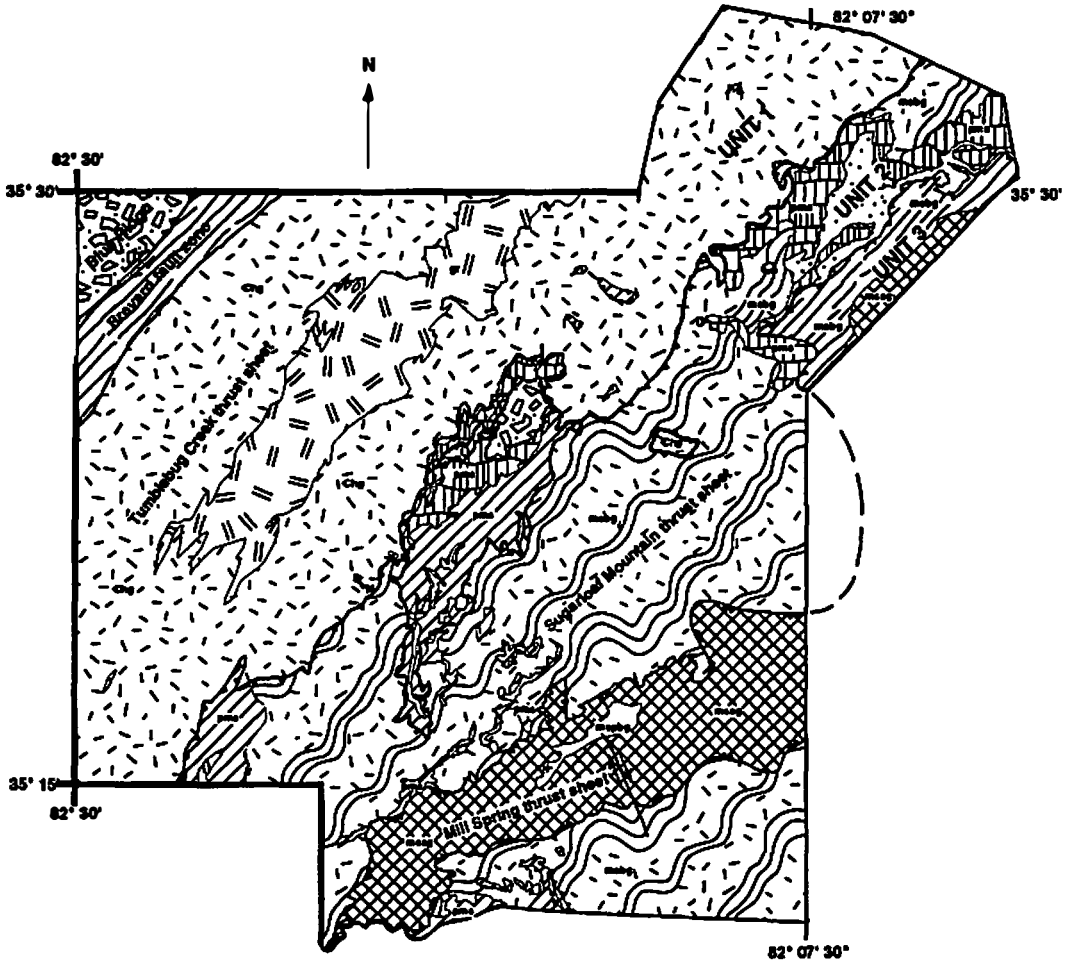
EXPLANATION

gr	438 Ma Granitoid
chg	Henderson Gneiss (535 – 600 Ma)

Poor Mountain Formation

ag	
pmq	Poor Mtn. amphibolite – quartzite
pma	Poor Mtn. amphibolite (local quartzite)
pmg	Granitic gneiss, biotite gneiss, and mica schist

Mill Spring Formation

Upper	msbg	Biotite gneiss - metagraywacke
Lower	mspbg	Porphyroblastic biotite gneiss-metagraywacke
		Migmatitic amphibolite gneiss and granite

0 _____ 10 km

Lynchburg, and Sandy Springs/New Georgia Group (Hatcher and Goldberg, 1990). A more detailed discussion is given by Davis (1993a).

Chauga belt stratigraphy (Poor Mountain Formation, Chauga River Formation, and Henderson Gneiss) is extensive throughout the Inner Piedmont of southwestern North Carolina, South Carolina, and northeastern Georgia. The extent of the Chauga belt to the north and south is unknown because these parts of the Inner Piedmont remains unmapped. Shufflebarger (1961), however, suggested that the Poor Mountain Formation may be correlative with the Evington Group of Virginia, a variable sequence of pelitic schist, marble, quartzite, and metabasalt (Brown, 1951, 1958; Espenshade, 1954). Furthermore, the Evington Group has been correlated with the Alligator Back Formation by Rankin and others (1973), Wehr and Glover (1985), and Patterson (1988). Wehr and Glover (1985) further suggested that the Evington Group may be the deep-water equivalent of the Chilhowee Group in the western Blue Ridge of Virginia. The Poor Mountain and Chauga River Formations have also been correlated with the Jackson's Gap Group and Ropes Creek Amphibolite in the Inner Piedmont of Alabama by Bentley and Neathery (1970) and Davis (1993a).

III. STRUCTURAL GEOLOGY

Rocks of the western Inner Piedmont have undergone a complex history of deformation recording multiple episodes of folding and faulting, similar to deformation in other parts of the high grade southern Appalachian internides. While structures in the Blue Ridge and Valley and Ridge indicate NW-directed transport, structures in the Inner Piedmont indicate W- to SW-directed shearing or orogen-oblique to orogen-parallel transport. This aspect of the Inner Piedmont has only recently been recognized (Hopson and Hatcher, 1988; Liu, 1991; Davis, 1993a) and is interpreted to be synchronous with upper amphibolite facies metamorphism (M_2). This W- to SW-directed transport predates a later Alleghanian episode of dextral strike-slip motion (Edelman and others, 1987; Liu, 1991; Davis, 1993a).

In the study area, at least four episodes of deformation have been recognized and involve four episodes of folding and at least one episode of faulting (Table 3.1). The extent of D_1 deformation is unknown since virtually all of its structures have been transposed by later deformation. D_2 and D_3 are the two episodes that are of most interest in this study resulting in virtually all the strain that can be observed in the rocks. D_2 deformation involved formation of penetrative structures, erased virtually all evidence of pre-peak metamorphic deformation, and is synchronous with peak M_2 metamorphism. D_3 occurred during the waning stages of M_2 metamorphism and involved far less shear strain than D_2. D_4, the latest episode of unknown timing, involved minor, gentle folding.

The timing of D_2 and D_3 deformation is constrained by the age of metagranites in the Inner Piedmont. Metagranites within the Henderson Gneiss in the Carolinas were dated by Odom and Russell (1975) at 438 ± 22 Ma and by Harper and Fullagar (1981) at 423 Ma. These granitoids are strongly foliated and lineated, indicating that they predate M_2 metamorphism. Dallmeyer (1988), using Ar closure temperatures for hornblende, biotite, and muscovite, suggested a Late Devonian age for M_2 metamorphism. Because of the parallel

Table 3.1. Summary of deformation events in the Columbus Promontory. D_1 and D_{2a} to D_4 have been recognized in the study area.

	FOLDS		FABRICS	FAULTS
	Style	Orientation		
D_1	Isoclinal, recumbent (F_1)	?	S_1 (indistinct)	—
D_{2a}				Tumblebug Creek fault Brevard fault
D_{2b}	Isoclinal recumbent dominant regional foliation (F_2)	E to NE	S_2 (dominant foliation)	Sugarloaf Mtn fault, Mill Spring fault
D_3	Isolated, upright or recumbent deforms regional foliation (F_3)	NE to SE	S_3 (indistinct)	Mesoscopic dextral strike slip
D_4	Upright broad, open to gentle (F_4)	N to NE	—	—
D_5	Upright broad, open to gentle (F_5)	NW	—	—

56

orientation of the metamorphic foliation, thrust faults, lithologic contacts, and fold axial planes, peak M_2 metamorphism is interpreted to be synchronous with D_2 deformation. In the vicinity of the Brevard fault zone, M_2 fabrics are overprinted by a foliation associated with greenschist-facies metamorphism (Hatcher, 1969, 1970; Lemmon, 1973; Edelman and others, 1987; Hopson and Hatcher, 1988; Liu, 1991). This episode of metamorphism has been dated by Sinha and others (1988) at 273 Ma using Rb/Sr data. These relationships imply that the age of D_2 deformation is Acadian.

SUMMARY OF DEFORMATION

D_1 DEFORMATION

Very little evidence of deformation prior to metamorphism exists because of extreme transposition during D_2 deformation. Such transposition has overprinted and reoriented earlier structures making them virtually impossible to study. Within the study area, isoclinal folds that appear to predate D_2 deformation are present in the Poor Mountain Amphibolite, but it is not clear whether or not these are D_1 folds or early D_2 folds. Outside of the study area, Hopson and Hatcher (1988) have found that D_1 deformation is associated with gneissic layering and a foliation. Davis (1993a) also observed such layering in the Columbus Promontory. Layering that predates D_2 deformation is present in the Poor Mountain Amphibolite but these layers are interpreted to be protolithic because their thickness is controlled, in part, by proximity to the Poor Mountain Quartzite.

D$_2$ DEFORMATION

The most important deformation event in the Inner Piedmont involved extensive transposition of previous structures and coincided with peak regional metamorphism (M$_2$). During this episode, intense ductile shearing produced the dominant foliation, mineral lineations, intrafolial folds, and S-C mylonite. Sheath folding, rootless intrafolial folds, and S-C fabrics all indicate high shear strains ($\gamma > 10$ as suggested for sheath folding by Park, 1983 and Skjernaa, 1989) throughout the study area. Because of the abundant evidence of high shear strains near and far away from the faults, the western Inner Piedmont has been interpreted as a crustal-scale shear zone (Davis, 1993a).

D$_3$ DEFORMATION

D$_3$ deformation occurred sometime after peak thermal metamorphism as rocks were cooling and were beginning to acquire a competency contrast between adjacent lithologies. It is associated with nonpenetrative recumbent to upright folding, boudinage, and outcrop-scale ductile strike-slip faulting. It is important to note that no significant time break occurred between D$_2$ and D$_3$ deformation but the associated structural styles are unique enough to warrant two separate events.

D$_4$ DEFORMATION

The latest episode of deformation recognized in the study area involved gentle to open, N to NE-trending folds. Such folding was so minor and widely scattered that the orientations

of the preexisting structures underwent little modification. These folds can be recognized at the outcrop scale as gentle, symmetric undulations of S_2 layering.

LATER EPISODES

In areas mapped in South Carolina and northeast Georgia, a fifth deformation event has been identified. This is associated with NW-trending, gentle, upright folding that interferes with D_4 folds resulting in a type 1 dome and basin pattern (Hopson and Hatcher, 1988; Liu, 1991). Cataclastic zones with a normal shear sense have also been identified throughout the Inner Piedmont and Blue Ridge and are interpreted to have a mid-Mesozoic age (Garihan and others, 1993). In the study area, normal faults with cm-scale offsets are present in the Poor Mountain Formation but it is not clear if these faults are mid-Mesozoic. These faults predate subvertical fractures that trend dominantly ENE and NNW.

MESOSCOPIC AND MICROSCOPIC FEATURES

The major types of mesoscopic structures in the study area include foliations and compositional layering, S-C fabrics, mineral lineations, folds, and fractures. The former four types formed during peak thermal metamorphism whereas the latter type formed sometime afterward. Based on the presence of mylonitic textures and other ductile fabrics, and the absence of cataclastic textures, I interpret those structures and fabrics synchronous with metamorphism formed in the ductile regime well below the 12-15 km depth where the ductile-brittle transition occurs (Sibson, 1977, 1983). Pressure-temperature relationships determined from metamorphic mineral assemblages are consistent with this interpretation. Each of these structures displays a diverse and complicated array of geometries due, in part, to polyphase deformation and will be treated separately in this section.

FOLIATION AND COMPOSITIONAL LAYERING

An early episode of deformation (D_1) and folding resulted in gneissic layering (S_1) and was subsequently transposed by the dominant S_2 foliation. The only evidence for S_1 layering and folding is preserved outside the field area in Poor Mountain rocks occurring below the Henderson Gneiss (Davis, 1993a) and in amphibolite boudins associated with a penetrative S_1 foliation (Hopson and Hatcher, 1988). Two stages of transposition (F_1 and F_2) have also been recognized in the eastern Blue Ridge (Hatcher and Butler, 1979; Quinn, 1991) and in other parts of the Inner Piedmont (Hopson and Hatcher, 1988; Liu, 1991). The S_2 foliation is the most pervasive structural element in the Columbus Promontory (Fig. 3.1). Davis (1993a) interpreted it as a mylonitic C-fabric from its relationships with shear-sense indicators and asymmetric S-C fabrics. The presence of S-C fabrics preserved within S_2 suggests that this C-fabric represents a regionally extensive shear surface characterized by a boundary-parallel noncoaxial flow (Lister and Snoke, 1984; Davis, 1993a).

The overall parallelism of the foliation, lithologic contacts, compositional layering, fold axial planes, and faults suggests that the S_2 foliation is the product of extensive transposition so that all preexisting foliations and layering were transposed into S_2 (Hatcher, 1990; Davis, 1993a). Davis (1993a) argues that the S_2 foliation represents a mylonitic C-fabric because of its strong planarity, the presence of mineral lineations on virtually all foliation surfaces, and its association with structures indicative of noncoaxial deformation such as S-C fabrics (Lister and Snoke, 1984), winged porphyroclasts (Simpson, 1986), and intrafolial folds. A more detailed discussion on the evolution of the S_2 foliation is given by Davis (1993a).

In isolated parts of the Poor Mountain Quartzite, two sets of layering with different

Figure 3.1. Foliations in the study area. A) Foliation and compositional layering in unit 3

biotite gneiss. Note that the layering and the foliation are parallel and have

subsequently been folded during later D3 deformation. Photo was taken a half mile

east of the Mullin Bible Camp, Shingle Hollow quadrangle. B) Foliation surface in

Henderson Gneiss showing mineral lineations formed by the parallel orientation of

mica, quartz and feldspar. The banding is formed by the tendency for the rock to

fracture into thin sheets parallel to the foliation surfaces and along the lineations.

Lens cap in both photos is 50 mm in diameter. The photo was taken in Chimney Rock

Park, Bat Cave quadrangle.
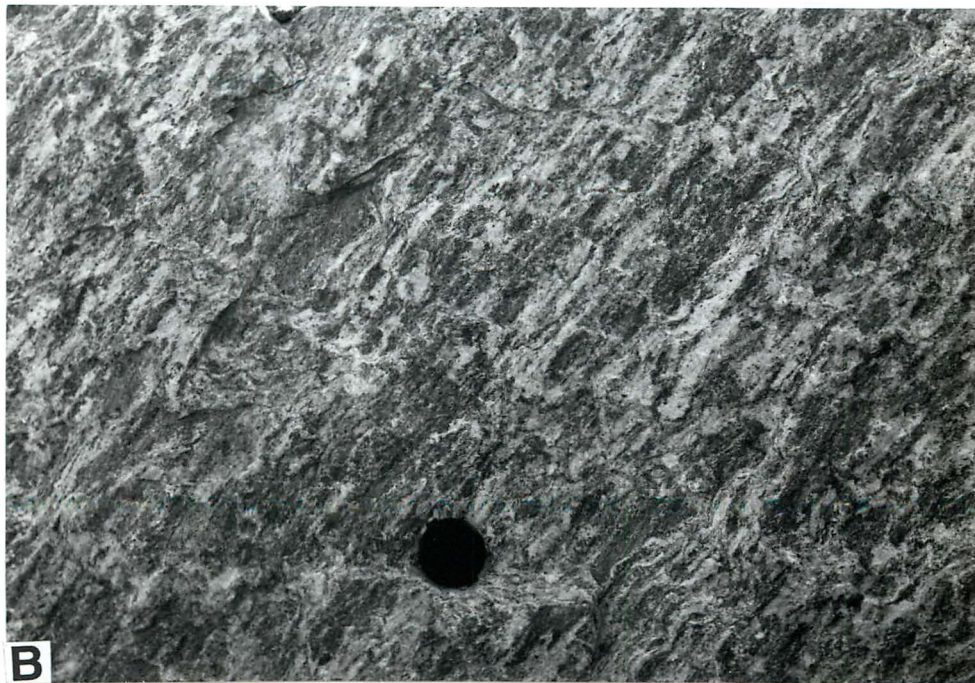
orientations occur. Both sets strike in the same direction, but dip to both the SE and NE. The intersection lineation, in general, trends NE and plunges gently in both directions, roughly parallel to the L_2 mineral lineation. Petrographically, these two foliations are defined by two different orientations of mica. The two types of mica mutually crosscut each other and this indicates that they formed at the same time.

About 1700 measurements of the S_2 foliation were made during this study and the data were subsequently divided into three domains by lithotectonic unit. Compositional layering is parallel to the foliations in all but a few cases, and no distinction was made between the two types of layers during mapping and stereonet analysis (Fig. 3.2). In general, the foliations strike NE and dip gently to the SE and show minor amounts of scatter.

While girdles demonstrating post-D_2 deformation are present, they tend to be poorly defined. This indicates that later folding (F_3 and F_4) was relatively minor and did little to alter the orientation of the S_2 foliation after metamorphism. At the outcrop scale, F_3 and F_4 folding is present and does affect the orientation of the foliation, but their effects are isolated.

A weakly developed, nonpenetrative foliation postdating the S_2 foliation has been observed in the hinge zones of F_3 folds. This foliation is composed mostly of fine-grained muscovite and is usually oriented parallel with the axial plane of the fold. A weak, secondary foliation has also been observed in the Inner Piedmont of northeast Georgia by Hopson and Hatcher (1988), in South Carolina by Hatcher (1969, 1970) and Liu (1991), and in the Columbus Promontory by Davis (1993a). While the study area underwent chlorite-grade retrograde metamorphism, the minerals associated with such metamorphism are usually randomly oriented. Outside of the study area, however, such minerals are associated with a foliation and lineation that is related with Alleghanian deformation in the Brevard fault zone (Lemmon, 1973; Sinha and others, 1988; Vauchez and Brunel, 1988).

Figure 3.2. Lower hemisphere, equal-area projections of poles to foliation measured in the study area and subdivided by lithotectonic unit. Scatter diagrams are shown on the left and contoured plots are shown to the right. Location of the lithotectonic units is shown in Fig. 2.3.

Poles to foliation

Uncontoured　　　　**Contoured**

Unit 1
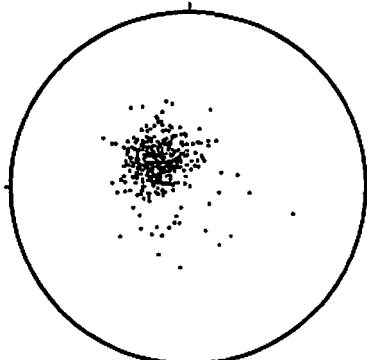
N = 488
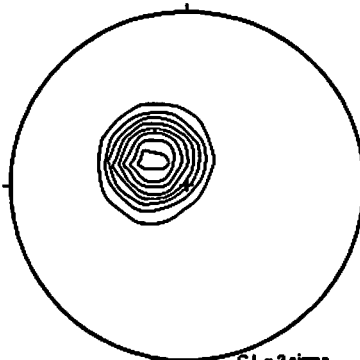
C.I. = 3 sigma

Unit 2
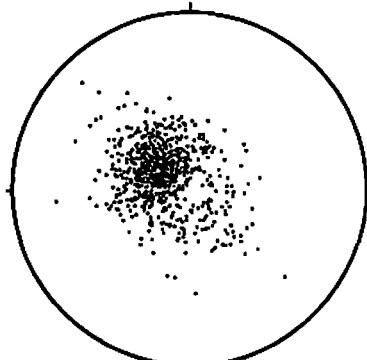
N =919
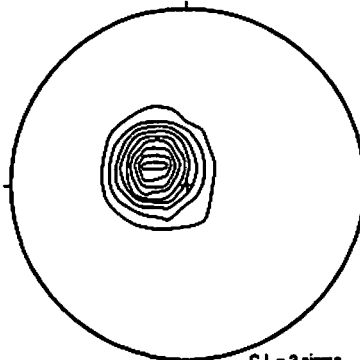
C.I. = 3 sigma

Unit 3
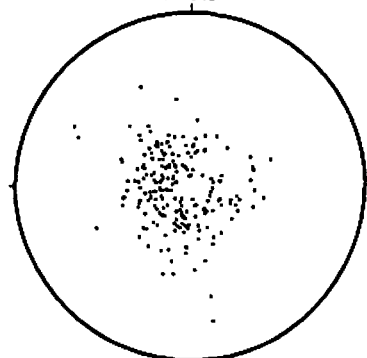
N =222
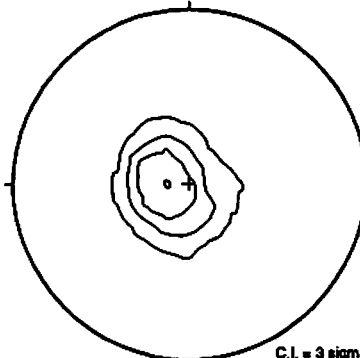
C.I. = 3 sigma

All units
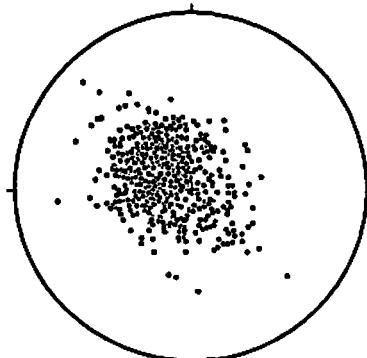
N =1629
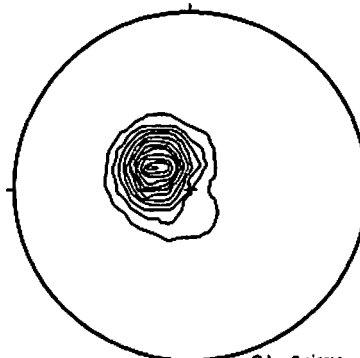
C.I. = 3 sigma

LINEATIONS

A variety of styles and orientations of lineations were observed in the study area. The majority, however, are the result of the parallel orientation of elongated minerals and trend NE and plunge gently (usually less than 10°) NE or SW. Other styles include mineral segregation lineations which result from the segregation of light and dark minerals, intersection lineations, and stretched feldspar porphyroclasts. All occur on foliation surfaces and locally parallel each other, suggesting that they formed during the same metamorphic event (Fig. 3.1). As expected, lineations are most distinct in lithologies that abound in elongated minerals such as amphibolite, which is rich in hornblende, and gneiss and schist, which are rich in mica. But even in the quartzites, which are relatively poor in elongate or platy minerals, lineations made up of slightly elongated quartz and feldspar plus trace amounts of mica are still visible.

Approximately 600 lineations of all types were measured in the study area, were subdivided by lithotectonic unit, and plotted on an equal-area net (Fig. 3.3). They were also plotted on a map to show macroscopic variations in orientation (Fig. 3.4 and 3.5). The map and the equal area nets show a gradual change in orientation of the lineations from ENE in the southeastern part of the study area to NE in areas to the west. Farther southeast, the mineral lineations become more E-W oriented (Fig. 3.5; Davis, 1993a). This change in orientation may be due to oblique shearing along the Brevard fault zone with reverse dip slip and dextral strike slip components (Lemmon, 1973; Davis, 1993a). Orientations do not change drastically across the ductile thrust faults and indicate that strain partitioning did not occur across the thrust faults. In unit 2, anomalous orientations within the Poor Mountain amphibolites produce considerable scatter on the stereonet (Fig. 3.3). Single measurements of anomalous orientations are present in all other lithologies, but in the Poor Mountain Amphibolite, such orientations are present over relatively large areas (up to 2.5 km^2; Plate I). These anomalous

Figure 3.3. Lower hemisphere, equal-area plots of mineral lineations measured in the study

area and subdivided by lithotectonic unit. Scatter diagrams are shown on the left

and contoured diagrams are shown on the right. Location of lithotectonic units is

shown in Figure 2.3.

MINERAL LINEATIONS

UNCONTOURED   CONTOURED

UNIT 1
(N = 182)

UNIT 2
(N = 334)

UNIT 3
(N = 71)

ALL UNITS
(N=587)
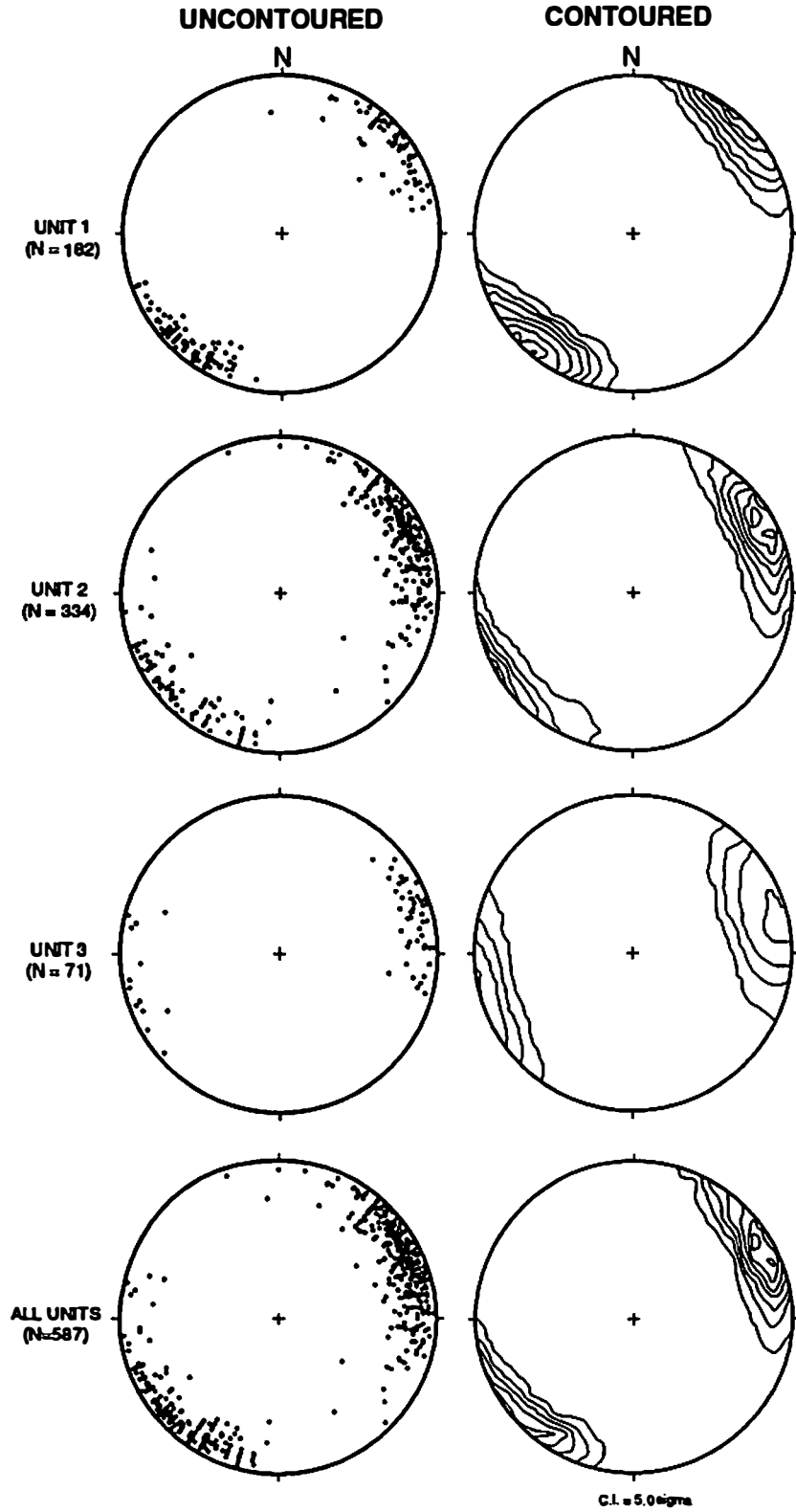
C.I. = 5.0 sigma

Figure 3.4. Distribution of representative L$_2$ mineral lineations measured in the study area.

Arrowheads indicate direction of plunge of the mineral lineations.
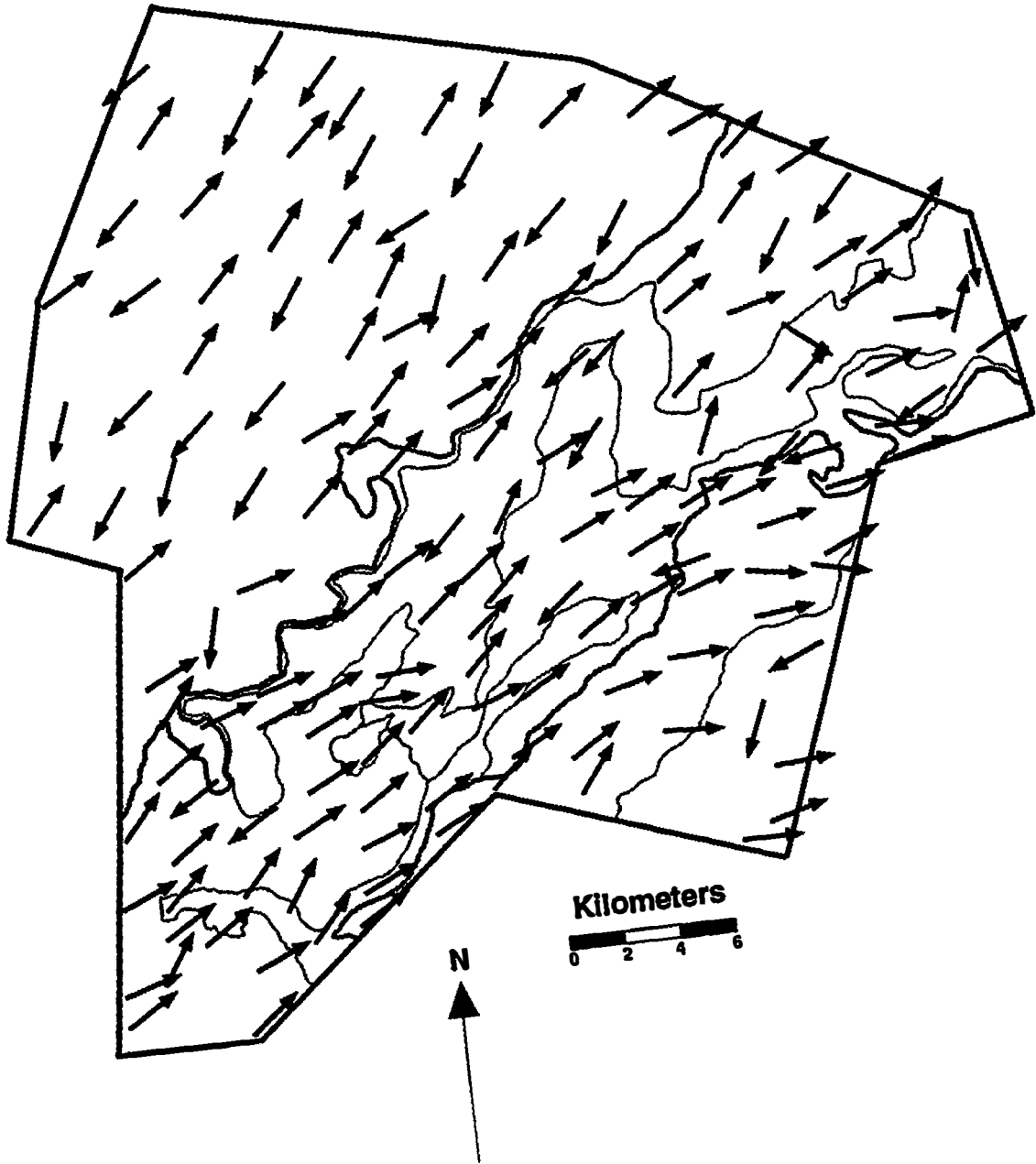
Figure 3.5. Distribution of mineral lineations in the western Inner Piedmont in part of

southwestern North Carolina. The study area is located in the northeast corner of

the map. The map includes data compiled from Lemmon (1973), Davis (1993), and

Tabor (unpublished). Map is derived from Davis (1993).
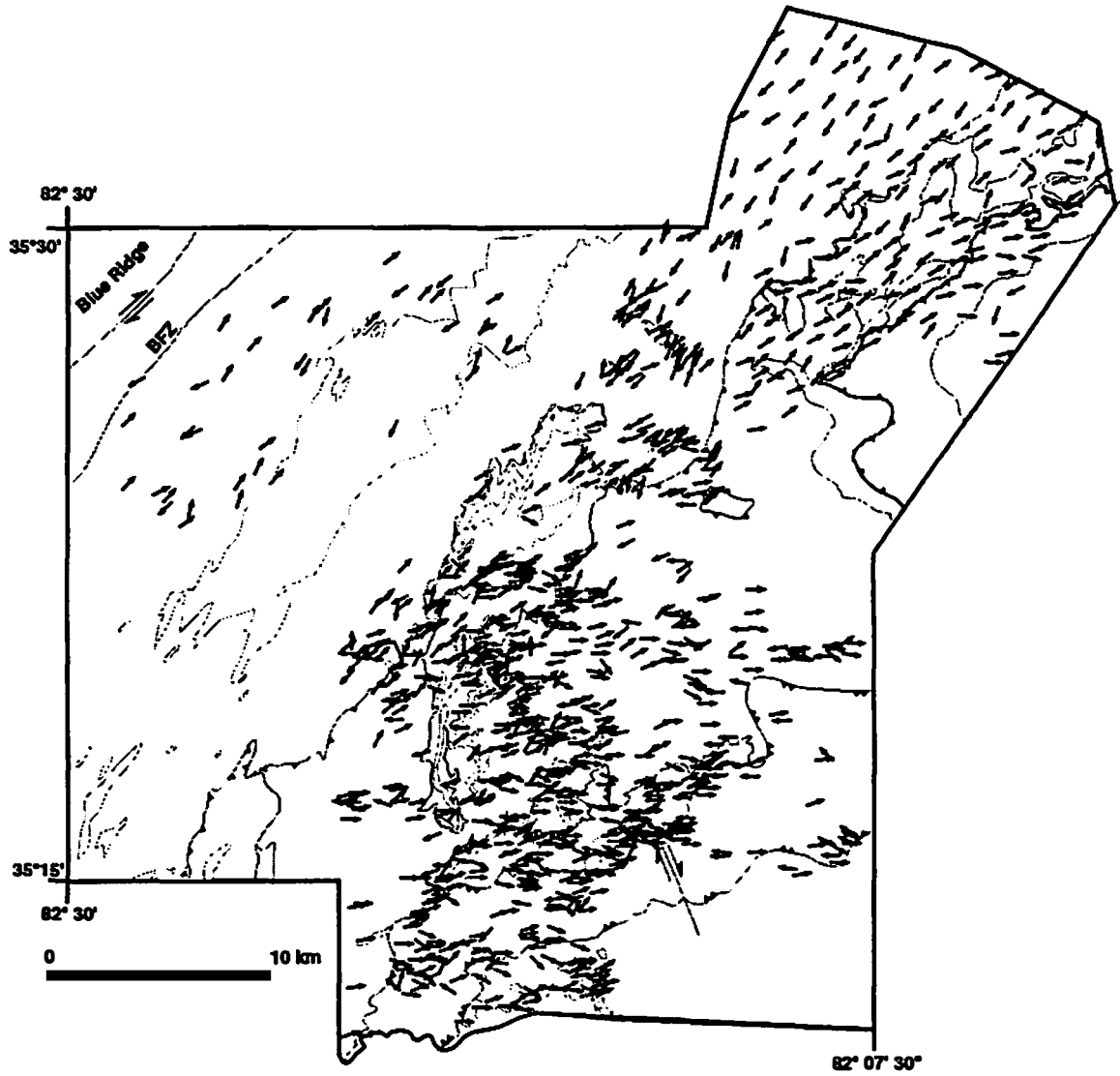
orientations probably record localized changes in the shear direction but it is not clear why these changes occurred.

The mineral lineations measured in the study area are often associated with shear fabrics (tailed porphyroclasts, mica fish, and other mylonitic textures) and are interpreted to be produced by ductile progressive simple shear. They are therefore interpreted to represent a transport lineation (Davis, 1993a). Such lineations, in conjunction with other structures, serve as useful indicators for the orientation of shearing (Simpson, 1986; Hatcher, 1990).

DUCTILE THRUST FAULTS

Two large, map-scale faults have been identified in the study area: the Sugarloaf Mountain fault of Davis (1993a), separating unit 1 from unit 2, and the Mill Spring fault, separating unit 2 from unit 3 (Plate I). The exact displacement on each fault is unknown, but is probably at least 10 to 15 kilometers because they juxtapose rocks of markedly different lithology.

Recognition of faults in the Columbus Promontory as well as much of the Inner Piedmont is complicated by the fact that textures and structures indicating high-shear conditions (e. g., S-C fabrics, winged porphyroclasts, intrafolial folds) are regionally penetrative. The pervasiveness of these structures prompted Davis (1993a) to interpret the Inner Piedmont as a crustal-scale ductile shear zone. Thrust faults in the Columbus Promontory, however, have been recognized as areas of relatively high strain and the contact between rocks juxtaposed by these faults are often very sharp. Criteria for their recognition include grain-size reduction in the vicinity of the fault and truncation of lithologic units and compositional layering along the fault. In addition, most fault contacts were folded no earlier than during D_3 deformation suggesting that faulting occurred during or after D_2. Lithologic contacts, however, were folded during D_2 into recumbent isoclines. Exceptions include the Tumblebug Creek fault in the

Columbus Promontory (Davis, 1993a) and the Cedar Creek thrust in South Carolina (Liu, 1991), interpreted to be correlative with the Tumblebug Creek fault (Davis, 1993a). Thrusting along these faults are interpreted to have occurred during early D_2 deformation (D_{2a}). Like the lithologic contacts, these faults were folded by D_2 into recumbent isoclines and subsequently truncated by the Sugarloaf Mountain fault during later D_2 deformation (D_{2b}— Davis, 1993a).

The Sugarloaf Mountain fault unequivocally satisfies all the above criteria. The Henderson Gneiss, in particular, shows a significant decrease in grain size with proximity to the fault. Augen in the Henderson Gneiss are stretched with a length-to-width aspect ratio exceeding 10:1 (it rarely exceeds 2:1 in gneiss farther away from the fault) indicating intense shearing in the vicinity of the fault. The Mill Spring fault in the study area juxtaposes Upper Mill Spring biotite gneiss on top of Poor Mountain Quartzite along most of its length. The actual contact between the gneiss and quartzite, however, is very poorly exposed and was never observed at the outcrop scale. Biotite gneiss in the vicinity of the fault is typically fine grained and the consistent absence of exposure along the fault contact suggests that a fine-grained schist or phyllonite that is relatively susceptible to weathering is present. Chris Jayne (pers. comm., 1991) did see the contact and observed truncated layering and foliation as on the Sugarloaf Mountain fault.

Outcrop-scale faults have also been observed and include mostly small thrust faults with displacements that rarely exceed 50 cm. They are oriented parallel to foliation and map-scale thrusts. Because most of these faults ductily deform the S_2 foliation, F_2 folds, and other D_2 structures, they are probably D_3 structures. In the Henderson Gneiss, shearing often occurs along pegmatite sills and dikes (Fig. 3.6). They are commonly oriented parallel to S_2 and have a SW-directed sense of displacement. Sometimes, they are observed offsetting earlier S_1 or S_2 gneissic bands. Outcrop-scale strike slip-faults are also present in the Henderson Gneiss. They strike E-W, and have a sinistral sense of displacement (Fig. 3.6).

Figure 3.6. Shear zones in the Columbus Promontory. A) Outcrop-scale ductile shear zone

located on the contact between Henderson Gneiss and a weakly foliated granitic

dike. The shear zone is E-W oriented, vertically oriented, and has a sinistral shear

sense. Width of the photograph is approximately 1 m and was taken on Youngs

Mountain, Lake Lure quadrangle. B) Pegmatite dikes in the Henderson Gneiss

behaving as ductile shear zones. Note the cross-cutting relationships and the

varying degrees of transposition of the dikes. Width of the photograph is

approximately 5 m and was taken at Chimney Rock Park, Bat Cave quadrangle.

A

B

This is consistent with a dextral component of shear along the NE-striking Brevard fault zone, as indicated by the orientation of the mineral lineations and shear-sense indicators. It is important to note, however, that this dextral motion predates a later episode of dextral shearing in the Brevard fault zon, which occurred during lower grades of metamorphism and is interpreted to be Alleghanian.

SHEAR-SENSE INDICATORS

Shear-sense indicators change gradually WSW-directed transport in areas to the southeast to SW-directed transport in areas to the northwest. This is reflected in the orientation of mineral lineations at the map-scale (Fig. 3.4). A more detailed discussion regarding their change in direction is given by Davis (1993a). Examples of shear-sense indicators include winged porphyroclasts, snowball garnets, S-C fabrics, and fold vergence, all of which exhibit W-to SW-directed transport. Fold vergence will be discussed later in this chapter.

Winged porphyroclasts are common in the Henderson Gneiss, biotite gneiss, granitoid gneiss, and are rare in the Poor Mountain Amphibolite. All are composed of microcline or plagioclase and are most numerous and well developed in the Henderson Gneiss where they form a variety of geometries but indicate SW-directed shear (Fig. 3.7). In general, there are three types of porphyroclast geometries— σ-type, δ-type, and θ-type (Passchier and Simpson, 1986; Hooper and Hatcher, 1988; Marshak and Mitra, 1988). θ-type porphyroclasts (Hooper and Hatcher, 1988) were not recognized in the study area. The Henderson Gneiss contains mostly σ type with long tails indicating the porphyroclasts formed during high recrystallization and strain rates (Passchier and Simpson, 1986; Hanmer and Passchier, 1991). Petrographically, the porphyroclasts typically consist of a core of optically continuous feldspar surrounded by a rim of fine-grained, recrystallized feldspar. The wings are also

Figure 3.7. S-C fabrics in the study area. A) Photomicrograph showing mica fish in Upper

Mill Spring complex schist. The mica fish are common in type I S-C mylonites

(Lister and Snoke, 1984). Width of the photomicrograph is approximately 2 mm.

Sample was collected on the summit of Youngs Mountain, Lake Lure quadrangle. B)

Large, well-defined, sigmoid porphyroclasts in mica-rich pods of the Henderson

Gneiss, interpreted to be a type I S-C mylonite (Lister and Snoke, 1984). The

photograph was taken on the north summit of Youngs Mountain, Lake Lure

quadrangle.
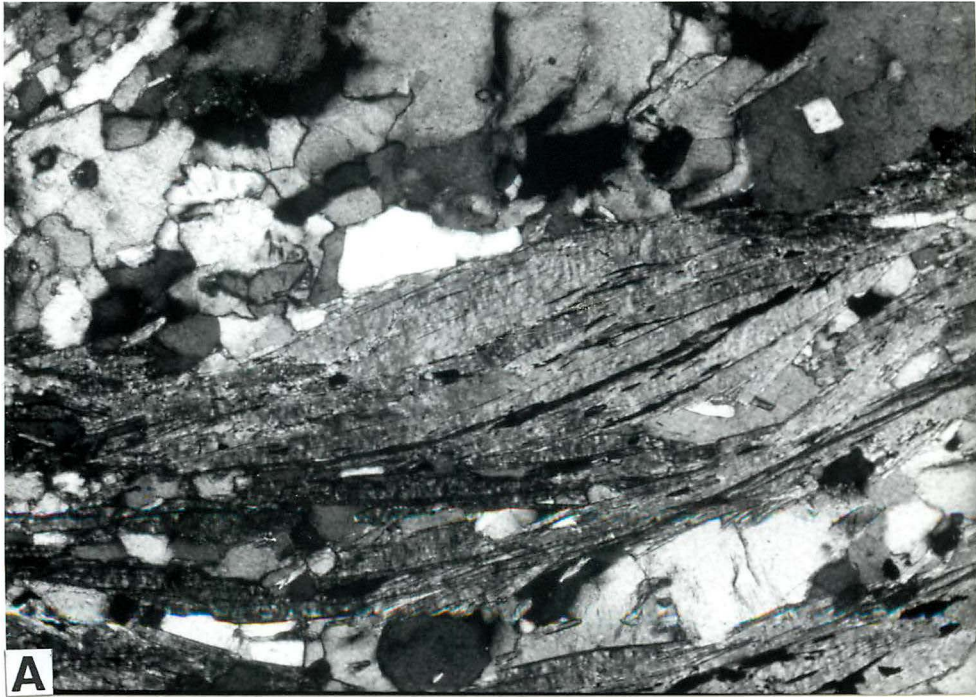
composed of fine-grained feldspar with individual grains measuring 0.2 mm or less across. White (1976) suggested that the centers of the porphyroclasts behaved as relatively rigid cores while the rims were soft, deforming into the wings on either side. In areas that presumably were deformed by a high strain rate, such as in the vicinity of the thrust faults, the cores are polycrystalline but remain coarse grained relative to the rims. Here, the cores become so flattened that, in hand sample, they are often difficult to distinguish from the wings.

Although C-surface mylonites are dominant in the Columbus Promontory, S-C fabrics are also common in the schists and biotite gneisses where mica content is high and optimal for the development for these fabrics. They are defined as textures that contain two foliations that formed at approximately the same time—S-surfaces, related to areas of accumulated finite strain, and C-surfaces, areas of high shear strain (Lister and Snoke, 1984). Two types S-C mylonites have been defined— type I, present mostly in rocks of granitic composition and type II, characterized by the presence of flame-shaped buttons of mica more commonly referred to as "buttons" or "mica fish" (Lister and Snoke, 1984; Hatcher, 1990). In the study area, both types of mylonites exist depending on the composition of the rock in which they exist. It is no surprise that the Henderson Gneiss, a granitic augen gneiss, is a type-I S-C mylonite (Fig. 3.7a). It has been classified as such because it contains two foliations, both of which appear to have formed at the same time and because feldspar, not mica, makes up the porphyroclasts. The entire Henderson Gneiss, however, is not characterized by type I S-C textures. In the biotite-rich pods where the porphyroblasts are composed of mica, type II textures are also present. Elsewhere, type II textures dominate in schist and in mica-rich parts of biotite gneiss, and granitoid gneiss (Fig. 3.7b). Mica fish are the most distinct feature in these schists and can be seen on the surfaces of the foliation as well as in sections cut parallel to the lineation.

BOUDINAGE

In the study area, two generations of boudinage occurred during D_2 and D_3. D_2 boudins are most common in granitoid and biotite gneiss, such as the Henderson Gneiss, where quartzofeldspathic layers were extended to form asymmetric boudinage. The neck lines are always oriented NW-SE so that the axis of extension (perpendicular to the neck lines) is parallel to the mineral lineation and further indicates that the lineation formed by transport. D_2 boudins are typically asymmetric and may be genetically related to the feldspar porphyroclasts in biotite and granitoid gneiss where the some of the porphyroclasts represent boudins. D_3 boudins are rarely asymmetric or slightly so, and the competent layer is nearly always granitoid gneiss (Fig. 3.8). This boudinage is most common in Poor Mountain Amphibolite but can also occur in Poor Mountain quartzite and biotite gneiss. Surprisingly, neither the quartzite layers in the amphibolites form boudinage nor do thin layers of amphibolite within the quartzites form boudinage or mullions. D_3 boudinage and folds, however, suggest that the rocks in the study area were beginning to acquire some degree of competency.

Only about 10 D_3 boudinage neck lines were measured because of their lack of three-dimensional exposure and paucity in the study area. Five of the boudins trend W or SW, parallel to D_2 lineations, revealing a paradox. While the mineral lineations predate the boudins, Hansen analysis of F_3 folds, which are coeval with the boudins, indicate that the shear direction did not change significantly between D_2 and D_3 deformation. Therefore, the boudins should be oriented normal to the lineations. Some boudins may have undergone rotation during simple shear or they may represent localized changes in the shear-direction. Such localized changes in shear-direction were present during D_2 deformation and are indicated by anomalous orientations of mineral lineations (Plate I). Complete resolution of

Figure 3.8. D3 boudin composed of granitic gneiss in Poor Mountain Amphibolite. In this case, the neck line is oriented NW-SE and plunge gently to the SE, nearly perpendicular to the mineral lineation. Photograph was taken at upper Youngs Creek, Lake Lure quadrangle.

this problem, however, may be impossible because of the paucity of D_3 boudinage within the study area.

<div align="center">FOLDS</div>

Rocks in the study area have undergone at least four episodes of folding, recognized on the microscopic, mesoscopic, and map scales (Table 3.1). These episodes can be distinguished from one another on the basis of geometry, the relationships with foliation, and fold interference patterns (Fig. 3.9). Of particular interest are the middle two episodes (F_2 and F_3) which are distinguished on the basis of their associated structural styles. The two episodes probably formed during different phases of the same period of metamorphism. They may also represent two stages of a single episode of deformation during which the rheological properties of the rocks changed, giving rise to the distinctive styles associated with each fold event. The possibility that these two events represent a single episode of deformation will be discussed later in this chapter.

F_1 **Folding.** F_1 folds are the earliest distinguishable folds in the study area, and they have only been recognized in the Poor Mountain Amphibolite. They are isoclinal and are difficult to recognize because they are premetamorphic and have been transposed by later deformation. They may also have similar geometries to later F_2 folds. F_1 folds have also been recognized in other parts of both the Piedmont (Hopson and Hatcher, 1988; Liu, 1991) and the Blue Ridge (Hatcher and Butler, 1979; Quinn, 1991). Liu (1991) and Quinn (1991) concluded these folds formed during the Penobscotian-Taconian orogeny. Like folds in other parts of the Blue Ridge and Piedmont, F_1 folds are highly variable in orientation due to overprinting by later folding. They have not been recognized at the map scale in the study area.

Figure 3.9. Selection of fold geometries commonly observed in the study area. The interpreted

fold generation that each geometry belongs to as well as any associated fabrics are

indicated on the drawings. A) occurs in Poor Mountain Amphibolite and was found

on Mike Mountain, Sugar Hill quadrangle. B) and C) were found in Poor Mountain

Amphibolite on the southeast ridge of Youngs Mountain, Lake Lure quadrangle. D)

was found in Poor Mountain Amphibolite on Grassy Mountain, Sugar Hill

quadrangle. E) occurs in Poor Mountain Quartzite with minor amphibolite and was

found in the Whitehouse community, Sugar Hill quadrangle. F) occurs in granitoid

gneiss in the upper Mill Spring complex and was found at Gringer Branch near

Montford Cove, Sugar Hill quadrangle.

(A)

(B) sheath fold

S₂

F₂

S₂

F₂?

F₃   F₃

1 cm

1 cm

(C) F₂

S₂

F₂

10 cm

F₄

(D)

F₃

F₃

F₃

S₂

F₂

S₂

1 cm

(E)

granite

quartzite and amphibolite

F₃

S₂ layering

F₃

1 m

(F) coarse-grained granitoid gneiss

S₂

fine-grained granitoid gneiss

coarse-grained granitoid gneiss

F₃

vein quartz

F₃

10 cm
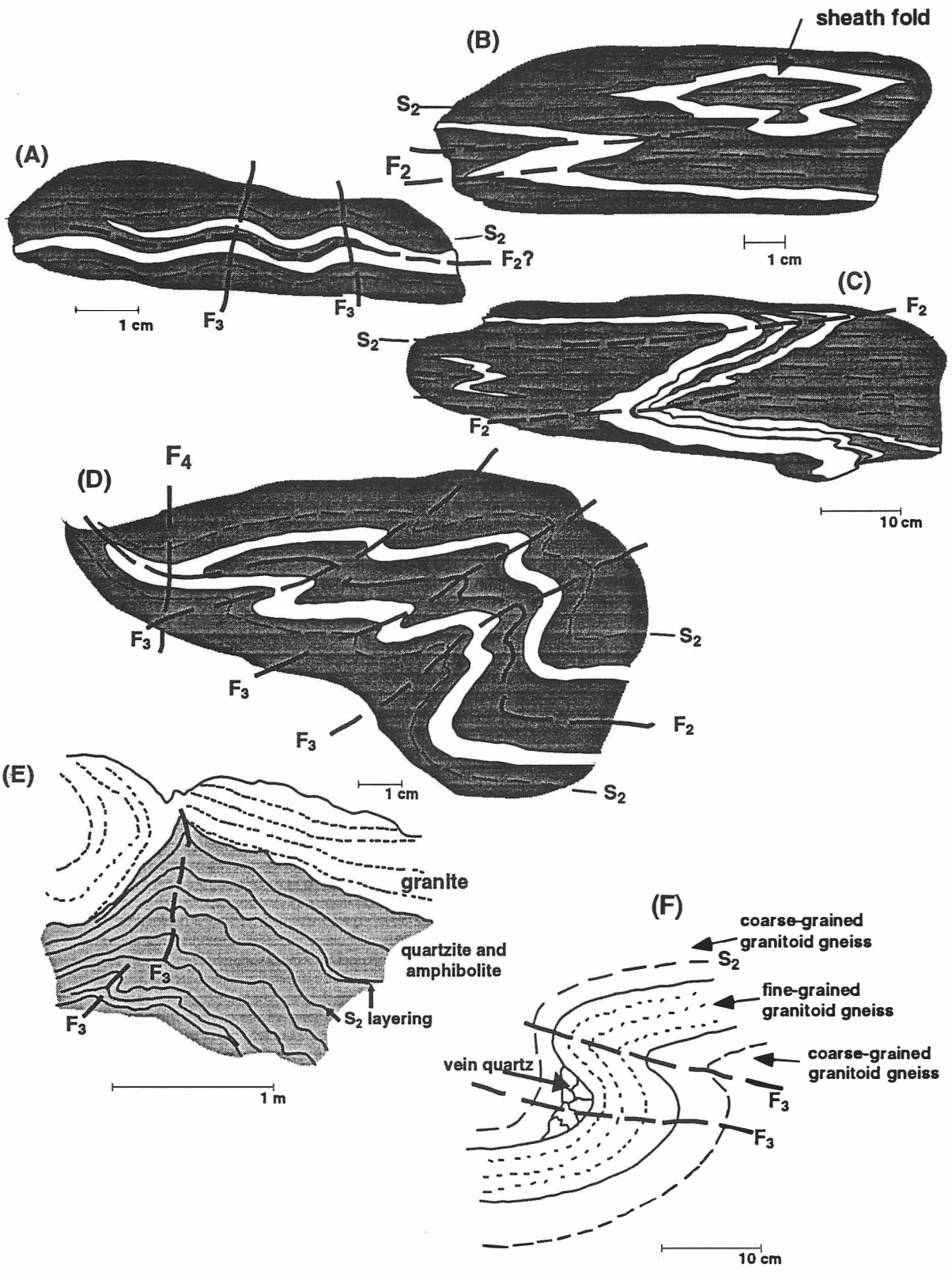
F$_2$ Folding. F$_2$ folds represent the dominant penetrative folding episode in the study area and can be recognized in all rock units on all scales. Most F$_2$ folds have an isoclinal geometry, are axial planar with the S$_2$ foliation, and are intrafolial (Fig. 3.9; Fig. 3.10). At the outcrop scale, most F$_2$ folds are characterized by cylindrical geometries but noncylindrical geometries do exist. Most of the noncylindrical folds are sheath folds whose limbs are typically oriented parallel to L$_2$ and verge WSW to SW. Sheath folds develop where gently bowed domes and basins in an initially cylindrical fold become amplified under conditions of high shear to form very acute, pointed structures (Cobbold and Quinquis, 1980). Ramsay and Huber (1987) defined them as folds with a hinge line variation of more than 90°. Skjernaa (1989) suggested a more rigorous definition where the hinge angle, ω, is less than 90° and an $x{:}y$ of the finite strain ellipsoid greater than 0.25 whereas a tubular fold, a tight sheath fold, has an $\omega < 20°$ and $x{:}y$ >1 (Fig. 3.11). Sheath folds are indicative of zones of high shear strain but do not necessarily indicate proximity to a shear zone (Ramsay and Huber, 1987), as is the case with rocks in the Inner Piedmont. Shear zones in the Columbus Promontory have been recognized as areas of relatively intense shearing (Davis, 1993a), but there is abundant evidence for intense, pervasive shearing including S-C fabrics and winged porphyroclasts. Sheath folds are further evidence that high shear strains were present in the Inner Piedmont during D$_2$ deformation.

Sheath folds are, in general, most common in rocks that appear to have some degree of competency contrast (Skjernaa, 1989), but can also occur where the folded layering has no rheological contrast with the surrounding matrix (Cobbold and Quinquis, 1980; Mies, 1993). The latter appears to be the case with the quartzofelspathic layers in the Poor Mountain Amphibolite where sheath folds are most commonly recognized. They have been also recognized in relatively homogenous rock by Davis (1993a). Therefore, these folded layers may only be indicators of passive flow in the rocks. The extent of sheath folds in the field area is difficult to assess because of the absence of three-dimensional exposure. They have

Figure 3.10. F$_2$ fold geometries: A) eye pattern in Poor Mountain amphibolite that is indicative of sheath folding. Photo was taken on the southeast ridge of Youngs Mountain, Lake Lure quadrangle. B) rootless intrafolial folds in Poor Mountain amphibolite. Photo was taken at same locality as (A). C) Same folds as (B) from a different angle showing three dimensional relationships. The strike of the left face is approximately parallel to the mineral lineation whereas the right face is nearly perpendicular. D) Transposed quartz vein in granitic gneiss of unit 2. Photo was taken in the Bills Creek Community, Lake Lure quadrangle. Photo was taken at Cove Creek near Anderson Shoal, Shingle Hollow quadrangle.

Figure 3.11. Diagram of a sheath fold showing its relationships with the principal strain axes, mineral lineation, and ω as defined by Skjernaa (1989).

Mineral lineation
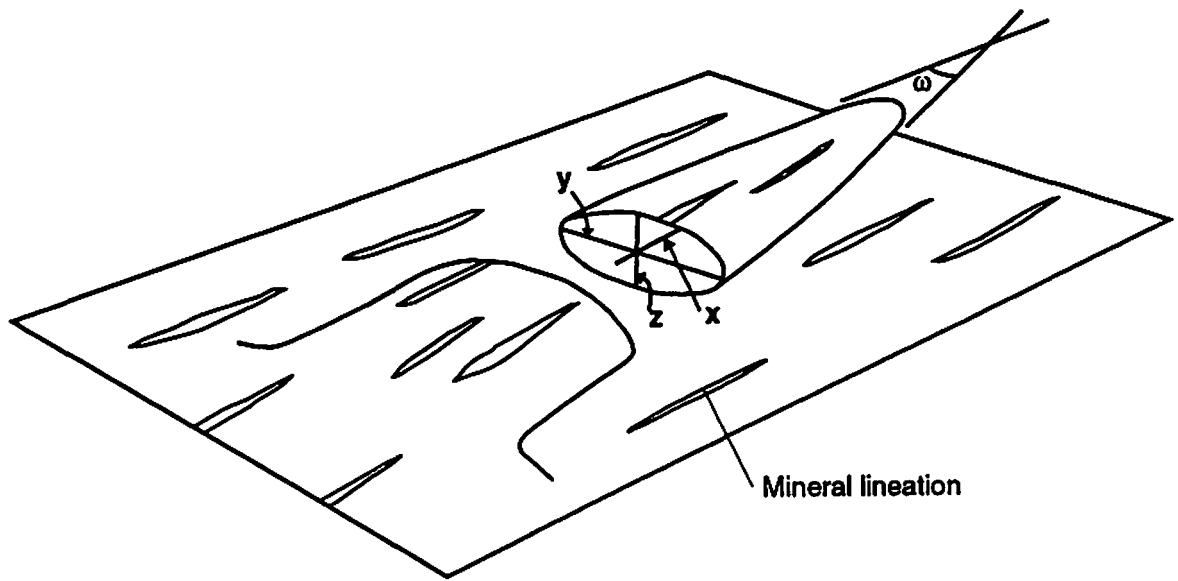
been only recognized at outcrop scale (Fig. 3.9B; Fig. 3.10A), but given the penetrative nature of D_2 structures and the high strains involved with its deformation, it is likely that sheath folds are penetrative at all scales. Complex outcrop patterns in the Chauga belt also indicate that sheath folds may be present at the map-scale. If this is the case, then most cylindrical isoclinal recumbent F_2 folds may represent the limbs of large-scale sheath folds.

The profile of F_2 folds in two-dimensional exposures indicate very small interlimb angles that formed under conditions of high shear strain. In general, however, it was difficult to ascertain the three-dimensional geometry of the sheath folds and therefore, was virtually impossible to measure the parameters outlined by Skjernaa (1989). Evidence for the existence of these folds consists of elongated bull's-eye and arrowhead sections, as well as folds with very small interlimb angles (Fig. 3.10a). Such patterns can be easily confused with type 1 fold interference patterns or dome-and-basin structures in folds created by inhomogeneities during a single folding event. Many folds, however, also have sections parallel and perpendicular to the mineral lineations are exposed. In sections perpendicular to the lineation, a bull's-eye pattern can be observed, whereas in sections parallel to the lineation, an elongate fold with a narrow interlimb angle appears. These exposures are consistent with a sheath fold geometry rather than fold interference patterns (Fig. 3.10C; Fig. 3.12).

Many folds also have a fold-nappe-style geometry where parasitic folds on the limbs verge in opposite directions and have variable axial-planar orientations (Ramsay, 1981; Ramsay and Huber, 1987). Good examples most commonly occur in granitoid and biotite gneiss and more rarely in the Henderson Gneiss and Poor Mountain Amphibolite.

F_2 folds have been recognized in all lithologies in the study area but are most easily recognized in rocks with compositional layering such as the Poor Mountain Amphibolite and the banded gneisses. Two types of F_2 folds have been recognized based on their relationships with the S_2 foliation: intrafolial folds and ordinary folds (folds that deform the foliation). Both fold types are penetrative, are isoclinal recumbent, and have hinge lines that are

Figure 3.12. Schematic block diagram showing typical relationships between F_2 folds, L_2, and S_2. These relationships are consistent with a sheath fold geometry for most F_2 folds.

S$_2$ foliation surface

L$_2$
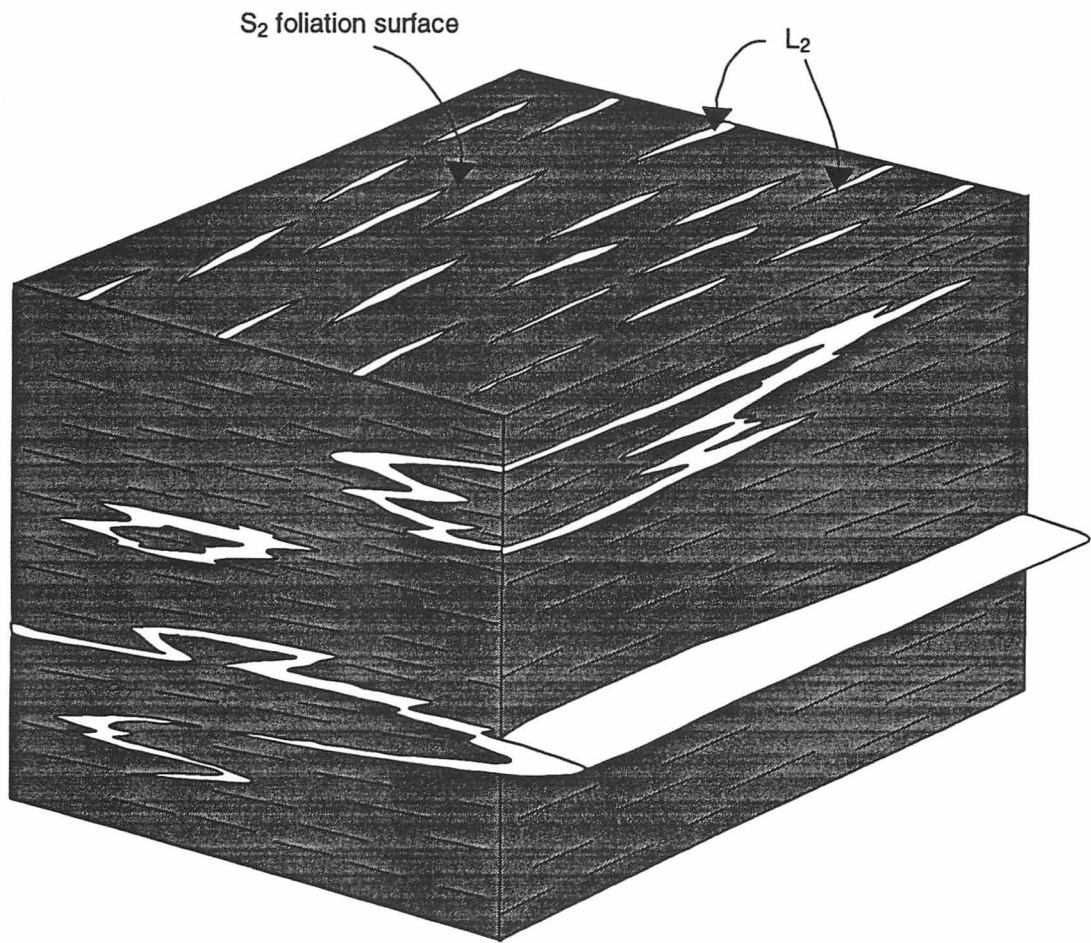
typically oriented parallel to the L_2 mineral lineation. These relationships suggest that both fold types are coeval with other D_2 structures and should not be classified as separate fold generations.

Davis (1993a) suggested that most F_2 folds represent an artifact of high shear strains within the S_2 foliation and are the result of perturbations within the shear plane. These folds probably formed by a process similar to that described by Cobbold and Quinquis (1980) where the perturbations within the shear plane are passively amplified to produce sheath folds. Under continued shearing, the limbs of the sheath folds will approach parallelism with the shear direction. Most F_2 folds, which are highly cylindrical at the outcrop scale and parallel the L_2 mineral lineation, may represent the limbs of sheath folds whose axial culminations remain unexposed (Fig. 3.12). These relationships suggest that rocks in the Columbus Promontory probably underwent very high shear strains ($\gamma >> 10$) in order for the limbs of the sheath folds to approach parallelism with L_2. Similar relationships between sheath folds and cylindrical isoclinal folds were also described by Bryant and Reed (1970), Carreras and others (1977), Evans and White (1984), Maneilly and Storey (1986), Mies (1991, 1992, 1993), and Davis (1993a).

F_3 folding. While F_2 folds were created by passive flow processes, F_3 folds appear to have formed by flexural flow. Rocks were probably cooling by this time and a competency contrast was developing between adjacent layers. F_3 folds differ from F_2 folds in two main respects: (1) F_3 folds deform the foliation, unlike most F_2 folds, which are typically intrafolial; (2) the folded layers in F_3 folds tend maintain original thicknesses around the hinges and limbs whereas F_2 folds have thickened hinges and attenuated limbs. Many F_3 folds also include chevron folds and crenulations in the schists. A weak, nonpenetrative fabric composed of sericite has been observed in the hinge regions of some F_3 folds. This fabric and general

characteristics of F3 folds are consistent with observations made by Griffin (1967, 1969, 1974), Hatcher (1969, 1978), Hopson and Hatcher (1988) and Liu (1991).

F3 folds vary from tight to closed, and from nearly-isoclinal recumbent to open, nearly upright (Fig. 3.9 and Fig. 3.13). Occasionally they interfere with one another resulting in type 3 interference patterns (Fig. 3.13d; Ramsay, 1962; Ramsay, 1967; Thiessen and Means, 1980). Furthermore, relationships between F3 folds and S2 layering suggest that tight, gently inclined folds formed under ductile conditions whereas open upright folds formed in relatively competent rock. These observations suggest a relationship between the relative age of the F3 fold and its geometry as defined by the orientation of the axial surface and interlimb angle— the more gently inclined and tighter the fold is, the older it is. This relationship, however, does not apply to F2 folds since virtually all of them have identical geometries.

The wide range of geometry and orientation displayed by F3 folds reflects the relatively low shear strains sustained during D3 deformation, and gradually decreasing temperatures, which increased the competency contrast between different rock layers. Folds were probably nucleating continuously throughout D3 deformation. Under continued shearing, the geometries of these folds were modified toward smaller interlimb angles and more gently-dipping axial planes. The low shear strains involved with D3 deformation, however, did not allow F3 folds to take on similar forms and orientations as F2 folds. Therefore, the wide variety of geometry of F3 folds represents folds frozen in various stages of development under varying degrees of shear strain. This interpretation is consistent with the observation that older folds tend to be tight to closed and recumbent whereas older folds are open to gentle and steeply inclined.

F4 Folding. The last fold event identified in the study area involved open to gentle upright folding. These folds are typically symmetric, are widely distributed, and typically appear as gentle undulations in the foliation. Because these folds usually have large interlimb angles

Figure 3.13. Photographs of F3 folds: A) three-dimensional exposure of a recumbent fold in Poor

Mountain Quartzite. The actual fold is the second wrinkle seen below the

hammer. The fold deforms the D_2 foliation, the surface of which is exposed in

this picture. The bulge behind the fold (hammer) crosscuts the foliation and is not

a fold. Photo was taken near junction of Rts. 1336 and 1008, Lake Lure quadrangle.

B) Folded layering in Mill Spring biotite gneiss. Width of the photograph is

approximately 2 m. Photo was taken on I-26 at the Saluda exit, Cliffield

Mountain quadrangle. C) Folds in Poor Mountain Quartzite and Amphibolite

related to the boudinage of granitic gneiss just outside the field of view. Photo was

taken near the junction of County Routes 1008 and 1001, Sugar Hill quadrangle. D)

Interference patterns of recumbent and upright folds in Poor Mountain

Amphibolite. The interference patterns clearly show that the upright folds

postdate recumbent folds. Sample was found on Harris Mountain, Sugar Hill

quadrangle.

and are widely scattered, their overall effect on the orientation of previous structures, such as the S_2 foliation, is minimal (Fig. 3.2). Based on map patterns, field observations, and stereonet analysis, the axes trend N-S to NE-SW, have steep to subvertical axial planes, and are not associated with a penetrative fabric. The interplay of topography and F_2 folding makes recognition of F_4 folds difficult at map scale. With their upright geometry and gentle interlimb angles, however, they are easily recognizable in cross-section (Plate 2). Because these folds are oriented parallel to subparallel to most F_2 and F_3 folds, it is possible that they may have formed shortly after D_3 deformation under the same orientation of the strain ellipsoid, but fabric relationships reveal no evidence for its absolute timing.

Other fold sets have been recognized in the Inner Piedmont in South Carolina and northeast Georgia. Hopson and Hatcher (1988) and Liu (1991), for example recognized two late postmetamorphic fold sets that are both similar in geometry to F_4 folding in the study area. The two fold sets, designated as F_4 and F_5 in northeast Georgia, however, have fold axes that intersect nearly at right angles and interfere with one another resulting in type 1 dome-and-basin patterns. F_5 folds, however, have not been recognized in the Columbus Promontory.

STRUCTURAL ANALYSIS OF F_2 AND F_3 FOLDS

Structural analysis of folds focused mostly on F_2 and F_3 folds because limited data precluded such analysis of F_1 and F_4 folds. Stereonet analysis of foliations reveals some scattering and indistinct girdle patterns, but, in general, indicates that post-F_2 deformation was insignificant in reorienting the S_2 foliation (Fig. 3.2). This conclusion is supported by the observation that F_3 and F_4 folds are widely distributed, by stereonet analysis of lineations which reveals little scatter or the distinctive patterns indicative of post-F_2 folding, and by map patterns where evidence for post-F_2 folding is present but widely scattered. Intrafolial

F_2 folds formed coeval with the dominant foliation and did not alter orientation of the C-fabric. Ordinary F_2 folds could significantly alter the orientation of the foliation but they are typically isoclinal and are parallel axial planar with the foliation. Consequently, the foliation on the limbs of these folds are usually parallel to the undeformed foliation.

Fold Axes and Axial Planes. Data used for stereonet analysis of folds were subdivided into fold axes and axial surfaces (Fig. 3.14). These data were further subdivided into F_2 and F_3 subsets and reveal a number of differences as well as similarities between the two generations. Analysis of the fold axes shows, for both fold events, that they define a girdle that approximates the orientation of the S_2 foliation (Fig. 3.14). Most F_2 folds trend ESE to NE, roughly parallel to the mineral lineation, with the greatest concentration of axes oriented ENE. Many of the folds that do not trend ESE to NE commonly occur in areas where the mineral lineation trends have anomalous trends. This contrasts with F_3 folds which exhibit large deviations from the NE to ENE arc and the best-fit great circle. The F_3 best-fit great circle, however, is parallel to the F_2 best fit great circle and S_2. While most F_3 folds also trend ESE to NE, orientations are, in general, more dispersed than F_2 folds.

Equal area plots of axial surfaces also indicate similarities as well as differences (Fig. 3.14). F_2 folds and F_3 folds to a lesser extent, reveal a bull's-eye pattern that defines a plane striking NE and dipping gently SW, virtually coplanar with the orientation of the dominant foliation (Fig. 3.14). F_3 axial surfaces reveal considerably more scatter, as they did in plots of fold axes. Most poles that cluster around the bull's-eye are axial surfaces of folds define recumbent, closed to tight folds, whereas most poles that are scattered elsewhere define the steeply-dipping axial surfaces of the more open, upright folds.

Plots of fold axes for the two fold phases indicate nearly identical orientations for the fold girdle and similarly for both fold phases, plots of axial surfaces yield roughly the same bull's-eye pattern (Fig. 3.14). This consistency indicates that the regional strain field did not

Figure 3.14. Lower-hemisphere, equal-area plots of fold axes and poles to fold axial

surfaces. Plots include the best-fit great circle for fold axes and the mean

plane of poles to axial surfaces and its pole (black great circles), and the best-

fit great circle for the foliations (gray circles). Additional unpublished data

provided by Christopher Jayne.

hinge lines

axial surfaces

N

N

F₂ folds

N=50

N=41

F₃ folds

N=43

N=37

F₂ and
F₃ folds

N=117

N=92
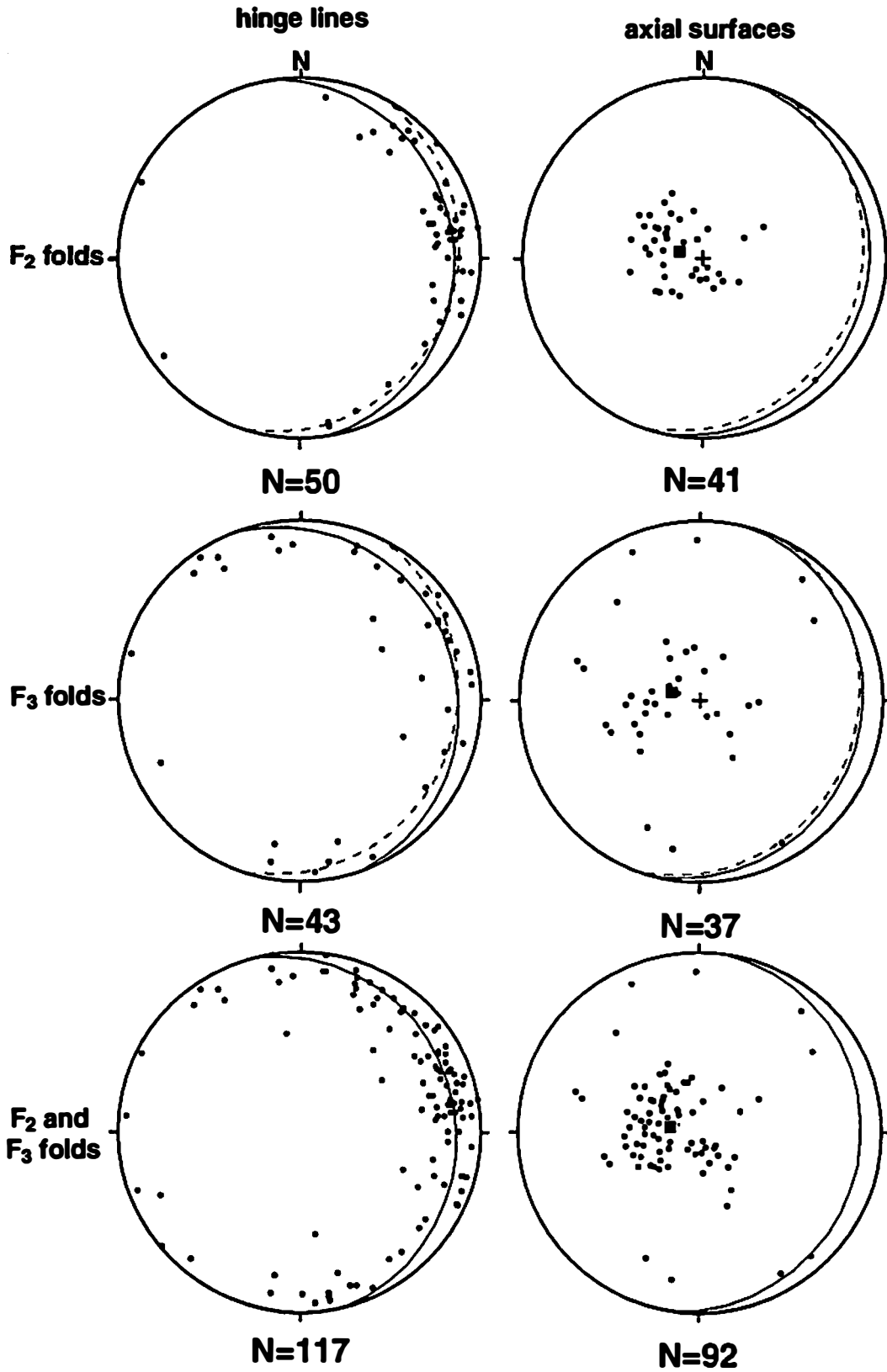
change appreciably between formation of F_2 and F_3 folds. On the other hand, the axes of F_3 folds are considerably more scattered than F_2 folds indicating a difference in fold mechanisms for each generation (Fig. 3.14). This scatter confirms field observations that the total shear strain during F_3 folding was significantly less than that during F_2 folding and thus, resulted in incomplete rotation of the axes into parallelism with the mineral lineation. Likewise, axial surfaces were probably oriented vertically when the folds first nucleated, and subsequently rotated during progressive simple shear into parallelism with the shear plane and S_2. All F_2 axial surfaces are parallel to subparallel with the S_2 foliation but many F_3 axial surfaces dip at a high angle to S_2. Again, this variation in geometry suggests incomplete rotation of the axial surfaces into parallelism with S_2 as a result of decreasing shear strains during D_3 deformation.

Hansen Analysis of Folds. Equal-area plots of the axes and axial surfaces (Fig. 3.14) have suggested that F_2 and F_3 folds in the study area formed at roughly the same time or, at least, the regional stain field did not significantly change throughout the evolution of F_2 and F_3 folds. The Hansen method uses the vergence of these folds to estimate the regional slip-line direction (Hansen, 1971). The slip-line direction is produced by the relative motion of two reference points in successive layers during deformation (Hatcher, 1990). The L_2 transport lineation is an example of a structure indicating slip-line direction. Slip lines may also be imaginary lines that can be determined from fold vergence (Hatcher, 1990). The vergence of an asymmetric fold was defined by McClay (1987) as the horizontal direction of movement of the upper component of a fold relative to the lower component, or direction of overturning (Hatcher, 1990). The vergence of asymmetric folds can serve as a shear sense indicator (Marshak and Mitra, 1988), but in the study area and many other parts of the Appalachians, axial orientations vary as much as 180° in the same plane making such interpretations ambiguous. Furthermore, folds may verge in opposite directions, even in the same outcrop.

These relationships are probably related to noncylindrical folding (sheath folding). The Hansen method links all these seemingly random folds to determine the slip-line direction during fold development. Imagine, for example, a thrust sheet that dips east where asymmetric folds developed within the sheet as a result of west-directed shearing. Folds that develop first will have either a northerly or southerly trend. With continued shearing, northerly trending folds will rotate counterclockwise, whereas southerly trending folds will rotate clockwise (note that vergence is always described with a down-plunge view). Plotted on an equal-area net, the fold hinges plot along a great circle that approximates the orientation of the thrust fault. This great circle can be separated into two domains of clockwise and counterclockwise folds separated by a narrow gap. The gap between these two fields is called the separation arc and the slip line or transport direction of the thrust fault lies within this arc.

About 75 folds were measured in the study area plus an additional 20 in the area immediately south by C. Jayne. Of these, the vergence of about 50 could be determined in the field. While abundant evidence for sheath folding was observed in the study area, only one had sufficient 3-dimensional exposure for measurement of its axes and vergence. Another was measured to the south in areas mapped by Davis. Sheath folds are useful for this analysis because they yield the exact direction of shear and, therefore, should plot within the separation arc given by the analysis. All the data were plotted on one equal area projection, then subdivided and plotted by fold generation (Fig. 3.15).

Hansen analysis of all folds shows considerable overlap of the two fields of clockwise and counterclockwise folds revealing a wide zone of overlap (overlap arc) of about 40° within which the separation arc occurs. The range of orientations of the overlap arc corresponds with the range of transport directions exhibited by other shear-sense indicators and the mineral lineations which yield a W to SW directed transport. The two sheath folds also plot within the overlap arc. When the data are subdivided into F_2 and F_3 fold sets, little difference is

Figure 3.15. Lower-hemisphere, equal-area projections of F_2 and F_3 fold axes and their vergences (indicated by the clockwise or counterclockwise arcs). The arrows indicate the orientation and vergence of two sheath folds, one measured in the study area, the other measured by T. L. Davis. Like Figs. 3.12 and 3.13, the data have been subdivided by fold generation and are shown in the top two diagrams (A and B). The lower diagram is a compilation of all folds (C). Additional unpublished data provided by Christopher Jayne.

(A) F₂ FOLDS

OVERLAP ARC

N = 31

(B) F₃ FOLDS

OVERLAP ARC

N = 20

(C) ALL FOLDS

OVERLAP ARC

N = 51
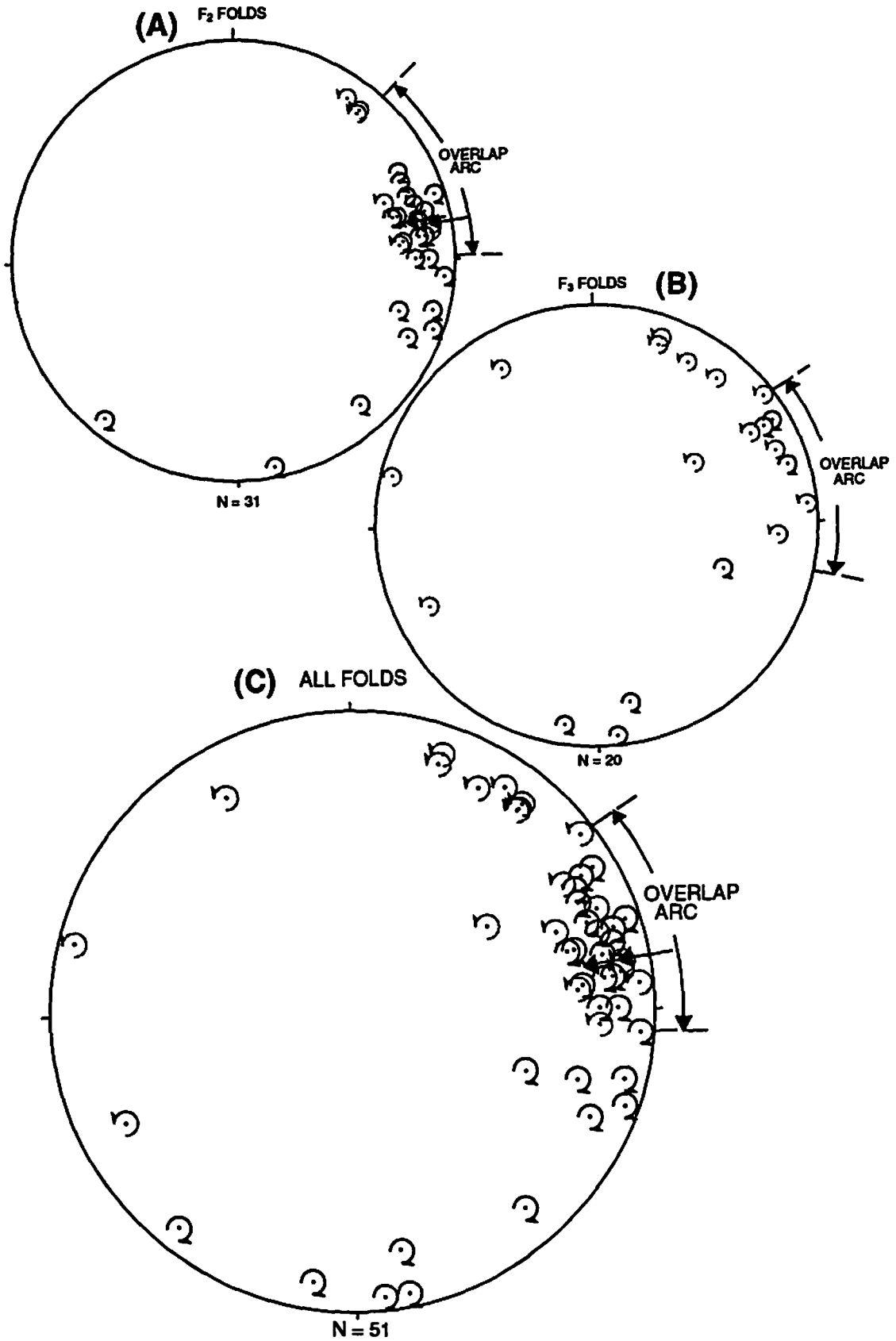
evident between the two generations indicating that transport directions did not change significantly between D_2 and D_3 deformation. This evidence, along with fabric evidence discussed earlier, suggests that D_2 and D_3 may represent a single continuous episode of deformation.

A limitation of the application of the Hansen method in the study area is that it cannot resolve whether shearing was W-directed in the southeastern parts of the study area and SW-directed in the NW part, which is indicated by the mineral lineations and other shear sense indicators. Subdivision of data sets into SE and NW domains for each fold generation may resolve this ambiguity but the size of the data sets would be too small for this analysis. In addition, F_3 folds are very rare toward the southeast, making such an analysis nearly impossible.

MACROSCOPIC STRUCTURES

Large-scale relationships in the Columbus Promontory were studied using geologic maps and cross sections. Cliff exposures and quarries outside the study area also provided insight into large-scale relationships. Geologic mapping was conducted at a scale of 1: 24,000 and about 1,700 field stations were recorded in a 180 km^2 (70 mi^2) area, an area slightly larger than a quadrangle at this latitude (Plate I). Two cross sections were also constructed along NW-SE lines, roughly perpendicular to strike (Plate II). Plate III is a compilation of data collected in the Lake Lure quadrangle for this study and data collected by Davis, Tabor, and Lemmon and Dunn (Davis, 1993a).

Both the map (Plate I) and the cross sections (Plate II) show the dominance of D_2 deformation over the orientation of the contacts and thrust faults. This dominance is indicated by the parallel orientation of the lithologic contacts, thrust faults, and axial surfaces of F_2 folds. While the lithologic contacts have been isoclinally folded, the faults

remain relatively planar, suggesting they postdate F_2 folding. Fabric relationships within the faults, however, suggest that thrusting is contemporary with F_2 folding. Such folding appears to be intimately related to faulting, especially along the Sugarloaf Mountain thrust. Here, the lower limb of a map-scale F_2 antiform has been stretched out along the fault (Plates I and II). This relationship is common among thrust sheets that form in ductile terranes (e.g., Milnes and Pfiffner, 1977; Dennis and others, 1981; Ramsay, 1981) and were termed tectonic slides by Fleuty (1964), type 3 thrust sheets by Hatcher and Williams (1986), and type F thrust sheets by Hatcher and Hooper (1991). Type F thrust sheets are characterized by penetrative ductile deformation and occur within the high-grade core of the orogen (Hatcher and Hooper, 1991). These are characteristics typical of the Inner Piedmont in the Columbus Promontory.

Recognition of map-scale F_2 folds is controlled by the occurrence of rock units of contrasting lithology. They are best-recognized in unit 2 where such units occur. Contrasting lithologies are also present in unit 3 but the complex outcrop-scale interlayering of these lithologies makes resolution of map-scale relationships impossible. The homogeneity of rocks in unit 1 also makes recognition of map-scale F_2 folds nearly impossible, but outcrop patterns of the 438 Ma (Odom and Russell, 1975) granitoid gneiss within the Henderson Gneiss (Lemmon, 1973) and recognition of F_2 folds on the scale of 10's to 100's of meters in quarries and cliff exposures outside the study area (Fig. 3.16) suggests that map-scale F_2 folds are present in unit 1.

Recognition of sheath folds at the map scale is enigmatic because patterns characteristic of sheath folds can be confused with stratigraphic variations or fold interference patterns. The widely distributed bodies of biotite-rich Henderson Gneiss located near the Sugarloaf Mountain fault, for example, may either represent sheath folds or variations in the composition of the protolith. In the southern part of the study area, thin (<10 m) layers of Poor Mountain Amphibolite appear within the upper Mill Spring complex. Like the biotite-

.

Figure 3.16. Large-scale folds in the Henderson Gneiss. The light-colored layers are younger

intrusions of pegmatite and granite whereas the dark rock is Henderson Gneiss.

Approximate width of the photograph is about 75 m and was taken at a quarry in

Hendersonville, Hendersonville quadrangle.

rich pods in the Henderson Gneiss, it is not clear if these layers of amphibolite represent sheath or isoclinal folding or if they are protolithic. The geometry and orientation of map-scale isoclinal folds, however, are consistent with a sheath fold geometry. They indicate the presence of WSW to SW-trending sheath folds and based on outcrop-scale shear-sense indicators, they probably verge to the SW.

Post-D_2 folding at the map-scale is recognized by broad warps and swales of the thrust sheets in cross-section (Plate II). They are more difficult to recognize on the map because of the expression of the low fault dip on the topography (Plate I). Most post-D_2 folds are probably F_4 folds because they have large interlimb angles (>120°) and are upright to steeply inclined, but some folds with smaller interlimb angles (Plate II) may represent F_3 folds. The broad dome-and-basin patterns created by the interference of F_4 and F_5 folds in northwestern South Carolina and northeastern Georgia (Hopson and Hatcher, 1988; Liu, 1991) have not been recognized in the Columbus Promontory. Both the map and the cross sections show that post-D_2 deformation was relatively minor and was insignificant in reorienting earlier structures. This observation is supported by equal-area plots of D_2 structures such as foliations, lineations, and folds (Figs. 3.2, 3.3, and 3.14). These plots show only minor scatter due to later deformation.

RELATIONSHIPS BETWEEN D_2 AND D_3 STRUCTURES

Figure 3.17a is a schematic diagram that shows the wide variety of D_2 structures and the control of lithology over their presence. Several relationships among these structures warrant discussion. As the diagram shows, the sheath fold at the top of the diagram and the recumbent fold at the bottom appear to verge in different directions. The tubular element of sheath folds, however, may be conceptually thought of as two cylindrical, isoclinal folds joined together at the limbs (Mies, 1993). By this analogy, the two folds therefore have

Figure 3.17. Block diagrams showing relationships of D_2 (A) and D_3 (B) structures with the strain ellipsoid in the study area. Shear direction for both generations is from left to right parallel to the X axis of the strain ellipsoid. (A) The numbers to the left of D_2 diagram indicates the following lithologies and associated structures: 1— mica schist containing S-C fabrics, 2— granitic augen gneiss containing sigmoid porphyroclasts, and 3— amphibolite and biotite gneiss which often contain intrafolial isoclinal recumbent folds. The foliations and lineations are present in all lithologies, including quartzite and metagraywacke (not shown). Sheath folds are also common in amphibolite and biotite gneiss. (B) D_3 structures, shown on the right, include recumbent folding, shown here, as well as upright folding. Note also that D_2 foliations and lineations, shown in this diagram, were being passively deformed during D_3. The sheath fold terminology in (A) is from Mies (1992, 1993).

(A)

S₂ C-fabric surface
L₂ lineation
tubular element
cap
sheath fold

(B)
L₂ lineation
S₂ foliation surface
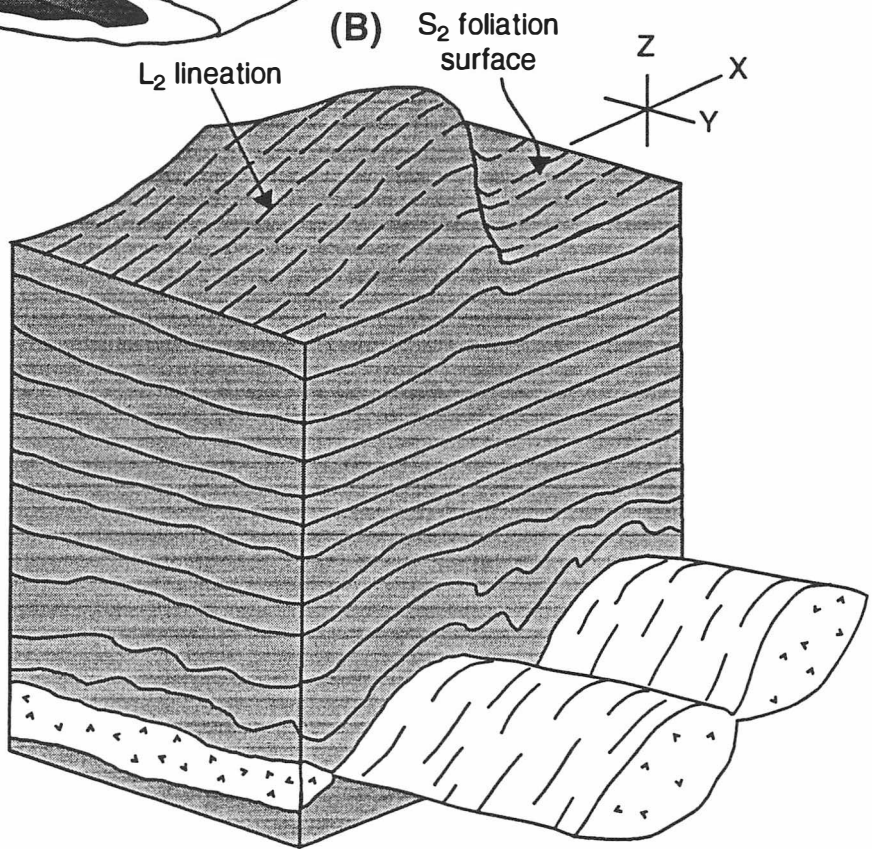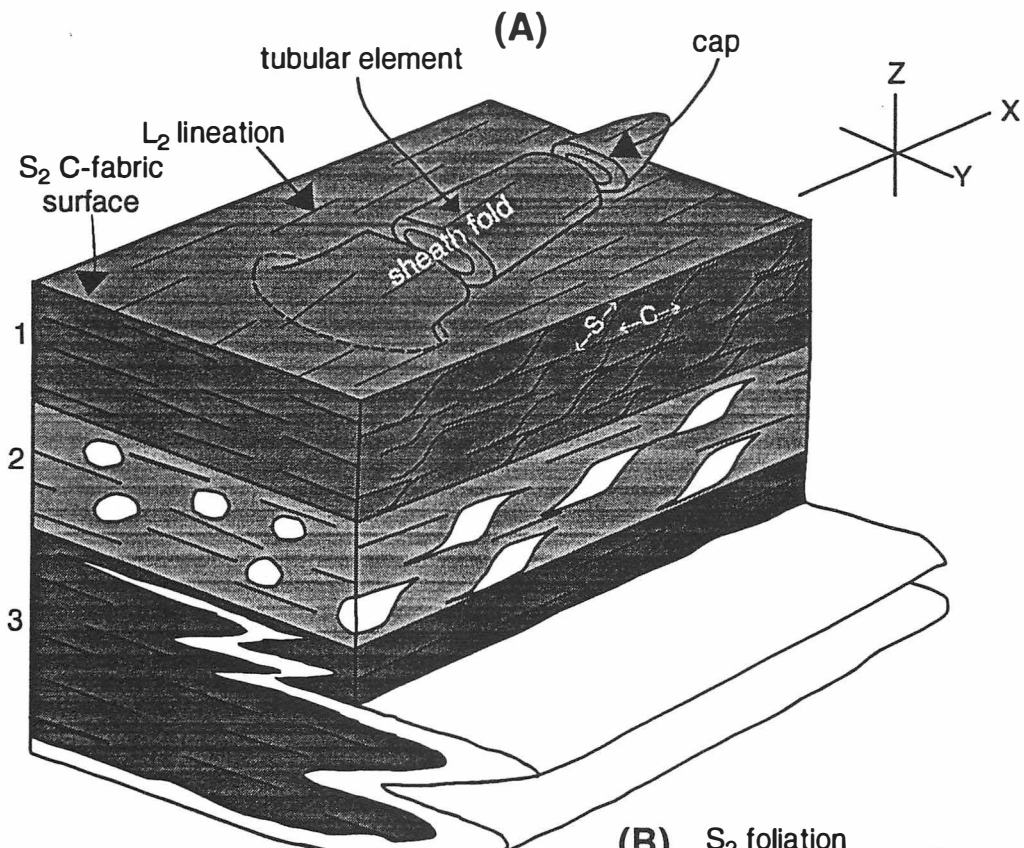
similar vergence. Many F_2 isoclines probably represent the limbs of larger-scale sheath folds. Caps of sheath folds, using the terminology of Mies (1992, 1993; see also Figure 3.17), were never observed in the Columbus Promontory, probably because these parts represent a volumetrically small part of the fold. Tubular elements of some folds are exposed in the premetamorphic Tumblebug Creek fault southwest of the study area. Estimated values of ω (see Fig. 3.11) from these tubular elements are very small and suggest that very high shear strains, probably greater than 50 based on computer modeling by Mies (1993), were involved with D_2 deformation.

The presence of S-C fabrics (Lister and Snoke, 1984) indicates that deformation in the Columbus Promontory was characterized by noncoaxial-laminar flow (Davis, 1993a). Furthermore, the presence of this fabric as well as sheath folds and intrafolial isoclinal folds strongly suggests that progressive heterogeneous simple shear was the dominant deformation process (Lister and Snoke, 1984; Mies, 1991, 1993). Simple shear was probably also an important process during D_3 deformation, but the absence of S-C fabrics, sheath folds, and other fabrics makes this interpretation more ambiguous.

Textural relationships between D_2 and D_3 indicate that they represent early and late phases of a single continuous episode of deformation. Evidence includes F_3 folds growing by progression after F_2 folds in South Carolina (Liu, 1991), and the similarity in geometry and orientation between older F_3 folds and younger F_2 folds. Furthermore, most F_3 folds, based on their relationship with the S_2 foliation, formed under highly ductile conditions, suggesting that these folds formed during the waning stages of M_2 metamorphism. An alternative interpretation is that these folds formed during a separate metamorphic event (M_3?). An indistinct fabric composed of chlorite and sericite (Hopson and Hatcher, 1988) can be found in the hinges of many F_3 folds but these minerals are interpreted to represent a retrograde assemblage that formed along the same P-T path as M_2 metamorphism (Davis, 1993a). A still later episode of chlorite-grade metamorphism (Lemmon, 1973; Sinha and others, 1988;

Vauchez and Brunel, 1988) also occurred, but the associated minerals in the study area tend to be randomly oriented and appear to have no involvement with D_3 deformation.

Equal-area plots of F_2 and F_3 folds also provide strong evidence for a link between D_2 and D_3 deformation. The hinge lines of both fold generations plot along a great circle that approximates the orientation of the S_2 foliation (Fig. 3.11). Plots of the axial surfaces also indicate that the majority of F_2 and F_3 folds are parallel axial planar to the foliation. Mies (1991) suggested that such relationships between folds and foliation may indicate a coeval origin. Textural relationships confirm that F_2 folds and the S_2 foliation are contemporary, but that F_3 folds postdate S_2. The parallelism between the great circle defined by F_3 hinge lines, the axial surfaces, and the S_2 foliation, however, suggests that the orientation of the strain ellipsoid did not change significantly between D_2 and D_3 deformation. This interpretation is further supported by Hansen analysis of F_2 and F_3 folds which indicates that transport directions remained W to SW-directed during D_2 and D_3. Therefore, I conclude that D_2 and D_3 represent two phases of a single deformation event during which rheological properties of the rocks changed as a result of gradual cooling following peak-M_2 metamorphism.

Tabor and others (1990) argued that the change in shear sense from W to SW-directed transport represented two distinct episodes of movement. Davis (1993a), however, proposed that W-SW-directed transport and emplacement of thrust sheets occurred coevally at upper amphibolite facies. This change in shear sense was interpreted by Davis (1993a) to result from partitioned, SW-directed orogen-parallel displacement along the primordial Brevard fault zone and Chauga belt and W-directed orgen oblique to origin parallel deformation in the Inner Piedmont. In the study area, all mineral lineations and kinematic indicators, regardless of orientation, are defined by minerals associated with middle to upper amphibolite facies metamorphism storngly suggesting a contemporary origin for both W and SW-directed transport. Hansen analysis also suggests that these movement directions occurred coevally throughout D_2 and D_3 deformation (Yanagihara, 1993).

Davis (1993b) has suggested that the thrust sheets were stacked in a foreland to hinterland progression (northwest to southeast). In the study area, the Sugarloaf Mountain and Mill Spring faults are both D_2 faults that contain middle to upper amphibolite facies mineral assemblages, and have fabrics indicating high shear strains under ductile conditions. This indicates that both faults were active at the same time relative to peak M_1 metamorphism and do support the interpretations of Davis (1993b). It should be emphasized, however, that the Sugarloaf Mountain and Mill Spring faults are adjacent faults and more accurate assessment of their relative timing of emplacement is virtually impossible to assess.

Outside the study area, cross-cutting relationships indicate that the Tumblebug Creek fault, the northwesternmost fault in the Columbus Promontory above the Brevard fault zone, formed before the Sugarloaf Mountain and Mill Spring faults. Similarly, the Stumphouse Mountain fault, the northwesternmost fault in the Inner Piedmont of South Carolina, was isoclinally folded during D_2 deformation and is interpreted to be correlative with the Tumblebug Creek fault (Liu, 1991; Davis, 1993aa). In northeastern Georgia and South Carolina, retrograde mineral assemblages and textures, and cross cutting relationships indicate that the Toccoa Falls-Shorts Mill fault emplaced the Alto Allochthon during D_3 deformation and subsequent to the metamorphic peak (Hopson and Hatcher, 1988). The Alto Allochthon probably represents a klippe of the Six Mile thrust sheet of Griffin (1967, 1969, 1971a), exposed farther to the southeast (Nelson, 1985; Hopson and Hatcher, 1988). This fault is the southeasternmost, structurally highest fault mapped in the Inner Piedmont of South Carolina (Griffin, 1974). These relationships support an interpretation for a foreland to hinterland stacking order for the Inner Piedmont whose earliest discernable thrusting occurred during early D_2 deformation (D_{2a}) prior to peak M_1 metamorphism with emplacement of the Tumblebug Creek and Stumphouse Mountain thrust sheets. The latest recognized thrusting event involved emplacement of the Six Mile nappe (Griffin, 1969, 1974), and the Alto Allochthon (Hopson and Hatcher, 1988) subsequent to the metamorphic peak during D_3

deformation. The Sugarloaf Mountain, Mill Spring, and Cedar Creek faults were all active during D_2 deformation and peak M_1 metamorphism after emplacement of the Tumblebug Creek and Stumphouse Mountain thrust sheets, but before emplacement of the Six Mile nappe.

STRUCTURAL RELATIONSHIPS SOUTH OF THE STUDY AREA

Structural relationships observed in the study area, in general, coincide with those observed by others working SW of the study area. Griffin (1967, 1971a, 1971b, 1974) first recognized the dominance of recumbent folding (which he designated F_1), and later open, upright folding (F_2), but failed to recognize that the two geometries could be subdivided into several constituent generations (Table 3.2). Hatcher (1978), Hatcher and Butler (1979), Hopson and Hatcher (1988), Liu (1991), and Davis (1993a) each recognized at least five episodes of folding including two episodes of isoclinal, recumbent folding (Table 3.2). In the case of Hopson and Hatcher (1988), D_1 and D_2 are identical in their characteristics as those of the study area. As in the study area, F_1 folds have an isoclinal geometry, and have been transposed and reoriented by D_2 deformation. D_2 involved the most pervasive deformation observed in the Inner Piedmont and is similar to D_2 structures observed in the Columbus Promontory. D_3 deformation in the Alto allochthon area is associated with a weakly developed retrograde foliation defined by sericite and chlorite. F_3 folds are characterized by vertical to steeply dipping axial surfaces and have axes that trend N to NE. Such geometries are common in the study area but recumbent geometries are also common. The similarity of D_3 structures and their relationship with the S_2 foliation in Georgia and South Carolina to D_3 structures in the study area suggest that structures designated as D_3 in the two areas are coeval. Furthermore, these observations confirm that D_3 deformation developed after peak M_2 metamorphism but before complete cooling of the rocks (Hopson and Hatcher, 1988). D_4 and D_5 probably occurred after the rocks cooled completely following M_2 metamorphism and

Table 3.2. Comparison of deformation events in the study area with deformation events in other parts of the Inner Piedmont and eastern Blue Ridge.

Deformation event in study area	Style	Dominant Orientation	Fabric	Study area	Davis (1993)	Griffin (1974)	Hopson and Hatcher (1988)	Liu (1991)	Hatcher and Butler (1979)
F_1	Isoclinal, recumbent	?	S_1 (isolated)	D_1	D_1	(not recognized)	D_1	D_1	D_1
F_2	Isoclinal recumbent	NE	S_2 (dominant regional foliation)	D_2	D_2	D_1	D_2	D_2	D_2
F_3	Isolated, isoclinal to open	NE	S_3 (isolated)	D_3	D_3	D_2	D_3	D_3	D_3 / D_4
F_4	Upright, open to gentle	NE		D_4	D_4	(not recognized)	D_4	D_4	D_5
F_5	Upright, open to gentle	NW		(not recognized)	D_5	(not recognized)	D_5	D_5	D_6

produced broad, open folding that interfered to create a dome-and-basin pattern (Hopson,
1984). In the study area, only one episode of broad, open folding, D_4, was recognized.

Structural relationships in South Carolina are also similar to those in the study area,
including NE-SW striking foliations that dip gently to the SE and E-W trending lineations
that change gradually westward to NE-SW. The style of the first two episodes of Liu (1991)
and Hopson and Hatcher (1988) are very similar to that in the study area (Table 3.2). The
early, possibly Taconian, stages of D_2 (termed D_{2a}) deformation were marked by thrusting
along the Stumphouse Mountain fault (Liu, 1991). This fault was subsequently folded and
transposed by D_{2b} deformation. Sharp truncation of footwall lithologies and structures
indicate that this fault was active under brittle to semi-brittle conditions. Later, D_{2b},
deformation, much like D_2 deformation in the study area, occurred under ductile conditions.
Equal-area plots of folds show NE-trending, NW-verging folds with flat axial surfaces (Liu,
1991).

As in North Carolina, northwestern South Carolina, and northeastern Georgia, D_3
structures developed shortly after peak thermal metamorphism, are widely scattered, and
are nonpenetrative. More importantly, Liu (1991) recognized a close relationship in South
Carolina between D_2 and D_3 structures, including F_3 folds that formed by progression of F_2
folds. These relationships strongly indicate there was no significant time break between
formation of D_2 and D_3 structures and that they represent a single continuous episode of
deformation. D_3 faults include Six Mile thrust (Griffin, 1967, 1969, 1974; Liu, 1991) and the
Toccoa Falls-Shorts Mill fault bounding the Alto allochthon (Hopson and Hatcher, 1988).
Both faults are associated with a retrograde fabric, designated as S_3 (Hopson and Hatcher,
1988; Liu, 1991). F_3 folds deform S_2 foliations, but a weakly developed, secondary foliation
(S_3) axial planar to these folds is present and is probably coeval with late fabrics observed in
D_3 faults (Hopson and Hatcher, 1988; Liu, 1991). As in my field area, these folds have an
upright or recumbent geometry. Postmetamorphic deformation produced broad and open

flexural-slip folding that trends NE-SW and brittle thrusting, including the Rosman fault (Lemmon, 1973; Edelman and others, 1987; Hopson and Hatcher, 1988; Liu, 1991).

The sequence of deformation in the Inner Piedmont can also be correlated across the Brevard fault zone into the eastern Blue Ridge. Blue Ridge deformation includes two earlier episodes of isoclinal recumbent folding, F_1 and F_2, a later episode of upright tight to isoclinal folding, F_3, crenulation cleavage, F_4, and two episodes of postmetamorphic upright, open folds, F_5 and F_6 (Hatcher and Butler, 1979; Quinn, 1991). F_1, F_2, F_3, and F_5 correspond well with those in the Inner Piedmont both in terms of folding style and timing relative to metamorphism. F_4 in the Blue Ridge is associated with a crenulation cleavage that has been identified in the Inner Piedmont, but is interpreted to be related to F_2 or F_3 folding (Hopson and Hatcher, 1988). F_6 in the Blue Ridge has been linked to F_5 folding in the Inner Piedmont of northeast Georgia and northwestern South Carolina (Hopson, 1984; Liu, 1991).

IV. METAMORPHISM

Rocks of the Inner Piedmont record a complex history of polymetamorphism. Lemmon (1973) and Hopson and Hatcher (1988) have suggested an early episode of metamorphism in the Inner Piedmont. This study and those conducted by Davis (1993a) have found no evidence supporting such an event. M_1 regional metamorphism is coeval with D_2 ductile deformation and most of the mineral assemblages seen in rocks of the study area (Lemmon, 1973, 1982; Yanagihara and Davis, 1992; Davis, 1993a). The age of metamorphism is constrained by radiometric age dating. Odom and Fullagar (1973) dated the Henderson Gneiss at 535±27 Ma using Rb-Sr but was later revised by Sinha and others (1989) to 509 Ma. A granitoid gneiss that intrudes the Henderson Gneiss west of the study area was dated at 438±22 Ma by Odom and Russell (1975). Because both gneisses contain S_2 foliations, their intrusion predates M_1 metamorphism. Dallmeyer (1988) determined that the age of regional M_1 metamorphism was late Devonian based on the timing of $^{40}Ar/^{39}Ar$ closure temperatures in hornblende (480°), biotite (300°), and muscovite (350°). Some time after M_1 metamorphism, the Inner Piedmont was affected by an episode of chlorite-grade metamorphism that overprints D_2 fabrics. Sinha and others (1988) dated this episode at 273 ±30 Ma using Sr/Sr and Rb/Sr. These data suggest that Inner Piedmont metamorphism is Acadian.

Like the Inner Piedmont in northwestern South Carolina and northeastern Georgia (Hatcher, 1969, 1970; Griffin, 1969, 1971a, 1971b; Hopson and Hatcher, 1988; Horton and McConnell, 1990; Davis, 1993a), metamorphism in the study area is interpreted to be Barrovian based on mineral assemblages in pelitic schist. Rocks bearing mineral assemblages produced by discontinuous reactions, however, are uncommon. Calcareous rocks are unknown, and "ideal" pelitic schist bearing aluminum silicate minerals are rare in the study area, making determination of metamorphic conditions difficult. Mineral assemblages in amphibolite, which are common in the study area, provide some information on metamorphic

conditions, but this is not nearly as precise as pelitic schist. "Ideal" pelitic schist is present as scattered interlayers and pods in Poor Mountain quartzite in unit 2, and unit 3 gneiss. They become increasingly rare in the western half of unit 2 and are absent in unit 1. Therefore, metamorphic conditions in these areas must be inferred from a comparison of textures in areas that lack pelites with textures in areas that do.

Analysis of metamorphism in the study area includes petrography as well as field observations. The main limitation of this study is the lack of geochemical data for the purpose of determining metamorphic conditions. More detailed studies using microprobe analysis, however, were conducted by Davis (1993a) in pelitic schist and by Liu (1991) in amphibolite and pelitic schist. Their work will be discussed where relevant.

ISOGRADS

The existence of sillimanite and muscovite indicating first sillimanite metamorphism in the southeastern half of the study area precludes the existence of any major isograds (e.g., staurolite, kyanite, second sillimanite zone) in that part. The absence of pelitic schist in the northwestern half makes identification of isograds using Barrovian mineral assemblages impossible, but the presence of migmatitic textures suggests that metamorphic conditions remained in the first sillimanite zone. Hornblende and plagioclase along with the absence of pyroxene, chlorite, and epidote in a single sample of amphibolite obtained within the Henderson Gneiss, indicate that metamorphic conditions were clearly in the amphibolite facies. In the far northwest corner of the study area, however, the Henderson Gneiss is dominated by fine-grained textures and could suggest lower grades of metamorphism, but more likely indicate other factors such as increased shearing near the Brevard fault zone resulting in grain-size reduction. This interpretation is supported by mineral assemblages in the fine-grained lithology which are identical to those in coarse-grained lithologies. Furthermore,

fine-grained textures are dominant in the Poor Mountain Amphibolite and Quartzite where sillimanite-bearing schist is present. Fine-grained textures are also present as interlayers within migmatite in the upper Mill Spring gneiss of units 2 and 3. Lemmon (1973) and Butler (1990) interpreted the contact between the Henderson Gneiss and Poor Mountain Formation above it (Sugarloaf Mountain thrust) as the sillimanite isograd. Davis (1993a), however, concluded that the contact is only a function of changes in rock type and does not constitute a metamorphic isograd. Evidence supporting this conclusion include mineral lineations defined by synkinematic sillimanite in the Sugarloaf Mountain fault, which can be traced into lineations in the Henderson Gneiss that are defined by elongated K-feldspar and other minerals (Davis, 1993a). Relationships observed in the study area are consistent with this interpretation.

The interpretation that the entire study area, including the western two thirds of the Chauga belt and a part of the Inner Piedmont, is in the sillimanite zone correlates with observations made by Davis (1993a), but vary with those made in South Carolina and northeast Georgia. Here, metamorphic conditions in the Chauga belt are upper-greenschist to lower amphibolite facies (Hatcher, 1969, 1970; Griffin, 1969, 1971a, 1974; Liu, 1991). The Walhalla and Six Mile nappes, farther east, reached middle to upper amphibolite facies as indicated by the presence of kyanite and sillimanite (Griffin, 1974; Liu, 1991). Sillimanite, however, is the only aluminum silicate mineral present in the Columbus Promontory.

MIGMATITE

Migmatitic textures are present in all three units in the study area and are most common in rocks that have greater mica content, such as granitoid gneiss and pelitic schist. Migmatite is composed of three principal components: (1) the leucosome, composed mostly of light-colored minerals; (2) the melanosome or restite, composed mainly of dark-colored minerals; and (3)

the paleosome, the unaffected schist (Mehnert, 1968). They are also classified into three main textural types: stromatic, nebulitic, and vein-type (Yardley, 1989). Nebulitic textures, where the leucosomes form nebulous patches and have obscure contacts with the adjacent melanosome, are present in widely scattered areas of the pelitic schists in unit 3. Stromatic textures, where the leucosome and melanosome segregate into distinct layers parallel to the foliation, are by far the most common migmatitic texture in the study area (Fig. 4.1).

The origin of migmatite has been the subject of much controversy but most authors agree they form by one of four mechanisms: (1) partial melting; (2) metamorphic differentiation; (3) *lit par lit* injection of granitic magma; and (4) metasomatism (Mehnert, 1968; Olsen, 1983, 1984). Winkler (1976) experimentally determined that pelite begins to melt at conditions slightly above the first sillimanite isograd to produce a liquid of granitic composition.

Most leucosomes in the study area, as determined by modal analysis, have a trondjhemitic composition (lacking K-feldspar). Tracy and Robinson (1983) noted that leucosome in New England, composed mostly of plagioclase and quartz, is characteristic of migmatite that forms in the first sillimanite zone or lower grades, whereas migmatite occurring above the K-feldspar + sillimanite isograd is rich in plagioclase, quartz, and K-feldspar. They speculated that the former originated as a result of metamorphic differentiation, whereas the latter formed by partial melting. This deduction, however, is only applicable to a few gneisses because subsolidus migmatite has been found to contain K-feldspar (Sawyer and Barnes, 1988) and anatectic migmatite can lack K-feldspar (Evans and Speer, 1984; Jones and Brown, 1990; Ashworth and Brown, 1990).

I interpret migmatites in the study area to have evolved by partial melting, because they formed at metamorphic grades substantially high enough to initiate partial melting. This interpretation is further supported by the presence of stromatic textures in which mineral assemblages are similar to those in other migmatites that are proven to have been produced by partial melting using more sophisticated techniques including electron microprobe analysis

Figure 4.1. Folded migmatite in unit 3 biotite gneiss (upper Mill Spring complex) at Cove Creek, Shingle Hollow quadrangle. The banded gneiss is typical of stromatic textures that dominate migmatites throughout the study area. Width of the photo is approximately 80 cm.

(e.g., Jones and Brown, 1990; Cartwright, 1990). The presence of highly contorted structures also suggests that migmatite layers were in a semi-molten state during deformation. Such observations have also been noted by Mason (1978), Winkler (1979), and McLellan (1983, 1988). This interpretation is supported by work conducted by Griffin (1969), Hopson (1984), Liu (1991), and Quinn (1991) who concluded that migmatite in the Inner Piedmont and eastern Blue Ridge also formed by partial melting. McClellan (1987) concluded that migmatite in the Coweeta Group in the Tray Mountain area of Georgia and North Carolina originated by injection of granitic magma but later acknowledged an origin by partial melting (McClellan, 1989).

MINERAL ASSEMBLAGES

Characteristic mineral assemblages and associated textures were identified petrographically. Those listed minerals are interpreted to represent the prograde assemblage. Minerals associated with a later episode of retrograde metamorphism are also common, but they tend to be randomly oriented and represent a substantially lower grade of metamorphism and thus, are easy to distinguish from the prograde assemblage. Davis (1993a) has presented evidence that at least some of his prograde mineral assemblages that are nearly identical to those identified in the study area evolved along the retrograde portion of the P-T path. The implications that these interpretations have for rocks in the study area will be discussed later in this chapter.

PELITIC SCHIST

Pelitic schist exists in unit 2 as widely scattered interlayers and pods in the Poor Mountain Quartzite and Amphibolite. To the south, pelitic schist is more common, forming a

distinct mappable unit. This unit continues into the study area but contains greater amounts of granitoid gneiss. The two lithologies have identical mineral assemblages but differ compositionally in that mica content is less than 15% in granitoid gneiss and greater than 25% in biotite gneiss. The contact between the two lithologies is typically gradational. While biotite gneiss is common in this unit, it rarely contains aluminum silicate minerals. In unit 3, pelitic schist forms a distinct mappable unit (upper Mill Spring complex of Davis, 1993a). Sillimanite is common not only in this unit, but also in the upper, undifferentiated unit.

Mineral assemblages in pelitic schist can be summarized as follows (see Table 4.1 for key to abbreviations):

(1) Qz + Pl + Ms ± Sil ± Bio ± Gt ± Kf ± Opq (unit 2)

(2) Qz + Pl + Ms ± Sil ± Bio ± Gt ± Opq (unit 3)

K-feldspar, while observed in pelitic schist, was never observed with sillimanite. Opaque minerals, composed mostly of pyrite, ilmenite, magnetite, and rutile were identified using reflection petrography. Many garnets in pelitic schist are optically zoned, suggesting two periods of growth. The zoning is easily discernible because it is composed of an inner core of inclusion-rich garnet and an outer core that is relatively clear. The inclusions are usually ilmenite, plagioclase, and in rare cases, biotite. Optically unzoned garnets are usually clear. Garnet also occurs in a variety of shapes ranging from euhedral forms with sharp, angular crystal surfaces to deeply embayed or skeletal forms (Fig. 4.2). Many of the embayments are occupied by prograde minerals and textures such as biotite and muscovite that are oriented parallel to the foliation. Davis (1993a) also observed sillimanite growing on the rims and in the embayments of anhedral garnet. Davis (1993a) suggested that these relationships indicate that consumption of garnet occurred during prograde metamorphism rather than during a later episode of retrograde metamorphism.

Sillimanite is most common as tiny, acicular, fibrolitic needles (usually less than 0.5 mm long and substantially less than 0.1 mm wide). It is also common as inclusions inside quartz and

Table 4.1. Key to mineral abbreviations

Aluminum silicate	Als	Muscovite	Ms
Biotite	Bio	Opaque minerals	Opq
Clinozoisite	Cz	Plagioclase	Pl
Chlorite	Chl	Anorthite	An
Epidote	Ep	Albite	Ab
Garnet	Gt	Quartz	Qz
Almandine	Alm	Sillimanite	Sil
Grossular	Gr	Sphene	Sph
Hornblende	Hbl	Staurolite	St
Ilmenite	Ilm	Zircon	Zr
K-feldspar	Kf		

Figure 4.2. Two typical morphologies of garnet in pelitic schist. (A) Skeletal embayed garnet

in a lens of pelitic schist in Poor Mountain Quartzite. Note that some of the

embayments are occupied by prograde mica. The sample was collected at Cove Creek

near Toms Mountain. (B) Optically zoned garnet in unit 3 pelitic schist of the upper

Mill Spring formation. Note the internal fabric defined mostly by ilmenite giving a

sense of shear (top to the left) consistent with other structural features (e.g., folds

and winged porphyroclasts). The sample was collected by T. L. Davis in the

Cliffield Mountain quadrangle. The width of both photos is 4 mm.

A

B
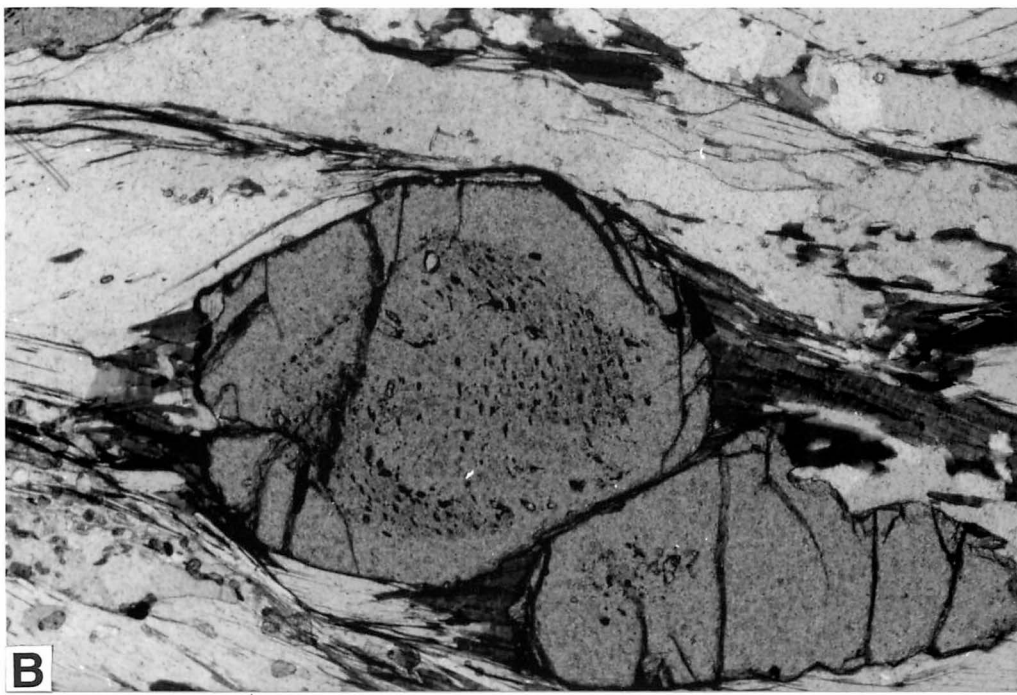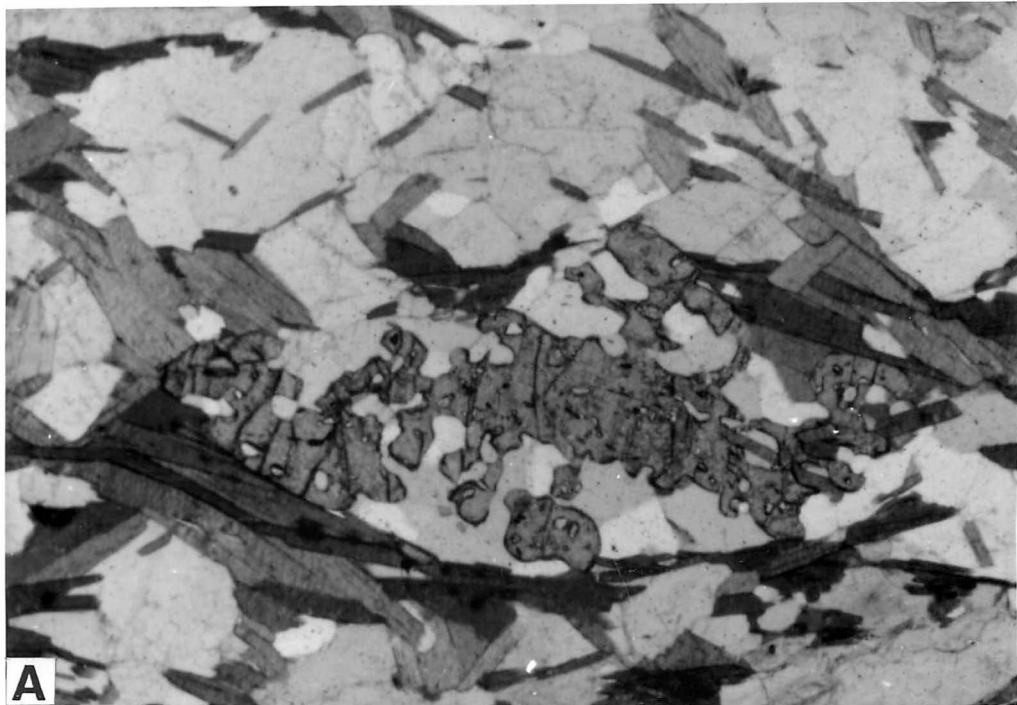
muscovite, and as prismatic intergrowths with biotite (Fig. 4.3). Davis (1993a) also observed fibrolite reaction rims enclosing muscovite and garnet. Such relationships were also observed in the study area in muscovite. In one sample, however, muscovite crystals are zoned with a sillimanite-rich core and a sillimanite-poor rim. In this thin section, sillimanite also is present on the rims of some crystals. Prismatic sillimanite was observed in a sample collected less than 35 m from the Shingle Hollow fault (Fig. 4.3c). The crystals are often intergrown with biotite suggesting simultaneous growth and range up to 0.2 mm wide and up to 1 mm long.

Based on observations made in pelitic schist, I deduce peak thermal metamorphic conditions reached the first sillimanite zone (sillimanite + muscovite). Sillimanite + orthoclase were never observed petrographically and thus, preclude the possibility that metamorphic conditions reached the second sillimanite zone (granulite facies).

AMPHIBOLITE

Amphibolite is common throughout unit 2 and unit 3, whereas only two localities were found in unit 1. In unit 2, they form a distinct mappable unit and have been correlated with the Poor Mountain Formation of South Carolina. In unit 3, they form a significant portion of the undifferentiated unit and occur as isolated lenses in the biotite gneiss.

The determination of metamorphic conditions is more difficult in amphibolite than in pelitic schist. Reactions in these rocks involve a relatively small number of phases but a large number of components. These phases contain extensive solid solutions and change compositions continuously with increasing pressure and temperature. Consequently, the absence of discontinuous reactions in amphibolites makes accurate identification of pressure-temperature relationships more difficult than in pelitic schist (Yardley, 1989). Furthermore, the lack of electron microprobe data in this study prohibits detailed geochemical analysis of the mineral assemblages, which can provide more accurate information on pressure-temperature

Figure 4.3. Photomicrographs showing some morphologies of sillimanite. (A) Fibrolitic

sillimanite growing on the rims of plagioclase in unit 2 pelitic schist. The two grains

in the center of the photo which sharply truncate the needles are quartz. All other

grains are plagioclase. The needles are intergrown with chlorite and gives the

clusters their dark color. The sample was collected on Grassy Mountain, Sugar Hill

quadrangle. (B) Fibrolitic sillimanite in a muscovite crystal in unit 3 biotite gneiss.

Sample was collected on Glaghorn Mountain, Sugar Hill quadrangle. (C) Prismatic

sillimanite and biotite in unit 3 pelitic schist collected near Harris Creek, Sugar

Hill quadrangle. The interfingering of the two phases strongly suggests

contemporary growth. The field of view for all three photographs is 2 mm.
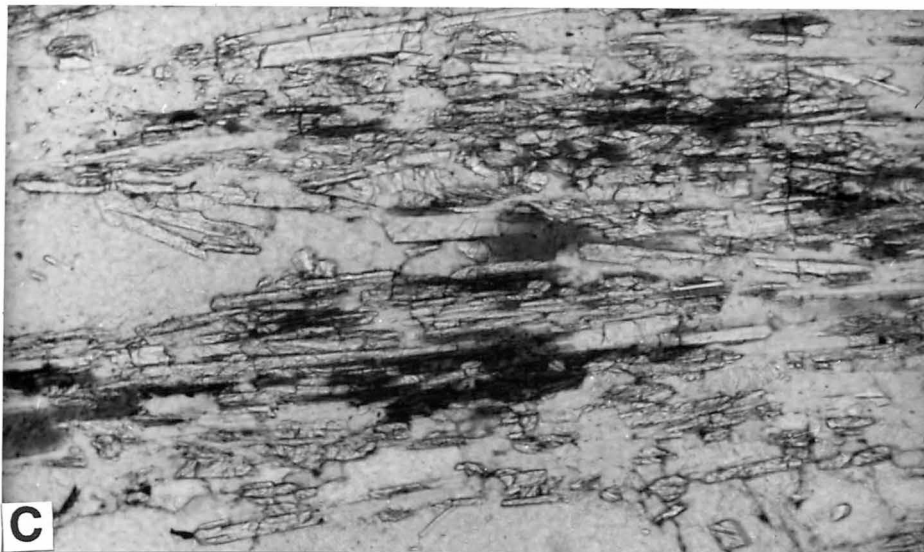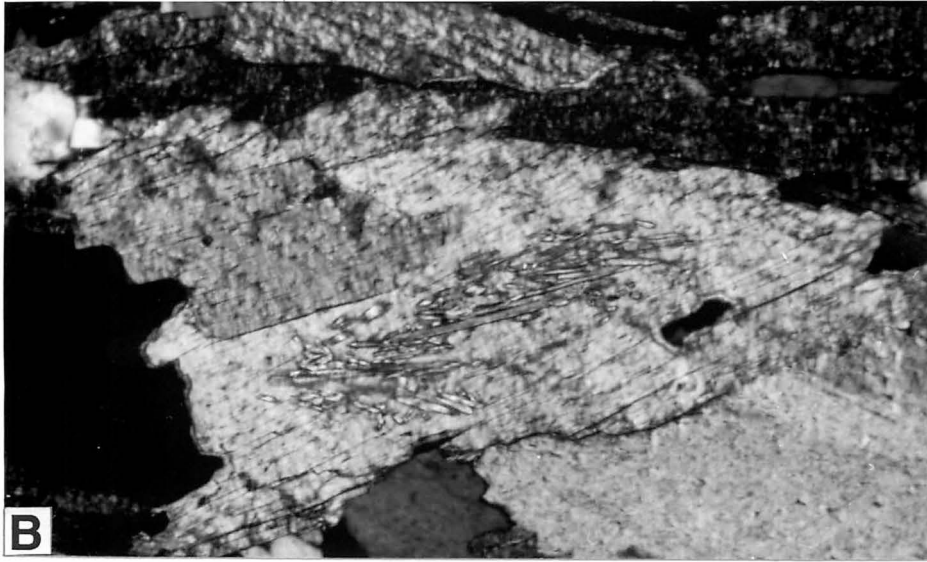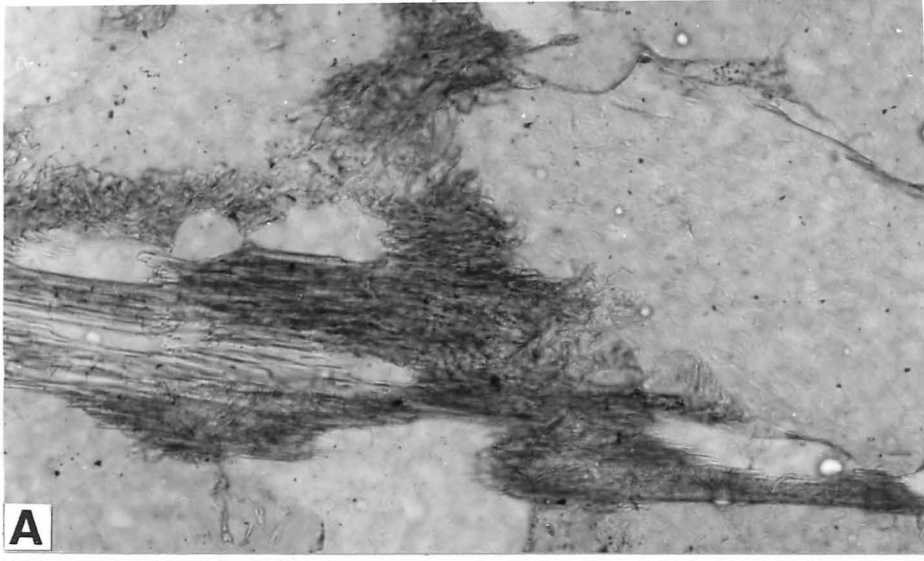
relationships. Nevertheless, the information provided by field observations and petrographic analysis of amphibolite, in conjunction with observations made in pelitic schist, yields valuable information on metamorphic conditions in the study area.

Prograde metamorphic assemblages in the amphibolites are summarized as follows:

(1) Am + Pl + Bio + Qz + Sph + Zr + Opq (unit 1)

(2) Am + Pl + Qz ± Sph ± Zr ± Bio ± Gt ± Ms ± Opq ± Chl (unit 2)

(3) Am + Pl + Qz ± Opq (unit 3)

Like pelitic schist, amphibolite contains a number of retrograde minerals (epidote, clinozoisite, and chlorite) that are not included in the above assemblages. Prograde chlorite usually has dark green-brown color in plane-polarized light and is oriented parallel to the S_2 foliation, whereas retrograde chlorite is light green and randomly oriented. Prograde epidote and clinozoisite have been found in other parts of the Inner Piedmont (e.g., Griffin, 1969; Hatcher, 1969, 1970; Hopson, 1984; Liu, 1991), but while the two minerals can grow in upper amphibolite facies conditions, this study has not found evidence for the presence of prograde epidote and clinozoisite. All three minerals can be stable under amphibolite facies conditions, but in the study area, they are typically randomly oriented and replace peak-M_1 minerals. Metamorphic assemblages in unit 1 are based on one thin section (one other sample of ultramafic rock was found, but was retrograded to chlorite and clinozoisite), while assemblages in units 1 and 2 are based on 8 and 4 thin sections, respectively. Hornblende, plagioclase, and quartz are consistently present in most of the samples collected. In a few samples, hornblende composed most of the rock, with trace amounts of opaque minerals. Reflection petrography of the opaque minerals reveals ilmenite as the dominant phase plus variable amounts of sulfide minerals (including pyrite and chalcopyrite), magnetite, and rutile.

Several observations constrain determination of metamorphic conditions in the amphibolites. The dominant mineral assemblage is hornblende + plagioclase and indicates

amphibolite facies conditions (Yardley, 1989). The absence of actinolite, chlorite, prograde epidote, and prograde clinozoisite precludes the possibility that metamorphic conditions did not exceed greenschist facies. The lack of pyroxene (hypersthene) or olivine indicates the rocks did not reach granulite facies. These observations correlate well with the first sillimanite zone metamorphism observed in pelitic schist.

ASSESSMENT OF P-T CONDITIONS

P-T conditions can be estimated using mineral assemblages observed in thin section and comparing them to stability fields determined experimentally by previous authors. The following observations are important for assessing peak metamorphic conditions:

1. The presence of muscovite + sillimanite.

2. The absence of K-feldspar + sillimanite.

3. The presence of migmatitic textures indicating the onset of partial melting.

4. The presence of hornblende + plagioclase (An_{30-35}, as determined by the Michel-Levy method) in the amphibolites.

5. The absence of clinopyroxene, orthopyroxene, or olivine in the amphibolites that would show the onset of granulite facies metamorphism.

Based on the presence or absence of these mineral assemblages and textures, the pressure and temperature range during peak metamorphic conditions can be constrained to a relatively small area in P-T space (Fig. 4.4). This indicates temperatures ranged from approximately 625° to 700°C and pressures from 3.5 to 8.0 kbars.

More quantitative calculations of P-T conditions were made by Davis (1993a) based on the Fe-Mg exchange reactions between garnet and biotite, the garnet-plagioclase-muscovite-biotite (GPMB) barometer, and garnet-plagioclase-sillimanite-quartz (GASP) barometer of Ghent and Stout (1981). From these barometers, Davis (1993a) calculated a peak temperature

Figure 4.4. Petrogenetic grid showing metamorphic relationships in the study area indicated

by the shaded area. The reaction lines for mafic schists are adapted from Yardley

(1989); the Al_2SiO_5 triple point is from Holdaway (1971); reaction 1 is from Luth

and others (1964); and reaction 2 is from Chaterjee and Johannes (1974).
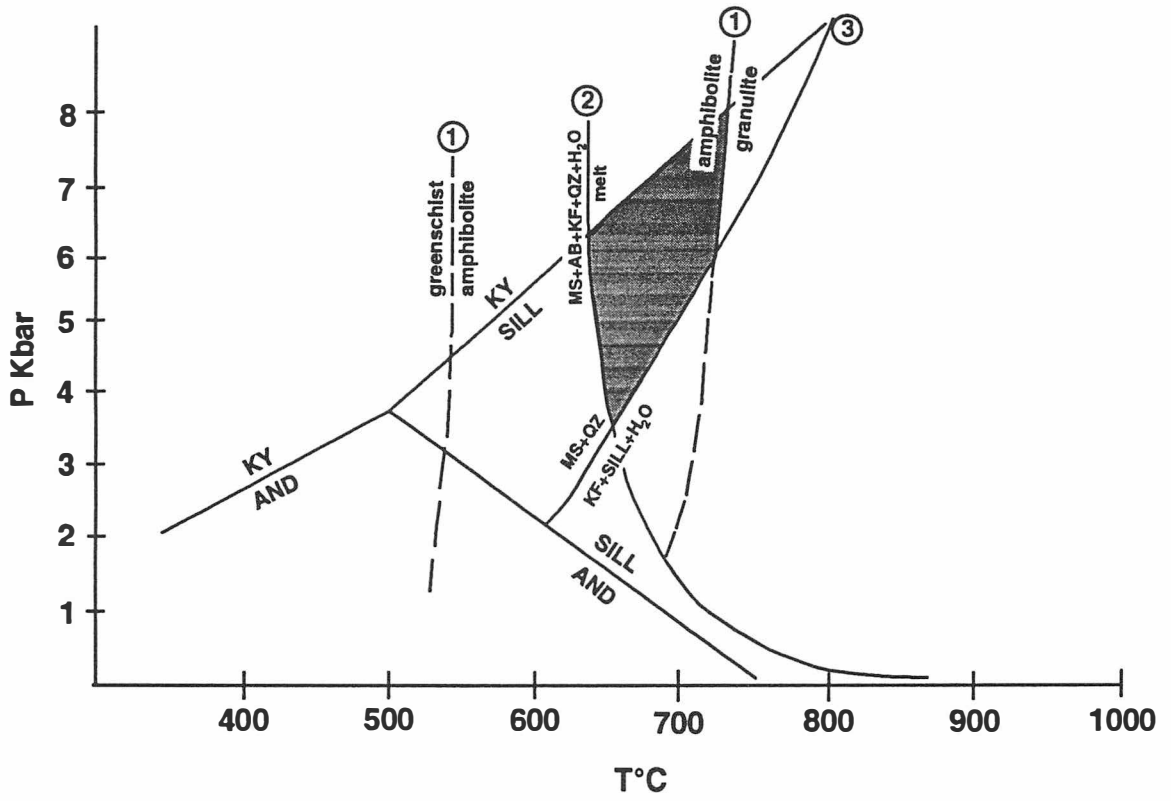
in the range of 535°-565°C plus one anomalous reading of 690°C, and a peak pressure of 3-5 kbars. Davis (1993a) speculated, however, that these calculations probably represent termination of the garnet-biotite exchange reaction along the retrograde P-T path rather than peak temperatures and pressures. Similar figures have been reported in other high-grade terranes, including areas that presumably experienced very high grades of metamorphism (Spear and Peacock, 1989). Liu (1991), based on the garnet-biotite exchange reaction, estimated temperatures in the Chauga belt to be in the range of 490°-550°C and 608°-714° in the Six Mile thrust sheet. Pressures in the Chauga belt were calculated to be about 5.3 to 6.3 kbars.

PETROGENESIS

Development of prograde mineral assemblages, herein referred to as assemblage A_1, in the Columbus Promontory involved consumption and both early and late-stage growth of garnet as well as the growth of sillimanite, biotite, and quartz. Garnets contain abundant inclusions of ilmenite and quartz as well as sparse inclusions of plagioclase, biotite, and muscovite indicating that these phases grew continuously throughout growth of garnet (Davis, 1993a). Many garnets, however, are optically zoned, with inclusion-rich cores and inclusion-poor rims. Microprobe analysis by Davis (1993) of some of these garnets indicates an increase in Ca content on the rims. This change in composition does not occur in the same area as the change in optical zoning (Davis, 1993a). Other garnets are deeply embayed or skeletal suggesting that garnet was both growing and being consumed during late-stage peak metamorphism.

Based on textural relationships, sillimanite is interpreted to have developed by more than one reaction (Davis, 1993a). Sillimanite is often intergrown with biotite in the study area and as inclusions inside muscovite and quartz (Fig. 4.3). Davis (1993a) also observed

fibrolite needles on the rims of garnet and muscovite and as intergrowths with biotite. While the growth of sillimanite can be explained by a number of reactions, it is unlikely that it grew by polymorphic transition from kyanite because this reaction is probably very sluggish (Yardley, 1989). Furthermore, relict kyanite has not been observed in the Columbus Promontory. More commonly, sillimanite grows at the expense of staurolite (Miyashiro, 1973; Turner, 1981; McLellan, 1985; Yardley, 1989):

$$6\,St + 4\,Ms + 7\,Qz = 4\,Bio + 31\,Sil + 3\,H_2O \quad (1)$$

The possibility that this reaction occurred in the study area is supported by the observation that sillimanite is commonly intergrown with biotite and muscovite, but is refuted by the absence of staurolite. Migmatitic textures suggest that a substantial amount of water necessary for initiation of partial melting was generated. This reaction provides at least some of the water necessary for partial melting. While there is no petrographic evidence for staurolite, it has been found in other parts of the Inner Piedmont (Bryant and Reed, 1970; Roper and Dunn, 1973; Hatcher, 1978). It is possible that staurolite was completely consumed during formation of sillimanite

There is evidence that garnet was both being consumed and was growing during the formation of assemblage A$_1$ in the Columbus Promontory (Lemmon, 1973; Davis, 1993a). The consumption of garnet in favor of sillimanite can be summarized by the following reaction:

$$Gt + Ms = 2\,Sil + Bio + Qz \quad (2)$$

Like reaction (1), reaction (2) is consistent with the observation that biotite and sillimanite grew together and that sillimanite grew on the rims of garnet and muscovite. It does not provide the water necessary for the initiation of partial melting.

Many euhedral garnets (A$_1$ garnets) in pelites south of the study area have increased grossular components at the rims (Davis, 1993a). This increase in Ca in the garnets can be characterized by (Spear and others, 1990):

$$3\,An = Gr + 2\,Sil + Qz \quad (3)$$
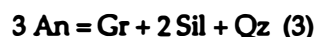
Petrographic evidence supporting this reaction in the study area is ambiguous. Sillimanite was observed on the rims of plagioclase in one sample but garnet is absent (Fig. 4.3a). Elsewhere, textural evidence for reaction (3) is largely absent, but growth of grossular can only occur at the expense of anorthite because anorthite is the only other Ca-bearing phase in the pelites.

Of the three sillimanite-producing reactions presented, equations (2) and (3) are the most likely to have been operating in the study area based on the available petrographic and geochemical data. Proving that equation (1) was also operating in the pelites is complicated by the absence of staurolite and that equation (2) produces nearly identical mineral assemblages as equation (1). It is possible that staurolite was completely consumed during formation of sillimanite. Based on the available evidence, however, I believe equation (1) probably did not produce significant amounts of sillimanite in the study area.

Textural information indicates that the formation of migmatite and the growth of sillimanite and assemblage A_1 probably occurred coevally. Evidence includes the parallel orientation of gneissic banding and sillimanite crystals due to synmetamorphic transposition, and the observation of sillimanite growing on the rims of muscovite that is oriented parallel to migmatitic layering within the melanosomes. These two processes can be explained by the following reaction (Tracy, 1978; Tracy and Robinson, 1983):

$$Ms + Bio + Qz + H_2O = Sil + melt \quad (4)$$

This reaction begins slightly below the second sillimanite isograd, but there is no evidence in the study area that metamorphic conditions exceeded the first sillimanite zone nor are the mineral assemblages of the leucosomes in the Columbus Promontory consistent with such a reaction. Therefore, this reaction was probably not important in producing significant amounts of partial melting in the study area. An alternative reaction is (Thompson and Algor, 1977; Thompson, 1982):

$$Ms + Kf + Ab + Qz + H_2O = melt \quad (5)$$
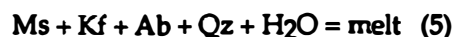
Reactions (4) and (5) produce melts that are granitic in composition. Most migmatites in the Inner Piedmont, including those in the study area, lack K-feldspar (Griffin, 1969, 1971a, 1974; Hopson, 1984; Liu, 1991; Davis, 1993a). In the study area, I believe the absence of K-feldspar is a function of bulk composition because K-feldspar is absent in both the leucosomes and the melanosomes. None of the sillimanite producing reactions that are interpreted to have been operating in the Columbus Promontory, however, provide the water necessary for the initiation of partial melting. Such water could have been provided by another reaction, involving the dewatering of muscovite or other water-bearing phase. Textural relationships and mineral assemblages provide no evidence for such a reaction. It is also possible that water came from an external source but the available data can neither support nor refute such a hypothesis.

Biotite, muscovite, plagioclase, and quartz were also growing during development assemblage A_1. Based on textural relationships and microprobe analysis, Davis (1993a) interpreted that the development of assemblage A_1 is characterized by a series of continuous reactions. Growth of these minerals probably occurred along the retrograde portion of the P-T path. This conclusion is supported by textural relationships such as garnet embayed by sillimanite and microprobe analysis of zoned garnets adjacent to the study area (Davis, 1993a). This analysis indicates increasing almandine, increasing Fe/Fe+Mg, and decreasing pyrope at the rims suggesting growth during decreasing temperatures (Davis, 1993a). Metamorphic textures observed in the study area, including zoned garnets, embayed garnets, and the growth of sillimanite on the rims of muscovite, are consistent with this interpretation. Such relationships involving continuous reactions in pelitic schists are not uncommon and have been observed in other high-grade terranes (e.g., Tracy and Robinson, 1983; Olsen, 1984; Mohan and others, 1989; Spear and others, 1990).

RETROGRADE METAMORPHISM

Sometime after peak thermal metamorphism, rocks in the study area underwent a period of retrograde metamorphism. Minerals associated with this episode are in general randomly oriented, widely scattered, and indicate relatively low-grade metamorphism (Fig. 4.5). Occasionally, these minerals parallel the S_2 foliations but this is probably related to pseudomorph development.

Minerals associated with retrograde metamorphism include chlorite, muscovite, chloritoid, and biotite in the pelitic schists and epidote, clinozoisite, actinolite, and chlorite in the amphibolites. Epidote and clinozoisite in the study area are interpreted to be retrograde because it is randomly oriented and replaces prograde minerals. These assemblages suggest that conditions during retrograde metamorphism reached the chlorite zone in pelitic schist and greenschist facies in amphibolite. The granitoid gneisses and quartzites also contain widely scattered chlorite and muscovite. In quartzite, muscovite forms large (up to 10 mm), optically continuous crystals that grew around and enclose preexisting phases, and is interpreted to be the result of hydrothermal alteration.

Retrograde metamorphism in the study area was probably synchronous with retrograde metamorphism in the Brevard fault zone. Mineral assemblages in the fault zone include chlorite, muscovite, quartz, epidote, and sphene and indicate a similar grade of metamorphism to that in the study area. In other parts of the Inner Piedmont, retrograde metamorphism in the Henderson Gneiss has been the most extensively studied (e.g., Sinha and others, 1988; Vauchez and Brunel, 1988; Liu, 1991). In areas in and adjacent to the fault zone, retrograde minerals are associated with shear bands superimposed on the preexisting S_2 foliation. The shear bands decrease in frequency with increasing distance from the fault zone (Edelman and others, 1987; Sinha and others, 1988; Vauchez and Brunel, 1988). Samples collected from the Henderson Gneiss in the study area contain a few retrograde minerals that

Figure 4.5. Retrograde minerals in the study area. (A) Chlorite replacing garnet in Poor Mountain Amphibolite. The sample collected on the southwest slope of Toms Mountain, Shingle Hollow quadrangle. (B) Well-developed chloritoid crystals in unit 3 pelitic schist (upper Mill Spring formation) collected near Harris Creek, Sugar Hill quadrangle. Note the preexisting fabric, composed mostly of muscovite and biotite, that it overprints. The crystals are truncated sharply by quartz-rich layers wherein composition is unfavorable for the formation of chloritoid. In other parts of this same thin section, chloritoid has formed after garnet.(C) Epidote (center of photograph) in Poor Mountain Amphibolite collected on Harris Mountain, Sugar Hill quadrangle. The elongated crystals above and below the epidote are prograde hornblende. The field of view for all three photomicrographs is 2 mm.
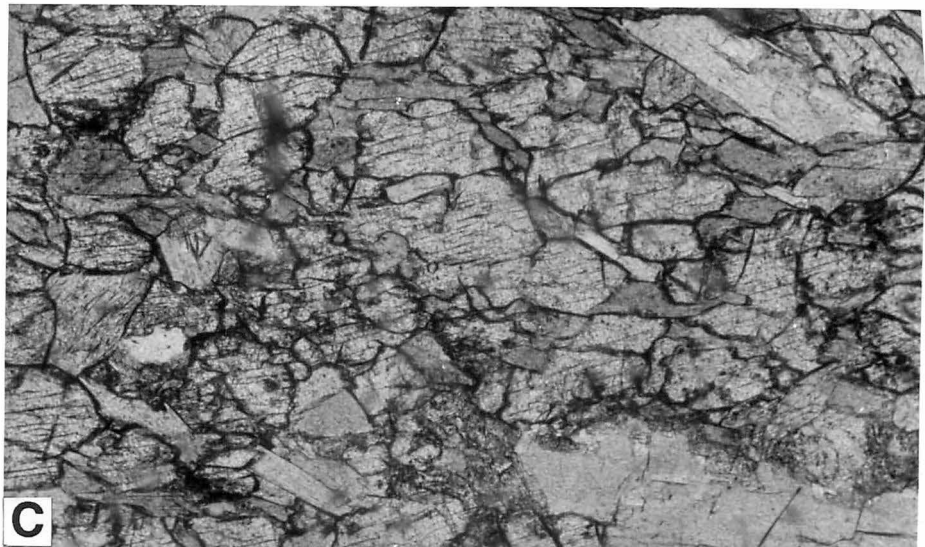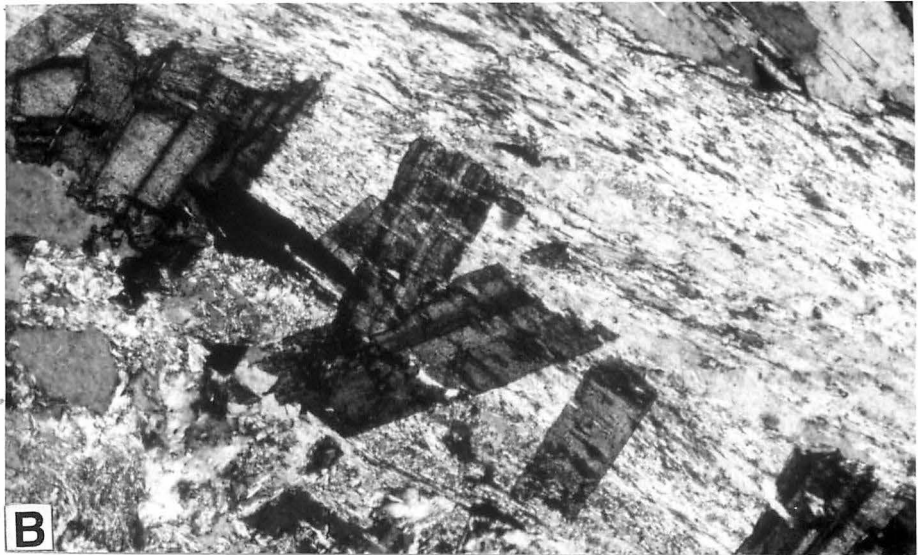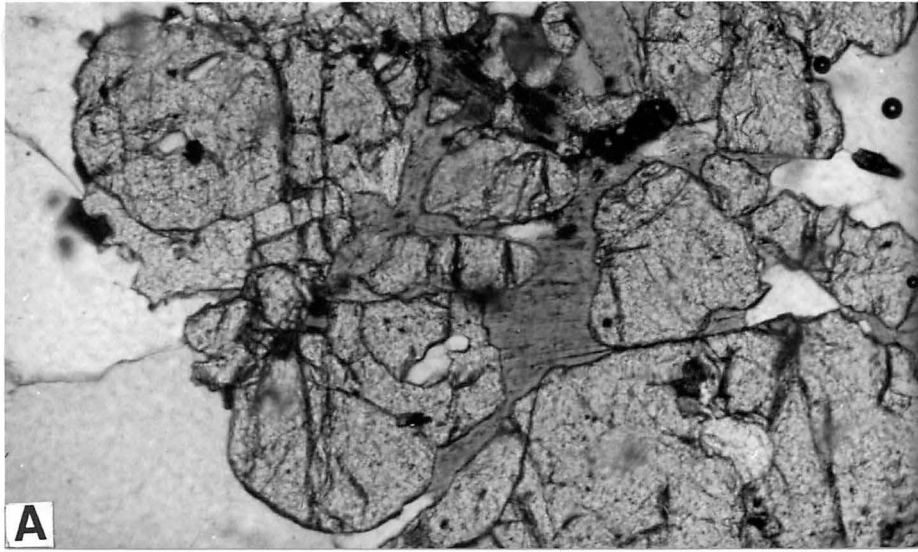
are often randomly oriented. This difference in the behavior of the retrograde minerals is interpreted to be a function of proximity to the Brevard fault zone (samples collected in the study area were never closer than 8 km). Sinha and others (1988), using Rb^{87}/Sr^{86} and Sr^{87}/Sr^{86} ratios in Henderson Gneiss, calculated the age of retrograde metamorphism as 273 ± 30 Ma.

V. GEOCHEMISTRY OF THE AMPHIBOLITES

Mafic schists are common throughout much of eastern Blue Ridge and Inner Piedmont but their origin has been the subject of some controversy. Due to high-grade metamorphism, thrusting, and severe transposition, protolithic mineral assemblages, textures, and other features have been mostly erased. Therefore, the use of whole-rock geochemical analysis is the best method available for providing primary information on the origin of these rocks.

The use of whole-rock analysis to determine the protolith of mafic schists has been used in a number of studies in the eastern Blue Ridge (e.g., Achaibar, 1983; Eggers, M. R., 1983; Hatcher and others, 1984; McConnell and Abrams, 1984; Misra and McSween, 1984; Misra and Conte, 1991; Quinn, 1991) and in the Inner Piedmont (Conley, 1978; Achaibar and Misra, 1984; Stow and others, 1984; Neilson and Stow, 1986; Davis, 1993a). Shaw and Wasserburg (1984) conducted isotopic studies of various mafic/ultramafic complexes throughout the Appalachian orogen, including rocks in the eastern Blue Ridge of North Carolina. These studies have indicated a variety of protoliths including continental, oceanic, and island arc affinities (Misra and McSween, 1984). Others have further suggested a back-arc basin origin for those metabasalts with an oceanic affinity (Neilson and Stow, 1986; Gillon, 1989; Misra and Conte, 1991; Davis, 1993a).

This chapter focuses mostly on the Poor Mountain Amphibolite whose fine felsic laminations and relationships with adjacent metasedimentary rocks prompted Hatcher (1969, 1970) to interpret them as an impure calcareous sediment. Subsequent studies using whole-rock geochemical data have shown them to be metabasalt (Davis, 1993a). In addition, several samples of lower Mill Spring amphibolite were collected for comparison with rocks of the Poor Mountain Formation but extensive weathering and hydrothermal alteration in these samples prevented accurate analysis in all but one of the samples.

TECHNIQUE AND LIMITATIONS

22 samples were collected from the Poor Mountain Formation in unit 2 and one sample was collected from the lower Mill Spring formation in unit 3 (Fig. 5.1). The samples selected were relatively free of weathering and post-metamorphic alteration in hand sample. Thin sections were also cut from 8 of these samples and contained no petrographic evidence of weathering or hydrothermal alteration.

The values for 10 major oxides and 8 trace elements were determined using X-ray fluorescence (XRF) on an EG&G Ortec energy dispersive spectrometer at the University of Tennessee (Table 5.1). An igneous rock protocol was used to obtain these values and their accuracy was checked against several standards. The standards were run through the spectrometer once or twice and the calculations are listed in Appendix B. In general, calculated values did not deviate more than 10% for major elements and 20% for trace elements.

Tectonic discrimination diagrams used in this study are intended specifically for non-cumulative mafic lavas. Therefore, mafic lavas used in such studies should fall within the compositional range of 12%< [CaO + MgO] <20% (Pearce and Cann, 1973). 7 of the 23 samples collected for this study had values substantially higher (>1%) than 20%. Because elimination of the samples would reduce the number to 16, these seven samples were, nevertheless, included in this study. Instead, they have been designated a symbol distinctive of those samples that fall within the 12 to 20% screen. In all of the plots used, none of the samples that failed the screen plotted in regions significantly distant from those samples that passed. Therefore, it is possible that the greater than 20% values may be due to other factors rather than the presence of cumulate minerals.

The use of tectonic discrimination diagrams brings up several questions when trying to determine the protolith of a metabasalt using whole-rock geochemical analysis. In the study

Figure 5.1. Geologic map of the study area showing the location of samples collected for whole-rock analysis. The corresponding XRF data are shown in Table 5.1.
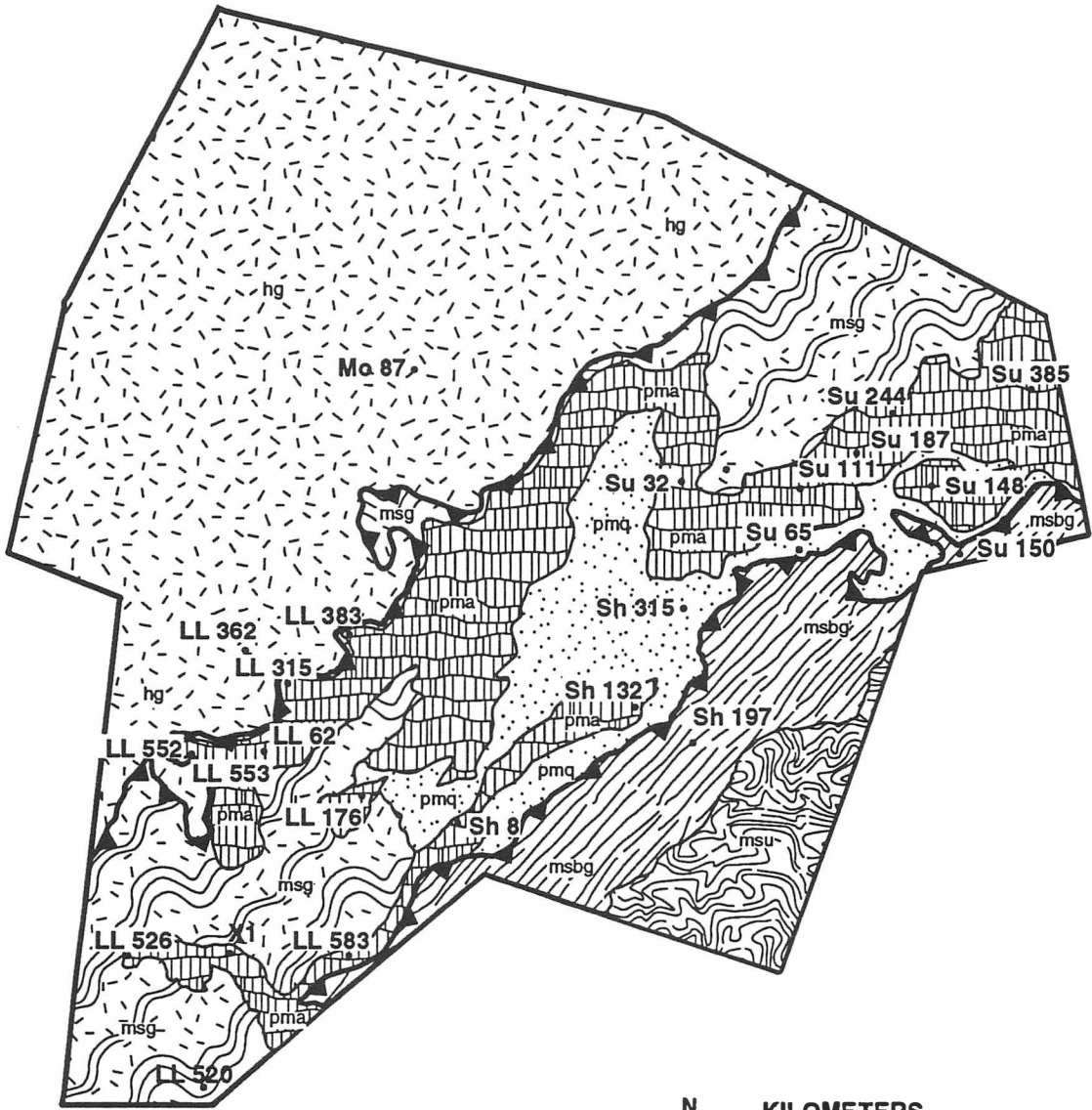
ROCK UNITS

msu	Unit 3, Mill Spring undifferentiated
msbg	Unit 3, Mill Spring biotite gneiss
pmq	Unit 2, Poor Mtn. quartzite
pma	Unit 2, Poor Mtn. amphibolite
msg	Unit 2, Mill Spring gneiss
hg	Unit 1, Henderson gneiss

N

KILOMETERS

0 1 2 3
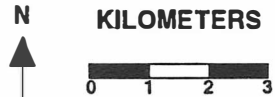
Table 5.1. XRF analysis of amphibolites from the study area.

	Su 150	Su 32	Su 244	LL 553	LL 62	LL 552	LL 500	LL 383	LL 62	Su 385	Sh 132	Sh 315	Su 111	Sh 8
major elements (wt% oxide)														
Na$_2$O	1.27	2.31	2.08	2.45	2.39	2.26	4.03	2.84	2.22	2.33	2.14	3.51	2.23	2.99
MgO	7.65	7.60	7.35	8.61	10.35	5.45	8.26	6.23	9.32	8.20	9.33	6.23	9.22	8.24
Al$_2$O$_3$	11.65	15.69	16.00	15.62	16.38	14.49	14.31	17.02	17.28	15.15	17.62	14.34	14.82	16.19
SiO$_2$	65.27	49.92	48.83	48.90	49.38	48.71	54.30	50.84	51.60	46.80	51.65	52.52	47.57	49.58
P$_2$O$_5$	0.056	0.15	0.20	0.15	0.13	0.25	0.14	0.26	0.17	0.27	0.14	0.34	0.10	0.34
K$_2$O	0.12	0.39	0.51	0.30	0.37	0.35	0.04	0.56	0.23	0.33	0.23	0.20	0.64	0.26
CaO	7.03	10.60	13.13	11.49	10.23	15.04	7.22	10.99	10.39	12.75	10.33	8.65	10.60	10.16
MnO	0.18	0.21	0.20	0.19	0.20	0.23	0.15	0.21	0.17	0.18	0.17	0.20	0.54	0.19
TiO$_2$	0.13	1.55	1.60	1.07	0.75	2.25	1.03	1.34	0.67	1.81	0.67	1.74	0.48	1.59
FeO	6.75	12.95	11.24	11.83	10.19	12.32	9.28	10.68	10.35	14.12	10.23	13.00	13.55	12.43
TOTAL	101.11	101.37	101.14	100.61	100.37	101.35	98.76	100.97	102.40	101.94	102.51	100.73	99,75	101.97
trace elements (ppm)														
Cr	238	175	232	220	406	129	262	115	188	258	202	60	247	160
V	63	372	423	332	223	503	188	295	247	439	225	319	263	334
Ni	61	54	97	70	150	20	130	40	60	102.2	56	23	83	65
Rb	5	6.1	6.9	7.5	10	9.7	3.2	6.7	4.1	6.8	3.3	3.1	8.3	5.3
Sr	194	269	222	173	102	225	89	191	194	277	194	276	119	333
Y	11	29	33	24	24	40	31	31	21	29	20	37	19	35
Zr	65	100	98	64	53	115	70	79.1	59	99	60	118	43	111
Nb	1.9	3.6	3.2	1	2.1	4.1	1.9	1.2	0.8	3.5	0.9	5.9	1.5	5

Table 5.1-continued.

	Su 244	Su 148	Su 187	LL 176	X1	Su 65	LL 315	LL 583	LL 526	LL 520	Su 58	LL 362	M 87	Sh 197
major elements (wt % oxide)														
Na$_2$O	2.43	1.98	2.10	1.97	1.27	1.78	1.31	1.94	1.83	3.70	3.96	3.94	3.55	4.23
MgO	7.72	4.21	6.96	11.72	10.37	7.15	7.50	12.71	8.35	1.20	0.088	2.05	0.61	2.87
Al$_2$O$_3$	16.24	14.72	17.47	12.98	11.31	15.34	16.90	15.86	12.10	17.17	17.00	15.76	14.70	15.29
SiO$_2$	47.03	46.26	44.70	50.37	49.63	47.85	48.26	48.38	46.82	68.15	67.70	68.30	71.22	70.84
P$_2$O$_5$	0.23	0.38	0.20	0.099	0.026	0.20	0.12	0.21	0.32	0.19	0.14	0.073	0.12	0.011
K$_2$O	0.55	4.17	0.85	0.063	0.11	0.41	0.21	0.13	0.33	3.98	6.79	3.22	4.96	1.64
CaO	12.58	7.55	14.85	10.56	15.09	16.13	18.60	10.21	15.11	2.55	2.08	1.77	1.94	1.87
MnO	0.20	0.22	0.31	0.26	0.19	0.19	0.18	0.19	0.25	0.085	0	0.13	0.059	0.10
TiO$_2$	1.31	1.77	1.39	0.33	0.26	1.73	0.92	0.97	1.70	0.48	0.37	0.37	0.36	0.18
FeO	12.88	12.73	12.64	10.27	9.29	10.63	8.74	11.96	12.84	3.15	1.44	4.00	2.29	3.77
TOTAL	101.17	93.99	101.47	98.62	97.55	101.41	102.74	102.56	99.65	100.66	99.57	99.61	99.81	100.8
trace elements (ppm)														
Cr	244	222	312	840	804	204	162	288	352	0	0	0	0	0
V	394	311	460	195	201	497	410	266	470	33	21	12	6.1	0
Ni	78	101	70	202	154	41	68	150	151	0	0	2.5	0	0
Rb	9.8	70	10.6	3.7	6.3	8.1	8.1	4.9	8.1	112	172	83	134.8	34.7
Sr	274	134	211	141	134	260	192	208	164	281	760	152	211.5	130.9
Y	24	33	28	14	12	28	22	23	31	43	6.8	43	34.1	32.5
Zr	85	96	86	52	50	110	76	76	100	266	380	157	227.8	136.8
Nb	3.9	5.6	2.3	0.8	0	5.9	0.2	2.7	2.2	22	5.8	12	22.1	7.5

area, rocks have undergone upper amphibolite facies metamorphism that resulted in a high degree of differentiation, recrystallization, and local partial melting. These rocks have also been interpreted to have undergone an earlier episode of metamorphism that may have reached high grades and produced gneissic banding (Lemmon, 1973; Hopson and Hatcher, 1988). These two events erased virtually all preexisting textures and structures, and completely changed the mineral assemblages in the rock. In addition, most basalts undergo sea-floor hydrothermal metamorphism that can reach as high as amphibolite facies (Humphris and Thompson, 1978). Finally, rocks in the study area contain evidence for post-metamorphic hydrothermal alteration in the form of sulfide minerals (chalcopyrite, pyrite), quartz and epidote veins, and large (up to 1 cm) muscovite crystals growing around M_2 mineral assemblages. Petrographic evidence suggests that this alteration is isolated and minor, particularly in the amphibolites.

The effects of postmetamorphic alteration and weathering can be avoided by careful inspection of the samples prior to analysis. Marine hydrothermal metamorphism generally occurs at greenschist facies or below. Under these conditions, SiO_2, FeO, CaO, Na_2O, and K_2O are the most mobile oxides whereas most other elements remain immobile (Pearce and Cann, 1973; Humphris and Thompson, 1978; Wilson, 1989). Many studies conducted in high-grade terranes such as the eastern Blue Ridge and Inner Piedmont (e.g., Achaibar and Misra, 1984; Stow and others, 1984; Quinn, 1991; Davis, 1993a) have shown that regional upper amphibolite facies metamorphism did not significantly alter the bulk-rock chemistry of metabasalts, particularly with respect to elements such as Ti, Zr, P, and the rare earth elements, which have small ionic radii and high field strengths. These elements consequently tend to be relatively immobile and are most useful in studies that are conducted on highly altered basalts (Pearce and Cann, 1973; Shervais, 1982; Misra and McSween, 1984).

ORIGIN OF AMPHIBOLITE

Paraamphibolites and orthoamphibolites at high grades can look virtually identical in both outcrop and in thin section (Yardley, 1989). As discussed earlier in this chapter and in Chapter II, the presence of fine, felsic laminations suggests that the Poor Mountain Amphibolite may have been metamorphosed from a calcareous sediment, but Davis (1993a) has subsequently presented evidence that these rocks have an igneous origin. Orthoamphibolites and paraamphibolites can be distinguished from one another, however, by whole-rock geochemical data. Leake (1964) showed that the two types follow different patterns when plotted on a ternary diagram of Niggli values. Figure 5.2 shows such a plot of amphibolites collected and analyzed in the study area, and while they tend to cluster in the upper part of the plot, they clearly show an igneous trend at a high angle to the sedimentary trend.

Harker covariation diagrams have been constructed to further demonstrate an igneous origin for the amphibolites. Such diagrams are often used to graphically calculate how a melt changes composition as a particular mineral crystallizes or as a contaminant is added (Cox and others, 1979). Davis (1993a) conducted similar studies in the Inner Piedmont immediately south of the study area. This study will attempt to establish such relationships only for the purpose of further establishing an igneous origin for the amphibolites. A more detailed discussion of the igneous petrogenesis of amphibolites very similar to those in the study area, however, is given by Davis (1993a).

Most authors use SiO_2 as the fractionation index in Harker covariation diagrams when analyzing unmetamorphosed basalts (Wilson, 1989). In metamorphosed terranes, however, SiO_2 is highly mobile and its use tends to produce widespread scatter. One such variation diagram was constructed using $Na_2O + K_2O$ vs. SiO_2 and shows surprisingly little scatter despite the high mobility of all three oxides used in the diagram (Pearce, 1975; Fig. 5.3). It shows that most amphibolite samples form an indistinct trend in the basalt and basaltic

Figure 5.2. Niggli *mg* vs. *c* vs. *al-alk* plot of samples from the study area (from Leake, 1964) where *mg* = 100× [MgO/FeO+MnO+MgO], *c* = CaO, and *al-alk* = [Al$_2$O$_3$]-[Na$_2$O+K$_2$O].
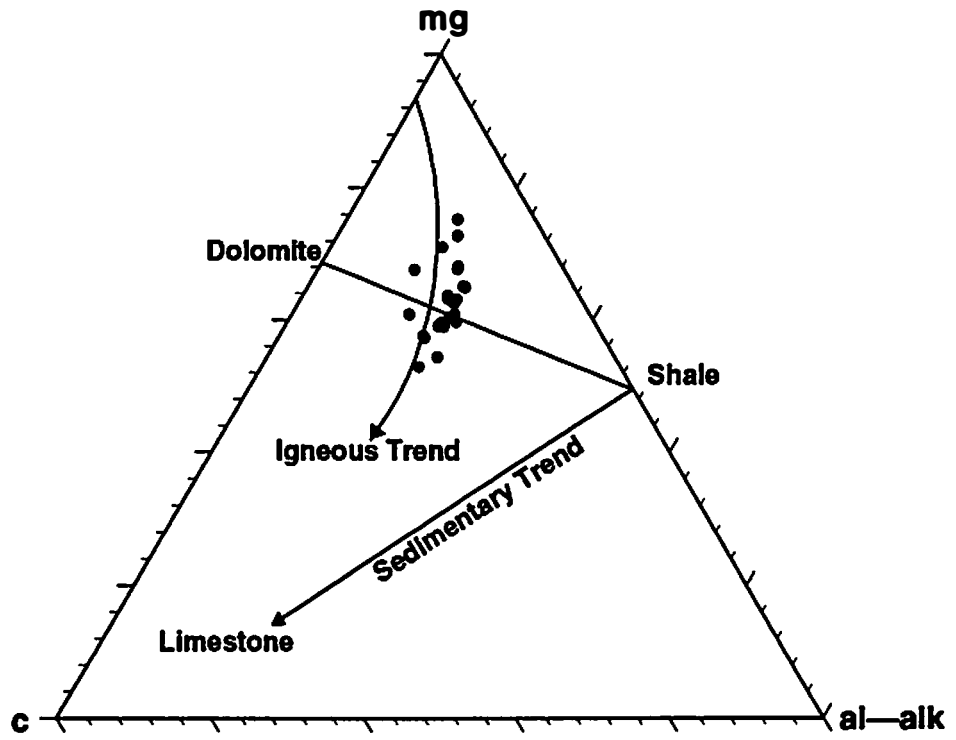
Figure 5.3. Harker covariation diagram plotting $Na_2O + K_2O$ vs. SiO_2 for samples in the study area. The squares denote amphibolite samples whereas the circles denote granitoid gneiss samples. The two different rock types are genetically unrelated.
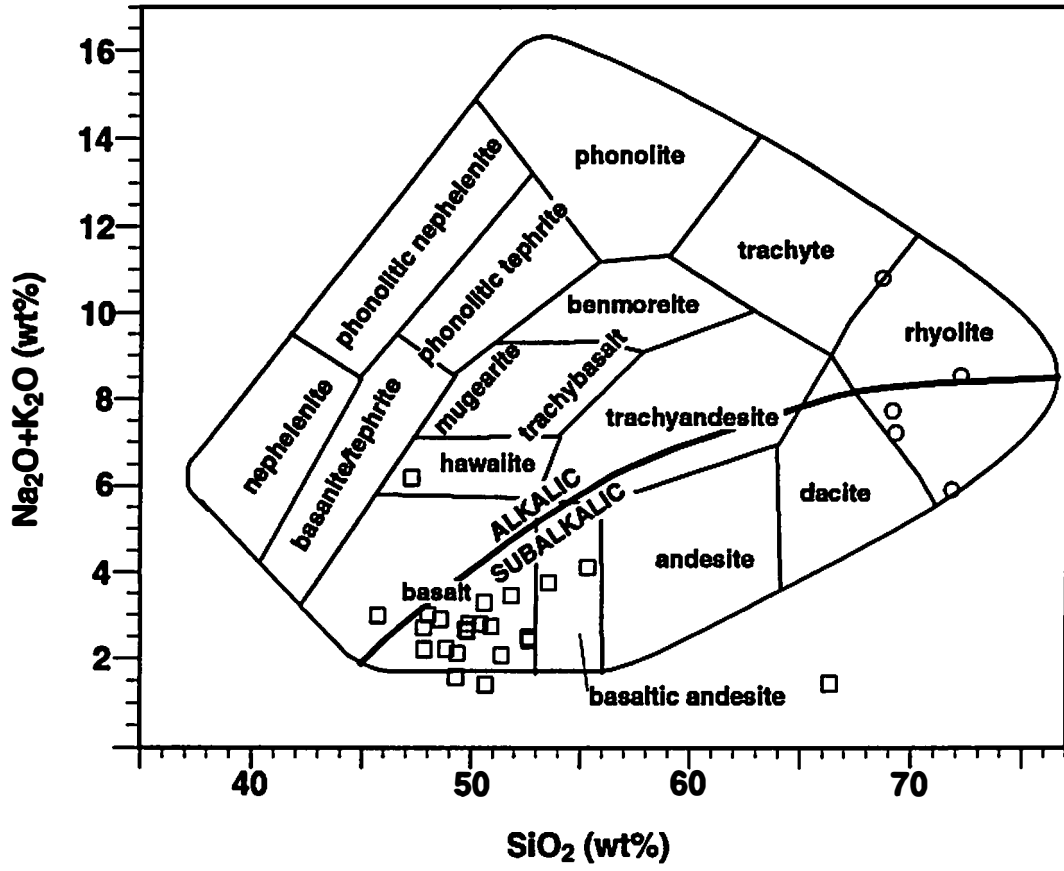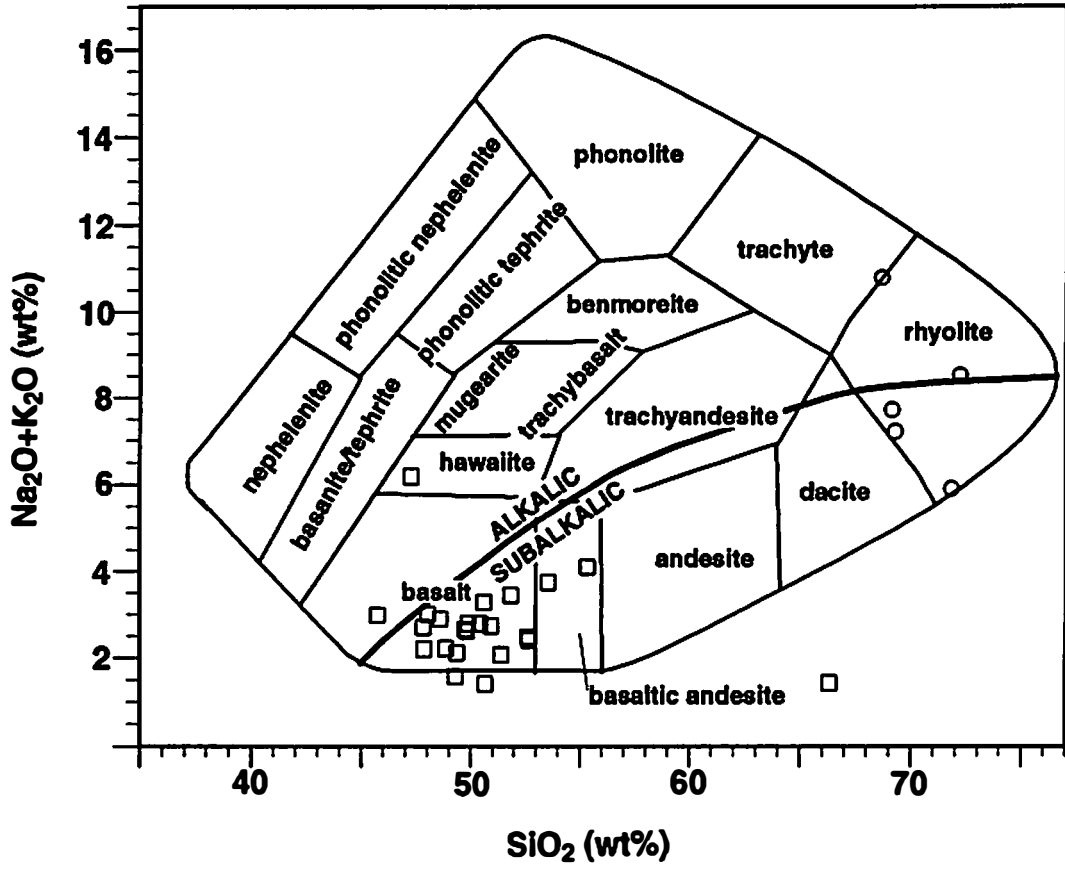
Figure 5.4. Covariation diagrams using Zr as the differentiation index. (a) plots Zr against major elements and (b) plots Zr against trace elements.

(A)
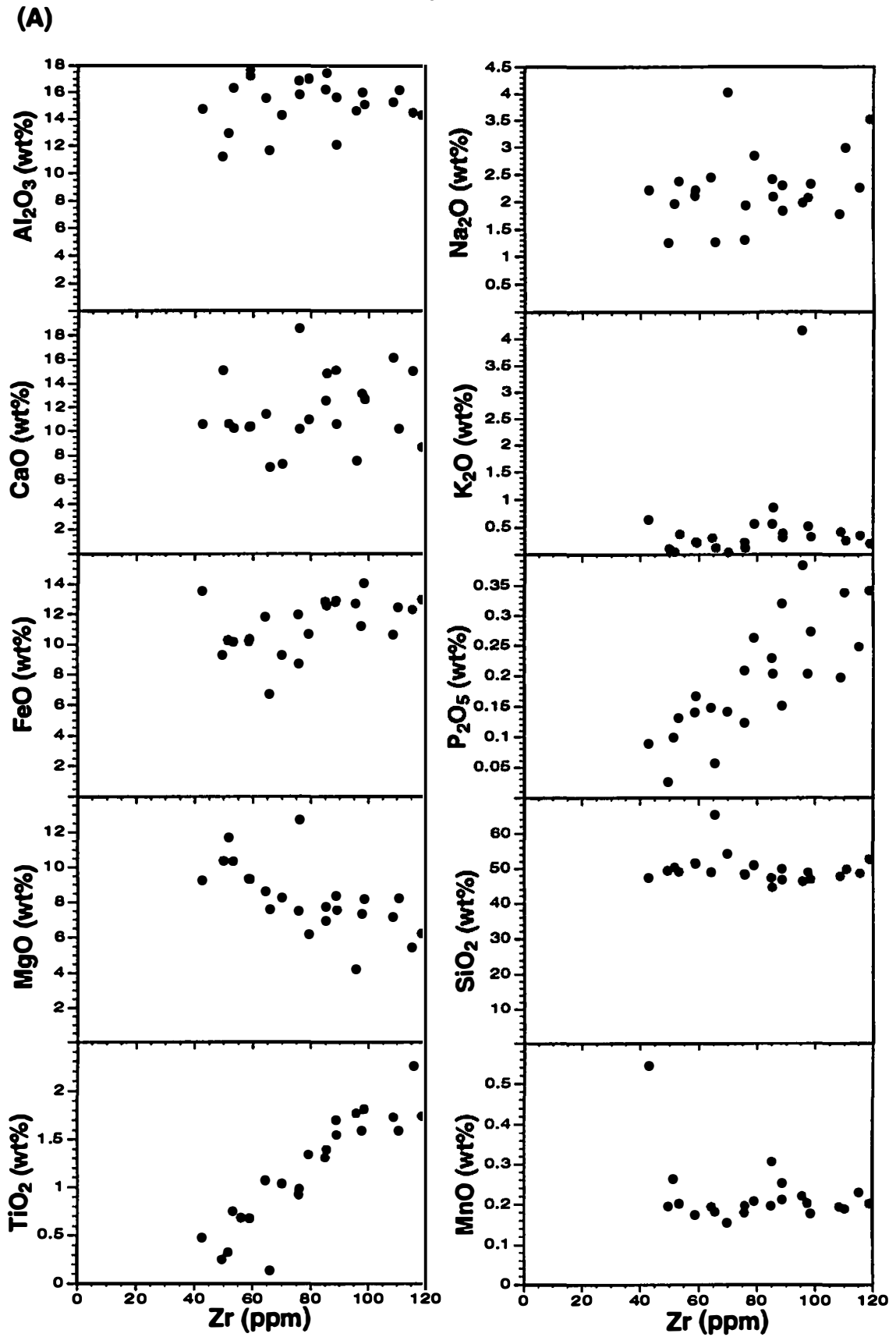
(B)
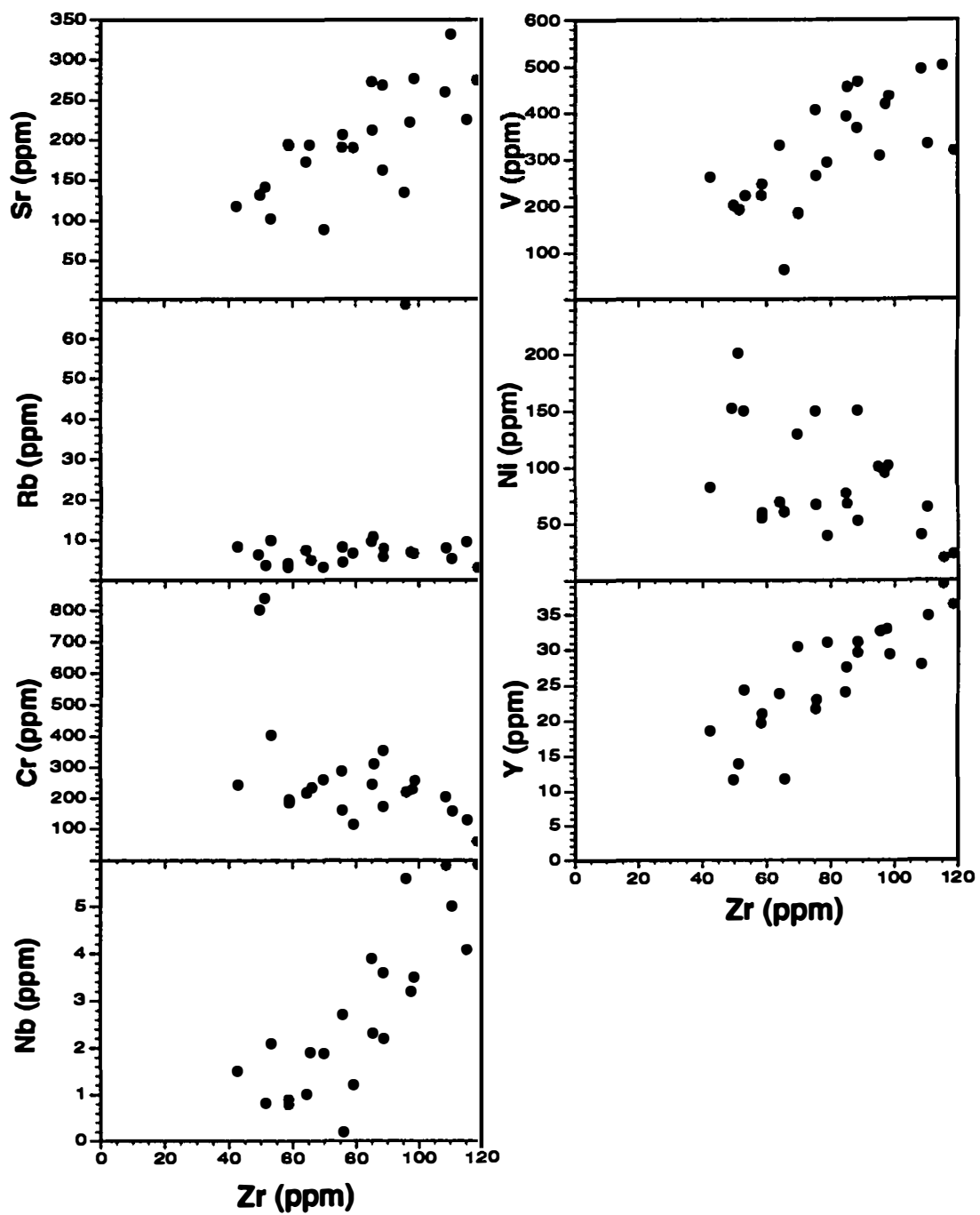
Figure 5.5. Covariation diagrams for selected elements using the Mg number (MgO/(MgO+FeO total) as the differentiation index. Note trends for elements plotted against the Mg number are opposite those plotted against Zr (Fig. 5.4).

MgO/(MgO+FeO total)

MgO/(MgO+ total)
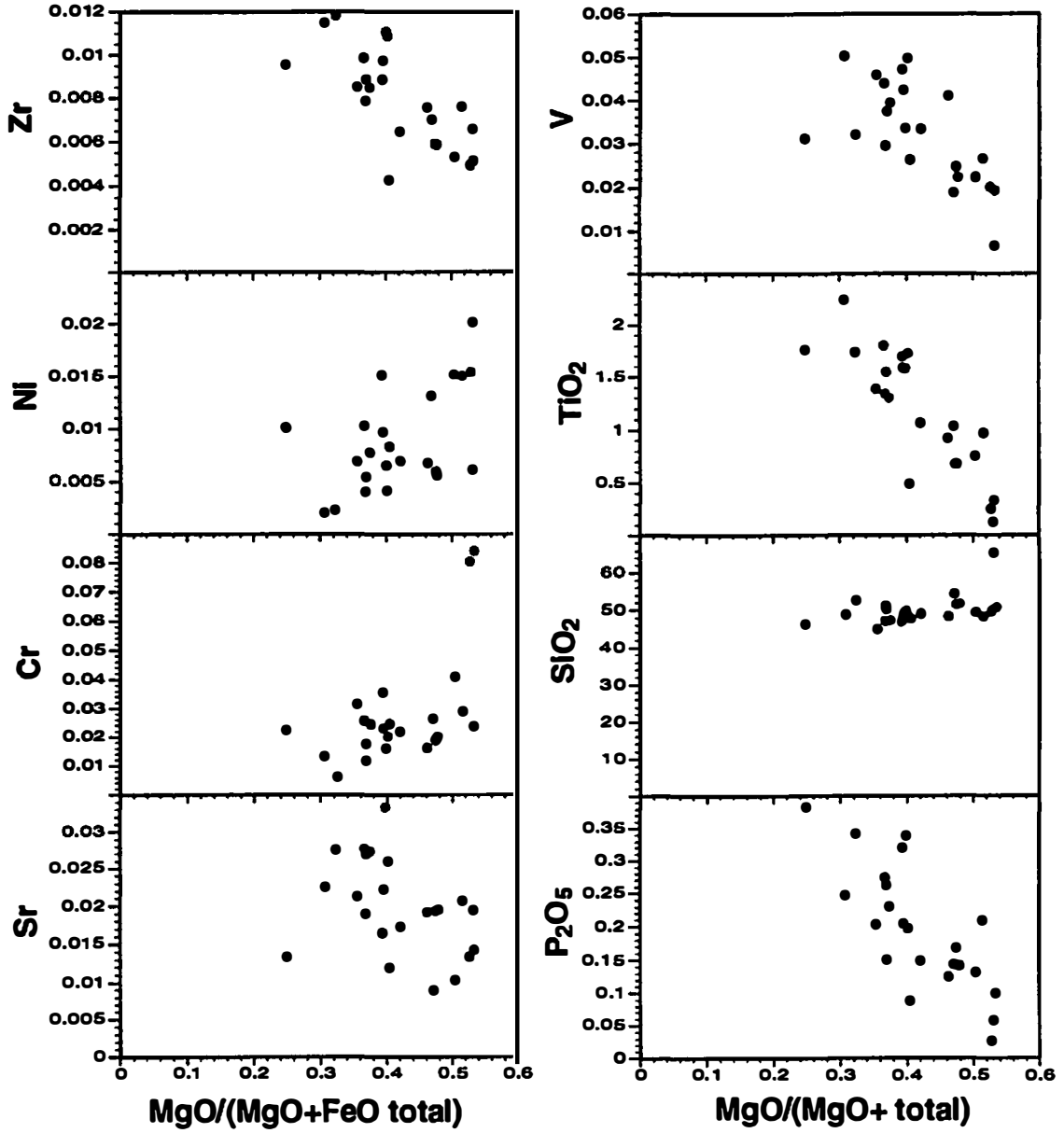
TECTONIC DISCRIMINATION DIAGRAMS

Many tectonic discrimination diagrams focus on the relatively mobile elements and oxides such as SiO_2, K_2O, or Na_2O (Wilson, 1989). Figure 5.6 is an AFM diagram utilizing three relatively mobile elements. The plotted amphibolites cluster surprisingly tightly within the calk-alkaline trend. This contrasts with most amphibolites in the eastern Blue Ridge and Inner Piedmont, which generally plot in the tholeiitic trend (Misra and McSween, 1984; Stow and others, 1984; Misra and Conte, 1991; Quinn, 1991; Davis and others, 1992; Davis, 1993a). Furthermore, this pattern plots roughly in the dacite-andesite field, which contradicts other plots made in this study, including Figure 5.3. Given the relative mobility of Al_2O_3, FeO, and MgO, it is probable that this anomalous pattern is due to modification by metamorphism.

In order to differentiate more precisely what type of basalt these rocks are, however, elements that are less sensitive to postmagmatic alteration are needed. TiO_2, P_2O_5, Zr, Nb, and Y are among those elements used in this study that undergo the least modification during metamorphism and hydrothermal alteration, and are therefore, ideal for discriminating between the various possible tectonic settings (Pearce and Cann, 1973; Floyd and Winchester, 1975; Wood and others, 1979).

Two ternary plots using Ti-Zr-Y (Pearce and Cann, 1973) and Nb-Zr-Y (Meschede, 1986) indicate the basalts are derived from a MORB setting although some scatter into the island arc field occurs (Fig. 5.7). Plots of Zr/Y-Zr (Pearce and Norry, 1979) and Ti-Cr (Pearce, 1975) show some clustering but fail to define the tectonic setting of the metabasalts. Diagrams using TiO_2-Zr (Pearce, 1980), V-Ti (Shervais, 1982), and Cr-FeO/MgO (Miyashiro and Shido, 1975) show some scatter into the adjacent fields but appear to favor a MORB origin (Fig. 5.7).

Figure 5.6. AFM ternary plot for amphibolites from the study area where A=Al$_2$O$_3$, F=FeO total, and M=MgO. The boundary between the tholeiitic and calc-alkaline fields is from Irvine and Baragar (1971).
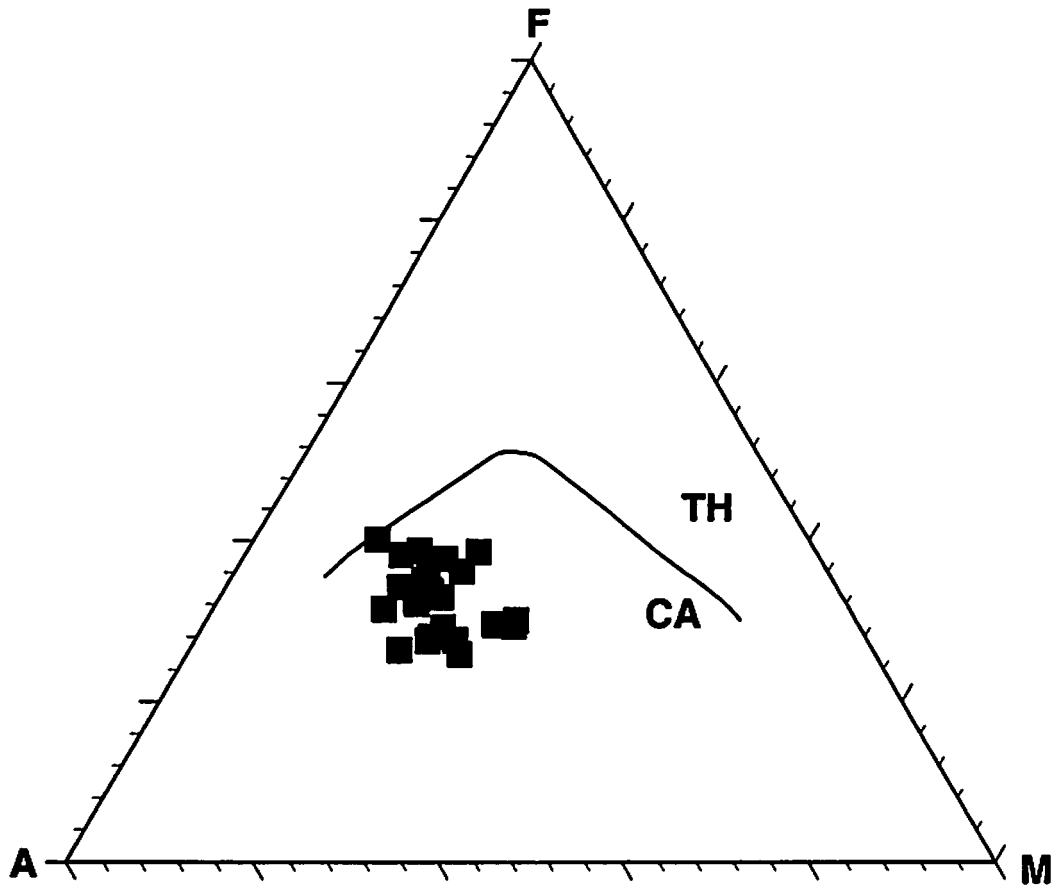
Figure 5.7. Tectonic discrimination diagrams of amphibolites from the study area. (A) plots Ti

vs. Zr vs. Y and is derived from Pearce and Cann (1973). Abbreviations:

WPB=within plate basalt; LKT=low-K tholeiite; MORB=mid-ocean ridge basalt;

CAB=calc-alkaline basalt. (B) Nb vs. Zr vs. Y (from Meschede, 1986).

Abbreviations: WPA=within plate alkali basalt; WPT=within plate tholeiite;

VAB=volcanic arc basalt; P-MORB=plume MORB; N-MORB= normal MORB. (C)

TiO_2 vs. Zr (Pearce, 1980). Abbreviations are defined above. (D) V vs. Ti (Shervais,

1982). (E) Cr vs. FeO/MgO (Miyashiro and Shido, 1975). In all graphs, squares

denote samples that have between 12 and 20% CaO and circles denote samples that

have more than 20% CaO.

(A)

Tl/100

Zr

3Y

IAT

WPB

CAB

MORB and IAT

(B)

2Nb

Zr/4

Y

WPA

P-MORB

N-MORB

WPT

VAB

(C)

(D)

(E)
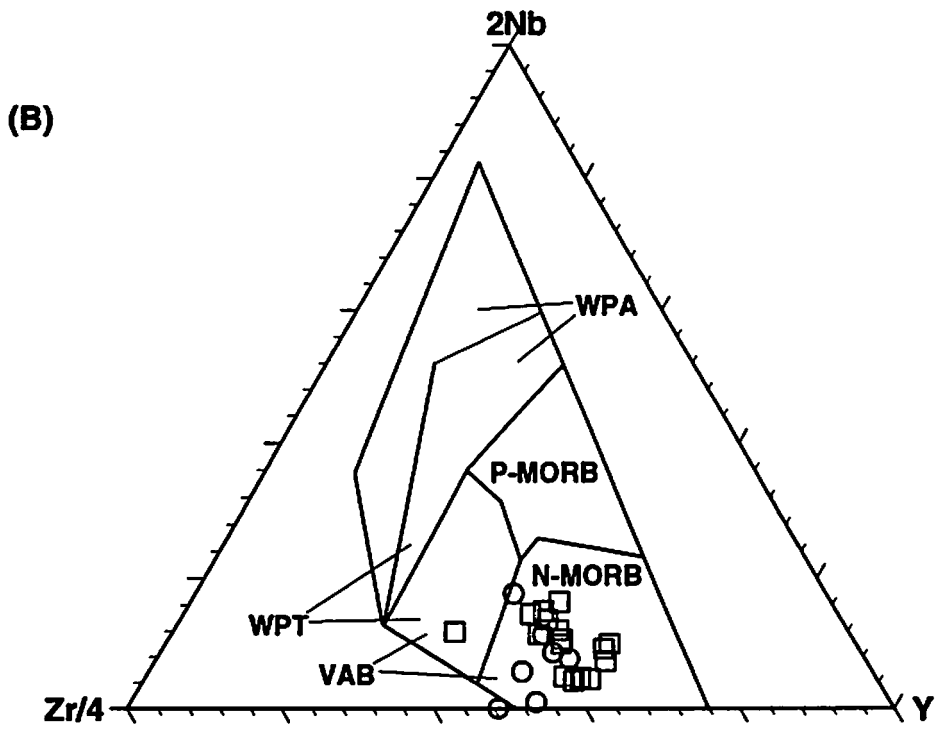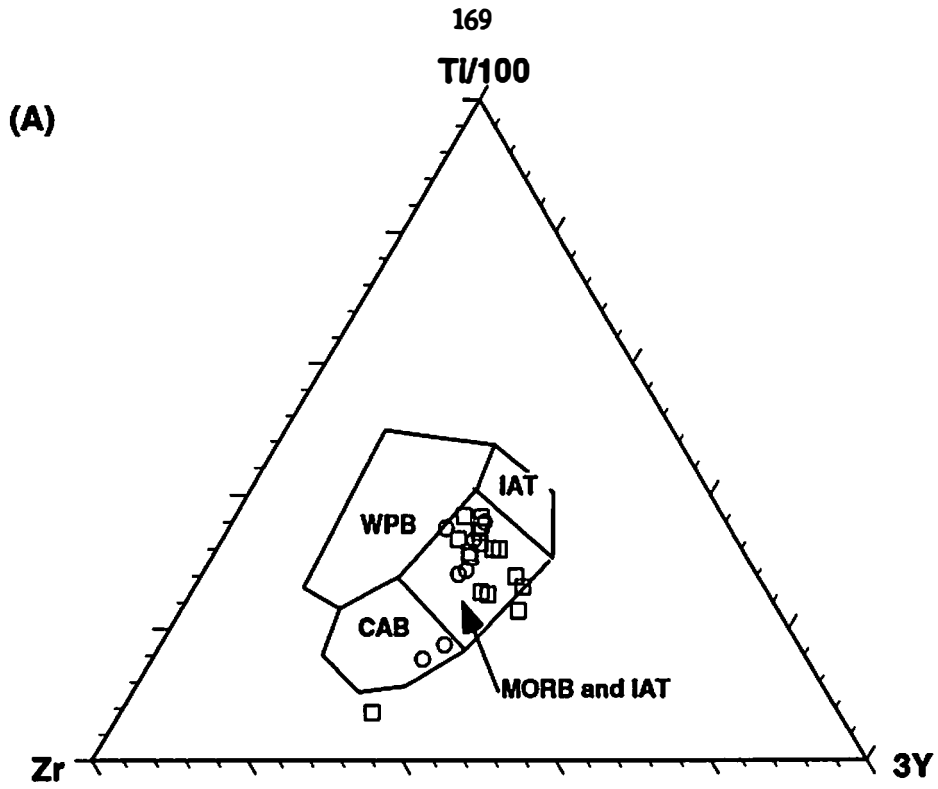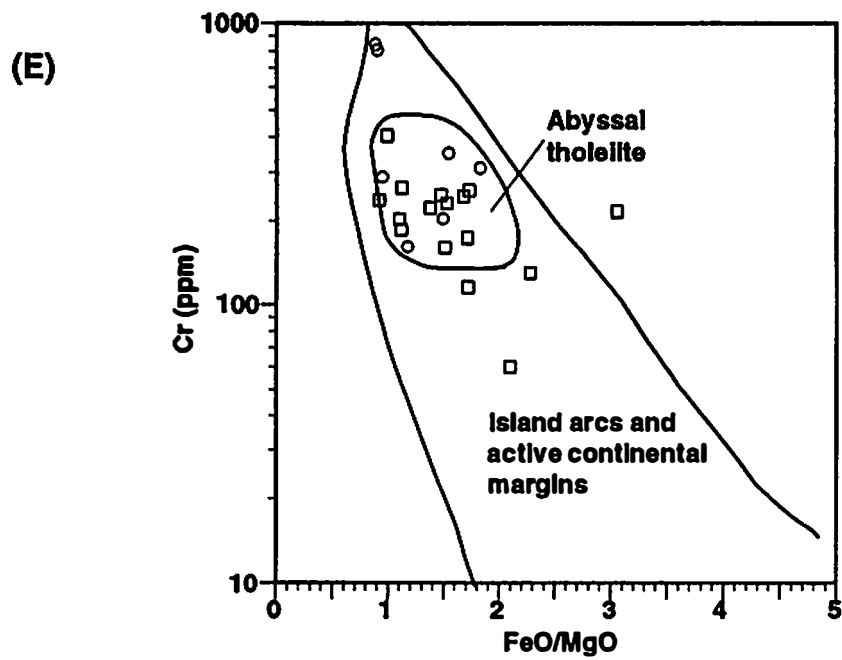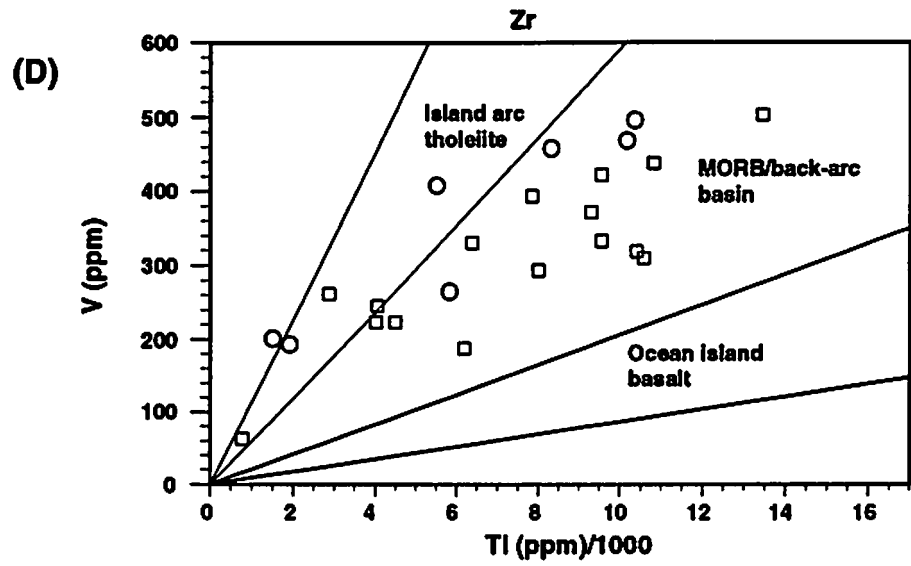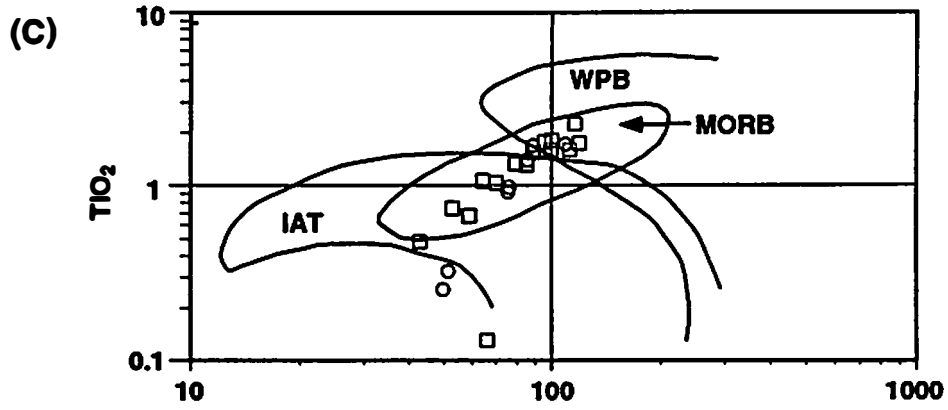
DISCUSSION

The interpretation that amphibolites in the study area have a MORB origin is consistent with those made in other parts of the Inner Piedmont (Achaibar and Misra, 1984; Stow and others, 1984; Davis, 1993a) as well as those made in the eastern Blue Ridge (McConnell and Abrams, 1984; Gillon, 1989; Misra and Conte, 1991; Quinn, 1991). Island arc affinities, however, are also present in the Alabama Inner Piedmont (Stow and others, 1984; Neilson and Stow, 1986) and eastern Blue Ridge (Tull and Stow, 1979; Eggers, 1983; Hopson, 1989; Walters, 1990). To further document an ocean floor basalt protolith for the amphibolites, spider diagrams normalized to both MORB and to island arc tholeiite were constructed (Fig. 5.8). Both diagrams exhibit some scatter, some of which is probably due to metamorphism. For the more immobile elements, however, metabasalts from the study area more closely correlate with MORB than with island arc tholeiite. Therefore, I conclude that amphibolites from the study area have a MORB affinity. This interpretation is consistent with the covariation diagrams, wherein trends are characteristic of tholeiitic basalt, and the tectonic discrimination diagrams, which, in general, favor a MORB setting.

Geochemical signatures of amphibolites of the Ashe and Alligator Back Formation prompted Misra and Conte (1991) to speculate that they evolved in a back-arc basin. Alternatively, they argued for multi-stage melting of an upper mantle source adjacent to a mantle plume in a MORB environment. A back-arc basin origin for metabasalt in other parts of the Blue Ridge and Inner Piedmont has also been speculated by McConnell and Abrams (1984), Stow and others (1984), Gillon (1989), Neilson and Stow (1986), and Davis (1993a).

Back arc basins have been hypothesized by Karig (1971) and Crawford and others (1981) to evolve as a diapiric upwelling of deep asthenospheric mantle intrudes beneath an island arc system. While arc volcanism ceases, isothermal decompression of the upwelling leads to partial melting, producing MORB-like back-arc basin basalts (Wilson, 1989). During the early

Figure 5.8. Spider diagrams normalized to mid-ocean ridge basalt (A) and island-arc tholeiite (B). The diagrams show average values as well as the standard deviation for the samples. Normalizing values are from Pearce (1982) for MORB and Wilson (1989) for island arc tholeiite.
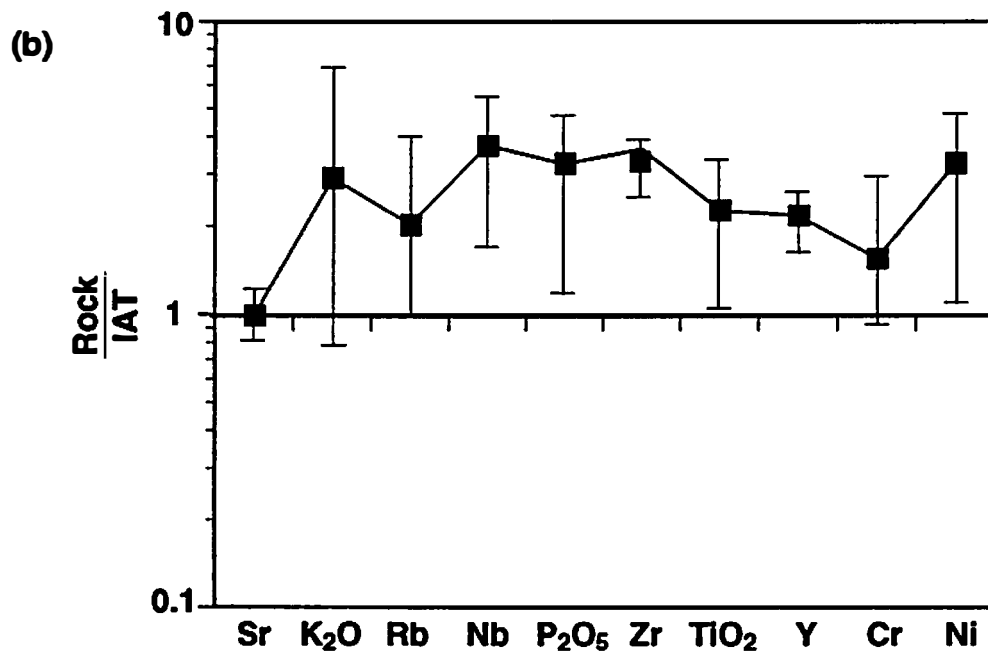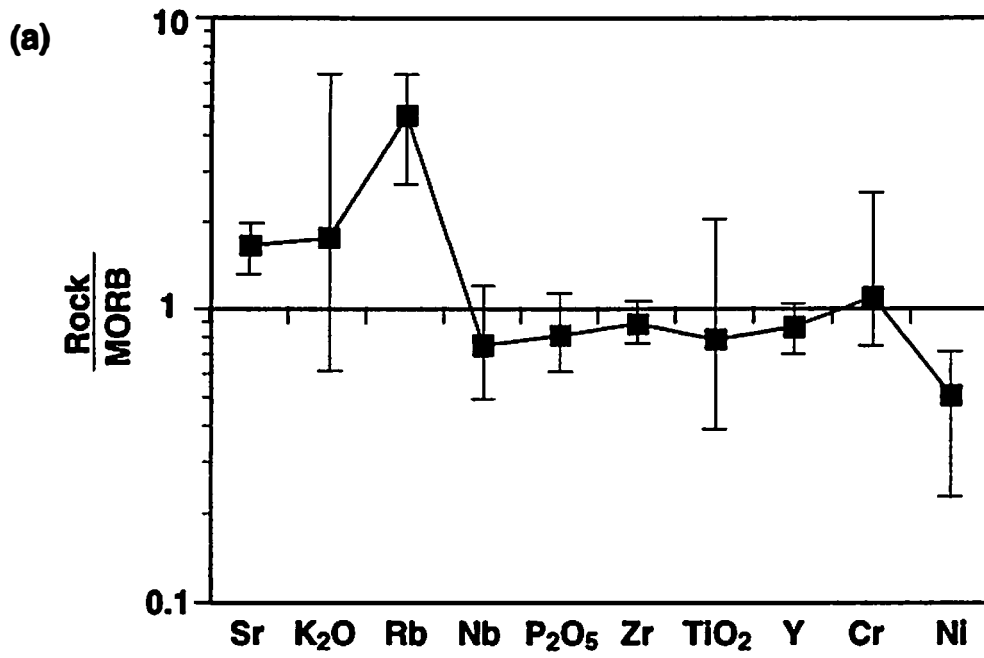
stages of back-arc rifting, when the spreading center remains close to the trench, fluids derived from the subducting slab may alter the chemistry of the back-arc basalts. As spreading proceeds, however, the influence of these fluids diminishes and the composition of the back-arc basalts gradually approaches an N-type MORB (Tarney and others, 1977; Wilson, 1989). The geochemistry of back-arc basin basalts typically are subject to a number of complex variables that may influence the chemistry of the associated basalts, particularly during the incipient stages of basin development. Such variables include the source components available for the production of back-arc basalts, the degree of partial melting, varying P_{H_2O} and P_{O_2} conditions during melting, and the influence of slab-derived fluids. As a consequence, while the major element geochemistry for back-arc basalt is identical to MORB, the trace element chemistry tends to be complex, showing both island arc and MORB affinities (Wilson, 1989).

The geochemical data collected for this study can neither definitively support nor refute a back-arc basin origin for metabasalts in the study area. Spider diagrams of metabasalts from the study area reveal an enrichment in elements such as Sr, K, and Rb and a depletion in Ni relative to MORB, a pattern reflected by many back-arc tholeiites (Saunders and Tarney, 1979; Humphris and others, 1985; Wilson, 1989). This evidence remains largely circumstantial, however, because whole rock analysis conducted for this study lacks key elements (e.g., Ba, Th, Ta) useful for comparisons with modern back-arc basalts. Furthermore, Sr, K, and Rb are relatively mobile during regional metamorphism, although covariation diagrams suggest that Sr and Rb retain their protolith concentrations. Future studies on similar metabasalts could benefit by the addition of such trace elements as Ba, Th, Ta, and Hf, plus rare earth elements and radiogenic isotopes.

The variety of affinities displayed by metabasalts throughout the Inner Piedmont and eastern Blue Ridge and their relationships with adjacent rocks suggest a complex history of development of the Laurentian margin and its subsequent destruction. The diversity of these rocks is consistent with continental rifting, subsequent development of an ocean basin, possibly a

back-arc basin, and island-arc volcanism proposed in the tectonic models of Rodgers (1970),

Brown (1970) Hatcher, (1972, 1978, 1987, 1989), Rankin (1976), and Thomas (1976, 1977, 1991).

Amphibolites in the study area have chemical compositions reflective of extrusion in an ocean

basin or possibly, a back-arc basin environment.

VI. CONCLUSIONS

1. The study area is composed of three major lithotectonic units, each separated by a ductile thrust fault. The lower boundary of unit 1, the structurally lowermost lithotectonic unit, is outside the study area but is underlain by the premetamorphic Tumblebug Creek fault in areas outside the study area. The upper boundary of unit 3 is also outside the area and the nature of this boundary is unknown in the Columbus Promontory.

2. The stratigraphy of the study area consists of three mappable units that include the Henderson Gneiss, the Poor Mountain Formation, and the Mill Spring complex. Unit 1 is composed almost entirely of Henderson Gneiss. Unit 2 is composed of upper Mill Spring biotite gneiss and granitoid gneiss and is overlain by the Poor Mountain Formation. The Poor Mountain Formation can be subdivided into a lower unit of amphibolite and an upper unit of quartzite. Unit 3 is composed of a lower unit of upper Mill Spring biotite gneiss and biotite-muscovite schist and an upper unit of undifferentiated biotite gneiss, granitoid gneiss, and amphibolite.

3. Four major episodes of deformation have been recognized in the study area. The first episode (D_1) involves premetamorphic isoclinal folding that was subsequently transposed by D_2 deformation. D_2 occurred during peak M_2 metamorphism and accounts for virtually all the shear strain observed in the Inner Piedmont.

4. D_2 deformation is characterized by pervasive ductile shearing. Associated structures include a mylonitic C-fabric, a mineral transport lineation, type 1 and type 2 S-C mylonites,

ductile thrust faults, and intrafolial folds and sheath folds. Most D_2 structures are penetrative and formed under conditions of progressive noncoaxial flow.

5. D_3 deformation occurred after peak M_2 metamorphism but prior to complete cooling of the rocks. It involved considerably less shear strain than D_2 deformation. Its associated structures, including folds deforming the S_2 foliation, boudinage, and outcrop-scale faults, are nonpenetrative.

6. Orientation of mineral lineations and other shear-sense indicators, such as S-C fabrics, winged porphyroblasts, snowball garnets, and Hansen analysis of folds, suggest that shear sense varied gradually from ESE in areas to the southeast to SE in areas to the northwest. This change in transport direction may be related to a dextral component of shear along the primordial Brevard fault zone.

7. Hansen analysis of F_2 and F_3 folds indicate that shear-sense did not significantly change between D_2 and D_3 deformation. This evidence as well as observations of F_3 folds growing by amplification of F_2 folds and the similarity in the geometry and orientation of old F_3 folds and young F_2 folds suggests that D_2 and D_3 represents a single continuous episode of deformation. During this episode, the rheological properties of the rocks changed giving rise to the distinctive fold geometries associated with each event.

8. Mineral assemblages indicate that the metamorphic grade reached the first sillimanite zone in pelitic schist and upper amphibolite facies in amphibolite. Based on these mineral assemblages and the interpretation that migmatitic textures indicate partial melting, temperatures in the study area probably ranged from 625° to 700°C and pressures probably ranged from 3.5 to 8.0 kbars.

9. Mineral assemblages in pelitic schist are characterized by two periods of mineral growth. This is supported by zoning patterns in garnet as well as the tendency for garnet to appear in both euhedral and anhedral skeletal forms. Growth of sillimanite probably occurred by consumption of anorthite, garnet, and muscovite.

10. The study area underwent a period of retrograde metamorphism that reached the chlorite zone in pelitic schist and greenschist facies in amphibolite. These mineral assemblages are similar to those observed in the Brevard fault zone and are probably coeval. This suggests that the age of retrograde metamorphism is Alleghanian.

11. Based on whole-rock geochemical analysis and tectonic discrimination diagrams, the protolith of the Poor Mountain Amphibolite is interpreted to be a tholeiitic basalt.

12. Spider diagrams and tectonic discrimination diagrams suggest that the amphibolites originated in a mid-ocean ridge setting (MORB)

REFERENCES CITED

REFERENCES CITED

Achaibar, J., 1983, A petrologic and geochemical study of some amphibolite bodies in the Smith River allochthon, Virginia (M. S. thesis): Knoxville, University of Tennessee, 93 p.

Achaibar, J., and Misra, K. C., 1984, Amphibolites of the Smith River allochthon, southwest Virginia, southern Appalachians: Geological Society of America Abstracts with Programs, v. 16, p. 121.

Ashworth, J. R., and Brown, M., 1990, High-temperature metamorphism and crustal anatexis: London, Unwin Hyman, 407 p.

Bentley, R. D., and Neathery, T. N., 1970, Geology of the Brevard zone and related rocks of the Inner Piedmont of Alabama: Alabama Geological Society, Eighth Annual Field Trip Guidebook, 119 p.

Bobyarchick, A. R., 1984, A late Paleozoic component of strike-slip in the Brevard zone, southern Appalachians: Geological Society of America Abstracts with Programs, v. 16, p. 126.

Bobyarchick, A. R., Edelman, S. R., and Horton, J. W., Jr., 1988, The role of dextral strike-slip in the displacement history of the Brevard zone, in Secor, D. T., ed., Southeastern Geological Excursions: Geological Society of America Southeastern Section Field Trip Guidebook, p. 53-154.

Brown, W. R., 1951, Major structural features in the Lynchburg quadrangle, Virginia: Virginia Journal of Science, v. 2, p. 346-347.

Brown, W. R., 1958, Geology and mineral resources of the Lynchburg quadrangle, Virginia: Virginia Division of Mineral Resources, Bulletin 74, 99 p.

Brown, W. R., 1970, Investigations of the sedimentary record in the Piedmont and Blue Ridge of Virginia, in Fisher, G. W., Pettijohn, F. J., Reed, J. C., and Weaver, K. N., eds., Studies in Appalachian geology: Central and southern: New York, Wiley— Interscience, p. 336-349.

Bryant, B., and Reed, J. C., Jr., 1970, Geology of the Grandfather Mountain window and vicinity, North Carolina and Tennessee: U. S. Geological Survey Professional Paper 615, 190 p.

Butler, J. R., 1990, Metamorphism, in Horton, J. W., Jr., and Zulio, V. A., eds., The Geology of the Carolinas, Carolina Geological Society Fiftieth Anniversary Volume: Knoxville, The University of Tennessee Press, p. 127-141.

Carreras, J., Estrada, A., and White, S., 1977, The effects of folding on the c-axis fabrics of a quartz mylonite: Tectonophysics, v. 39, p. 3-24.

Cartwright, I., 1990, Prograde metamorphism, anatexis, and retrogression of the Scourian Complex, north-west Scotland, in Ashworth, J. R., and Brown, M., eds., High-temperature metamorphism and crustal anatexis: London, Unwin Hyman, 407 p.

Cazeau, C. J., 1967, Geology and mineral resources of Oconee County, South Carolina: South Carolina Division of Geology Bulletin, v. 34, 38 p.

Chaterjee, N. D., and Johannes, W., 1974, Thermal stability and standard thermodynamic properties of synthetic 2M1 muscovite, $KAl_2AlSi_3O_{10}(OH)_2$: Contributions to Mineralogy and Petrology, v. 48, p. 89-114.

Clark, G. M., 1993, Quaternary geology and geomorphology of part of the Inner Piedmont of the southern Appalachians in the Columbus Promontory upland area, southwestern North Carolina and northwestern South Carolina, *in* Hatcher, R. D., Jr., and Davis, T. L., eds., Studies of Inner Piedmont Geology with a focus on the Columbus Promontory, Carolina Geological Society Guidebook, p. 67-84.

Cobbold, P. R., and Quinquis, H., 1980, Development of sheath folds in shear regimes: Journal of Structural Geology, v. 2, p. 119-126.

Conley, J. F., 1978, Geology of the Piedmont of Virginia: Interpretation and problems: *in* Contributions to Virginia Geology— III, Virginia Division of Mineral Resources Publication 7, p. 115-149.

Conley, J. F., and Drummond, K. M., 1963, Brecciated dikes in the southern Piedmont and mountain regions of North Carolina: Geological Society of America Special Paper 76 (abstract), p. 241.

Conley, J. F., and Drummond, K. M., 1965, Ultramylonite zones in the western Carolinas: Southeastern Geology, v. 6, p. 201-211.

Conley, J. F., and Drummond, K. M., 1981, Geologic map and mineral resources summary of northeast 1/4 Marion quadrangle, North Carolina: North Carolina Department of Natural Resources and Community Development Map 202 NW, scale 1/24,000.

Conley, J. F., and Henika, W. S., 1973, Geology of the Snow Creek, Martinsville East, Price, and Spray quadrangles, Virginia: Virginia Division of Mineral Resources, Report of Investigations 33, 71 p.

Coruh, C., Costain, J. K., Hatcher, R. D., Jr., Platt, T. L., Williams, R. T., and Phinney, R. A., 1987, Results from regional VIBROSEIS profiling: Appalachian ultra-deep core hole site study: Geophysical Journal of the Royal Astronomical Society, v. 89, p. 147-156.

Cox, K. G., Bell, J. D., and Pankhurst, R. J., 1979, The interpretation of igneous rocks: London, Allen and Unwin, 450 p.

Crawford, A. J., Beccaluva, L., and Serri, G., 1981, Tectonomagmatic evolution of the West Phillipine—Mariana region and the origin of boninites: Earth and Planetary Science Letters, v. 54, p. 346-356.

Dallmeyer, R. D., 1988, Late Paleozoic tectonothermal evolution of the western Piedmont and eastern Blue Ridge, Georgia: Controls on the chronology of terrane accretion and transport in the southern Appalachian orogen: Geological Society of America Bulletin, v. 100, p. 702-713.

Davis, T. L., 1993a, Stratigraphy, structure, and metamorphism of a crystalline thrust terrane, western Inner Piedmont, North Carolina (PhD dissertation): Knoxville, Tennessee, University of Tennessee, 245 p.

Davis, T. L., 1993b, Geology of the Columbus Promontory, western Piedmont, North Carolina, Southern Appalachians, *in* Hatcher, R. D., Jr., and Davis, T. L., eds., Studies of Inner Piedmont Geology with a focus on the Columbus Promontory, Carolina Geological Society Guidebook, p. 17-43.

Davis, T. L., and Tabor, J. R., 1988, Preliminary report on detailed mapping of the western Inner Piedmont, Cliffield Mountain quadrangle and surrounding area, North and South Carolina: Geological Society of America Abstracts with Programs, v. 21, p. 11.

Davis, T. L., Tabor, J. R., Hatcher, R. D., 1989, Orogen-parallel to orogen-oblique ductile deformation and possible late Paleozoic (?) ductile deformation of the western Piedmont, southern Appalachians: Geological Society of America Abstracts with Programs, v. 21, p. A65

Davis, T. L., Tabor, J. R., and Hatcher, R. D., Jr., 1990a, Possible late Paleozoic (?) ductile front exposed in the Columbus Promontory, North Carolina: implications for emplacement of the Blue Ridge-Piedmont thrust sheet, southern Appalachians and the kinematics of Paleozoic Africa-North America collision: Geological Society of America Abstracts with Programs, v. 22, p. A225.,

Davis, T. L., Tabor, J. R., and Hatcher, R. D., Jr., 1990b, Geologic mapping in the Columbus Promontory, western Piedmont: Polyphase development of a crystalline thrust complex: Geological Society of America Abstracts with Programs, v. 21, p. A65.

Davis, T. L., Hatcher, R. D., Jr., Liu, A., and Tabor, J. R., 1991a, Structural development of a progressively deformed crustal-scale shear zone, southern Appalachian Inner Piedmont, U. S. A.: The geometry of deformed rocks (John Ramsay Meeting) Mitt. aus den Geol. Inst. ETH Zurich, Neue Folge, p. 119-120.

Davis, T. L., Hatcher, R. D., Jr., Liu, A., and Tabor, J. R., 1991b, Southern Appalachian western Inner Piedmont: a crustal—scale shear zone: Geological Society of America Abstracts with programs, v. 23, p. A138.

Davis, T. L., Hatcher, R. D., Jr., and Misra, K. C., 1992, Regional comparisons of stratigraphic sequences and mafic geochemistry, southern Appalachian Inner Piedmont and eastern Blue Ridge: Constraints on Laurentian margin development, terrane accretion and tectonic models: Geological Society of America Abstracts with Programs, v. 24, p. 11.

Dennis, J. G., Price, R. A., Salem, J. K., Hatcher, R. D., Jr., Bally, A. W., Perry, W. J., Laubscher, H. P., Williams, R. E., Elliot, D., Norris, D. K., Hutton, D. W., Emmett, T., 1981, What is a thrust? What is a nappe?, *in* McClay, K. R., and Price, N. J., eds., Thrust and nappe tectonics: Geological Society of London Special Publication 9, p. 7-9.

Dewey, J. F., and Kidd, W. S. F., 1974, Continental collisions in the Appalachian-Caledonian orogenic belt: variations related to complete and incomplete suturing: Geology, v. 2, p. 543-546.

Edelman, S. H., Liu, A., and Hatcher, R. D., Jr., 1987, The Brevard zone in South Carolina and adjacent areas: An Alleghanian orogen-scale dextral shear zone reactivated as a thrust fault: Journal of Geology, v. 95, p. 793-806.

Eggers, M. R., 1983, Petrology, structure, and geochemistry of the Kimsey Bald mafic complex, North Carolina (M. S. thesis): Columbia, South Carolina, University of South Carolina, 72 p.

Espenshade, G. H., 1954, Geology and mineral deposits of the James River-Roanoke River manganese district, Virginia: U. S. Geological Survey Bulletin 1008, 155 p.

Evans, D. J., and White, S. H., 1984, Microstructural and fabric studies from the rocks of the Moine Nappe, Eriboll, NW Scotland: Journal of Structural Geology, v. 6, p. 369-389.

Evans, N. H., and Speer, J. A., 1984, Low-pressure metamorphism and anatexis of Carolina Slate Belt phyllites in the contact aureole of the Lilesville pluton, North Carolina, U. S. A.: Contributions to Mineralogy and Petrology, v. 87, p. 297-309.

Fabbri, L. A., 1986, Geophysical interpretation of a portion of the southern Appalachian Blue Ridge and Inner Piedmont (M. S. thesis): Columbia, South Carolina, University of South Carolina, 68 p.

Favret, P. D., and Williams, R. T., 1988, Basement beneath the Blue Ridge and Inner Piedmont in northeastern Georgia and Carolinas: A preserved Late-Proterozoic, rifted continental margin: Geological Society of America Bulletin, v. 100, p. 1999-2007.

Fleuty, M. J., 1964, Tectonic slides: Geological Magazine, v. 101, p. 452-456.

Floyd, P. A., and Winchester, J. A., 1975, Magma type and tectonic setting discrimination using immobile elements: Earth and Planetary Science Letters, v. 27, p. 211-215.

Garihan, J. M., Ranson, W. A., and Preddy, M. S., 1993, Pattern of minimum principal stress trajectories affecting the Carolinas (Inner Piedmont and Charlotte belt) during two stages of mid-Mesozoic continental rifting: Geological Society of America Abstracts with Programs, v. 25, p. 16.

Ghent, E. D., and Stout, M. Z., 1981, Geobarometry and geothermometry of plagioclase-biotite-garnet-muscovite assemblages: Contributions to Mineralogy and Petrology, v. 76, p. 92-97.

Gillon, K. A., 1989, The geology of the eastern Blue Ridge thrust sheets in the vicinity of Helen, Georgia, in Fritz, W. J., Hatcher, R. D., Jr., and Hopson, J. L.: Georgia Geological Society Guidebook, v. 9, p. 133-169.

Griffin, V. S., 1967, Geology of the Six Mile quadrangle, South Carolina: South Carolina Division of Geology Map Series MS-14, scale 1: 24000.

Griffin, V. S., Jr., 1969, The migmatitic Inner Piedmont belt of northwestern South Carolina: South Carolina Division of Geology, Geologic Notes, v. 13, p. 87-104.

Griffin, V. S., Jr., 1971a, Inner Piedmont belt of the southern crystalline Appalachians: Geological Society of America Bulletin, v. 82, p. 1885-1898.

Griffin, V. S., Jr., 1971b, Stockwork tectonics in the Appalachian Piedmont of South Carolina and Georgia: Sonderdruck aus der Geologischen Rundschau, v. 60, p. 868-886.

Griffin, V. S., Jr., 1974, Analysis of the Piedmont in northwest South Carolina: Geological Society of America Bulletin, v. 85, p. 1123-1138.

Hadley, J. B., and Nelson, A. E., 1971, Geologic map of the Knoxville quadrangle, North Carolina, Tennessee, and South Carolina: U. S. Geological Survey Miscellaneous Geologic Investigations Map I-654, scale 1:250,000.

Hanmer, S., and Passchier, C., 1991, Shear-Sense Indicators: A Review: Geological Survey of Canada Paper 90-17, 72 p.

Hansen, E., 1971, Strain Facies: New York, Springer Verlag, 207 p.

Harper, S. B., and Fullagar, P. D., 1981, Rb-Sr age of granitic gneisses of the Inner Piedmont belt of northwestern North Carolina and South Carolina: Geological Society of America Bulletin, v. 92, p. 864-876.

Hatcher, R. D., Jr., 1969, Stratigraphy, petrology, and structure of the low rank belt and part of the Blue Ridge of northwesternmost South Carolina: South Carolina Division of Geology, Geologic Notes, v. 13, p. 105-141.

Hatcher, R. D., Jr, 1970, Stratigraphy of the Brevard zone and Poor Mountain area, northwestern South Carolina: Geological Society of America Bulletin, v. 81, p. 933-940.

Hatcher, R. D., Jr., 1971a, Structural, petrologic, and stratigraphic evidence favoring a thrust solution to the Brevard problem: American Journal of Science, v. 270, p. 177-202.

Hatcher, R. D., Jr., 1971b, The geology of Rabun and Habersham counties: The Geological Survey of Georgia, Department of Mines, Mining, and Geology, Bulletin 83, 48 p.

Hatcher, R. D., Jr., 1972, Developmental model for the southern Appalachians: Geological Society of America Bulletin, v. 83, p. 2735-2760.

Hatcher, R. D., Jr., 1978, Tectonics of the western Piedmont and Blue Ridge, southern Appalachians: Review and speculation: American Journal of Science, v. 278, p. 276-304.

Hatcher, R. D., Jr., 1987, Tectonics of the southern and central Appalachian internides: Annual Review of Earth and Planetary Sciences, v. 15, p. 337-362.

Hatcher, R. D., Jr., 1989, Tectonic synthesis of the U. S. Appalachians, in Hatcher, R. D., Jr., Thomas, W. A., and Viele, G. W., eds., The Appalachian—Ouachita orogen in the United States: Boulder, Colorado, Geological Society of America, The Geology of North America, v. F-2, p. 511-535.

Hatcher, R. D., Jr., 1990, Structural geology: principles, concepts, and problems: Columbus, Merrill Publishing, 531 p.

Hatcher, R. D., Jr., and Acker, L. L., 1984, Geology of the Salem quadrangle, South Carolina: South Carolina Geological Survey, MS-26, 23 p., scale 1/24,000

Hatcher, R. D., Jr., and Butler, J. R., 1979, Guidebook for southern Appalachian field trip in the Carolinas, Tennessee, and northeastern Georgia: International Geological Correlation Program— Caledonide Orogen Project 27: Chapel Hill, North Carolina, University of North Carolina, 117 p.

Hatcher, R. D., Jr., Costain, J. K., Coruh, C., Phinney, R. A., and Williams, R. T., 1987, Tectonic implications of new Appalachian ultradeep core hole (ADCOH) seismic reflection data from the crystalline southern Appalachians: Royal Astronomical Society Geophysical Journal, v. 89, p. 157-162.

Hatcher, R. D., Jr., and Goldberg, S. A., 1990, The Blue Ridge geologic province, in Horton, J. W., Jr., and Zullo, V. A., eds., The geology of the Carolinas, Carolina Geological Society Fiftieth Anniversary Volume: Knoxville, The University of Tennessee Press, p. 11-35.

Hatcher, R. D., Jr., and Hooper, R. J., 1991, Evolution of crystalline thrust sheets in the internal parts of mountain chains, in McClay, K. R., ed., Thrust Tectonics: Chapman and Hall, London, p. 217-234.

Hatcher, R. D., Jr., Hooper, R. J., Petty, S. M., and Willis, J. D., 1984, Structure and petrology of three southern Appalachian mafic—ultramafic complexes and their bearing on the tectonics of emplacement and origin of Appalachian ultramafic bodies: American Journal of Science, v. 284, p. 484-506.

Hatcher, R. D., Jr., and Williams, R. T., 1986, Mechanical model for single thrust sheets Part I: Taxonomy of crystalline thrust sheets and their relationships to the mechanical behavior of orogenic belts: Geological Society of America Bulletin, v. 97, p. 975-985.

Holdaway, M. J., 1971, Stability of andalusite and the aluminum silicate phase diagram: American Journal of Science, v. 271, p. 97-131.

Hooper, R. J., and Hatcher, R. D., Jr., 1988, Mylonites from the Towaliga fault zone, central Georgia: products of heterogeneous non-coaxial deformation: Tectonophysics, v. 152, p. 1-17.

Hopson, J. L., 1984, Stratigraphy and structure of the Alto Allochthon, Ayersville Quadrangle, Georgia: Columbia, South Carolina; University of South Carolina, 151 p.

Hopson, J. L., 1989, Structure, stratigraphy, and petrogenesis of the Lake Burton mafic-ultramafic complex, in Fritz, W. J., Hatcher, R. D., Jr., and Hopson, J. L., eds., Georgia Geological Society Guidebook, v. 9., p. 93-110.

Hopson, J. L., and Hatcher, R. D., Jr., 1988, Structural and stratigraphic setting of the Alto allochthon, northeast Georgia: Geological Society of America Bulletin, v. 100, p. 339-350.

Horton, J. W., Jr., and McConnell, K. I., 1990, The western Piedmont, in Horton, J. W., Jr., and Zulio, V. A., eds., The Geology of the Carolinas, Carolina Geological Society Fiftieth Anniversary Volume: Knoxville, The University of Tennessee Press, p. 36-58.

Humphris, S. E., and Thompson, G., 1978, Hydrothermal alteration of oceanic basalts in seawater: Geochemica et Cosmochimica Acta, v. 42, p. 107-125.

Humphris, S. E., Thompson, G., Schilling, J. G., and Kingsley, R. A., 1985, Petrological and geochemical variations along the Mid-Atlantic Ridge between 46°S and 32°S: influence of the Tristan de Cunha mantle plume: Geochimica Cosmochimica Acta, v. 49, p. 1445-1464.

Irvine, T. N., and Baragar, W. R. A., 1971, A guide to the chemical classification of common rocks: Canadian Journal of Earth Science, v. 8, p. 523-548.

Jones, K. A., and Brown, M., 1990, High-temperature 'clockwise' P-T paths and melting in the development of regional migmatites: an example from southern Brittany, France: Journal of Metamorphic Geology, v. 8, p. 551-578.

Karig, D. E., 1971, Origin and development of marginal basins in the western Pacific: Journal of Geophysical Research, v. 76, p. 2542-2561.

Keith, A., 1905, Description of the Mount Mitchell quadrangle (North Carolina-Tennessee): U.S. Geological Survey Atlas, Folio 124, 10 p.

Keith, A., 1907, Description of the Pisgah quadrangle (North Carolina—South Carolina): U. S. Geological Survey Geologic Atlas, Folio 124, 10 p.

Leake, B. E., 1964, The chemical distinction between ortho-and para-amphibolites: Journal of Petrology, v. 5, p. 238-254.

Lemmon, R. E., 1973, Geology of the Bat Cave and Fruitland quadrangles and the origin of the Henderson Gneiss, western North Carolina (Ph.D. dissertation): Chapel Hill, North Carolina, University of North Carolina, 145 p.

Lemmon, R. E., 1982, Evidence for an Acadian tectonic event in the western Inner Piedmont: Geological Society of America Abstracts with Programs, v. 14, p. 34.

Lemmon, R. E., and Dunn, D. E., 1973a, Geologic map and mineral resources of the Bat Cave quadrangle, North Carolina: North Carolina Department of Natural Resources and Community Development Map GM 202 NW, scale 1/24,000.

Lemmon, R. E., and Dunn, D. E., 1973b, Geologic map and mineral resources of the Fruitland quadrangle, North Carolina: North Carolina Department of Natural Resources and Community Development Map GM 202 NW, scale 1/24,000.

Lemmon, R. E., and Dunn, D. E., 1975, Origin and geologic history of the Henderson Gneiss from Bat Cave and Fruitland quadrangles, western North Carolina: Geological Society of America Abstracts with Programs, v. 7, p. 509.

Lister, G. S., 1993, Do smoothly curving, spiral-shaped inclusion trails signify porphyroblast rotation?: Comment and reply: Geology, v. 21, p. 479-480.

Liu, A., 1991, Structural geology and deformation history of the Brevard fault zone, Chauga belt, and Inner Piedmont, northwestern South Carolina and adjacent areas (PhD Dissertation): Knoxville, Tennessee, University of Tennessee, 200 p.

Liu, A., and Davis, T. L., and Hatcher, R. D., Jr., 1991, Thrusting in orogenic process: observations from the Chauga belt and Inner Piedmont, southern Appalachians: Geological Society of America Abstracts with Programs, v. 23, p. 59.

Luth, W. D., Jahns, R. H., and Tuttle, O. F., 1964, The granite system at pressures of 4 to 10 kilobars: Journal of Geophysical Research.

Maneilly, A. W., and Storey, B. C., 1986, Ductile thrusting within subduction complex rocks on Signey Island, South Orkney Islands: Journal of Structural Geology, v. 8, p. 457-472.

Marshack, S., and Mitra, G., 1988, Basic methods of structural geology: Englewood Cliffs, Prentice-Hall, 446 p.

Mason, R., 1978, Petrology of the metamorphic rocks: London, George, Allen and Unwin, 245 p.

McClay, K. R., 1987, The mapping of geological structures (Geological Society of London handbook): England, Open University Press, 162 p.

McClellan, E. A., 1987, Geologic history of a portion of the eastern Blue Ridge, southern Appalachians: Tray Mountain and Macedonia 7 1/2' quadrangles, Georgia (M. S. thesis): Knoxville, Tennessee, University of Tennessee, 179 p.

McClellan, E. A., 1989, The Coweeta Group in the Tray Mountain area and northeast, Georgia and North Carolina: Georgia Geological Society Guidebooks, v. 9, p. 75-92.

McLellan, E. L., 1983, Contrasting textures in metamorphic and anatectic migmatites: an example from the Scottish Caledonides: Journal of Metamorphic Geology, v. 1, p. 241-262.

McLellan, E. L., 1985, Metamorphic reactions in the kyanite and sillimanite zones of the Barrovian type area: Journal of Petrology, v. 26, p. 789-818.

McLellan, E. L., 1988, Migmatite structures in the Central Gneiss Complex, Boca de Quadra, Alaska: Journal of Metamorphic Geology, v. 6, p. 517-542.

McConnell, K. I., and Abrams, C. E., 1984, Geology of the greater Atlanta region: Georgia Geological Survey Bulletin 96, 127 p.

Mehnert, K. R., 1968, Migmatites and the origin of granitic rocks: Amsterdam, Elsevier, 393 p.

Meschede, M., 1986, A method of discriminating between different types of mid-oceanic ridge basalts and continental tholeiites with the Nb-Zr-Y diagram: Chemical Geology, v. 56, p. 207-218.

Mies, J. W., 1991, Planar dispersion of folds in ductile shear zones and kinematic interpretation of fold-hinge girdles: Journal of Structural Geology, v. 13, p. 281-297.

Mies, J. W., 1992, Sheath folds in the Sylacauga marble, Talladega County, Alabama: Geological Society of America Abstracts with Programs, v. 24, p. 53.

Mies, J. W., 1993, Structural analysis of sheath folds in the Sylacauga Marble Group, Talladega slate belt, southern Appalachians: Journal of Structural Geology, v. 15, p. 983-993.

Milnes, A. G., Pfiffner, O. A., 1977, Structural development of the Infrahelvetic complex, eastern Switzerland: Eclogae Geologicae Heletiae, v. 70, p. 83-95.

Misra, K. C., and Conte, J. A., 1991, Amphibolites of the Ashe and Alligatorback Formations, North Carolina: Samples of Late-Proterozoic—Early Paleozoic oceanic crust: Geologic Society of America Bulletin, v. 103, p. 737-750.

Misra, K. C., and McSween, H. Y., 1984, Mafic rocks of the southern Appalachians: A review: American Journal of Science, v. 284, p. 294-318.

Miyashiro, A., 1973, Metamorphism and metamorphic belts: New York, Wiley and sons, 492 p.

Miyashiro, A., and Shido, F., 1975, Tholeiitic and calc-alkaline series in relation to the behaviours of titanium, vanadium, chromium, and nickel: American Journal of Science, v. 275, p. 265-277.

Mohan, A., Windley, B. F., and Searle, P., 1989, Geothermobarometry and development of inverted metamorphism in the Darjeeling-Sikkim region of the eastern Himilaya: Journal of Metamorphic Geology, v. 7, p. 95-110.

Neilson, M. J., and Stow, S. H., 1986, Geology and geochemistry of the mafic and ultramafic intrusive rocks, Dadeville belt, Alabama: Geological Society of America Bulletin, v. 97, p. 296-304.

Nelson, A. E., 1985, Major tectonic features and structural elements in the northwest part of the Greenville quadrangle, Georgia: U. S. Geological Survey Bulletin 1643, 22 p.

Odom, A. L., and Fullagar, P. D., 1973, Geochronologic and tectonic relationships between the Inner Piedmont, Brevard zone, and Blue Ridge belt, North Carolina: American Journal of Science, v. 273-A, p. 133-149.

Odom, A. L., and Russell, G. S., 1975, The time of regional metamorphism of the Inner Piedmont, North Carolina, and Smith River allochthon: Inference from whole-rock ages: Geological Society of America Abstracts with Programs, v. 7, p. 522-523.

Olsen, S. N., 1983, A quantitative approach to local mass balance in migmatites, in Atherton, M. P., and Gribble, C. D., eds., Migmatites, melting, and metamorphism: Shiva, Nantwich, p. 201-233

Olsen, S. N., 1984, Mass-balance and mass-transfer in migmatites from the Colorado Front Range: Contributions to Mineralogy and Petrology, v. 85, p. p. 30-44.

Park, R. G., 1983, Foundations of Structural Geology: Glasgow, Blackie, 135 p.

Passchier, C. W., and Simpson, C., 1986, Porphyroclast systems as kinematic indicators: Journal of Structural Geology, v. 8, p. 831- 843.

Patterson, J. G., 1988, Deformation in portions of the distal continental margin to ancestral North America: An example from the westernmost internal zone, central and southern Appalachian orogen, Virginia: Tectonics, v. 8, p. 535-554.

Pearce, J. A., 1975, Basalt geochemistry used to investigate past tectonic environments on Cyprus: Tectonophysics, v. 25, p. 41-67.

Pearce, J. A., 1980, Geochemical evidence for the genesis and eruptive setting of lavas from Tethyan ophiolites, in Panaylotou, A., ed., Ophiolites— Proceedings of the International Ophiolite Symposium: Cyprus, Geological Survey Department, p. 261-272.

Pearce, J. A., 1982, Trace element characteristics of lavas from destructive plate boundaries, in Thorpe, R. S., ed., Andesites: New York, Wiley, p. 525-548.

Pearce, J. A., and Cann, J. R., 1973, Tectonic setting of basic volcanic rocks determined using trace element analyses: Earth and Planetary Science Letters, v. 19, p. 290-300.

Pearce, J. A., and Norry, M. J., 1979, Petrogenetic implications of Ti, Zr, Y, and Nb variations in volcanic rocks: Contributions to Mineralogy and Petrology, v. 69, p. 33-47.

Pettijohn, F. J., 1954, Classification of sandstones: Journal of Geology, v. 62, p. 360-365.

Quinn, M. J., 1991, Two lithotectonic boundaries in western North Carolina: Geologic interpretation of a region surrounding Sylva, Jackson County (Masters Thesis): Knoxville, Tennessee, University of Tennessee, 223 p.

Ramsay, J. G., 1962, Interference patterns produced by the superposition of folds of "similar" type: Journal of Geology, v. 60, p. 466-481.

Ramsay, J. G., 1967, Folding and fracturing of rocks: New York, McGraw-Hill, 568 p.

Ramsay, J. G., 1981, Tectonics of the Helvetic nappes, in McClay, K. R., and Price, N. J., eds., Thrust and nappe tectonics, Geological Society Special Publication No. 9: Oxford, Blackwell Scientific Publications, p. 293-309.

Ramsay, J. G., and Huber, M. I., 1987, The techniques of modern structural geology, Volume 2: Folds and fractures: London, Academic Press, 392 p.

Rankin, D. W., 1970, Stratigraphy and structure of Precambrian rocks in northwestern North Carolina: in Fisher, G. W., Pettijohn, F. J., Reed, J. C., and Weaver, K. N., Studies of Appalachian Geology: central and southern: New York, Wiley-Interscience, p. 227-245.

Rankin, D. W., 1975, The continental margin of eastern North America in the southern Appalachians: the opening and closing of the Proto-Atlantic Ocean: American Journal of Science, v. 273-A, p. 298-336.

Rankin, D. W., 1976, Appalachian salients and recesses: Late Precambrian continental breakup and the opening of the Iapetus Ocean: Journal of Geophysical Research, v. 81, p. 5605-5619.

Rankin, D. W., Espenshade, G. H., and Shaw, K. W., 1973, Stratigraphy and structure of the metamorphic belt in northwestern North Carolina and southwestern Virginia: a study from

the Blue Ridge across the Brevard fault zone to the Sauratown Mountains anticlinorium: American Journal of Science, v. 273A, p. 1-40.

Reed, J. C., and Bryant, B., 1964, Evidence for strike-slip faulting along the Brevard fault zone in North Carolina: Geological Society of America Bulletin, v. 75, p. 1177-1196.

Reed, J. C., Bryant, B., and Myers, W. B., 1970, The Brevard zone: a reinterpretation, *in* Fisher, G. W., and others, eds., Studies of Appalachian geology: central and southern: New York, Wiley Interscience, p. 261-269.

Rodgers, J., 1970, The tectonics of the Appalachians: New York, Interscience Publishers, 271 p.

Roper, P. J., and Dunn, D. E., 1973, Superposed deformation and polymetamorphism, Brevard zone, South Carolina: Geological Society of America Bulletin, v. 84, p. 3373-3386.

Saunders, A. D., and Tarney, J., 1979, The geochemistry of basalts from a back-arc spreading center in the East Scotia Sea: Geochimica et Cosmochimica Acta, v. 43, p. 555-572.

Sawyer, E. W., and Barnes, S. J., 1988, Temporal and compositional differences between subsolidus and antectic migmatite leucosomes from the Quetico metasedimentary belt, Canada: Journal of Metamorphic Geology, v. 6, p. 437-450.

Shaw, H. F., and Wasserburg, G. J., 1984, Isotopic constraints on the origin of the Appalachian mafic complexes: American Journal of Science, v. 284, p. 319-349.

Shervais, J. W., 1982, Ti-V plots and the petrogenesis of modern and ophiolitic lavas: Earth and Planetary Science Letters, v. 59, p. 101-118.

Shufflebarger, T. E., 1961, Notes on relationships of Piedmont sedimentary rocks with emphasis on the Poor Mountain-Chauga River area, Oconee County, South Carolina: South Carolina Division of Geology, Geologic Notes, v. 5, p. 31-38.

Sibson, R. H., 1977, Fault rocks and fault mechanisms: Journal of the Geological Society of London, v. 133, p. 191-213.

Sibson, R. H., 1983, Continental fault structure and the shallow earthquake source: Journal of the Geological Society of London, v. 140, p. 741-767.

Simpson, C., 1986, Determination of movement sense in mylonites: Journal of Geological Education, v. 34, p. 246-261.

Sinha, A. K., Hewitt, D. A., and Rimstidt, J. D., 1988, Metamorphic petrology and strontium isotope geochemistry associated with the development of mylonites: an example from the Brevard fault zone, North Carolina: Amercian Journal of Science, v. 288-A, p. 115-147.

Sinha, A. K., Hund, E. A., and Hogan, J. P., 1989, Paleozoic accretionary history of the North American plate margin (central and southern Appalachians): Constraints from the age, origin, and distribution of granitic rocks, *in* Hillhouse, J., (ed.) Deep structure and past kinematics of accreted terranes: American Geophysical Union Monograph Series, p. 219-238.

Skjemaa, L., 1989, Tubular folds and sheath folds: definitions and conceptual models for their development, with examples from the Grapesvare area, northern Sweden: Journal of Structural Geology, v. 11, p. 689-703.

Sloan, E., 1908, Catalogue of the mineral localities of South Carolina: South Carolina Geologcial Survey Bulletin, 2, 4th series, 505 p.

Spear, F. S., Hickmont, D. D., and Selverstone, J., 1990, Metamorphic consequences of thrust emplacement, Fall Mountain, New Hampshire: Geological Society of America Bulletin, v. 102, p. 1344-1360.

Spear, F. S., and Peacock, S. M., 1989, Metamorphic pressure-temperature time paths: American Geophysical Union Short Course in Geology, v. 7, 102 p.

Stow, S. H., Neilson, M. J., and Neathery, T. L., 1984, Petrography, geochemistry, and tectonic significance of the amphibolites in the Alabama Piedmont: American Journal of Science, v. 284, p. 416-436.

Stuckey, J. L., and Conrad, S. G., 1958, Explanation text for geologic map of North Carolina: North Carolina Department of Conservation and Development Board Bulletin, v. 71, 55 p.

Tabor, J. R., Davis, T. L., and Hatcher, R. D., Jr., 1990, Implications of late deformation in the Columbus Promontory, southern Appalachians for regional deformation and metamorphism in the Piedmont: Geological Society of America Abstracts with Programs, v. 22, p. 65.

Tarney, J., Saunders, A. D., and Weaver, S. D., 1977, Geochemistry of volcanic rocks from the island arcs and marginal basins of the Scotia Arc region, in Talwani, M., and Pitman, W. C., eds., Island arcs, deep sea trenches and back arc basins: Washington, American Geophysical Union, p. 367-377.

Thiessen, R. L., and Means, W. D., 1980, Classification of fold interference patterns: a reexamination: Journal of Structural Geology, v. 2, p. 311-316.

Thomas, W. A., 1976, Evolution of the Ouachita-Appalachian continental margin: Journal of Geology, v. 84, p. 323-342.

Thomas, W. A., 1977, Evolution of tha Appalachian-Ouachita salients and recesses from reentrants and promontories in the continental margin: American Journal of Science, v. 277, p. 1233-1278.

Thomas, W. A., 1991, The Appalachian-Ouachita rifted margin of southeastern North America: Geological Society of America Bulletin, v. 103, p. 415-431.

Thompson, A. B., 1982, Dehydration melting of pelitic rocks and the generation of H_2O-undersaturated granitic liquids: American Journal of Science, v. 282, p. 1567-1595.

Thompson, A. B., and Algor, J. R., 1977, Model systems for anatexis of pelitic rocks I: Theory and melting reactions in the system $KAlO_2$—$NaAlO_2$—Al_2O_3—SiO_2—H_2O: Contributions to Mineralogy and Petrology, v. 63, p. 247-269.

Tracy, R. J., 1978, High grade metamorphic reactions and partial melting in pelitic schist, west-central Massachusetts: American Journal of Science, v. 278, p. 150-178.

Tracy, R. J., and Robinson, P., 1983, Acadian migmatitic types in pelitic rocks of Central Massachusetts, *in* Atherton, M. P., and Gribble, C. D., eds., Migmatites, melting, and metamorphism: Shiva, Nantwich, p. 163-173.

Tull, J. F., and Stow, S. H., 1979, Regional tectonic setting of the Hillabee Greenstone, *in* Tull, J. F., and Stow, eds., The Hillabee metavolcanic complex and associated rock sequences: Alabama Geological Society 17th Annual Field Trip Guidebook, p. 30-33.

Turner, F. J., 1981, Metamorphic petrology: New York, McGraw Hill, 524 p.

Van der Plas, L., and Tobi, A. C., 1965, A chart for judging the reliability of point counting results: American Journal of Science, v. 263, p. 87-90.

Vauchez, A., 1987, Brevard fault zone, southern Appalachians: A medium-angle, dextral Alleghanian shear zone: Geology, v. 15, p. 669-672.

Vauchez, A., and Brunel, M., 1988, Polygenetic evolution and longitudinal transport within the Henderson mylonitic gneiss, North Carolina: Geology, v. 16, p. 1011-1014.

Walters, K. A., 1990, Geochemistry and trace-element models for the petrogenesis of the mafic rocks in the Hayesville thrust sheet, Georgia-North Carolina Blue Ridge (Ph.D. dissertation), Knoxville, Tennessee, Unversity of Tennessee.

Wegmann, C. E., 1935, Zur Deutung der Migmatite: Geologische Rundschau, v. 26, p. 303-350.

Wehr, F., and Glover, L., 1985, Stratigraphy and tectonics of the Virginia-North Carolina Blue Ridge: Evolution of a late-Proterozoic hinge zone: Geological Society of America Bulletin, v. 96, p. 285-295.

White, S. H., 1976, The effects of strain on microstructures, fabrics and deformation mechanisms in quartzites: Philosophical Transactions of the Royal Geological Society of London, v. A283, p. 69-86

Williams, H., and Hatcher, R. D., Jr., 1983, Appalachian suspect terranes, *in* Hatcher, R. D., Jr., Williams, H., and Zietz, I., eds., Contributions to the tectonics and geophysics of mountain chains: Geological Society of America Memoir 158, p. 33-53.

Wilson, M., 1989, Igneous petrogenesis: London, Unwin Hyman, 466 p.

Winkler, H. G. F., 1976, Petrogenesis of metamorphic rocks: New York, Springer-Verlag, 334 p.

Wood, D. A., Joron, J. L., and Treuil, M., 1979, A re-appraisal of the use of trace elements to classify and discriminate between magma series erupted in different tectonic settings: Earth and Planetary Science Letters, v. 45, p. 326-336.

Yanagihara, G. M., Davis, T. L., and Hatcher, R. D., Jr., 1992, Structural relationships in the western Inner Piedmont, North Carolina: Geological Society of America Abstracts with Programs, v. 24, p. 74.

Yanagihara, G. M., and Davis, T. L., 1992, Relationships between deformation and metamorphism in the western Inner Piedmont, North Carolina: Geological Society of America Abstracts with Programs, v. 24, p. 238.

Yanagihara, G. M., 1993, Evolution of folds associated with D_2 and D_3 deformation and their relationship with shearing in a part of the Columbus Promontory, North Carolina, *in* Hatcher, R. D., Jr., and Davis, T. L., eds., Studies of Inner Piedmont Geology with a focus on the Columbus Promontory: Carolina Geological Society Guidebook, p. 45-54.

Yardley, B. W., 1989, An introduction to metamorphic petrology: Essex, England, Longman, 248 p.

APPENDICES

APPENDIX A
STRUCTURAL DATA

station no.	foliation	lineation	fold axis	axial plane
1	010/13E			
2	010/16E			
3	025/19E			
4	170/23E			
5	054/12S			
6	040/18E			
7	007/22E			
8	065/36S			
9	165/15E			
10	010/18E			
11	040/12W			
12	010/18E			
13	040/20E			
14	015/25E			
15	055/16S			
16	006/13E			
17	066/14S			
18	007/17E			
19	070/25S			
20	040/20E			
21	160/15E			
22	155/20E			
23	045/30E			
24	050/20S			
25	160/15E	15/070		
26	050/20S			
27	045/25E	10/050		
28	060/20S			
29	160/30E	15/048		
30	035/25E			
31	070/25S			
32	070/25S			
33	010/30E			
34	033/43E			
35	140/30E			
36	026/23E			
37	085/20S			
38	166/09W	04/194		
39	115/10N			
40	040/35E			
41	060/21S			
42	015/18E	10/052		
43	030/21E			
44	035/15E			
45	015/16E			
46	035/26E	01/040		
47	040/26E			
48	085/15S			
49	015/15E	10/045		
50	028/14E			
51	060/10S			
52	056/15S	05/220		
	070/38S	05/240		
53	165/08E	08/065		
54	010/16E			
55	023/21E	10/062		
56	060/17S			
57	080/10S			
58	105/10S			
59	073/18S	06/230		
60	056/11S			

station no.	foliation	lineation	fold axis	axial plane
820	023/32E			
821	026/33E			
822	041/38E			
823	035/23E			
824	038/30E	13/068		
825	065/20S			
826	095/30S			
827	030/15E			
828	035/30E			
829	018/38E			
830	020/15E	12/068		
831	170/45E			
832	025/15E			
833	005/25E			
834	170/15E			
835	070/15S			
836	027/38E			
837	168/22E	20/050		
838		14/020	175/20E	
839	065/20S			
840	022/36E			
841	015/17E			
842	030/28E			
843	050/20S	07/216		
844	065/05S			
845	015/15E			
846	030/10E	07/073		
847	050/25S			
848	035/10W			
849	020/15E			
850	040/10E			
851	025/20W	05/189		
852	175/27W	16/109		
853	025/17E			
854	060/18S			
855	0155/26W	05/340		
856	085/20S			
857	170/10E			
858	055/20S			
859	015/10E			
860	050/17S	04/207		
861	178/26E			
862	176/33E	05/023		
863	045/30E			
864	105/20S			
865	035/17W			
866	018/12E	05/085		
867	130/19N	08/100		
868	170/10W			
869	140/15E			
870	135/28E			
871	018/23E	12/058		
872	162/10W			
873	120/22S	17/245	17/245	120/22S
874	022/15E	15/107		
875	177/21E			
876	055/23S			
877	110/20S			
878	050/16S			
879	160/35E			
880	035/16E	05/050		

no.	foliation	lineation	fold axis	axial surface	no.	foliation	lineation	fold axis	axial surface
61	096/08S	08/215			881	093/20S			
62	055/29S				882	070/10S	02/088		
63	113/23S				883	043/19E	06/068		
64	030/17E	06/042			884	080/12S			
65	107/38N				885	055/14S			
66	067/34S				886	058/24S	05/086		
67	035/17E				887	085/24S			
68	003/36E				888	118/10S			
69	063/25S				889	065/13N	07/260		
70	035/25E				890	160/10W			
71	048/14S	06/216			891	010/08E			
72	020/25E				892	095/09S			
73	056/11S	06/225			893	182/18W	18/235		
74	030/23E				894	058/14S			
75	045/15E					078/18N			
76	045/27E	09/202			895	035/19E			
77	025/10E				896	120/20N			
78	010/10E	08/051			897	110/10S			
79	043/13E	05/070			898	010/10E	07/075		
80	130/24N				899	040/16E			
81	020/18E				900	100/23N			
82	035/31E	08/042			901	100/24S		13/068	085/24S
83	038/28E				902	125/20N			
84	085/17S	15/215			903	165/20E	18/080		
85	050/28S	17/080			904	170/07E			
86	100/21S	18/210			905	145/16W			
	180/18E	10/033			906	020/25E			
87	043/23E				907	065/30S			
88	030/28E	08/190			908	140/33W			
89	020/25E	08/040			909	096/25N			
90	063/21S	05/078			910	098/18S			
91	175/15E				911	125/16N			
92	045/15E	03/060			912	110/19S			
93	015/23E	05/033E			913	100/09S			
94	084/25S				914	065/08S			
95	045/25E	10/205			915	060/30S	07/233		
96	054/47S	10/221			916	030/08E	04/050		
97	110/16S	10/250			917	114/21S	19/260		
98	031/16E	07/050			918	035/23E	20/095		
99	043/27E	06/055			919	060/13N	01/070		
100	036/25E	05/208			920	022/25E	25/110		
101	060/15S				921	110/18S			
102	165/23W	13/219			922	095/23S			
103	055/26S	05/215			923	040/07E			
104	060/17S	08/215			924	015/07E	05/070		
105	078/21S				925	100/20N			
106	105/10S	10/208			926	050/16N			
107	020/10E				927	030/17E	16/110		
108	050/20S	10E/070			928	048/23S	08/210		
109	078/41S	25/223			929	063/10S			
110	050/25S	18/201			930	006/45E	30/210		
111	174/23E				931	032/24E	08/185		
112	085/20S	10/228			932	022/26E	23/076		
113	046/29	14/202			933	120/19N	19/058		
114	040/20E	02/050			934	043/17E	05/215		
115	043/23E				935	010/14E			
116	067/22S	07/225			936	040/27E	14/080		
117	040/23E				937	070/19S			
118	107/13S	10/211			938	045/20E			
119	045/30E	06/210			939	010/24E			
120	040/22E	10/200			940	145/32W			

no.	foliation	lineation	fold axis	axial surface	no.	foliation	lination	fold axis	axial surface
121	020/28E				941	035/40E	22/080		
122	023/22E	04/035			942	095/08S			
123	105/38S	25/205			943	065/23S	07/235		
124	100/16S	13/233			944	105/25N			
125	080/21S	10/210			945	170/33W	33/235		
126	010/18E				946	037/40E	19/080		
127	035/17E	08/055			947	044/30E			
128	165/22E				948	116/27S	14/264		
129	130/25W	25/200			949	048/20S			
130	065/17S	10/207			950	080/43S	05/094		
131	065/15S	05/225			951	063/55S			
132	024/30E	10/058			952	081/20S			
133	160/28E	24/040			953	080/20N	02/070		
134	006/32E	26/070			954	042/16E			
135	050/22S				955	170/25E			
136	050/31S	10/068			956	048/28S	10/068		
137	010/14E				957	035/28E			
138	050/18S	05/210			958	015/22E			
139	045/31E	05/215			959	170/30E			
140	035/20E	05/060			960	010/13E			
141	100/28S	16/225			961	055/36S	10/083		
142	050/23S	08/220			962	100/26S			
143	055/12S	04/215			963	050/33S			
144	050/30S				964	050/25N			
145	080/15S	08/205			965	055/26S			
146	065/17S				966	076/35S			
147	073/29S	06/234			967	043/16W	05/245		
148	130/28N	25/020			968	115/36S	22/097		
149	050/15S	10/205			969	045/42E			
150	045/20E	05/210			970	100/23N			
151	050/23S	10/209			971	105/21N			
152	105/25N	25/042			972	105/19N			
153	006/28W	20/230			973	022/17E			
154	045/16E	05/200			974	018/14E			
155	173/13E				975	157/20E			
156	020/25E	07/040			976	030/22E	12/057		
157	063/30N	25/355			977	165/13E	10/230		
158	040/18E	05/060			978	085/15S			
159	115/21S	07/210			979	028/12E	05/074		
160	010/22E	14E/040			980	065/14S	06/083		
161		05/210			981	068/16S	03/073		
162	020/17E	05/043			982	080/18S			
163	045/12E				983	047/25S	09/215		
164	035/33E	02/045			984	035/13E			
165	043/27E	02/052			985	035/13E			
166	080/25S				986	075/10S	06/060		
167	060/18S	25/223			987	048/26S			
168	040/20E	05/210			988	065/20S			
169	065/23S	05/230			989	075/29S	08/243		
170	180/22E	06/030			990	082/11S	06/223		
171	025/22E	22/070			991	034/24E	07/052		
172	040/20E	05/050			992	047/23S			
173	050/18S	04/215			993	083/34S	04E/075E		
174	045/13E	03/210			994	110/21S			
175	031/40E	08/054			995	024/25E	25/115		
176	030/20E				996	046/22S	03/065		
177	020/16E	08/035			997	086/14S	07/250		
178		13/211		998	174/35E				
179	005/30E				999	073/20S			
180	175/30E				1000	053/23S	13/206		
181	045/20E	08/070			1001	054/24S			

no.	foliation	lineation	fold axis	axial surface	no.	foliation	lineation	fold axis	axial surface
182		10/043			1002	065/18S			
183	030/20E	10/055			1003	082/14S			
184	032/36E				1004	110/23S	20/235		
185	050/25S	07/215			1005	085/17S			
186	055/20S	04/220			1006	095/18S			
187	010/14W	02/215			1007	140/21W			
188	050/25S				1008	110/18S	17/205		
189	070/15S	03/230			1009	050/13S	08/200		
190	020/10E				1010	095/19S			
191	010/22E				1011	092/32S			
192	030/33E				1012	058/33S	33/185		
193	035/25E	09/205			1013	077/44S			
194	080/28S	22/210			1014	020/11E			
195	025/12E	07/050			1015	145/23E			
196	020/21E	04/035			1016	018/19E	09/056		
197	080/20S	11/235			1017	042/16E			
198	010/20E	05/045			1018	173/11E	11/055		
199	045/25E				1019	055/10N			
200	045/27E	12/060			1020	160/15E			
201	115/18N				1021	038/11E			
202	050/25S	05/215			1022	075/13S			
203	060/20S	03/230			1023	034/20E	10/054		
204	010/19E	03/040			1024	052/51S			
205	055/19S	09/215			1025	005/25W			
206	040/21E				1026	028/30E	23/094		
207	070/25S	08/220			1027	045/13E	03/060		
208	060/20S				1028	172/23E	19/047		
209	055/22S	08/225			1029	084/31S	08/245		
210	095/12S	05/235			1030	006/25E	20/125		
211	025/25E	10/040			1031	003/12E			
212	007/28E				1032	165/10E	04/135		
213	055/10S				1033	078/19S	14/129		
214	080/25S				1034	165/13E			
215	075/32S	08/080			1035	030/23E			
216	128/30N	04/097	09/350	150/15E	1036	165/06W			
217	120/06N		14/040	120/06	1037	030/20E			
218	050/25S				1038	040/25E		14/140	080/22S
219	025/20E				1039	068/25S	13/090		
220	070/35S				1040	075/18S			
221	080/15S				1041	015/13E	11/075		
222	160/15E				1042	020/17E			
223	080/30S				1043	026/22E			
224	170/34E				1044	015/21E			
225	020/20E				1045	170/08E			
226	020/22E	15/078			1046	035/30E	05/045		
227	040/11E				1047	101/19N	10/058		
228	040/12E	09/080			1048	175/19W	15/244		
229	160/19E				1049	005/06E			
230	158/19E	16/085			1050	155/14E			
231	015/25E				1051	040/24E			
232	040/25E				1052	156/21E			
233	020/25E				1053	010/16E	08/035		
234	033/14E				1054	165/13E			
235	070/22N				1055	010/15E			
236	045/25E				1056	115/20S			
237	075/43S				1057	055/12S	03/065		
238	040/23S				1058	030/20E			
239	065/25S				1059	135/33E			
240	019/16E				1060	032/27E	11/048		
241	175/30E				1061	122/24N	13/064		
242	045/21E				1062	080/10S			

no.	foliation	lineation	fold axis	axial surface	no.	foliation	lineation	fold axis	axial surface
243	040/19E				1063	120/32S			
244	050/20S				1064	085/30S	07/240		
245	047/21S				1065	104/21S	20/212		
246	030/24E	16/068			1066	170/36E			
247	028/33E		09/350	003/31E	1067	032/28E			
248	(No data)				1068	040/30E			
249	025/30E	19E/078			1069	010/17E	10/065		
250	170/28E				1070	038/19E	03/043		
251	013/12E				1071	030/32E			
252	016/15E				1072	015/18E			
253	164/22E	16/110			1073	025/23E	07/033		
254	155/28E	24/088			1074	038/16E			
		29/095			1075	060/15S	10/215		
255	170/22E				1076	038/24E			
256	033/26E				1077	040/20E			
257	120/20S				1078	033/29E	11/065		
258	020/20E				1079	015/25E			
259	120/20S				1080	020/21E			
260	050/27S		16/080	045/22E	1081	170/19E			
261	172/21E				1082	045/23E			
262	030/16E				1083	032/18E			
263	140/25E	23/060			1084	077/24S			
264	163/27E				1085	037/56E	49/125		
265	142/17E	14/063			1086	165/36E			
266	175/17W				1087	059/16S	09/092		
267	030/34E	16/076			1088	048/13S	10/086		
268	010/18E	10/064	17/083	040/11E	1089	063/18S	13/100		
269	156/15W				1090	040/27E			
270	045/10E				1091	040/44E	21/200		
271	059/24S				1092	050/13S			
272	050/23S				1093	020/26E			
273	059/17S				1094	018/16E			
274	053/14S				1095	050/20S	19/110		
275	025/24E				1096	018/23E			
276	034/20E				1097	034/19E			
277	031/22E				1098	053/20S	18/140		
278	043/24E						13/190		
279	020/24E				1099	005/26E			
280	008/15E				1100	162/19E			
281	052/24S				1101	169/21E			
282	065/05S	04/194			1102	045/21E	04/040		
283	053/21S				1103	050/15S			
284	027/28E				1104	072/10S			
285	048/26S				1105	060/30S			
286	016/21E				1106	010/12E			
287	029/28E				1107	100/43N			
288	055/25S				1108	032/25E	03/040		
289	041/24E				1109	30/42E			
290	065/24S				1110	033/20E			
291	051/18S				1111	170/23E			
292	064/19S				1112	025/43E			
293	063/12S	08/230			1113	018/30W			
294	041/14E				1114	026/10E	05/035		
295	042/29E				1115	055/11S			
296	160/20E				1116	030/14E			
297	031/19E				1117	060/25S			
298	015/30E	25/094			1118	025/22E			
299	112/11S				1119	055/22S	05/220		
300	022/25E	11/060			1120	080/18N			
301	034/27E	18/065			1121	030/41E			
302	017/27E				1122	060/30N	11/050	10/020	060/30N

no.	foliation	lineation	fold axis	axial surface	no.	folaiton	lineation	fold axis	axial surface
303	176/21E	19/072			1123	010/19E	10/060		
304	035/25E				1124	167/20E			
305	045/21 11/076				1125	055/20S	03/225		
306	010/21E	17/079			1126	070/20S	17/205		
307	020/30E				1127	045/10			
308	016/25E				1128	091/13S	11/190		
309	068/29S				1129	065/07S	05/195		
310	033E/16E				1130	130/23S	20/197		
311	035/32E				1131	030/25E			
312	045/27E				1132	105/16N			
313	050/15S				1133	070/05S			
314	070/12S				1134	053/33S			
315	050/20S				1135	010/23E			
316	030/23E				1136	045/75E			
317	018/16E				1137	040/25E			
318	006/12E				1138	170/14E	14/060		
319	056/31S		16/125	056/31S	1139	030/33W			
320	164/35E	27/072			1140	130/10S	10/215		
321	018/29E				1141	035/10W	05/020		
322	022/19E	10/062	096/10N		1142	030/20E	10/195		
323	050/14S				1143	080/21S	04/250		
324	018/12E	09/068			1144	170/16E			
325	028/19E				1145	015/20E			
326	005/24E	19/079			1146	040/15E			
327	177/21E				1147	130/20N			
328	049/16S	07/087			1148	020/05E	03/065		
329	027/20E				1149	085/33S			
330	064/34S				1150	105/33S			
331	046/28S				1151	075/25S	15/225		
332	072/30S	12/080			1152	070/14S	12/190		
333	030/21E				1153	035/25E	12/055		
334	170/12E				1154	160/20E			
335	055/25S				1155	045/15E			
336	072/31S				1156	065/29S	18/085		
337	005/18E				1157	065/18S			
338	015/25E				1158	045/17E	11/070		
339	172/10E				1159	060/15S	05/225		
340	006/13E				1160	060/15S	08/215		
341	163/15E				1161	150/27E	27/060		
342	176/20E				1162	085/24S	13/220		
343	016/34E				1163	120/14S	14/210		
344	175/24E				1164	115/15N	13/040		
345	011/25E				1165	060/25S			
346	157/23E	21/094			1166	100/12S			
347	170/18E				1167	050/22S	05/210		
348	048/37S	25/073			1168	010/25E			
349	045/18E				1169	085/05S			
350	015/21E	13/095			1170	020/28E	17/040		
351	010/11E		05/105	040/10W	1171	015/15E	07/055		
352	028/26E	18/065			1172	068/17S			
353	015/12E				1173	045/20E			
354	173/16E	07/095			1174	075/11S			
355	145/15E	13/088			1175	025/20E	08/050		
356	173/13E	13/093			1176	105/26S	18/242		
357	028/26E				1177	170/30E			
358	175/48E				1178	160/24E	24/065		
359	035/26E				1179	030/15E	09/065		
360	045/24E				1180	085/28S	20/215		
361	015/18E				1181	060/10S			
362	015/10E				1182	060/23S			
363	032/22E				1183	080/14S			

no.	foliation	lineation	fold axis	axial surface	no.	foliation	lineation	fold axis	axial surface
364	165/18E				1184	120/17S	17/215		
365	005/23E				1185	105/14S	11/210		
366	058/18E				1186	060/27S	07/075		
367	050/15S				1187	055/18S			
368	066/28S				1188	170/33E	33/080		
369	015/38E				1189	062/30S			
370	050/33S				1190	170/40E	31/035		
371	170/10E				1191	030/22E	10/105		
372	168/38E				1192	130/20N	20/040		
373	018/30E				1193	030/13E	03/055		
374	165/21E				1194	010/16E			
375	170/27E	20/109			1195	060/28S	20/185		
376	008/18E				1196	033/40E	13/195		
377	140/24E				1197	020/14E	05/030		
378	170/26E	17/070			1198	020/24E	12/175		
379	045/03E				1199	042/31E	16/190		
380	025/09E				1200	030/29E	10/195		
381	010/28E				1201	020/22E			
382	010/25E	17/065			1202	070/25S	08/230		
383	010/22E				1203	040/26E			
384	170/16E				1204	060/20S	15/215		
385	020/25E	17/065			1205	080/08S			
386	062/15N				1206	065/25S	13/228		
387	035/25E				1207	040/33E	06/050		
388	010/30E				1208	045/13E	03/072		
389	018/23E				1209	050/11S	04/225		
390	012/16E				1210	040/24E	05/055		
391	167/20E				1211	020/15E			
392	165/10E				1212	020/20E			
393	030/17W				1213	055/22S	10/210		
394	155/24E				1214	040/12E			
395	023/18E				1215	050/28S	09/216		
396	173/24E				1216	060/33S	11/225		
397	035/17E				1217	040/30E			
398	030/34E				1218	065/23S			
399	017/27E				1219	052/15S	05/225		
400	020/18E				1220	060/14S	04/228		
401	160/16E	10/085			1221	075/25S	14/230		
402	047/33S				1222	065/18S	14/215		
403	025/21E	16E/085			1223	070/18S	09/210		
404	055/09S				1224	070/24S	04/240		
405	015/24E				1225	020/15E			
406	017/19E				1226	115/10S	08/220		
407	034/26E				1227	042/12E			
408	042/29E	02/075			1228	061/13S	07/228		
409	027/19E				1229	070/13S			
410	060/20S	11/082	11/082	100/30N	1230	050/38S	19/210		
411	032/22E				1231	022/26E	08/040		
412	040/14E				1232	038/28E			
413	005/10E				1233	020/28E	09/047		
414	020/06E				1234	010/40E	23/045		
415	164/10E				1235	015/51W			
416	006/17E				1236	039/18E	06/059		
417	030/10E				1237	010/25E	09/062		
418	027/12E				1238	050/12S			
419	040/09E				1239	045/19E			
420	025/09E				1240	010/25E			
421	032/12E				1241	120/25N		10/020	025/15E
422	030/20E				1242	170/13E	12/050		
423	050/29S				1243	030/24E			
424	035/10E				1244	036/30E	12/052		

no.	foliation	lineation	fold axis	axial surface	no.	foliation	lineation	fold axis	axial surface
425	030/11E				1245	037/30E	14/200		
426	032/29E				1246	025/26E			
427	053/33S				1247	030/47E			
428	050/35S				1248	165/20E	11/020		
429	048/16S				1249	025/38E	04/035		
430	035/30E				1250		27/075	040/31E	
431	046/13S		11/162	120/09N	1251	050/20S	10/200		
432	(No data)				1252	045/18E	08/205		
433	030/23E				1253	070/14S	07/215		
434	060/27S				1254	050/16S	04/055		
435	055/11S						10/080		
436	030/14E	07/065			1255	170/20E			
437	048/13S				1256	052/23S	18/195		
438	030/20E				1257	030/20E	10/020		
439	035/33E				1258	024/26E	11/040		
440	050/29S				1259	040/23E			
441	025/15E				1260	065/13S	10/222		
442	037/25E				1261	062/23S	07/220		
443	025/20E				1262	023/15E	06/055		
444	020/31E				1263	080/16S	08/242		
445	046/26S				1264	030/16E	05/050		
446	033/20E				1265	035/31E	07/055		
447	023/32E				1266	070/28S			
448	010/31E				1267	075/16S	04/232		
449	010/27E				1268	012/25E	16/075		
450	040/20E				1269	060/23S	13/200		
451	010/15E				1270	073/25S			
452	050/30N				1271	065/10S	03/215		
453	035/18E				1272	060/44S			
454	020/23E				1273	026/31E	08/220		
455	020/23E				1274	015/29E	10/033		
456	025/24E				1275	020/25E			
457	018/32E				1276	145/40E	40/055		
458	028/22E				1277	020/30E			
459	030/20E				1278	074/15N	02/065		
460	040/33E				1279	171/23E			
461	030/20E				1280	028/23E			
462	025/22E				1281	045/22E			
463	056/33S				1282	039/10W			
464	025/27E				1283	060/15N			
465	043/33E				1284	034/14E			
466	043/30E				1285	065/20N			
467	048/20S				1286	032/19W			
468	049/26S				1287	095/10N			
469	042/28E	25/108			1288	022/36E			
470	041/17E				1289	136/30E			
471	037/29E				1290	108/45N			
472	032/21E				1291	087/14S	09/102		
473	003/31E	22/056			1292	140/10E			
474	027/36E	27/086			1293	165/20E			
475	056/36S	21/092	26/085	035/35E	1294		19/094	100/72N	
476	039/33E				1295	(No data)			
477	035/33E				1296	037/31E	09/067		
478	037/30E				1297	010/20E	10/072		
479	042/28E				1298	067/30N			
480	033/21E				1299	062/13S			
481	046/26S				1300	030/16E	02/119		
482	023/16E				1301	030/10E	05/055		
483	015/24E				1302	038/18E	04/065		
484	027/30E				1303	058/48S			
485	037/36E				1304	037/22E	06/051		

no.	foliation	lineation	fold axis	axial surface	no.	foliation	lineation	fold axis	axial surface
486	038/24E				1305	142/12E			
487	062/21S				1306	042/20E			
488	042/35E				1307	061/18S			
489	052/29S		05/170	034/25E	1308	068/11S			
490	047/29S				1309	050/10S			
491	032/22E				1310	042/22E			
492	048/12S				1311	030/20E	10/059		
493	041/23E				1312	054/21S			
494	039/24E	22/115			1313	027/20E			
495	062/33S				1314	029/26E	05/045		
496	035/20E					127/14N			
497	010/35E				1315	042/30E			
498	054/28S				1316	010/13E			
499	020/23E	14/060	18/065	020/23E	1317	049/20S	08/072		
500	180/34E				1318	041/22E	05/058		
501	043/09E				1319	105/24S	12/210		
502	048/19S				1320	039/32E	05/053	05/053	067/08N
503	044/18E	13/112			1321	037/10E			
504	010/18E				1322	040/17E			
505	048/16S	16/131			1323	137/25E	21/066		
506	016/21E				1324	011/36E			
507	028/24E				1325	177/31E	18/041		
508	037/19E				1326	028/13E			
509	021/22E				1327	168/19E	06/010		
510	049/23S	11/071			1328	142/24E			
511	039/23E				1329	020/20E			
512	038/20E				1330	020/30E			
513	066/33S	23/108			1331	028/31E	07/046		
514	048/33S				1332	173/19E			
515	052/31S				1333	057/16S			
516	026/31E				1334	041/21E			
517	024/25E				1335	053/21S			
518	046/37S				1336	045/27E			
519	033/23E				1337	050/18S	09/062		
520	039/10E				1338	039/55E			
521	059/24S				1339	082/25N	08/061		
522	168/28E				1340	065/40S			
523	176/24E				1341	038/24E	12/062		
524	174/22E				1342	036/20W			
525	022/18E				1343	043/37E			
526	172/26E				1344	046/21S			
527	012/33E				1345	170/16E			
528	036/18E	15/097			1346	041/33E			
529	046/23S				1347		08/233		048/82N
530	022/23E				1348	042/22E			
531	047/12S				1349	087/11N	08/048		
532	038/27E	13/079			1350	049/36S			
533	010/13E				1351	051/20S			
534	020/20E				1352	058/29S			
535	060/22S				1353	061/42S			
536	175/20E				1354	035/32W			
537	030/23E				1355	051/27N			
538	044/24E				1356	071/31N	16/056		
539	035/30E				1357	043/22E			
540	060/31S	17/078			1358	054/32W			
541	018/24E	21/084			1359	042/30E			
542	032/20E				1360	046/40S			
543	010/32E	31/078			1361	020/18W	07/232		
544	010/21E				1362	046/28N	05/235		
545	047/21S				1363	047/18S	05/067		
546	015/20E				1364	052/15S			

no.	foliation	lineation	fold axis	axial surface	no.	foliation	lineation	fold axis	axial surface
547	010/09E	08/073			1365	049/15S	05/077		
548	019/06E	02/160			1366	032/45E			
549	024/23E				1367	049/52S			
550	015/16E				1368	046/30S	01/221		
551	012/26E				1369	047/34N			
552	019/24E				1370	080/30S			
553	015/07E				1371	150/23E			
554	037/19E	10/165			1372	164/10E	09/058		
555	037/18E				1373	023/14E	06/046		
556	015/19E				1374	025/28E			
557	020/18E				1375	033/57E			
558	055/35S				1376	023/60E			
559	032/34E				1377	047/65S			
560	066/32S				1378	030/20E			
561	035/14E				1379	060/25S			
562	039/23E				1380	043/17E	01/047		
563	038/18E				1381	020/26E			
564	028/27E				1382	006/12W			
565	066/22S				1383	055/30S			
566	062/17S				1384	010/22E			
567	118/17S				1385	015/32E			
568	025/27E				1386	020/04E			
569	023/28E				1387	006/24E			
570	048/22S				1388	036/28E			
571	058/11S				1389	017/25E	16/063		
572	050/15S				1390	012/44E			
573	068/08S				1391	020/21E			
574	015/26E				1392	008/16E	06/032		
575	050/19S				1393	012/24E			
576	015/20E				1394	056/38S			
	072/30S				1395	030/08E			
577	005/08E				1396	020/13E	12/063		
578	040/15E				1397	047/13N	01/061		
579	037/31E				1398	048/17S			
580	028/27E				1399	060/12S			
581	113/19S				1400	062/24S			
582	003/24E				1401	043/11W			
583	010/26E	11/020			1402	146/11W			
584	177/18E				1403	105/24N			
585	010/20E				1404	050/19S	07/063		
586	012/23E				1405		13/060	060/13N	
587	029/19E						08/060	060/80N	
588	040/18E				1406	075/09S	01/230		
589	053/24S				1407	059/23S			
590	027/25E				1408	042/25W	05/248		
591	044/29E				1409	042/43W			
592	028/16E	04/055			1410	025/24E	07/061		
593	070/04				1411	030/15E			
594	020/17E				1412	030/15E	05/063		
595	036/21E				1413	085/21N			
596	010/10E				1414	055/19N			
597	026/23E				1415	095/21N			
598	036/16E	05/081			1416	169/33E			
599	020/24E				1417	045/15E	02/072		
600	062/24S	11/093			1418	020/19E			
601	032/33E				1419	051/26S			
602	065/25S				1420	163/25E	14/060		
603	019/21E				1421	080/05S			
604	073/23S				1422	170/14E			
605	072/20S				1423	043/28E			
606	068/23S				1424	043/63W			

no.	foliation	lineation	fold axis	axial surface	no.	foliation	lineation	fold axis	axial surface
607	020/15E				1425	087/50N			
608	030/10E				1426	057/55S			
609	003/17E				1427	040/14E			
610	176/28E				1428	083/07N			
611	010/11E				1429	020/15E			
612	175/34E				1430	015/30E	12/053		
613	173/13E				1431	155/50E			
614	025/23E				1432	105/38N	13/085		
615	108/17N				1433	082/16S	08/251		
616	165/12E				1434	050/22S			
617	064/34S				1435	052/27S			
618	023/25E				1436	040/25E			
619	044/22E				1437	153/31W		08/170	153/31W
620	015/24E				1438	170/20E			
621	010/14E				1439	160/15E			
622	018/17E				1440	138/20E			
623	033/15E				1441	110/33N	08/099		
624	010/25E				1442	170/22E	16/066		
625	021/19E				1443	043/37E			
626	011/18E				1444	158/18E	17/056		
627	032/13E				1445	095/33N			
628	008/12E				1446	222/31E			
629	015/14E				1447	170/14W			
630	019/14E				1448	058/27N	06/035		
631	160/13E				1449	059/18S	03/063		
632	010/20E				1450	145/32E			
633	065/37S				1451	125/36N	20/070		
634	020/26E				1452	157/27E			
635	025/25E				1453	140/15E			
636	030/10E				1454	160/15E			
637	046/12N				1455	163/34E	30/100		
638	003/24E				1456	160/22E			
639	178/04E				1457	177/24E			
640	036/10E	05/064	10/073	047/13S	1458	005/25E			
641	010/16E				1459	082/15N			
642	004/14E	10/228			1460	135/20E			
643	047/24S				1461	150/20E			
644	067/16N				1462	117/27N	18/085		
645	158/15E				1463	050/12S			
646	010/16E	11/062			1464	110/21N			
647	013/26E				1465	105/21N			
648	101/13N				1466	170/18E			
649	006/13E				1467	135/35E			
650	020/18W				1468	100/13N			
651	168/28E				1469	170/17E			
652	172/13E	11/052			1470	135/25E			
653	055/04S				1471	075/10N			
654	170/25E				1472	040/25W			
655	046/14S				1473	170/32E			
656	050/22S				1474	110/14N	05/088		
657	050/14S				1475	166/11E			
658	040/25E				1476	100/17S			
659	038/12E				1477	040/20E			
660	065/10S				1478	070/25S	09/088		
661	129/10N				1479	088/41N	11/080		
662	048/26S				1480	170/37E			
663	069/09S				1481	100/20N			
664	170/20E				1482	080/20S	05/240		
665	138/20E				1483	055/32S	05/075		
666	044/12E				1484	035/23E	10/058		
667	039/18E				1485	080/55N	17/075		

no.	foliation	lineation	fold axis	axial surface	no.	foliation	lineation	fold axis	axial surface
668	011/24E	17/055			1486	080/55N			
669	018/27E	14/052			1487	115/11N			
670	048/30N				1488	110/23N	08/087		
671	063/20S				1489	080/22N			
672	065/25S				1490	138/30E			
673	047/16S				1491	135/07W			
674	155/15W			1492	055/25S				
675	165/09E				1493	110/15N			
676	060/20S				1494	105/15N			
677	040/18E				1495	170/15E	07/051		
678	046/09N	05/068			1496	160/15E			
	082/08N				1497	017/24W	06/213		
679	060/10S				1498	045/11W			
680	046/25S				1499	008/10W			
681	075/15S				1500	050/20S			
682	050/20S				1501	040/15E			
683	099/21N				1502	016/14E	04/040		
684	020/14E				1503	175/30E			
685	010/08E				1504	170/17E			
686	155/15E				1505	050/16N			
687	095/30N				1506	035/17E			
688	032/39E				1507	013/22W	05/229		
689	020/15E				1508	020/20W			
690	169/14E				1509	025/23W			
691	049/28S				1510	015/17E			
692	045/10E				1511	030/10W			
693	040/30E				1512	005/20W			
694	170/25E				1513	130/21N			
695	035/15E				1514	035/13E		15/040	010/22E
696	166/18E	16/065				060/20N			
697	(No data)				1515	040/15E	08/067		
698	125/23N	23/035			1516	063/27N	02/052		
699	080/10S	05/232			1517	114/16N	12/067		
700	005/17W	11/250			1518	058/31N			
701	160/23E				1519	010/20W			
702	135/22E				1520	010/30E			
703	025/33E				1521	086/15S			
704	170/25E	23/067			1522	023/16E			
705	010/19E	16/075			1523	006/17E	11/051		
706	155/13E	13/065			1524	025/29E			
707	035/13E				1525	010/18E			
708	168/14E	10/066			1526	162/30W			
709	110/15N	08/070			1527	115/13N			
710	170/30E				1528	175/15E			
711	175/65E	07/000			1529	170/10W			
712	025/20E				1530	140/17E			
713	010/18E	13/046			1531	050/25S			
714	003/21E	20/065			1532	042/27E			
715	120/10N	10/040			1533	155/15E			
716	160/15E				1534	160/15W			
717	140/10E	10/053			1535	105/25S			
718	035/17E	08/055			1536	065/15N			
719	015/10E	06/060			1537	130/25N			
720	020/10E	08/080			1538	148/26E	20/087		
721	020/10E	08/070			1539	170/13W			
722	055/20S				1540	005/30E			
723	160/12E	10/050			1541	030/10W			
724		22/050			1542	010/18E			
725	165/30E				1543	053/15S			
726	140/13E	13/060			1544	015/20E			
727	175/35E	25/040			1545	160/10W			

no.	foliation	lineation	fold axis	axial surface	no.	foliation	lineation	fold axis	axial surface
728	005/20E	13/058			1546	125/10N			
729	120/35N				1547	020/10E			
730	005/10E	07/075			1548	004/09E			
731	010/08E				1549	020/10W			
732	010/13E	13/095			1550	030/25W			
733	065/07S	05/240			1551	025/25E			
734	015/14E	10/070			1552	070/30N			
		14/095			1553	132/25S	22/243		
735	005/25E				1554	025/15W			
736	023/40E	13/050			1555	174/28W			
737	015/13E	12/065			1556	010/08E			
738	028/20E	17/095			1557	030/15W			
739	160/16E	16/065			1558	161/40W			
740	169/16E	05/055			1559	005/30W			
741	045/13E	08/070			1560	165/30W			
742	030/10E				1561	022/24E			
743	040/20E				1562	070/25S			
744	005/25E	10/022			1563	170/20E			
745	015/20E	14/060			1564	145/20E			
746	010/24	05/035			1565	170/10W			
747	002/36E	24/060			1566	010/15E	09/088		
748	015/15E	09/040			1567	049/26S	13/073		
749	025/24E	03/040			1568	062/43S	06/226		
750	178/18E	17/105			1569	165/15E			
751	(No data)				1570	020/10E			
752	010/10E	05/063			1571	166/39E			
753	100/15N	10/055			1572	151/09W	09/242		
754	045/24E	03/060			1573	145/29E			
755	140/16E	18/055			1574	175/20E	10/060		
756	075/20N	03/263			1575	060/15N			
757	132/35N				1576	057/17S			
758	175/10E				1577	035/15E			
759	170/12E				1578	083/26N	07/075		
760	115/19N	10/057			1579	052/27S			
761	030/11W	05/070			1580	162/20E	15/100		
762	075/20N	09/050			1581	028/10E			
763	030/11W	05/250			1582	080/10N			
764	160/08E				1583	026/20W			
765	070/20N	09/045			1584	095/16S	11/068		
766	045/16E	07/210			1585	092/19S	05/250		
767	010/10E	08/047			1586	165/10E			
768	105/43N	21/040			1587	067/27N	04/257		
769	020/20E				1588	061/22S	05/260		
770	145/08E	08/050					08/247		
771	177/24E	19/060	19/060	177/24E	1589	020/10E			
772	020/25E	06/035			1590	015/22E	05/072	05/072	
773	042/30E				1591	018/27E	23/080		
774	005/17E	08/041			1592	068/31			
775	175/20E	20/065			1593	047/20S	05/059		
776	050/20S	05/210			1594	028/16E	12/066		
777	160/26E				1595	075/20S			
778	100/16N	10/060			1596	070/17S			
779	115/35N	20/070			1597	133/20N	15/075		
780	005/15E	10/065			1598	066/16S			
781	175/05E	05/080			1599	072/08S			
782	050/15N	07/035			1600	060/24S	07/075		
783	010/35E	12/040			1601	051/13S			
784	175/15E	10/070			1602	005/17E			
785	005/27E	20/040			1603	095/08S			
786	125/15N	10/075			1604	034/27E	23/080		
787	170/10E	05/060			1605	043/33E	12/072		

no.	foliation	lineation	fold axis	axial surface	no.	foliation	lineation	fold axis	axial surface
788	145/35E	35/070			1606	070/22N			
789	050/40N	05/240			1607	010/23E	18/062		
790	100/15N				1608	044/10E			
791	155/21E	21/065			1609	110/23N	05/078		
792		10/080	170/18E		1610	066/27S			
793	040/11E				1611	062/24S			
794	025/25E				1612	008/15E	14/073		
795	005/20E	14/040			1613	120/15N	08/078		
796	085/10N				1614	095/23S	05/105		
797	010/30E				1615	102/44N			
798	170/15E				1616	095/19N	03/184		
799	070/10N				1617	081/68N			
800	180/30E				1618	060/15N			
801	050/25S	10/215			1619	028/65E			
802	155/30E	20/055			1620	024/60E			
803	030/10E	02/195			1621	096/30N	10/068		
804	055/15S	03/065			1622	080/16N			
805	155/35E				1623	170/12E	11/104		
806	175/22E	10/020			1624	080/24S			
807	080/33S	25/210			1625	170/14E			
808	030/25E	10/055			1626	115/18N			
809	020/15E				1627	120/14N			
810	062/35S	08/225			1628	104/16N	08/048		
811	030/11E	05/060			1629	010/35W			
812	100/20N	20/035			1630	115/22S	17/240		
813	025/08E				1631	125/08N			
814	010/20E	07/040			1632	110/18S			
815	080/20S	09/230			1633	115/20N	09/102		
816	095/20S	08/235			1634	065/11S			
817	045/35E	08/060			1635	078/12S			
818	020/35E	18/045			1636	043/15E			
819	100/13S	11/215			1637	020/31W	05/140		

APPENDIX B
XRF CONDITIONS

.

Conditions of X-ray Flourescence Analysis

Instrument used: EG&G ORTEC X-ray flourescence spectrometer with an energy dispersive SiLi Detector (EDS)

	1	2	3
Elements analyzed:	Na, Mg, Al, Si, P, K, Ca, Mn	Ti, V, Cr, Fe, Ni	Rb, Sr, Y, Zr, Nb
Spectral region of interest (kV):	1.00-6.01	4.37-7.59	13.14-16.81
Accelerating voltage (kV):	10	35	45
Current (nA):	150	125	150
Counting Time (sec):	300	300	300
Filter:	open	Cu	In
Anode:	Rh	W	W

	Standard: BIR 1 (basalt)		Standard: SARM1B (granite)	
	Calculated Value	Standard	Calculated value	Standard
Na$_2$O	1.69	1.82	3.13	3.36
MgO	10.36	9.7	0.28	0.06
Al$_2$O$_3$	15.46	15.53	12.35	12.08
SiO$_2$	48.02	48.0	75.68	75.7
P$_2$O$_5$	0.059	0.021	—	0.01
K$_2$O	0.069	0.03	5.18	4.99
CaO	13.46	13.32	1.11	0.78
MnO	0.19	0.1750	0.041	0.21
TiO$_2$	0.92	0.96	—	0.09
V	0.037	1.031	—	0.0002
Cr	0.038	0.0373	—	0.0012
Fe$_2$O$_3$	11.11	11.33	2.01	2.02
Ni	0.017	0.166	—	0.0008
Rb	0.00035	0.002	0.036	0.032
Sr	0.011	0.011	0.0026	0.001
Y	0.0016	0.016	0.0089	0.0145
Zr	0.0041	0.018	0.031	0.03
Nb	0.0003	0.0002	0.0058	0.0053

Standard: BCR1F

	Calculated Values		Standard
Na$_2$O	3.04	3.16	3.30
MgO	3.27	3.25	3.48
Al$_2$O$_3$	13.98	13.92	13.72
SiO$_2$	54.81	54.62	54.53
P$_2$O$_5$	0.41	0.41	0.360
K$_2$O	1.72	1.70	1.70
CaO	6.93	6.89	6.97
MnO	0.20	0.19	0.18
TiO$_2$	2.23	2.25	2.26
V	0.020	0.030	0.042
Cr	0.0043	0.0068	0.0015
Fe$_2$O$_3$	13.35	13.35	13.40
Ni	0.0039	0.0041	0.001
Rb	0.035	0.0034	0.0047
Sr	0.034	0.035	0.033
Y	0.003	0.0033	0.0037
Zr	0.014	0.014	0.0185
Nb	0.0009	0.0012	0.0014

Standard: BHVO1

	Calculated Values		Standard
Na$_2$O	2.30	2.20	2.29
MgO	7.22	7.30	7.31
Al$_2$O$_3$	14.05	14.14	13.85
SiO$_2$	50.33	50.35	49.90
P$_2$O$_5$	0.25	0.26	0.28
K$_2$O	0.50	0.50	0.54
CaO	11.22	11.17	11.33
MnO	0.17	0.17	0.17
TiO$_2$	2.72	2.69	2.69
V	0.036	0.036	0.03
Cr	0.022	0.023	—
Fe$_2$O$_3$	12.23	12.24	12.23
Ni	0.010	0.010	0.012
Rb	0.00091	0.0010	0.00090
Sr	0.036	0.037	0.042
Y	0.0022	0.0023	—
Zr	0.013	0.013	0.018
Nb	0.0013	0.0014	—

VITA

Gregory Masakatsu Yanagihara was born a *yonsei* (4th generation Japanese American) on October 24, 1967 in Lancaster, California. His early interest in geology, the study of rocks, and mountaineering, the climbing of rocks, prompted his father to proclaim that his head was full of rocks (schist?). Greg spent his entire pre-college life in the Mojave Desert, less than five miles from the San Andreas Fault, where frequent earthquakes (including the San Fernando earthquake of 1971) sustained his interest in geology. He attended Antelope Valley High School and graduated in 1985.

After spending a year at Antelope Valley College (Tumbleweed Tech), Greg transferred to the University of California, Santa Barbara. Despite interests in art, history, and architecture, Greg's love for science and the outdoors prompted him to choose geology as a major. Living 50 yards from the beach, he enjoyed surfing, sea kayaking, rock climbing, and skiing as well as pranks with and on his roommates, volleyball, seafood, and Gaucho basketball. Greg entered graduate school at the University of Tennessee, Knoxville in Fall, 1990 and received his Masters degree in May, 1994. He has ambitions for a PhD, but wonders that if it took $3 \frac{1}{2}$ years to get his M.S., how long would it take to get a PhD? So for now, he has chosen to enjoy life in the real world.

When Greg graduated from high school in 1985, he wrote 100 things he would like to accomplish in life, among them— to stand on top of Mount Everest, to publish a novel, etc. The earning of his Masters degree marks the 28th accomplishment on his list.

PLATE I

GEOLOGIC MAP OF PARTS OF THE LAKE LURE, SHINGLE HOLLOW, SUGAR HILL, AND MOFFITT HILL QUADRANGLES, SOUTHWEST NORTH CAROLINA

by
Gregory M. Yanagihara
1993

Tectonic Units

Unit 3

| msu | Mill Spring complex undifferentiated: amphibolite, granitic gneiss, and biotite gneiss |

| msbg | Mill Spring biotite gneiss |

Mill Spring fault

Unit 2

| pmq | Poor Mountain quartzite and minor amphibolite |

| pma | Poor Mountain amphibolite and minor quartzite |

| msgg | Mill Spring biotite gneiss, metasiltstone, and granitic gneiss |

Sugarloaf Mountain fault

Unit 1

| Chga / Chgm | Chga: Henderson granitic augen gneiss
Chgm: Henderson migmatitic biotite gneiss |

| not exposed | Poor Mountain Formation |

Contacts

— — — — Lithologic contact, solid where precisely located, dashed where approximately located, short-dashed where concealed

▲▲▲▲▲ Thrust fault, solid where precisely located, dashed where approximately located, short-dashed where concealed

Structural Symbols

⟍₆₇ Strike and dip of schistosity, foliation, or compositional layering

↗⁸ Bearing and plunge of mineral lineation

Bearing and plunge of mesoscopic tight to isoclinal recumbent antiformal fold

Bearing and plunge of mesoscopic tight to isoclinal recumbent synformal fold

Bearing and plunge of mesoscopic upright antiformal fold

Bearing and plunge of mesoscopic upright synformal fold

Strike and dip of schistosity and bearing and plunge of mineral lineation measured at the same locality

Strike and dip of schistosity and bearing and plunge of mesoscopic fold measured at the same locality

Moffitt Hill | Sugar Hill
Lake Lure | Shingle Hollow

35° 30'

82° 07' 30"

Geology Completed
1991–1992

Scale 1:24,000

2 Miles
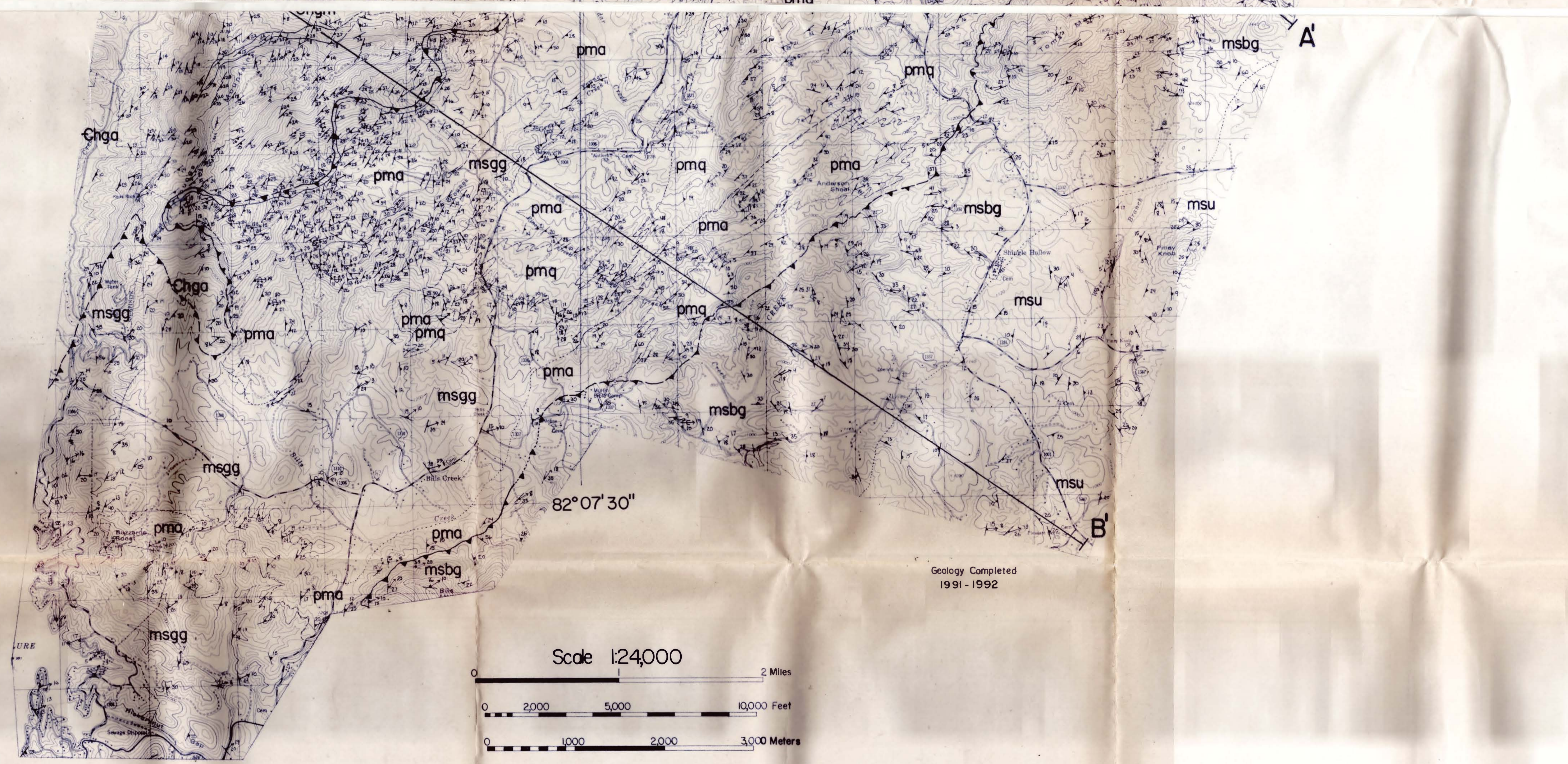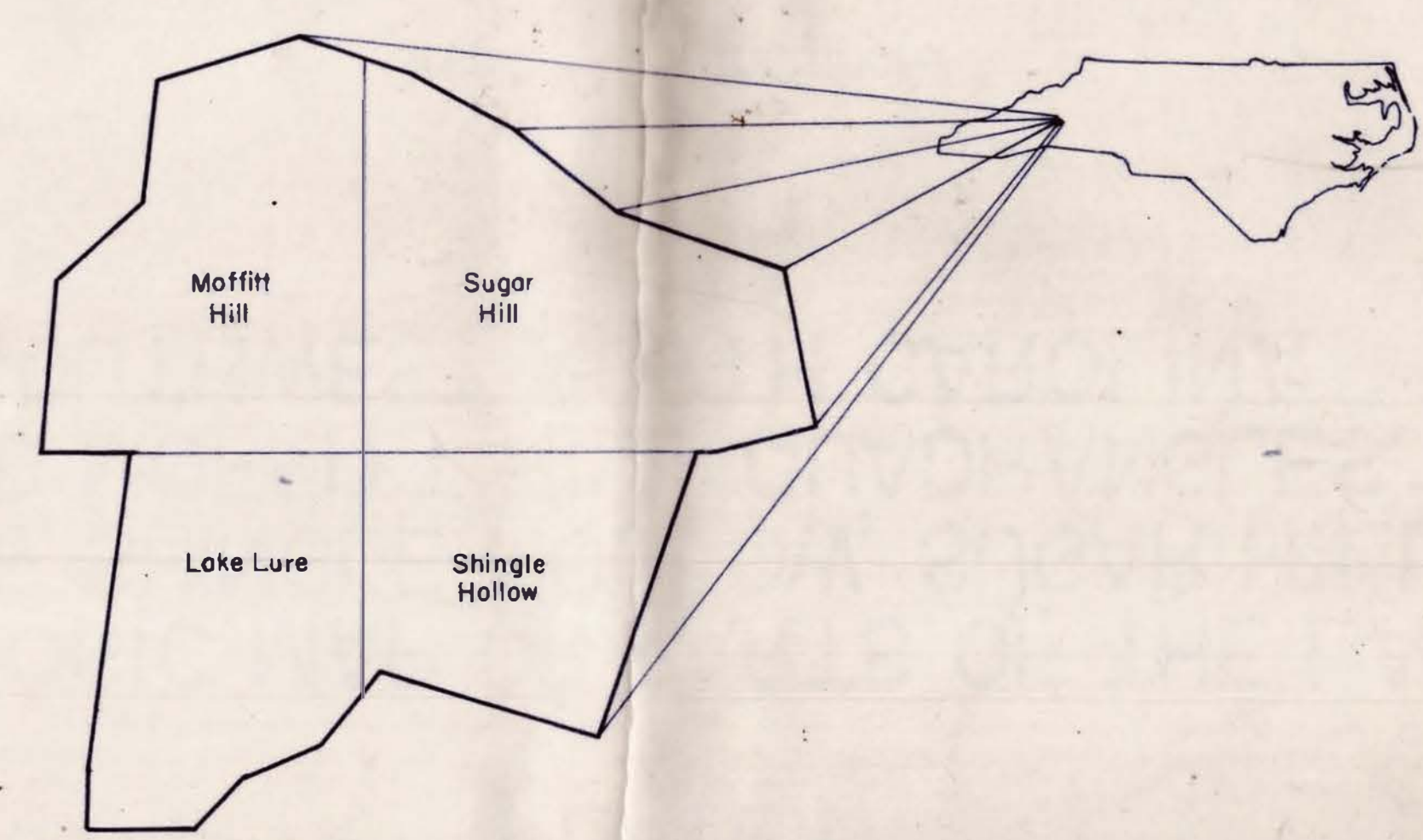
2,000   5,000   10,000 Feet

1,000   2,000   3,000 Meters

Contour Interval: 40 feet

A — A'
B — B'

# PLATE II: CROSS SECTIONS ALONG LINES A-A' AND B-B' ON PLATE I
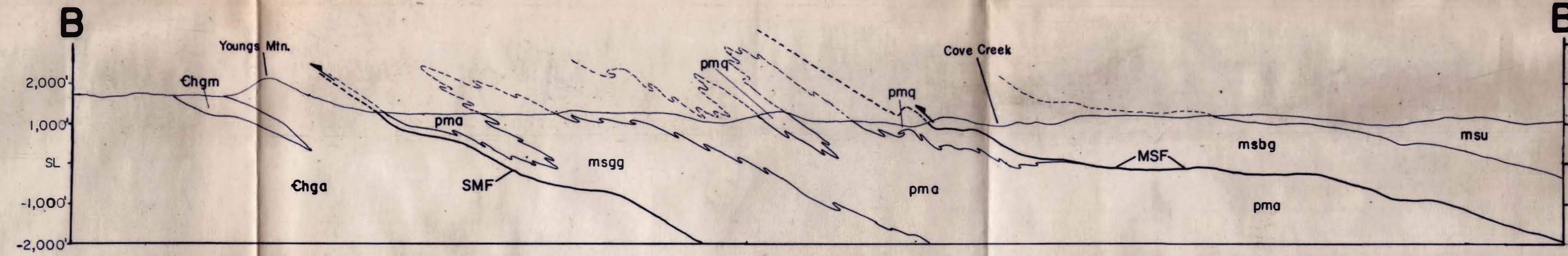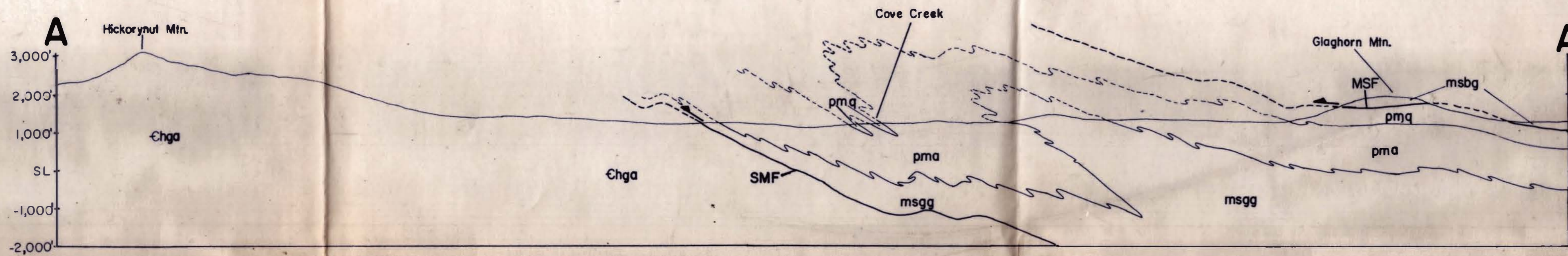
ABBREVIATIONS

SMF - Sugarloaf Mountain fault
MSF - Mill Spring fault

Єhga - Henderson augen gneiss
Єhgm - Henderson migmatitic biotite gneiss
pma - Poor Mountain Amphibolite
pmq - Poor Mountain Quartzite
msgg - Mill Spring biotite gneiss and granitic gneiss
msbg - Mill Spring biotite gneiss
msu - Mill Spring undifferentiated unit

Scale 1:24,000

No Vertical Exaggeration

PLATE III
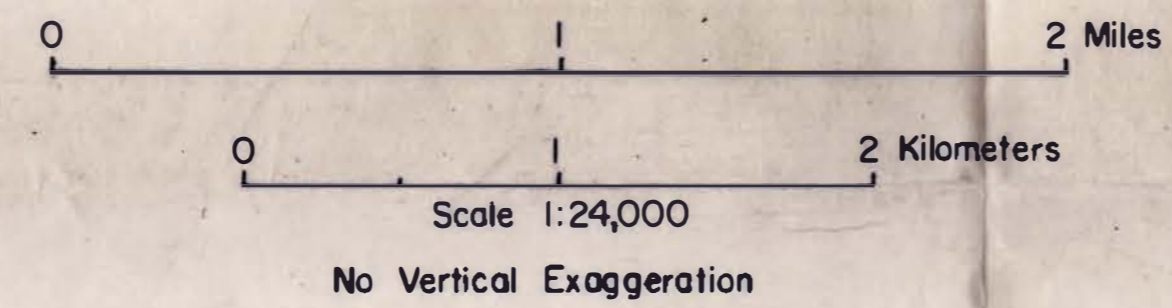
GEOLOGIC MAP OF THE COLUMBUS PROMONTORY, WESTERN INNER PIEDMONT, NORTH CAROLINA

compiled

by

Timothy L. Davis and

Gregory M. Yanagihara

1993
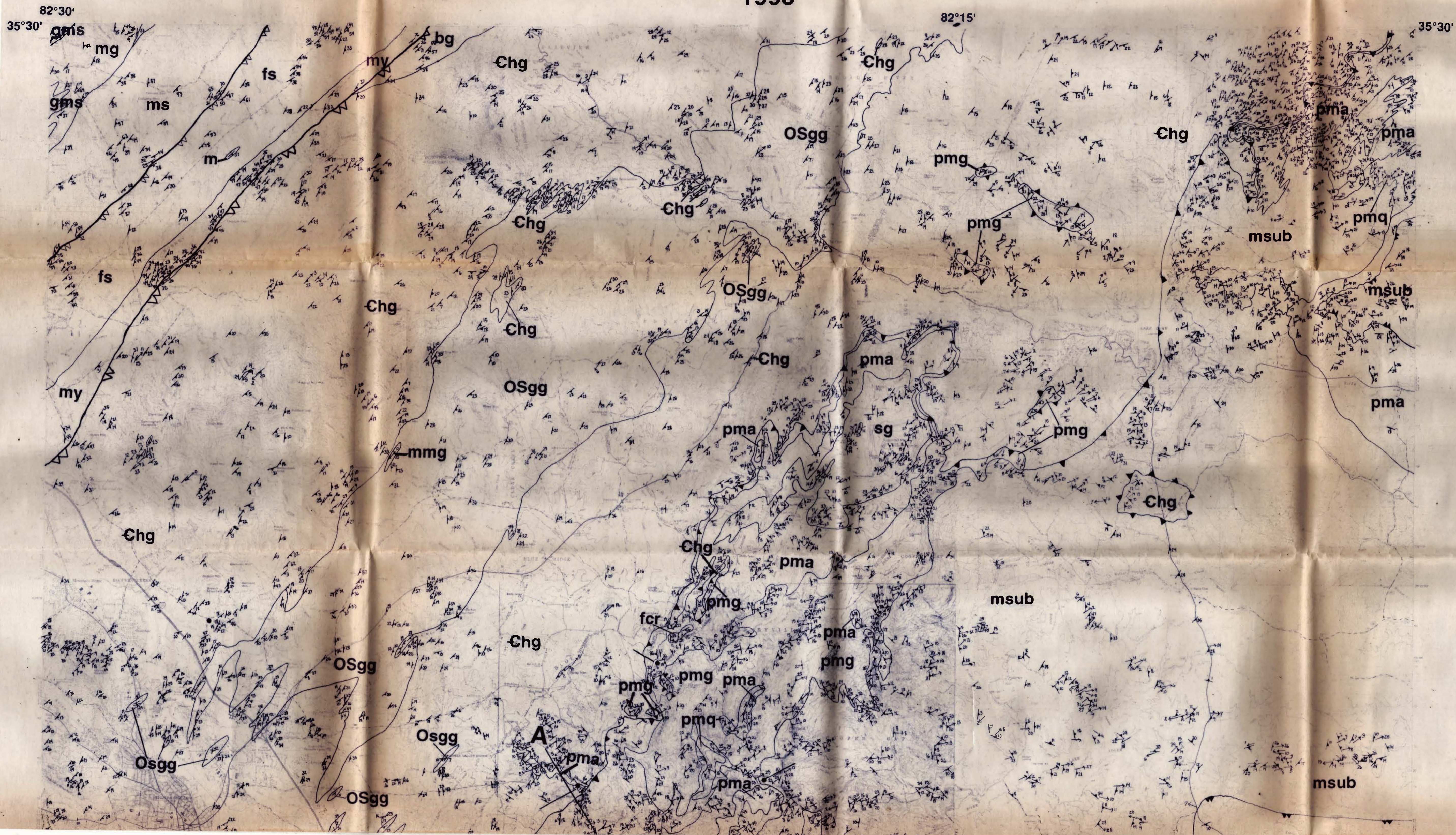
EXPLANATION

| fcr | flinty crush rock (Mesozoic) |

Blue Ridge (from Lemmon and Dunn, 1973b*)

gms	garnetiferous muscovite schist
mg	layered muscovite gneiss and schist
bw	biotite metasandstone
ms	garnetiferous muscovite and muscovite–biotite schist

Inner Piedmont (sensu lato)

Chauga Belt

Brevard Fault Zone (from Lemmon and Dunn, 1973b*)

my	porphyroclastic mylonite and ultramylonite
fs	cataclastic schist, phyllonite and mylonite
m	marble

OSgg	granitic gneiss (438 Ma; Odom and Russell, 1975*)
Chg	Henderson Gneiss (509 Ma; Sinha and others, 1989*)
bg	muscovite–biotite gneiss (Lemmon and Dunn, 1973b*)
mmg	mixed mica gneiss (from Lemmon and Dunn, 1973b*)
sg	Sugarloaf Gneiss (Davis, 1993* and this guidebook)

Poor Mountain Formation (Davis, 1993* and this guidebook)

pma	amphibolite – amphibole gneiss
pmq	quartzite
pmg	garnet-mica schist and quartzite
pmaq	interlayered amphibolite–quartzite

Inner Piedmont (sensu stricto)

Upper Mill Spring complex (Davis, 1993* and this guidebook)

| msub | migmatitic biotite gneiss–metagraywacke |

Lower Mill Spring complex (Davis, 1993* and this guidebook)

| mslb | porphyroclastic biotite gneiss – metagraywacke |
| msla | amphibolite – amphibole gneiss |

STRUCTURAL SYMBOLS

strike and dip of foliation

strike and dip of vertical foliation

trend and plunge of mineral lineation

trend and plunge of horizontal mineral lineation

CONTACTS

stratigraphic contact

FAULTS

Tumblebug Creek thrust – teeth on hanging wall

Sugarloaf Mountain thrust – teeth on hanging wall

Mill Spring thrust – teeth on hanging wall

DATA SOURCES

1	2	3
4	5	6
7		

1. Lemmon and Dunn (1973b*)
2. Lemmon and Dunn (1973a*)
3. Tabor (unpublished, 1988-1990) Yanagihara (unpublished, 1991-1992) Jayne (unpublished, 1991)
4. Lemmon (unpublished, 1975)
5. Davis (this study, 1987-1992)
6. Tabor (unpublished, 1988-1990)
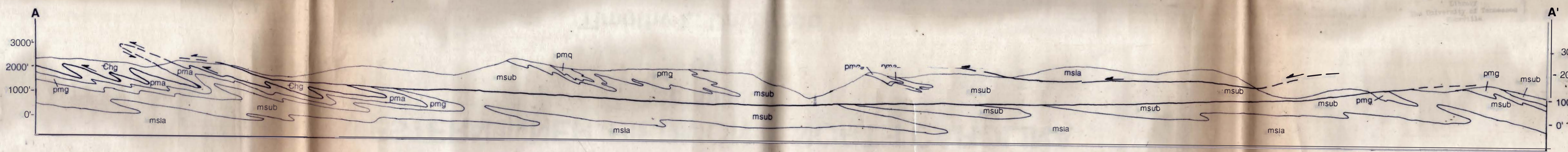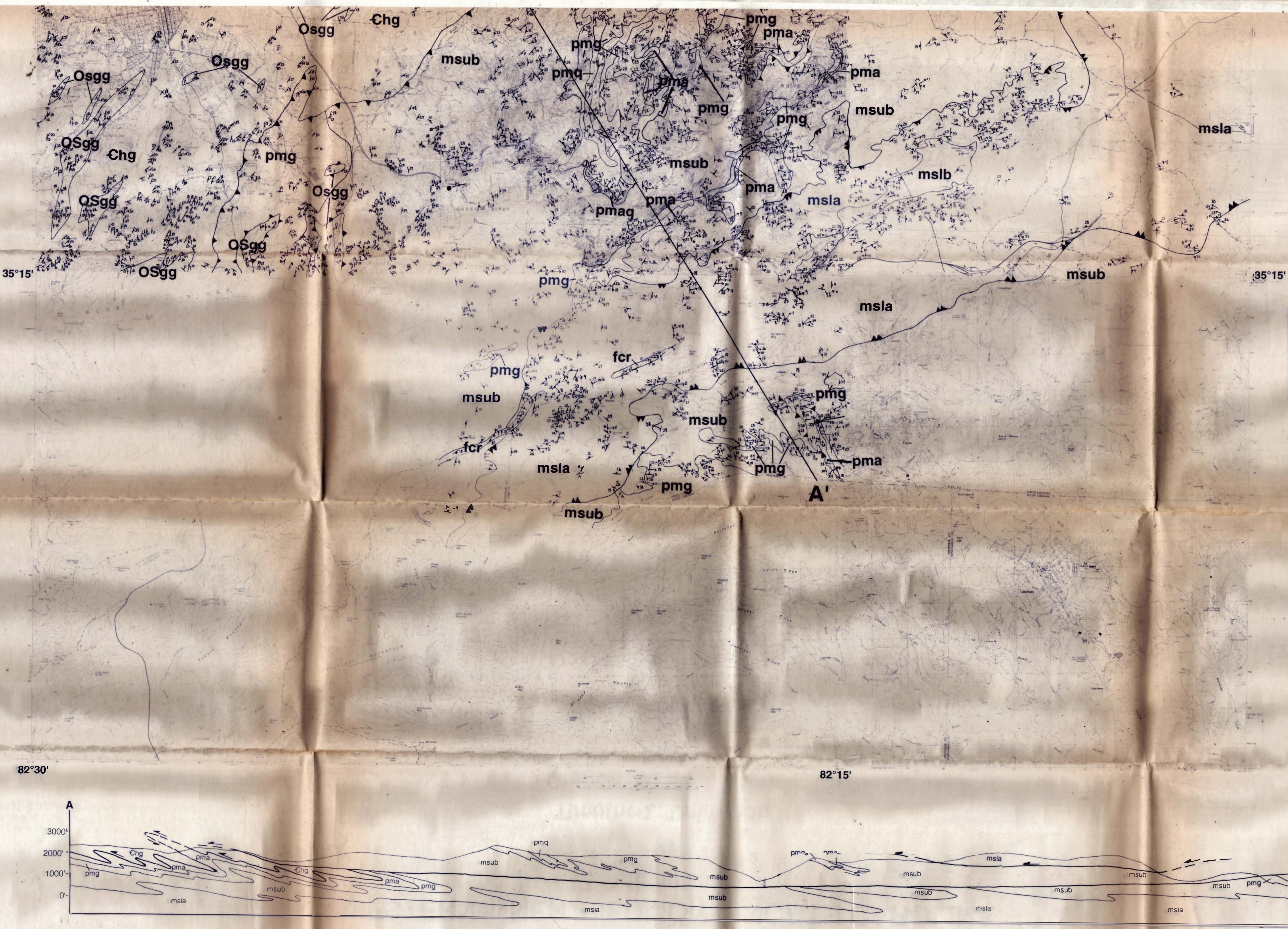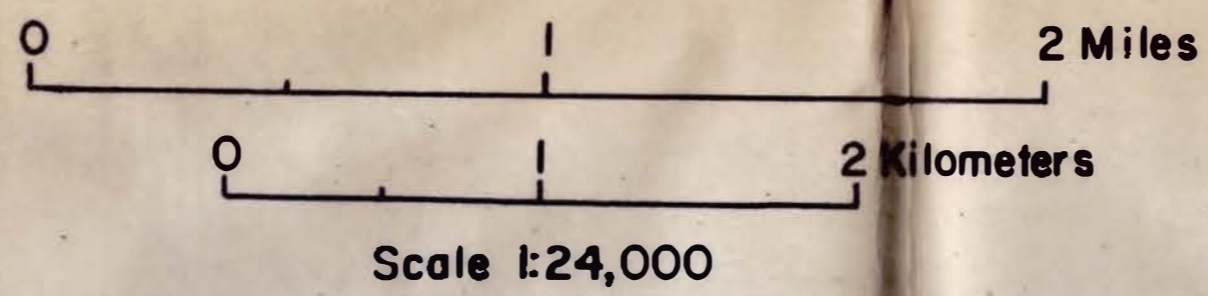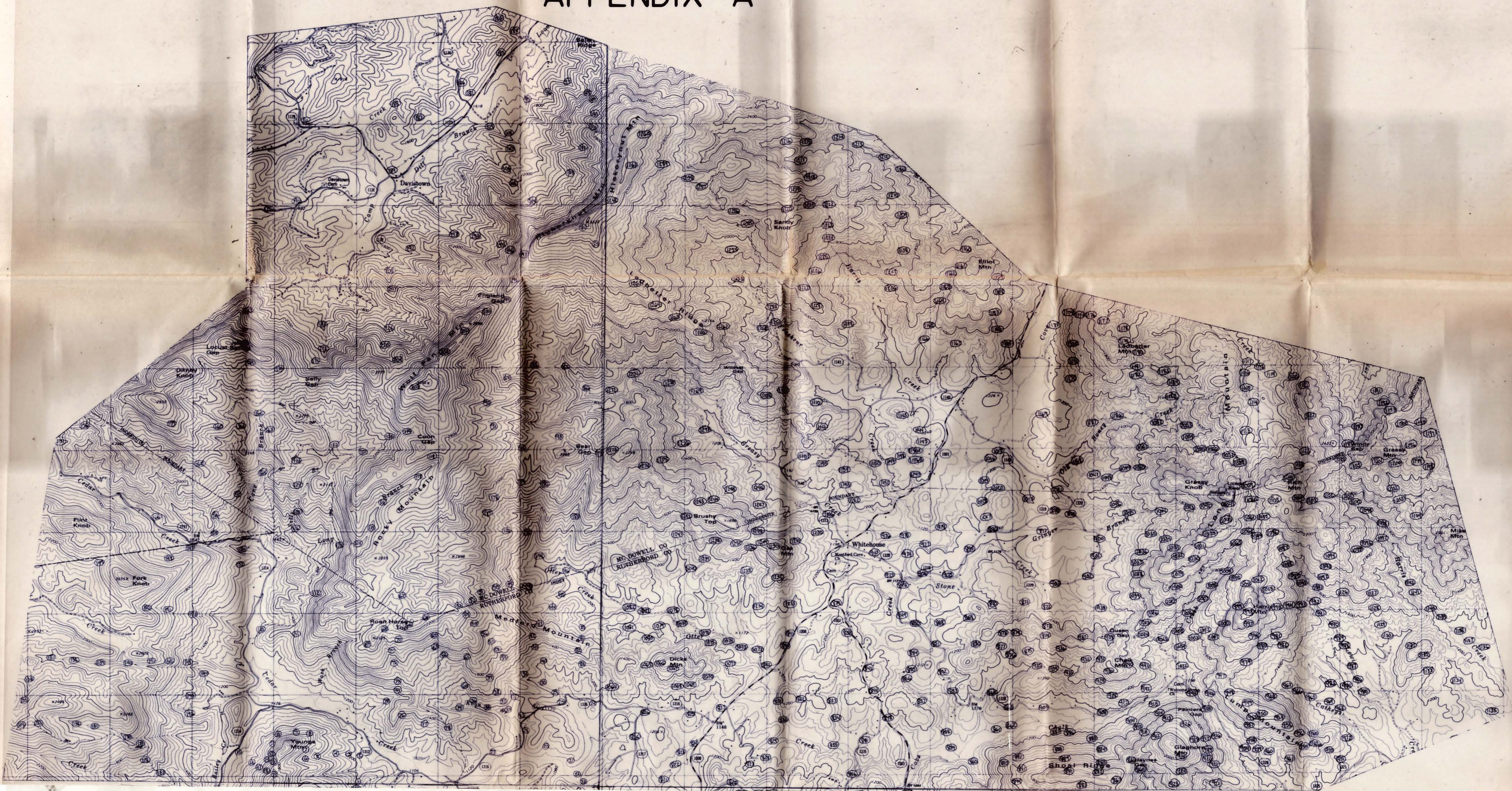7. Davis (this study, 1987-1992)

* Reference in Davis (this guidebook)

82°30′ 35°30′ 82°15′ 35°30′

35°15′ 35°15′

82°30′ 82°15′

A A′

3000′ 2000′ 1000′ 0′

PLATE IV

MAP SHOWING LOCATION OF STRUCTURAL MEASUREMENTS IN
APPENDIX A

Scale 1:24,000